REPORT DOCUMENTATION PAGE			
1. Recipient's Reference	**2. Originator's Reference**	**3. Further Reference**	**4. Security Classification of Document**
	AGARD-LS-151	ISBN 92-835-1547-1	UNCLASSIFIED

5. Originator Advisory Group for Aerospace Research and Development
North Atlantic Treaty Organization
7 rue Ancelle, 92200 Neuilly sur Seine, France

6. Title

MICROWAVE ANTENNAS FOR AVIONICS

7. Presented at

8. Author(s)/Editor(s)	**9. Date**
Various	April 1987
10. Author's/Editor's Address	**11. Pages**
Various	166

12. Distribution Statement This document is distributed in accordance with AGARD policies and regulations, which are outlined on the Outside Back Covers of all AGARD publications.

13. Keywords/Descriptors

Microwave antennas
Avionics
Radomes
Design
Improvement

14. Abstract

Even though considerable advances have been made in digital technology and signal processing, antennas continue to play a key role and their performance is often a dominating factor in defining the overall effectiveness of a system. New system requirements, and the need to provide electronic scanning capabilities have presented major challenges to the technology that require substantial improvements over what is currently available.

Over the last decade there have been notable advances in antenna and radome design, particularly in sidelobe reduction, electronic scanning, conformal arrays, printed circuit arrays, adaptive control and millimetre wave antennas. This Lectures Series will address many of these issues in a two-day programme of lectures by noted workers in the various fields of antenna technology. Future trends and new directions for technological innovation will be subjects for round table discussions.

This Lecture Series, sponsored by the Avionics Panel of AGARD, has been implemented by the Consultant and Exchange Programme of AGARD.

The material in this publication was assembled to support a Lecture Series under the sponsorship of the Avionics Panel and the Consultant and Exchange Programme of AGARD presented on 7—8 May 1987 in Rome, Italy, 11—12 May 1987 in Guenzburg, Germany and 14—15 May 1987 in Ankara, Turkey.

AGARD-LS-151

AGARD-LS-151

AGARD

ADVISORY GROUP FOR AEROSPACE RESEARCH & DEVELOPMENT

7 RUE ANCELLE 92200 NEUILLY SUR SEINE FRANCE

AGARD LECTURE SERIES No.151

Microwave Antennas for Avionics

NORTH ATLANTIC TREATY ORGANIZATION

NORTH ATLANTIC TREATY ORGANIZATION

ADVISORY GROUP FOR AEROSPACE RESEARCH AND DEVELOPMENT

(ORGANISATION DU TRAITE DE L'ATLANTIQUE NORD)

AGARD Lecture Series No.151

MICROWAVE ANTENNAS FOR AVIONICS

The material in this publication was assembled to support a Lecture Series under the sponsorship of the Avionics Panel and the Consultant and Exchange Programme of AGARD presented on 7—8 May 1987 in Rome, Italy, 11—12 May 1987 in Guenzburg, Germany and 14—15 May 1987 in Ankara, Turkey.

THE MISSION OF AGARD

The mission of AGARD is to bring together the leading personalities of the NATO nations in the fields of science and technology relating to aerospace for the following purposes:

— Exchanging of scientific and technical information;

— Continuously stimulating advances in the aerospace sciences relevant to strengthening the common defence posture;

— Improving the co-operation among member nations in aerospace research and development;

— Providing scientific and technical advice and assistance to the Military Committee in the field of aerospace research and development (with particular regard to its military application);

— Rendering scientific and technical assistance, as requested, to other NATO bodies and to member nations in connection with research and development problems in the aerospace field;

— Providing assistance to member nations for the purpose of increasing their scientific and technical potential;

— Recommending effective ways for the member nations to use their research and development capabilities for the common benefit of the NATO community.

The highest authority within AGARD is the National Delegates Board consisting of officially appointed senior representatives from each member nation. The mission of AGARD is carried out through the Panels which are composed of experts appointed by the National Delegates, the Consultant and Exchange Programme and the Aerospace Applications Studies Programme. The results of AGARD work are reported to the member nations and the NATO Authorities through the AGARD series of publications of which this is one.

Participation in AGARD activities is by invitation only and is normally limited to citizens of the NATO nations.

Published April 1987

ISBN 92-835-1547-1

Printed by Specialised Printing Services Limited
40 Chigwell Lane, Loughton, Essex IG10 3TZ

LIST OF SPEAKERS

Lecture Series Director: Dr R.J.Mailloux
Chief, Antenna Technology Branch
Antenna & RF Components Div.
Electromagnetic Sciences Directorate
Rome Air Development Center
Hanscom AFB, MA 01731
USA

SPEAKERS

Dr P.Balling
TICRA — A/S
13 Kronprinsensgade
DK 1114 Copenhagen K
Denmark

Dr P.Barton
STC Components Ltd
Microwave Subsystems
Electron Devices Division
Brixham Road
Paignton, Devon TO4 7BE
United Kingdom

Mr R.J.P.Douville
Chief, RF Circuits
Space Electronics Directorate
Communications Research Centre
3701 Carling Avenue
P.O. Box A90, Station H
Ottawa, Ontario K2H 8S2
Canada

Prof. D.Schaubert
Electrical and Computer Eng. Dept.
University of Massachusetts
Amherst, MA 01003
USA

Mr H.E.Schrank
MS-55
Westinghouse Electric Corp.
P.O. Box 746
Baltimore, MD 21203
USA

Dr F.Schwering
AMSEL-COM-TM-4
Dept. of the Army
HQ US Army Comm-Electronics Command
Fort Monmouth, NJ 07703-5000
USA

Dr K.Solbach
AEG Radio & Radar Systems Div.
D-7900 Ulm
Federal Republic of Germany

CONTENTS

	Page
LIST OF SPEAKERS	iii
	Reference
BASIC PARAMETERS OF ANTENNAS FOR AIRCRAFT, SATELLITES AND MISSILES by R.J.Mailloux	1
AIRCRAFT RADAR ANTENNAS by H.E.Schrank	2
AIRCRAFT ANTENNAS/CONFORMAL ANTENNAS. MISSILE ANTENNAS by K.Solbach	3
SPACECRAFT MULTI-BEAM AND CONTOURED-BEAM ANTENNAS by P.Balling	4
MILLIMETER WAVE ANTENNAS FOR AVIONICS by F.K.Schwering	5
ADAPTIVE ANTENNAS by P.Barton	6
MIC TECHNOLOGY FOR PHASED ARRAYS by R.Douville	7
PRINTED CIRCUIT ANTENNA TECHNOLOGY by D.H.Schaubert	8
BIBLIOGRAPHY	B

BASIC PARAMETERS OF ANTENNAS FOR AIRCRAFT, SATELLITES AND MISSILES

Robert J. Mailloux
Electromagnetics Directorate
Rome Air Development Center
Hanscom Air Force Base, MA 01731

1. INTRODUCTION

System requirements for airborne, satellite and missile antennas continue to place increasingly severe demands upon antenna technology. In general these requirements push toward the increased capability to control and modify antenna patterns, and away from the use of small antennas with broad radiation patterns. Increased control can imply several levels of added sophistication. At the lowest level it implies mechanical or electronic scanning of an antenna directive pattern, at the next level there are needs to produce precise low sidelobe radiation patterns, and at the highest level of complexity there is the need to actively suppress jammer interference through the use of adaptive control of a full array or an antenna with sidelobe cancellers. In addition x to increased control, there is also a trend toward higher frequencies, even to EHF frequencies where arrays of several thousand elements are necessary for some applicatons. At present it appears that the technology at millimeter wave frequencies will be radically different than the current state-of-the-art. System needs at these frequencies are thus seen as a major stimulus to technology.

2. Antennas for Radar and Communications

Airborne satcom antennas at UHF frequencies were required to have near hemispherical coverage. At L-band there is a need for some limited directivity and possible null steering for anti-jam purposes. At EHF frequencies of 20 and 44 GHz there are new requirements for mechanically steered apertures as well as flush mounted arrays. The development of arrays at these frequencies is seen as a major challenge to antenna technology. Sidelobe control is not presently an important factor at these frequencies.

Airborne radar requirements for tactical and strategic systems use antenna technology at frequencies from UHF through the SHF range. The major thrusts of this work have been to produce precise antennas for sidelobe control and to seek high reliability to minimize the cost of maintenance.

Satellite communication antennas have primarily been lens and reflector systems covering the frequency range mentioned for airborne terminals. At all frequencies the trends are toward electrically larger apertures for increased directivity. Sidelobe control and polarization purity have both been emphasized as a means of isolating nearby users, and once again this is a factor that pushes technology development. Adaptive pattern control has also become a major issue for space segment satcom antennas.

Missile antenna technology emphasizes extreme lightweight and conformal "wraparound" or very thin antenna structures, and it was this application that gave the first impetus to the development of microstrip patch antennas in the early 1970's. Present demands in this area emphasize wider bandwidth and operation through EHF frequencies.

2.1 Antenna Parameters

The most important properties of antennas pertinent to radar or communication system designers are the antenna gain, beamwidth, sidelobe levels, bandwidth and noise temperature. These are defined here for the sake of reference.

Directivity, Gain

The antenna gain is equal to the antenna directivity minus the losses and reflected power in the antenna and feed network. This directivity [1] is defined:

$$D = \frac{E(r_0)\, E^*(r_0)}{\frac{1}{4\pi}\int_0^{2\pi}\int_0^{\pi} E(r_0)\, E^*(r_0) \sin\theta \, d\theta \, d\phi} \qquad (1)$$

The maximum directivity (except for certain small apertures) is directly related to the antenna aperture area A as [1]:

$$D_{max} = \frac{4\pi A}{\lambda^2} \qquad (2)$$

a formula that is appropriate for aperture systems like reflectors and lenses, and for arrays in front of metallic ground screens.

Beamwidth

The usual beamwidth implied is that defined by the angles at which the antenna power pattern falls 3 dB below the main beam peak. This beamwidth is of the order of λ/L for an antenna with aperture length L at a wavelength λ. Lowering the antenna sidelobes usually increases the beamwidth, so it is convenient to write the beamwidth in terms of a beam broadening parameter B which is unity for a uniformally illuminated linear array or in the principal planes of a uniformally illuminated rectangular aperture.

$$\Theta_3 = 0.886\, B\, \lambda/L \tag{3}$$

Sidelobes

Antenna sidelobe levels are defined in a number of different ways, depending upon how they are seen to impair system operation. For example, Figure 1 shows two antenna patterns, one for a uniform illumination that has high near sidelobes, but very low far sidelobes, another for a 30 dB Dolph-Chebyshev distribution which has lower sidelobes near the main beam, but higher sidelobes away from the main beam. If the antenna were to track a target immersed in clutter, it might be better to have the near sidelobes be very low, and so the choice would be the 30 dB Chebyshev pattern, but if the clutter source were generally lower, but spread out over very wide angular sectors, then the uniformally illuminated antenna pattern may be preferable because its average sidelobes are so low.

Noise Temperature, Noise Figure

The noise temperature at the antenna terminal has two components, one due to the pattern itself, and which is a function of what the antenna "sees" within its receiving pattern and a part due to dissipative losses within the antenna or couplers, or whatever transmission medium may preceed the antenna terminals.

The antenna temperature for a lossless antenna is the integral of the observed brightness temperature $T_B(\Theta,\phi)$ weighted by the antenna gain, or [1]

$$T_A = \frac{\int_0^{2\pi}\int_0^{\pi} T_B(\Theta,\phi)\, D(\Theta,\phi) \sin\Theta\, d\Theta\, d\phi}{\int_0^{2\pi}\int_0^{\pi} D(\Theta,\phi) \sin\Theta\, d\Theta\, d\phi} \tag{4}$$

The antenna temperature measured at the antenna terminals, however, is modified by losses. If we define a loss factor so that α is the ratio of power at the output terminals to the total received power (note $\alpha \leq 1$), and the lossy material (or transmission line) is at temperature T_ℓ then the effective antenna temperature is [2,3]:

$$T_a = \alpha T_A + T_\ell (1-\alpha) \tag{5}$$

The effective system temperature relative to the preamplifier input is obtained by adding the input noise temperature of the preamplifier and those of following stages as:

$$T_s = T_a + T_1 + T_2/g_1 + T_3/(g_1 g_2) + \cdots \tag{6}$$

where T_1 is the preamplifier effective noise temperature T_n is the effective input temperature of the n'th cascaded element. g_n-1 is the gain or loss of any element in the cascaded chain (preceding the n'th element).

This expression emphasizes the well known result that the system temperature is mainly established by the overall antenna temperature T_a plus the preamplifier input noise temperature T_1, since all successive noise contributions are divided by large gain numbers.

In terms of system noise figure for any two port (with input noise temperature T_e

$$F = 1 + T_e/T_o \tag{7}$$

where here To is room temperature, the above result for the cascade of two-ports is written: (using Te = (F-1)To)

$$F_S = F_1 + \frac{F_2-1}{G_1} + \frac{F_3-1}{G_2} + \ldots \tag{8}$$

$$\text{where } F_1 = 1 + (T_a + T_1)/T_o$$

The effective noise power received at the preamplifier input over the bandwidth Δf thus is:

$$N = k\, T_S\, \Delta f \tag{9}$$

where k is Boltzman's constant (1.38×10^{-23} J/°K)

This noise power is used to calculate the signal to noise ratio at the preamplifier input for the radar range equation and Friis Transmission formula.

2.2 System Considerations

For polarization matched antennas aligned for maximum directional radiation and reception, the received power in a communication system is given:

$$P_r = (P_T G_T)\left(\frac{\lambda}{4\pi R}\right)^2 G_R \tag{10}$$

which is a reduced form of the Friis Transmission Equation.

The term $(\lambda/4\pi R)^2$ is the free-space loss factor, and accounts for losses due to the spherical spreading of the energy radiated by the antenna.

A similar form defining the received power for a monostatic radar system is given by the following reduced form of the radar range equation.

$$P_R = (P_T G_T)\,\sigma \left[\frac{\lambda}{4\pi R}\right]^2 \left(\frac{1}{R}\right)^2 G_R \tag{11}$$

where in this case, it is not assumed that $G_T = G_R$. The the receiver input, the sensitivity is determined by the signal to noise ratio. In either case the ratio is that of the received power to the noise (Eq 9) (12)

$$\underline{\text{Communications:}} \quad S/N = (P_T G_T)\left(\frac{G_R}{T_S}\right)\frac{1}{k\Delta f}\left(\frac{\lambda}{4\pi R}\right)^2 \tag{13}$$

$$\underline{\text{Radar :}} \quad S/N = (P_T G_T)\left(\frac{G_R}{T_S}\right)\frac{1}{k\Delta f}\left(\frac{\lambda}{4\pi R}\right)^2\left(\frac{1}{R}\right)^2$$

Subject to some minimum S/N ratio at the receiver therefore it is clear that the range of a communications system varies like the square root of $G_T P_T$ (called the EIRP or effective isotropic radiated power) and like the square root of G_R/TS. For a radar system the range varies like the fourth root of the transmit EIRP and receive $G_R T_S$.

These system aspects are of great significance when choosing between passive or mechanically scanned antennas and array antennas for a particular requirement, as will be illustrated later.

2.3 Fixed Beam Antennas

Needs to reduce sidelobe levels beyond what was acceptable a decade ago have led to very precise reflector antennas and the development of low sidelobe feeds for both reflectors and lenses. Off axis reflectors feeds have demonstrated extreme low sidelobe behavior (4,5) with wide instantaneous bandwidths. In addition, waveguide slot and stripline fed dipole arrays are being developed as elements in flat plate arrays with mechnical beam positioning in either one or two planes. This technology has advanced substantially and can produce extemely low sidelobe patterns over narrow bandwidths. Figure 2 shows an L-band low sidelobe array (6) developed by Westinghouse Corp., that demonstrated better than -36dB peak and -48 db RMS sidelobe levels over about 45% bandwidth.

Low sidelobe patterns can thus be produced by fixed beam antennas. As we shall see later, they can also be produced by scanned arrays. In either case there is a price in terms of increased beamwidth and correspondingly decreased gain. Figure 3 demonstrates these changes for several low sidelobe aperture distributions.

2.4 Scanning Array Antennas

New avionics system requirements are often only satisfied by electronically scanned array antennas. The constraints that ultimately dictate use of a phased array for a given application are the need for rapid scanning to track multiple communication system users, the need to provide stationary, conformal airborne antennas with variable angular coverage for airborne SATCOM, and requirements for airborne antennas with low radar cross section. Nevertheless, the specification of an array antenna to satisfy a given application should never be accepted lightly, for it is met only at great cost: monetary cost, and cost in terms of system performance.

Array Directivity/Gain

Phased array directivity is given conveniently by the formula below (7):

$$D = 32{,}400/(\theta_{x_3}\,\theta_{y_3}\sec\theta_o) \tag{14}$$

where θ_{x3} and θ_{y3} are the 3dB beamwidths of the pencil or elliptical beam at broadside. In this formula the beamwidths are in degrees.

This simple formula reveals the well known cosine scan dependence exhibited by planar arrays. The formula is exact for uniform illumination, and a good approximation for other array illuminations for all θ_0 except very near endfire, where more detailed analysis is required. It reduces exactly to equation 2 for a uniformally illuminated array, and so is consistent with aperture gain principles. Since the directivity varies like the cosine, one must account for this 3-dB loss at 60° scan.

In practice, the array impedance mismatch usually increases with scan and so the actual array gain varies more like $\cos^{3/2}(\theta)$, which would be 4.5 dB at 60° or $\cos^2\theta$ which is 6 dB. In addition there is loss in the phase shifters and power dividing network that can easily be another 3 dB (or more). For an array to provide the same gain at 60° scan as a fixed aperture with perhaps one dB loss, the array would have to have at least four times the area of the fixed aperture.

The second "cost" factor arises because the array is composed of a number of elements that must be spaced very closely across the aperture to suppress grating lobe radiation. This cost translates to the real monetary costs of phase controls, microwave power dividing networks and the elements themselves.

Element Spacing and Grating Lobes

Grating lobes result from an ambiguity in the array radiation pattern. Consider an array of "N" elements arranged in a line as shown in Figure 4 with element locations $x = nd_x$. In the far field the normalized array radiation pattern is given by:

$$A(\theta) = \sum I_n e^{jk_o n d_x \sin\theta} f_n(\theta) \tag{15}$$

where the I_n are complex weights assigned to each element, and $f_n(\theta)$ is the radiation pattern (or "element pattern") of the n'th element in the presence of the other array elements.

k_o is the free space wave number $= 2\pi/\lambda_o$ at frequency f_o.

If all the element patterns are assumed to be the same (an assumption that the elements are not inter-coupled), then one can create a maximum of A $A(\theta)$ in an given direction θ_o by choosing the weights I_n to be:

$$I_n = |I_n| e^{-jk_o n d_x \sin\theta_o} \tag{16}$$

The radiation pattern then has the familiar form of an array factor F (θ) times an element pattern f (θ)

$$A(\theta) = f(\theta)F(\theta) = f(\theta)\sum_n |I_n| e^{jknd_x(\sin\theta - \sin\theta_0)}$$

in which it is apparent that at $\theta = \theta_0$ the summation has its peak value. However, the summation also has a peak whenever the exponent is some multiple of 2π or when

$$\frac{2\pi}{\lambda_0} d_x (\sin\theta - \sin\theta_0) = 2\pi p \qquad (18)$$

for all integer "p". Such peaks are called grating lobes and are shown from the above to occur at angles θ_p such that: $\sin\theta_p = \sin\theta_0 + \frac{p\lambda}{d_x}$; $p = \pm 1, \pm 2 \cdots$

for values of p that define an angle with a real sine ($|\sin\theta_p| \leq 1$). (19)

If the element spacing exceeds a critical dimension, grating lobes occur in the array factor, as indicated in Figure 5. Since the far field is the product of an element pattern times the array factor, the grating lobe may be suppressed by the element pattern zero for a broadside array as shown in the figure. However, when the array is scanned (and the element pattern not), the grating lobe location moves out from null and can be a substantial source of radiation. A criterion for determining the maximum element spacing for a given scan angle θ_0 is to set $\sin\theta_{-1} = -1$ so that the nearest grating lobe is at the horizon. Using 19 this leads to

$$d_x/\lambda < \frac{1}{(1+\sin\theta_0)} \qquad \text{(Wide angle scan condition)} \qquad (20)$$

a condition that leads to spacing not much greater than $\lambda/2$ for wide angle scanning.

Similar relations hold for the two dimensional array, with the end result that element spacings are restricted to about half wavelength or slightly more for most applications. The area occupied per element for 60° scan lies between $0.29\lambda^2$ and $0.33\lambda^2$.

In practice, it is necessary to further reduce the element spacings (by 5-10%) in order to avoid pattern deterioration associated with slow wave coupling.

By taking advantage of suppression due to the element pattern, it is possible to design arrays with spacing larger than that given by equation (20) if the scan angle is limited to a few degrees (up to ± 10° or so). Several of these cases will be described later, but in all instances there remains a maximum element spacing for grating lobe suppression given by:

$$\frac{d_x}{\lambda} < \frac{0.5}{\sin\theta_{max}} \qquad \text{(Limited Angular Scan Condition)} \qquad (21)$$

This increased element spacing is available only through the use of very subtle feed techniques, and require arrays that become quite different than the conventional ones. Cost savings can be dramatic if the scan angles are significantly limited.

Phased Array Bandwidth

The third "cost" factor incurred because of the use of a phased array instead of a mechanically positioned aperture is that arrays have significantly narrowed bandwidth. The bandwidth limitation is because scanning control is performed by phase shifters, rather than by time delay devices. The result is pattern "squint" like that shown in Figure 6, in which the main beam scan angle is reduced for frequencies above the design frequency, an increased for frequencies below the design frequency. Assuming that bandwidth is defined by the frequency limits at which the gain is reduced to half power, the resulting fractional bandwidth is given by:

$$\frac{\Delta f}{f_0} = \frac{\theta_3}{\sin\theta_0} = 0.886\, B \left(\frac{\lambda}{L}\right) \frac{1}{\sin\theta_0} \qquad (22)$$

for an array with beamwidth θ_3. Clearly the bandwidth becomes smaller as the array is made larger or as the scan angle is increased. The array bandwidth restriction is, in many cases, a severe system limitation. It can be removed only at great cost by replacing phase shifters by time delay devices. Moreover, present day time delay units are switched transmission lines, and their bulk and weight make them unsuitable for most array applications. In general then, most avionics applications of arrays suffer the bandwidth limitation given by equation (22).

Tolerance Control, Sidelobes, Gain

Phased arrays can provide excellent pattern control, with very low sidelobe radiation. Such precise control is not without its cost however, for building a low sidelobe array requires very high tolerance phase controls.

In an array with random phase and amplitude errors, and including randomly failed elements, the average sidelobe level far from the beam peak is given by: (8,9).

$$\sigma^2 = \frac{\epsilon^2}{P_e N \eta} = \frac{[(1-P_e) + \bar{\Delta}^2 + P_e \bar{\delta}^2]}{P_e N \eta} \qquad (23)$$

where

$\bar{\Delta}^2$ is the amplitude error variance normalized to unity

$\bar{\delta}^2$ is the phase error variance

P_e is the probability of survival for any element in the array

η is the array efficiency

N is the total number of elements

This equation gives the normalized sidelobe level relative to the average array gain. The failed elements in the array are assumed to be randomly located, and the average value of the phase and amplitude errors is assumed to be zero. The sidelobe level above should be considered the average of a number of antenna patterns, not the average level of any one antenna.

The reduction in directivity due to these errors is given by:

$$\frac{D}{D_0} = \frac{P_e}{1 + \bar{\Delta}^2 + \bar{\delta}^2} \qquad (24)$$

Peak sidelobe levels are also given in the literature. A convenient result is obtained when the errors are sufficiently large compared to sidelobes or null depths that structured minor lobe radiation is negligible and the statistics of the field intensity pattern are described by a Rayleigh density function. In this case the probability that a particular sidelobe level v_0^2 is exceeded at any point is:

$$\text{Probability } (v > v_0) = \exp\left[\frac{-v_0^2}{\sigma^2}\right] \qquad (25)$$

where σ^2 is the average sidelobe level of Eq. 23.

Starting with the expression above, valid at particular point, Allen derives the following rule of thumb for the error $\bar{\epsilon}^2$ allowable for an array with gain G, far sidelobe level 1/R and using element lattice areas 0.5λ on a side:

$$\epsilon^2 \leq \frac{1}{10\pi} \frac{G}{R} \qquad (26)$$

which results in an allowable phase error of about 10° when the sidelobe level is numerically equal to the gain.

This important relationship explains why it is fairly easy to design arrays with sidelobes at the isotropic level, but to maintain sidelobes of 20 dB below the isotropic level would require 1° phase error, an extremely difficult goal and one barely within the present state of the art.

Discrete Phase Shifters

Low sidelobe arrays not only require precise phase shifters, but if the phase shifters have discrete phase states, they require additional states for low sidelobes.

A digitally controlled "P" bit phase shifter has 2^P phase states separated by phase steps of $2/(2^P)$ as shown in Figure 7. Miller (10) has analyzed the resulting peak and rms sidelobe levels for this staircase approximation to the desired linear phase progression and has shown the loss in array gain due to the triangular error distribution is approximately

$$\Delta G = \frac{1}{3}\frac{\pi^2}{2^{2P}} \tag{27}$$

which is on the order of 0.23 for a three bit phase shifter and 0.06 for a four bit phase shifter. More significant are the average sidelobe levels which, based upon an average array loss of 2 dB to account for illumination taper and scan degradation are:

$$\text{RMS Sidelobes} \simeq \frac{5}{2^{2P}N} \tag{28}$$

where N is the number of elements in the array. For a one-dimensionally scanned array N is the number of phase controls, and the RMS sidelobe level above is measured in the plane of scan. The net result is to require extreme precision for unidimensional scanned arrays. Figure 7 shows this sidelobe level for various phase shifter bits "P" and N up to 10,000 elements. For -50 dB rms sidelobes an array of 1000 elements requires 5-bit phase shifters, but an array of 10,000 elements can maintain 50 dB sidelobes with only 3-phase bits.

Of greater significance to antenna design is that the phase errors have a periodic variation across the array and tend to collimate as individual sidelobes, called phase quantization sidelobes, which are much larger than the rms levels. A detailed discussion of this phenomenon is given in Ref. 11 along with simple formulas for evaluating the resulting lobes. A perfectly triangular quantization error causes a quantization lobe level of $1/2^P$, which gives -30 dB for 5-bit phase shifters. Ref. 11 shows that for discrete phase shifters the error is not triangular, and that the maximum quantization lobe can be substantially larger.

One solution to the peak quantization lobe problem as suggested by Miller and in a more recent paper Smith and Guo (12) is to decorrelate the phase shifter errors. Decorrelation occurs naturally in space fed arrays, where the phase shifters collimate the beam as well as steer it. In such arrays the phase error is distorted from the triangular shape and the quantization lobe is substantially reduced. The efficiency of various procedures is described in reference 12.

Alternatively, in an array with in-phase power division one can introduce a phase error into each path and then program the phase shifter to remove the error in addition to steering the beam. Optimizing this error can reduce the peak sidelobes very close to the rms sidelobe level, but this consideration must be carefully accounted for in the array design.

An entirely different solution to the quantization lobe problem is often achieved at the system level by recycling all the phase shifters between consecutive radar pulses or between transmit and receive. This process, called beam dithering, (13) consists of adding a fixed phase shift to the phase command and re-computing phase shifts. The net result is to change all the phase states so that the quantization is made differently for each pulse (or between transmit and receive). By following this procedure one can use simple row-column steering but introduce randomness into the quantization steps to reduce the peak quantization lobes.

Before leaving the topic of arrays, it is of interest to go back to consider the comparison between fixed beam antennas and arrays in light of practical array losses. Typical losses through an array might be on the order of 3 dB, including phase shifter losses, element, polarizer and connector losses and losses in the power divider network. This compares to, for example, one dB dissipative loss for a moveable reflector with rotary joint and waveguide feed. Using equations and assuming that the two systems have the same antenna pattern (and antenna temperature TA of 20°K) then the net temperature at the antenna terminals is 75.6° for the dish, and 155° for the array. If the receiver reamplifier noise figure is 2.75 (a reasonable number up to 20 GHz) then T_1 = (F-1) 290° = 508°, then the system noise temperatures will be approximately 584° and 663° for the two cases, an increase of slightly over 0.5 dB. Moreover, if the antennas are the same size and the array scans out to where it's directivity is reduced to one half the boards, be directivity, then the array gain will be about 5 dB less than the dish with its 1 dB total dissipative loss.

The net S/N (Eq 13) for an array based radar system will thus be a factor of 10.5 dB less than the reflector based system unless this loss is compensated by some combination of increased transmitter power or increased transmit or receive apertures. For this reason the array aperture may be several times the size of the reflector it replaces.

Current Technology for Scanning and Multiple Beam Antennas

Phased arrays with waveguide and dipole radiators are now extensively used in airborne and ground based radar systems. A recently fielded system, the EAR (Electronically Agile Radar) array (Figure 8) is a multifunction airborne radar antenna developed by Westinghouse Corporation. The EAR antenna has 1818 phase shifters and was developed as a constrained fed array with azimuth and elevation beam steering via the phase shifters and drivers which are integrated into the radiating element.

The demands imposed by electronic countermeasures in military systems are leading to antenna systems with much lower sidelobes. The Air Force AWACS antenna system, an early warning surveillance system, was the first development to address this need. In addition, the Ultra Low Sidelobe Antenna (ULSA) system for the TPS-43 Search Radar (Figure 9) and the Army Hawk antenna system are all examples of antennas that scan in the vertical plane and maintain extremely low sidelobes in the azimuth plane. Designed by Westinghouse Corporation, these arrays use slotted waveguide row radiators and have multiple or scanned elevation beams.

Other low sidelobe arrays have been developed [14,15] using precision stripline feeds for wider band performance. Like the slot array geometries, these antennas are mechanically rotated in the azimuth plane, and rely on ultra precise row distribution networks for low azimuth sidelobes. Elevation coverage is provided electronically, but with substantially higher elevation plane sidelobes.

A recent paper by Tsandoulas [16] describes the development of an array of 252 waveguide elements arranged in 42 vertical columns and scanned in the azimuth plane. Through careful tolerance control in the power division network and extremely accurate phase shifters the array achieved azimuth scan patterns with all but the first sidelobe below -42 dB. This significant development represents the lowest scan plane sidelobes achieved to date.

Arrays for full two dimensional scanning tend to be bulky, heavy, and costly. The addition of special features, like wideband performance or adaptive pattern control, or performance at millimeter wave frequencies, all tend to make array cost unreasonable for many applications. One solution is offered by the new technology of printed circuit arrays.

Figure 10 shows a microstrip patch array developed by Ball Corporation. The array has 16 elements and a measured 15.7 dB gain (compared to the maximum area gain of 17.2 dB) at 4.6 Ghz. The beam was scanned to 55° in both E and H planes, VSWR was less than 2 to 1 at all beam positions, and gain fell off about 1.6 dB at $\pm$ 100 MHz around the design center frequency. Much larger arrays have been built but because of the losses in microstrip circuitry and the lack of space for a large power distribution network at the one radiating surface, it is necessary to build these larger arrays with multiple layers.

Separating feed and elements also permits a greater freedom in element placement. The antenna shown in Fig. 11 is a 3.5 λ, X-band monopulse array. The 24 elements are distributed in three rings and a separate corporate feed is used to excite each quadrant. The feed consists of an input three-way power divider, followed by three binary power dividers. Measured gain was 19.7 dB, corresponding to an aperture efficiency of 77 percent, while measured sidelobes were about -17.5 dB.

Figure 12 illustrates the use of multiple layer boards for phase scanned microstrip arrays. Extra layers are required for power division, phase shift circuitry and logic and DC bias lines. Often the logic board is itself a multiple layer board which must then be integrated into the array backplane structure. As shown on the figure, it is often convenient to organize such arrays into subarrays, and at EHF frequencies the subarrays could even include active devices, high power or low noise amplifiers to improve transmit array efficiency and receive array noise temperature.

Although microstrip array technology is a truly revolutionary development in phased array antennas, its application remains limited because of the narrow bandwidth of microstrip radiators. Arrays with low dielectric constant substrates have been made with approximately 6% bandwidth, but the bandwidth is less for higher dielectric constant substrates.

The final topic in the array area is the use of arrays or switched multiple beam feeds for electronic control of high directivity pencil-beam patterns within a limited field of view. Figure 13 illustrates a focussing lens (or reflector) used as a multiple beam structure by accessing the individual beams formed by feed elements displaced from the focus. In practice it is often necessary to construct the multiple beams using clusters of feeds for the sake of sidelobe control. Figures 13B and 13C indicate that in general such a multiple beam system can be organized as a scanning array by appropriately combining the output signals received at the individual multiple beam feed elements.

The primary reason for developing such scanning systems instead of simply using conventional arrays is that such systems need only a small fraction of the number of phase controls that would be required of a conventional system with the same aperture. A convenient rule-of-thumb is that the minimum number of required phase controls is roughly equal to the number of independent beams required to fill the scan sector. For the case of a rectangular scan sector, a rectangular aperture and orthogonal beams this minimum number is: minimum number is:

$$N_{min} = \left[\frac{\sin \theta_{max}^{(1)}}{\sin(\theta_3^{(1)}/2)}\right]\left[\frac{\sin \theta_{max}^{(2)}}{\sin(\theta_3^{(2)}/2)}\right] \qquad (28)$$

where $\theta^{(1)}$ max and $\theta^{(2)}$ max are the maximum scan angles in the two planes measured at the peak of each beam and the θ_3 values are the respective halt power beamwidths.

Most of these quasi-optical scanning systems require more controls than this minimum number, but still require far less than conventional arrays. Systems based on the use of a single array in the focal region of a reflector or lens (Fig. 14) typically require between 2 and three times the minimum number of elements, and in addition, requires an oversize main reflector. Other quasi-optical approaches combine an array, a subreflector or primary lens, and a main reflector or lens to produce scanning over a limited sector. Some examples are shown in Fig. 15, in which the figures 15B and D should be seen as performing the function of the "Transform" feed previously shown in Figure 13C. Systems with two focussing structures do not require such a large main aperture, because it's illumination does not move as a function of scan angle.

REFERENCES:

1. C.A. Balanis, "Antenna Theory, Analysis and Design", Ch 2, Harper and Row, Publishers, New York, 1982.

2. M. Skolnik Editor, Radar Handbook, McGraw Hill Book Co., New York, Ch 1.

3. A.B. Carlson, "Communication Systems", McGraw Hill Publishing Co., 1968. Appendix B.

4. R. Fante, P. Franchi, N. Kernweis, L. Dennett, "A Parabolic Cylinder Antenna with Very Low Sidelobes", IEEE Trans AP-28, pp. 53-59, Jan 1980.

5. E. Carlsson, A. Derneryd, E.R. Karlsson, J.O. Larsson "Doubly Curved Reflector Antenna with Extremely Low Azimuth Sidelobes", IEEE Symposium on Antennas and Propagation, pp. 249-252, Digest, 24 May 1982.

6. S. Winchell, "A Performance Analysis of Broadband Low Sidelobe Array Antennas", Report No. N60921-79-C-A236-100, Naval Surface Weapons Center, Dahlgren, Virginia, 1979.

7. R. Elliott, "The Theory of Antenna Arrays", Ch 1, Vol 2, p. 45 of Microwave Scanning Antennas, Academic Press, New York, Ed. R.C. Hanson, 1966.

8. M. Skolnik, Ch 6 in Antenna Theory, Part 1 McGraw Hill Book Co., N.Y. (1969), Edited by R.E. Collin and F.J. Zucker.

9. J.L. Allen, "The Theory of Array Antennas, MIT Lincoln Lab Tech. Report 323, 1963.

10. C.J. Miller, "Minimizing the effects of phase quantization errors in an electronically scanned array", Proc., 1964 Symp. on Electronically Scanned Array Techniques and Applications, RADC-TDR-64-225, 1:17-38, RADC, Griffiss AFB, New York.

11. R.J. Mailloux, "Array Grating Lobes due to Periodic Phase, Amplitude and Time Delay Quantization", IEEE Trans. AP-32, No. 12, pp. 1364-1368, 1984.

12. M.S. Smith and Y.C. Guo, "A Comparison of Methods for Randomizing Phase Quantization Errors in Phased Arrays", IEEE AP-31, No. 6, pp. 821-828, Nov 1983.

13. Brookner, E. (1977) Editor, Radar Technology, Artech House, Dedham, Massachusetts.

14. Evans, G.E., and Winchell, S.G. (1979) A wide-band ultra-low sidelobe antenna, Proceedings of the 1979 Antenna Applications Symposium.

15. Dahl, C.G., Fogelstrom, C.E., Gansz, W.W., and Merril, P.R. (1979) Low-sidelobe tactical radar antenna. The 1979 Antenna Applications Symposium, Univ. of Illinois, Urbana, Illinois.

16. Tsandoulas, G.N. (1980) Unidimensionally scanned phased arrays, IEEE Trans., AP-28 (No. 1): 86-98.

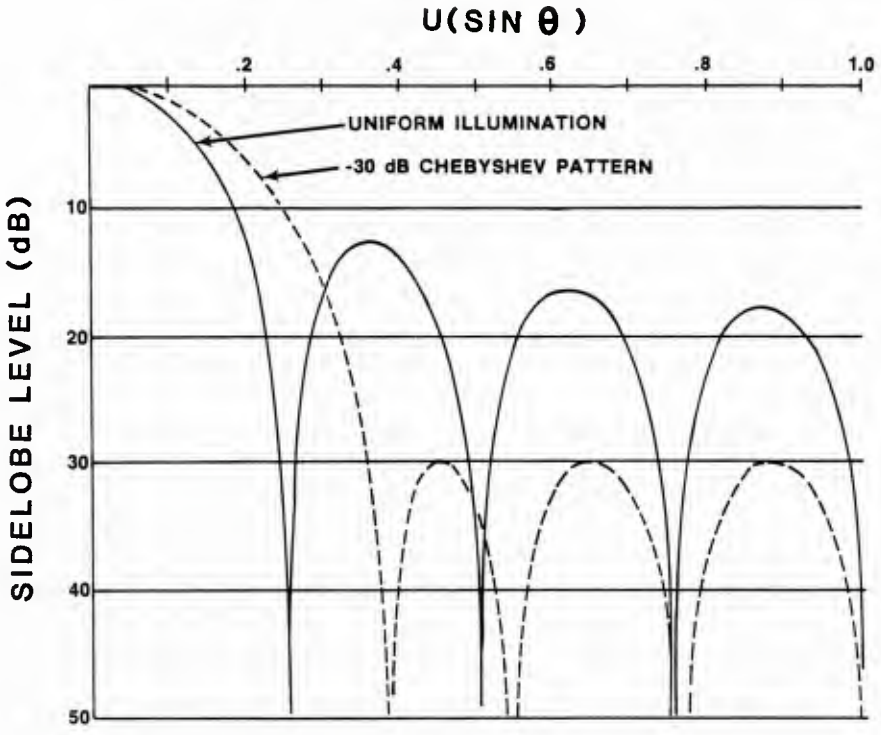

FIG. 1 COMPARISON OF PATTERN FROM UNIFORM AND LOW SIDELOBE ILLUMINATIONS

FIG. 2 LOW SIDELOBE L-BAND ARRAY (COURTESY OF WESTINGHOUSE CORPORATION)

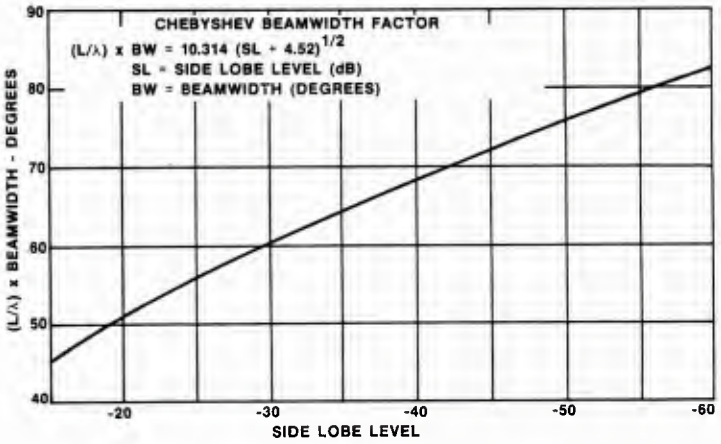

FIG.3 VARIATION OF ARRAY BEAMWIDTH WITH SIDELOBE LEVEL

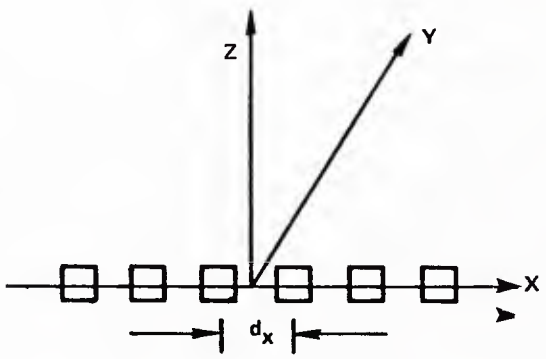

A. ONE DIMENSIONAL ARRAY

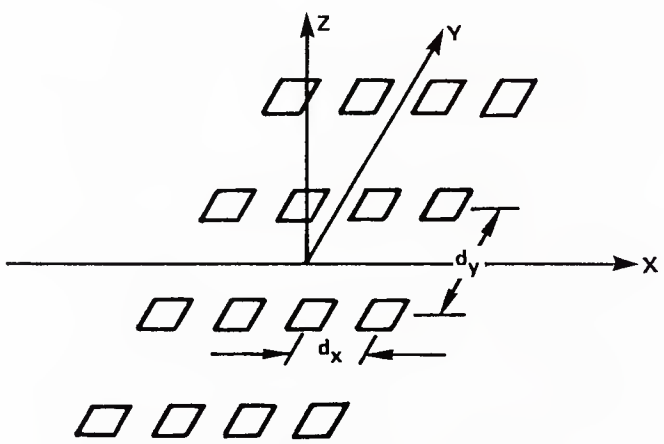

B. TWO DIMENSIONAL RECTANGULAR GRID ARRAY

FIG.4 ARRAY GEOMETRIES

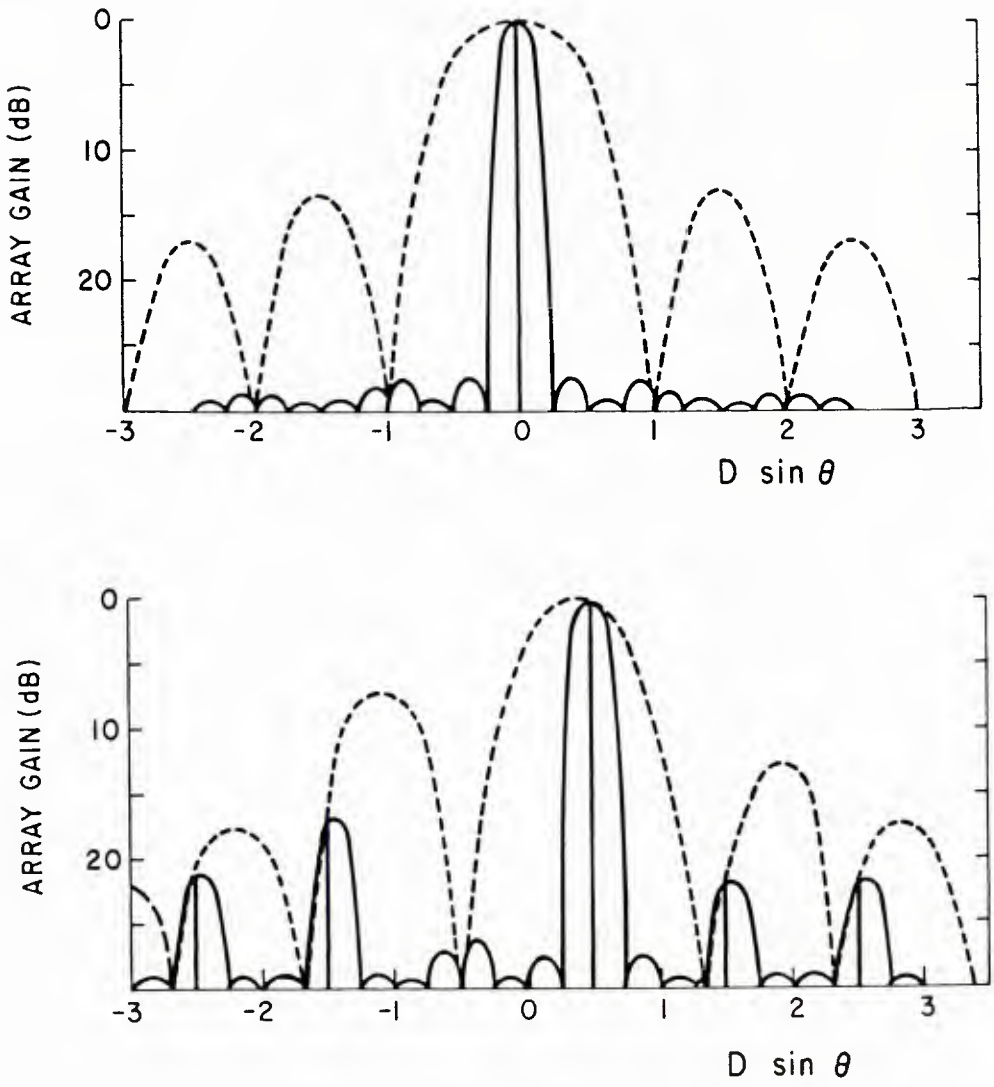

FIG.5 GRATING LOBE STRUCTURE FOR WIDELY SPACED ARRAYS

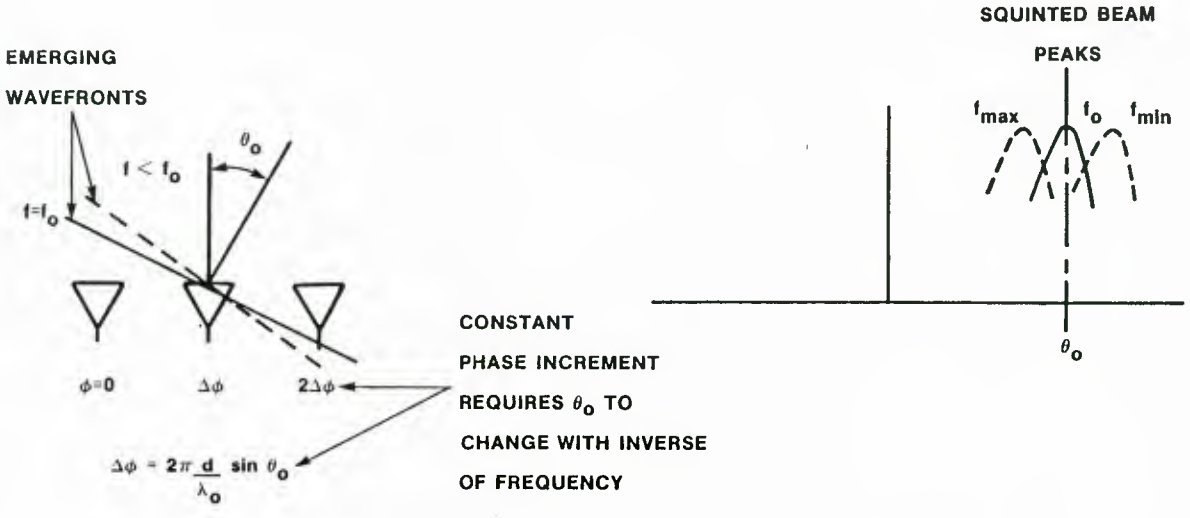

FIG.6 BEAM SQUINT IN PHASE STEERED ARRAY

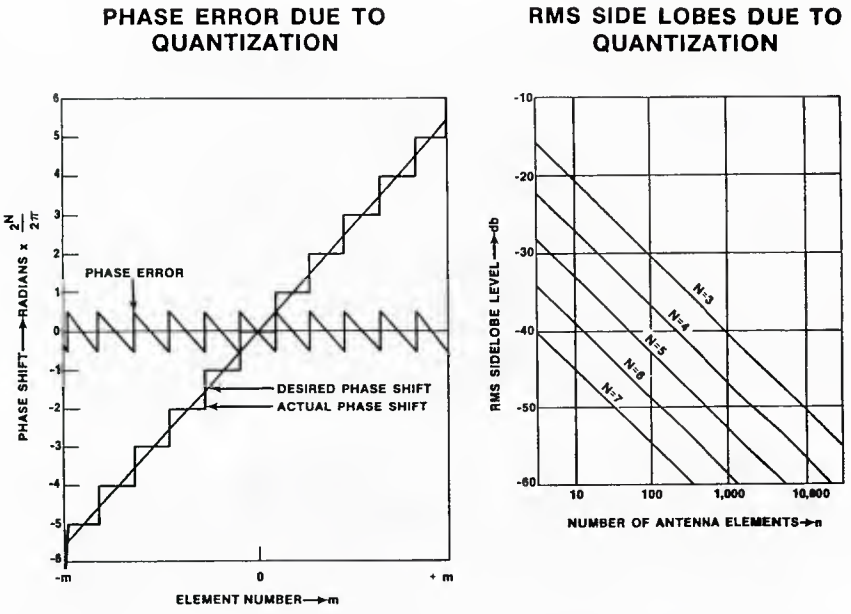

FIG.7 ILLUMINATION AND PATTERN ERRORS DUE TO PHASE QUANTIZATION

FIG.8 ELECTRONICALLY AGILE RADAR ARRAY (COURTESY OF WESTINGHOUSE CORPORATION)

FIG.9 ULTRA LOW SIDELOBE SEARCH RADAR ARRAY

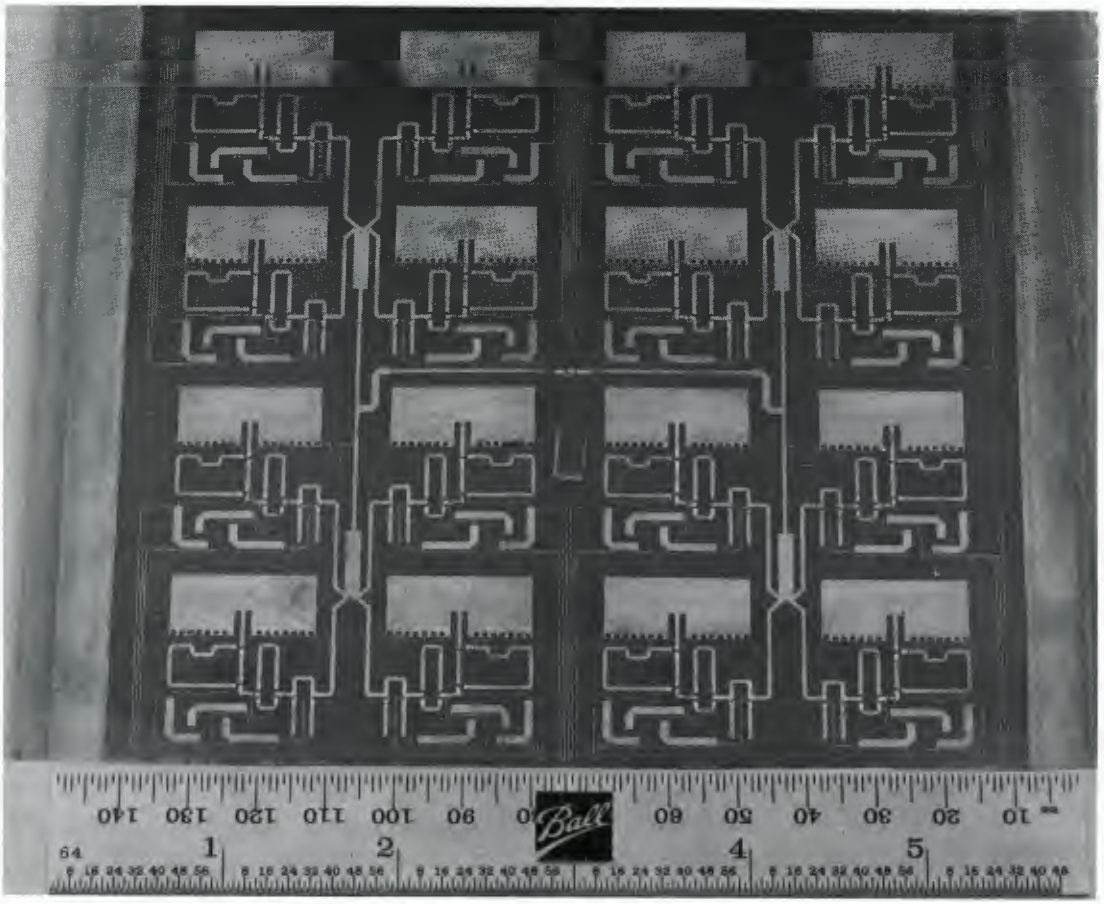

FIG.10 MICROSTRIP PATCH ARRAY
(COURTESY OF BALL AEROSPACE CO.)

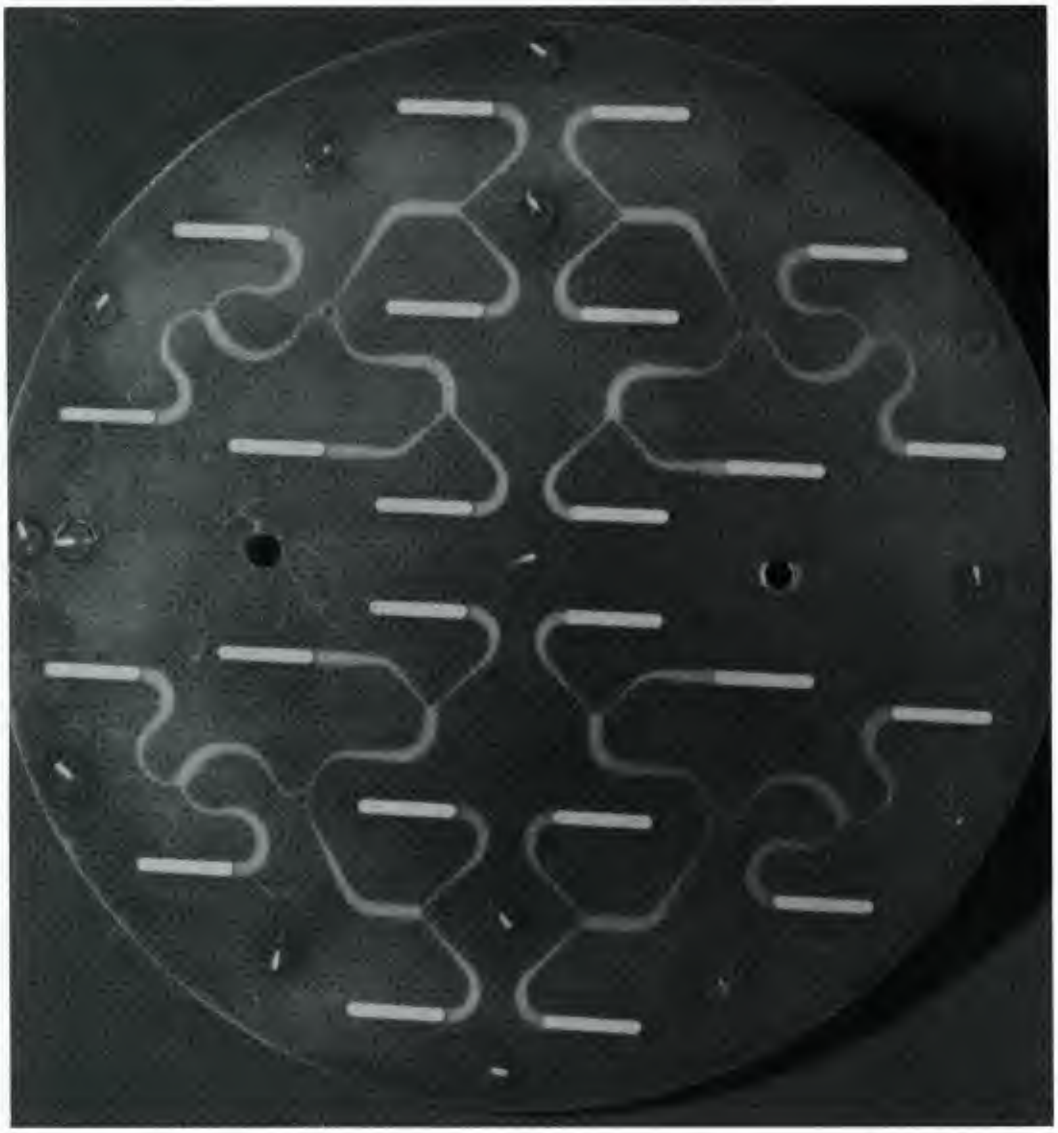

FIG. 11 PROXIMITY COUPLED MICROSTRIP DIPOLE ARRAY (COURTESY OF BALL AEROSPACE CO.)

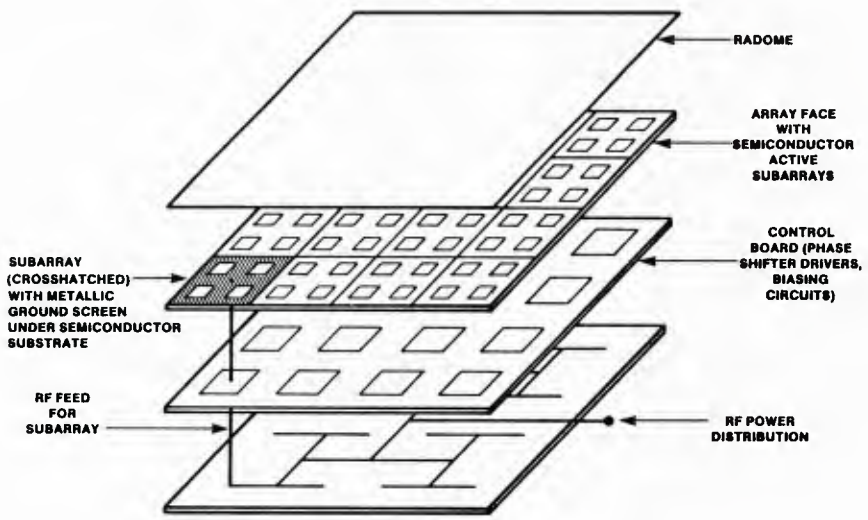

FIG. 12 MULTI LAYER CONSTRUCTION OF PRINTED CIRCUIT ARRAY

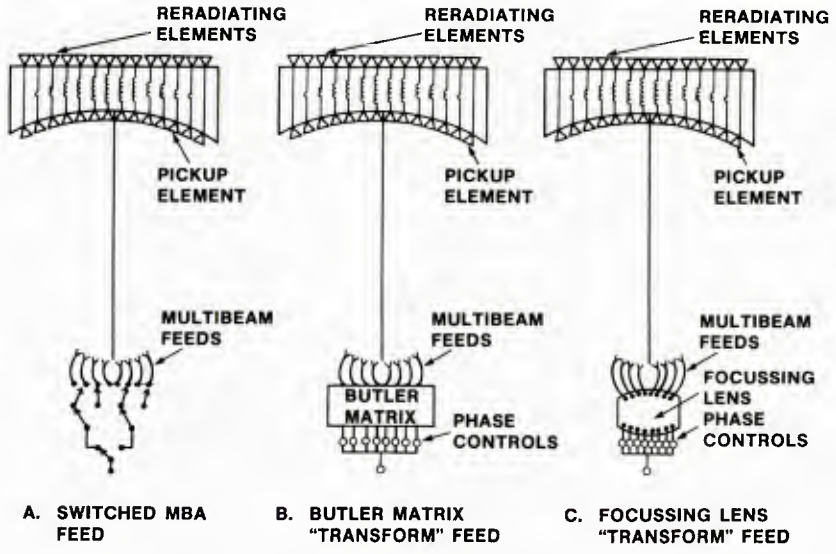

FIG. 13 ANTENNA CONCEPTS FOR LIMITED FIELD OF VIEW

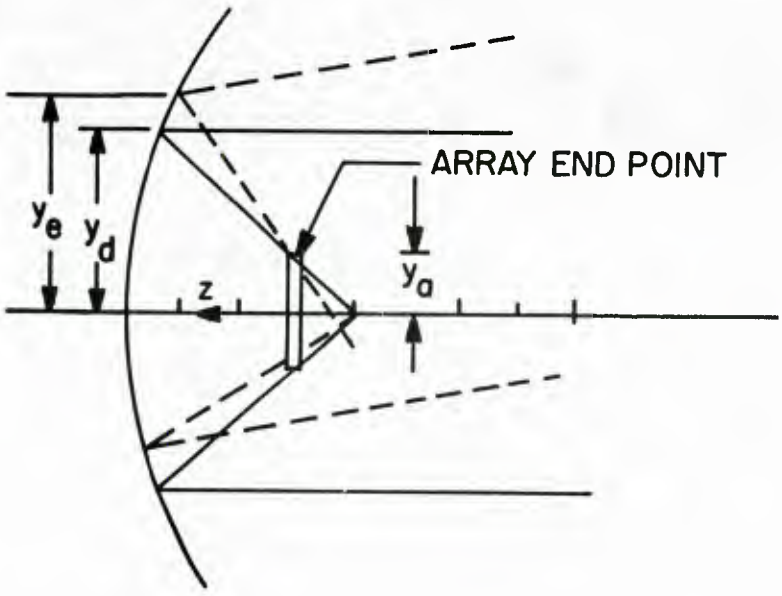

FIG. 14 REFLECTOR WITH ARRAY FEED

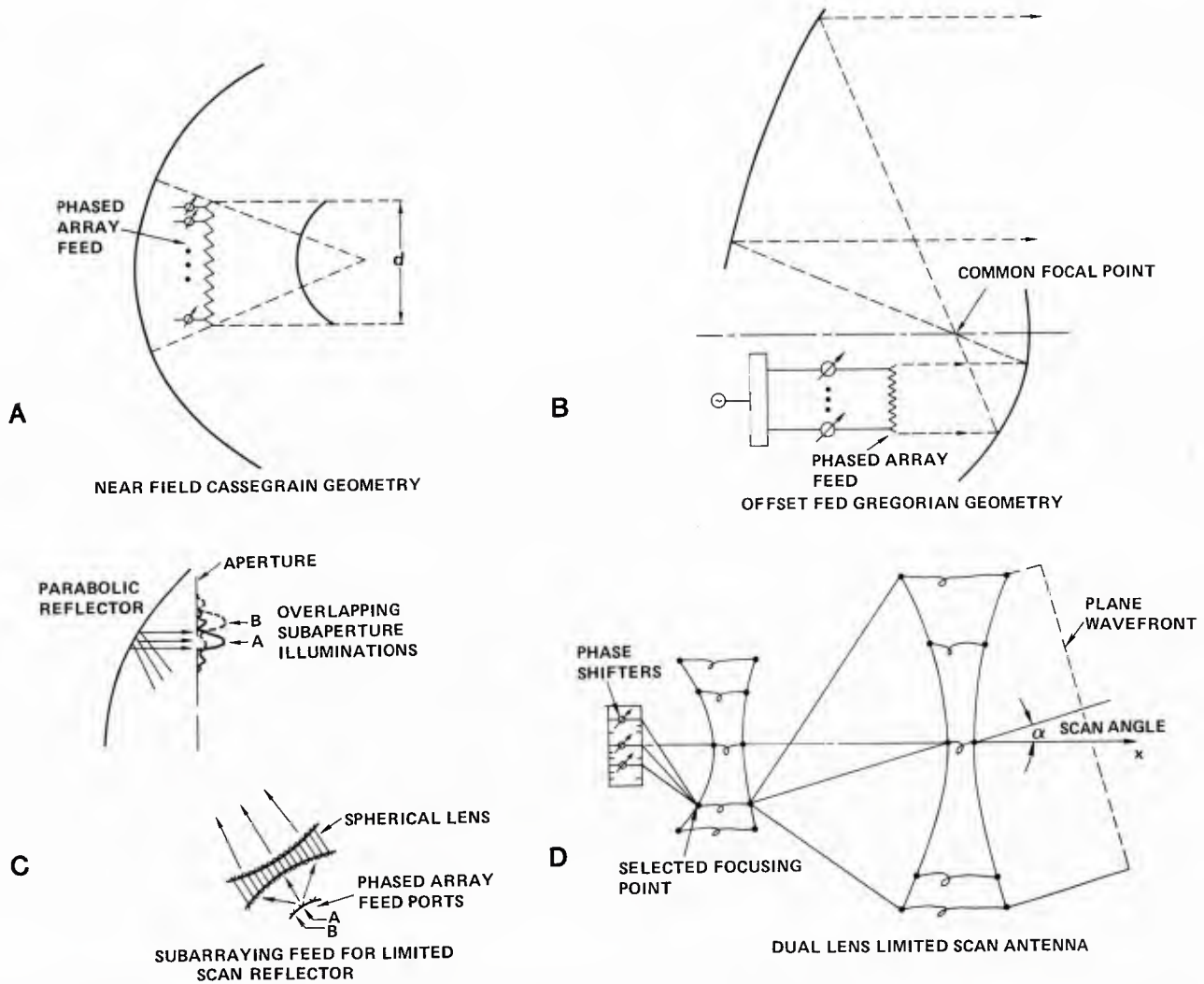

FIG. 15 ANTENNA CONFIGURATIONS FOR LIMITED FIELD OF VIEW ELECTRONIC SCANNING SYSTEMS

AIRCRAFT RADAR ANTENNAS

Helmut E. Schrank
Advisory Engineer - Antenna Development
Westinghouse Electric Corporation
Box 746, MS-55, Baltimore, MD 21203

SUMMARY

Many changes have taken place in airborne radar antennas since their beginnings over forty years ago. This lecture includes a brief historical overview of the advances in technology from mechanically scanned reflectors to modern multiple-function phased arrays. However, emphasis is not on history but on the "state-of-the-art" technology and trends for future airborne radar systems.

The status of rotating surveillance antennas is illustrated by the AN/APY-2 Airborne Warning and Control System (AWACS) slotted waveguide array, which achieved a significant breakthrough in sidelobe suppression. Gimballed flat-plate arrays in nose radomes are typified by the AN/APG-66 (F-16) antenna. Multifunction phased arrays are represented by the Electronically Agile Radar (EAR) antenna, which has achieved significant advances in performance versatility and reliability. Trends toward active aperture, adaptive, and digital beamforming arrays are briefly discussed. Antennas for future aircraft radar systems must provide multiple functions in less aperture space, and must perform more reliably.

HISTORICAL BACKGROUND

Radar technology had its beginnings in the mid-1930's (see "Radar in Retrospect" by T. Ival[1] and "Fifty Years of Radar" by M.I. Skolnik[2]) and by the mid-1940's aircraft radars were already in production. The first radars to fly operated at UHF and had fixed Yagi antennas mounted under the wing for search and navigation. The ASB-1 system was in operation by late 1941, but by 1946 higher frequencies were used to improve angular resolution. One of the earliest microwave airborne radars was the AN/APS-4, designed to provide carrier-based aircraft with high resolution search, navigation, and aircraft interception under conditions of fog and darkness. The entire radar was housed in a bomb-shaped container hung under the wing. It was an X-band (10 GHz) system with a 14.5 inch (37 cm) diameter paraboloidal "dish" antenna shown in figure 1. The antenna, typical of early aircraft radars, produced a pencil beam and was mechanically scanned to cover an azimuth sector of 150 degrees by an elevation sector of $\pm$30 degrees. Later airborne radars used larger apertures inside a nose radome to achieve higher gain with better angular resolution and accuracy, but basically the RF designs were all similar, using simple focal-fed paraboloids with waveguide feeds of various types.

While the RF designs remained relatively simple, the mechanisms for scanning the antenna developed in complexity. More powerful hydraulic systems replaced the earlier electric motor driven gear trains, and two-axis gimbal systems required waveguide rotary joints. When accurate target tracking became a requirement, conically-scanned feed mechanisms further complicated the mechanical designs until the monopulse technique replaced conical and sequential lobing. Figure 2 illustrates an airborne radar antenna of the late 1960's, the Westinghouse AN/APQ-120 radar used for target search and track as well as for weapon delivery. It operates at X-band and uses conical scan for tracking. It is typical of many similar radar antennas still in operational use.

SIDELOOKING RECONNAISSANCE ANTENNAS

Starting in the early 1950's and continuing into the 1960's, various airborne radars were designed for all-weather reconnaissance mapping purposes. These systems used fixed aperture reflector or array antennas mounted on the side of the aircraft fuselage (or on the side of a long pod) to form a fan beam aimed at the ground in a direction normal to the flight axis. Both real aperture and synthetic aperture systems were built, the former typified by the AN/APQ-56 radar (Ka-band) and the latter by the AN/APQ-97 radar (X-band), shown in figures 3 and 4, respectively. With these systems, (particularly the synthetic aperture type) extremely detailed radar maps can be made through clouds and/or at night, although not generally in real time because the signal processing was often done post flight. However, modern reconnaissance systems are capable of near real-time mapping in flight, as well as moving target enhancement by means of doppler processing.

SURVEILLANCE RADAR ANTENNAS

Another type of airborne antenna used in surveillance radar systems is the rotating antenna for 360 degree azimuth coverage. Some have been designed to operate in a belly radome under the aircraft fuselage, but this location severely limits the size of the antenna that can be used. More successful have been the top-mounted "rotodome" (rotating radome) antennas used in the E-2C (U.S. Navy) aircraft and in the E-3 (U.S. Air Force and NATO) Airborne Warning and Control System (AWACS). Figure 5 shows the NATO aircraft with the top-mounted 30 ft. (9.1m) diameter rotodome for long-range, 360 degree surveillance of high or low-flying aircraft as well as surface ships, providing an instant overview of more than 100,000 cubic miles (400,000 cubic Km). This S-band pulse doppler radar has achieved its successful high performance in large measure because of its unique phased array antenna shown in figure 6.

This S-band antenna represents a technology breakthrough in that it is the first production antenna to achieve ultralow sidelobes, which was necessary to reduce ground clutter. It is a planar array of over 4,000 waveguide slot radiators with an oval-shaped aperture approximately 25 ft. (7.6m) long by 5 ft. (1.5m) high. It produces a fan beam which can be electronically scanned in elevation while it is rotated mechanically in azimuth. This type of phased array is called a one-axis (or one-dimensional) phased array. The elevation scanning is done using precision ferrite phase shifters, especially developed for the AWACS program. These phase shifters are of the Fox (rotary field) type and have a phase accuracy of better than one degree RMS.

This AWACS radar was developed in the late 1960's and has been operational since 1972. Over 60 systems are operating around the globe, with an excellent reliability factor in addition to the high performance. NATO has 19 of these systems, which still out-perform any other airborne radar, including more recent designs.

GIMBALLED ARRAYS

The "flat-plate" slotted waveguide array antenna has largely replaced the parabolic dish antennas in modern nose-mounted airborne radars. This type of fixed-beam (not electronically scanned) array, when mechanically scanned in a two-axis gimbal mount, has many features superior to the parabolic dish antennas. First, it achieves higher aperture efficiency and lower sidelobes. Secondly, it can be made lighter with lower inertia and less swept volume than an equivalent dish antenna. Finally, it can be manufactured at lower cost.

Figure 7 shows the AN/APG-66 antenna in the nose of an F-16 fighter aircraft. This planar array of broadwall waveguide slots operates at X-band and produces a vertically polarized beam with low sidelobes. The array is fed in quadrants which provides sequential lobing on receive for tracking targets. It has low sidelobes and low cross-polarization even through the radome, which is carefully designed and manufactured to minimize reflection and distortion of the antenna pattern. The light-weight array antenna is precision machined (aluminum) using an automatic numerically-controlled milling machine.

The radar is used in several air-to-air and air-to-surface modes, including doppler beam sharpened mapping. Over 1500 systems are operational world-wide, and a field mean-flight-time-between-failures (MFTBF) in excess of 70 hours has been achieved. The highly reliable antenna contributed significantly to this achievement.

MULTIFUNCTION PHASED ARRAYS

The inertia of mechanically scanned antennas, whether dishes or flat-plate arrays, limits how rapidly they can be scanned. Even with more powerful servo drives and lower inertia antenna designs, the time came when mechanical scanning could not satisfy the ever-increasing requirements for tracking multiple, high velocity targets. To meet the new requirements, it was necessary to develop techniques for electronic beam scanning. Various techniques were investigated by many workers over the years, including switched beam arrays, frequency scanning, phase scanning, and combinations of these techniques. Experimental and prototype systems were built but they were generally bulky, heavy, and too expensive. Then in 1974, Westinghouse designed and built the Electronically Agile Radar (EAR) to demonstrate a cost-effective system with multimode performance for strategic missions. It is an X-band system with a two-axis electronically scanned phased array as illustrated in figure 8. This planar array of over 1800 closely-spaced radiators forms a low sidelobe pencil beam that can be rapidly scanned 60 degrees off broadside in any direction. The nominally circular aperture is 39 inches (1.0m) in diameter, and is fixed inside the precision nose radome.

The dielectric-filled circular waveguide radiating elements contain integral ferrite phase shifters as well as a polarizer for switching from linear to circular polarization for operation in rain. Figure 9 shows a typical phase control module. The elements are fed by a constrained waveguide manifold which provides a sum and two monopulse difference channels. The waveguide feed manifold uses half-height cross guide couplers to achieve a low sidelobe Taylor distribution.

This versatile and agile array, together with an advanced digital signal processor, provides a multifunction radar capable of high resolution Synthetic Aperture Radar (SAR) mapping, automatic terrain follow and avoidance (TF/TA), as well as the usual target detection and tracking. Extensive flight tests of the EAR system demonstrated not only successful performance but also high reliability and maintainability. Over a two-year test period, the few (less than 1 percent) phase shifter failures had almost negligible effect on system performance, due to the "graceful degradation" that represents one of the major advantages of phased array antennas. This technology is being applied to a number of other modern airborne radars.

TRENDS FOR FUTURE SYSTEMS

Future airborne radar systems will have challenging requirements to comply with new aircraft designs and ever-increasing operational demands. These challenges apply to the antenna designs as well as to the rest of the system. Modern military aircraft are designed for high speed and low radar observability. This rules out flat arrays behind large radomes, and instead dictates the use of conformal (non-planar) array antennas built into the aircraft structure. Because of space limitations on such aircraft, radars and their antennas must be capable of multiple functions as well as being able to adapt (in flight) to changes in the operational environment. The antennas must be agile, that is, they must be capable of rapid (electronic) beam scanning and beam shape modification for various functions. They must also be resistant to jamming, which dictates the need for low or ultralow sidelobes and low cross-polarization. Furthermore, they must be reliable and economically affordable.

These challenging requirements dictate the following trends in antenna designs currently under development, namely:

agile (implies electronically scanned arrays)
multifunction (often requires wide bandwidth)
adaptive (tends toward digital designs)
low-observable (the antenna must not increase the radar cross section (RCS) of the aircraft)
jam resistant (implies low sidelobes and low cross-pol)
reliable (tends toward active arrays)
cost-effective (implies automated manufacturing)

The need for high reliability leads antenna technology toward solid-state "active" phased arrays. In these, each radiating element contains its own RF power amplifier for transmitting as well as a low-noise amplifier (LNA) for receiving. In effect, this distributes the transmitter function over thousands of array elements instead of generating all the RF power in a single transmitter tube, such as a Klystron or travelling-wave tube source. This results in higher reliability because several elements can fail without seriously degrading radar performance, as compared to the catastrophic failure of a single tube transmitter.

Achieving these important goals can lead to the situation where the cost of the radar (and other avionics equipment) approaches 50 percent of the total fly-away cost, and the cost of antennas represents a large fraction of that cost. Therefore, it is important for the antenna designer to minimize the cost of manufacturing and testing the antenna as well as to provide all the necessary performance features.

To minimize the cost for high volume production of these transmit/receive (T/R) modules will require the insertion of monolithic microwave integrated circuits (MMICs). This technology, now emerging from the laboratories, combined with automated manufacturing methods will herald the beginning of a new generation of airborne radar antennas that promise the performance and reliability required for future systems.

CONCLUSION

This paper has given a brief historical review of airborne radar antenna development, described some typical operational designs, and presented an overview of the major trends toward future radar antennas. The emerging technologies will assure that the next generation of aircraft antennas will be quite different from any that are now operational.

REFERENCES

(1) T. Ival, "Radar in Retrospect", Electronics & Wireless World, August 1985

(2) M.I. Skolnik, "Fifty Years of Radar", Proc. IEEE, Vol. 73, No. 2, February 1985

(3) M.I. Skolnik, "Antenna Options in Radar Design", Microwave Journal, December 1983

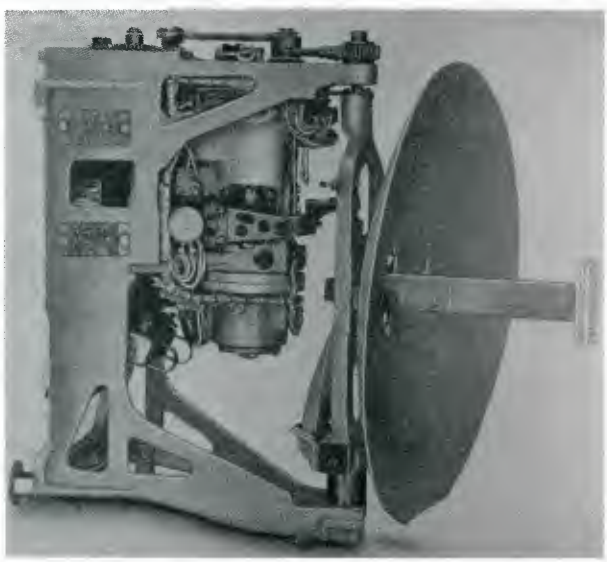

Figure 1. AN/APS-4 Radar Antenna (1944)

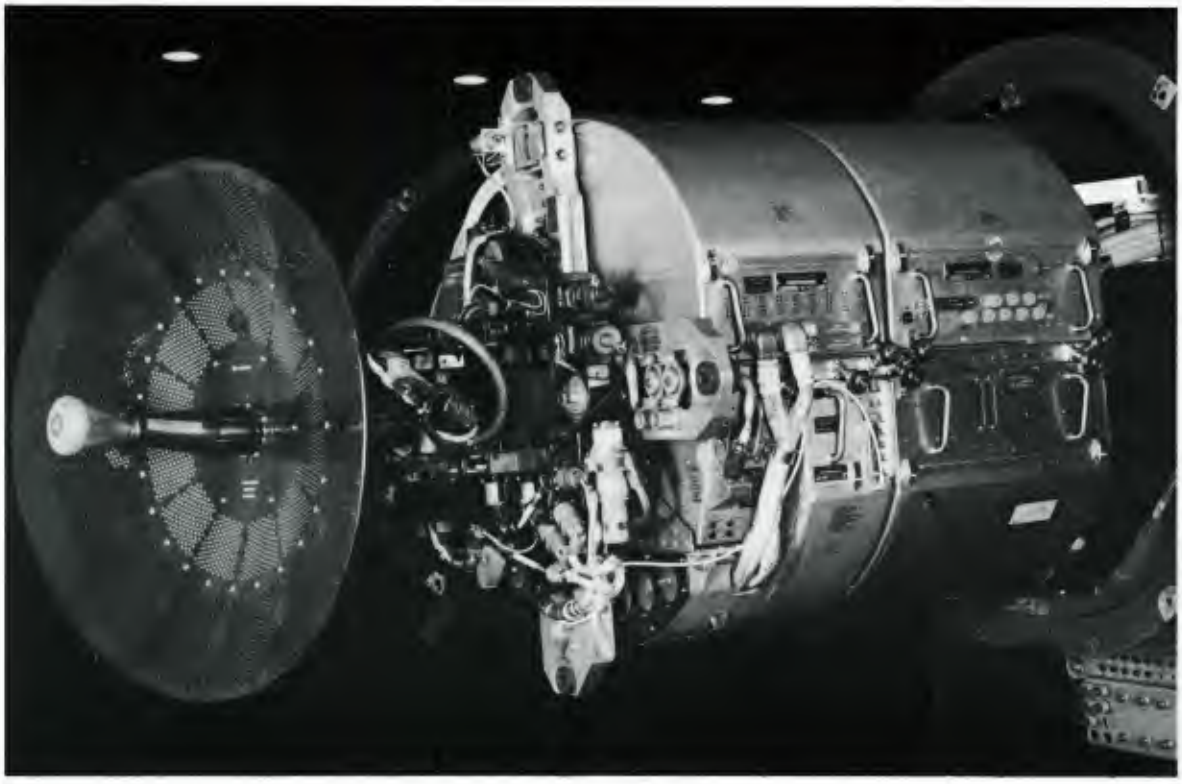

Figure 2. AN/APQ-120 Radar Antenna (1967)

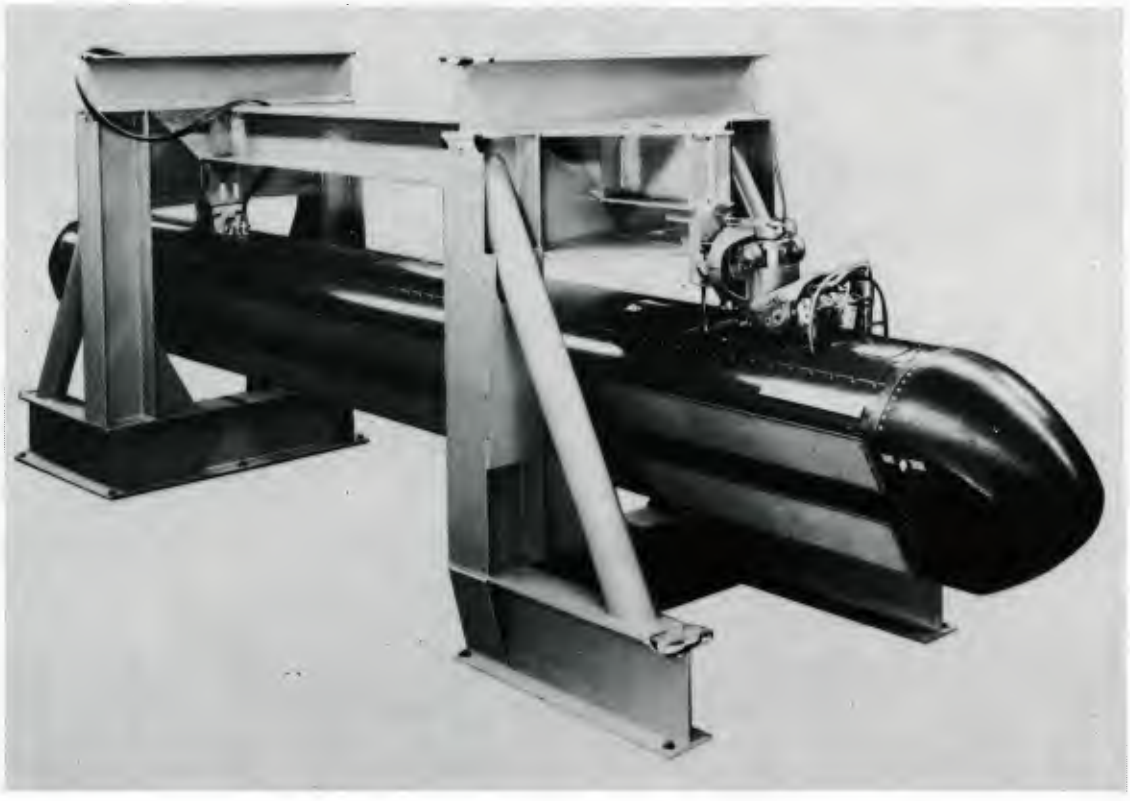

Figure 3. AN/APQ-56 Real Aperture Sidelooking Radar (1953)

Figure 4. AN/APQ-97 High Resolution Mapping Radar (1968)

Figure 5. NATO AWACS Aircraft (1982)

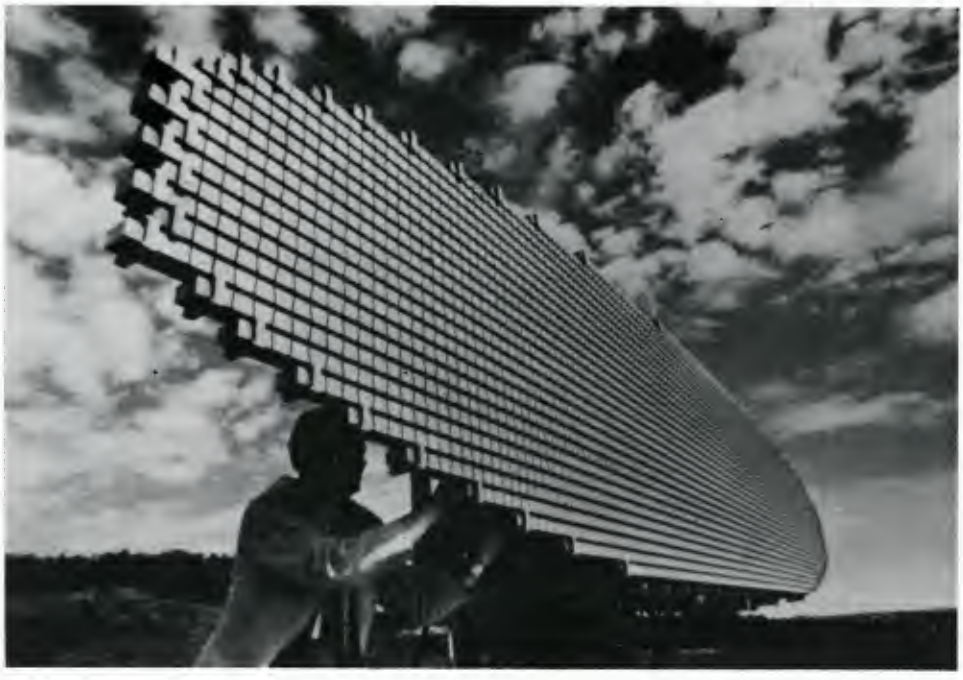

Figure 6. AWACS Slotted Waveguide Array Antenna (1975)

Figure 7. AN/APG-66 Radar Antenna (1975)

Figure 8. Electronically Agile Radar (EAR) Phased Array

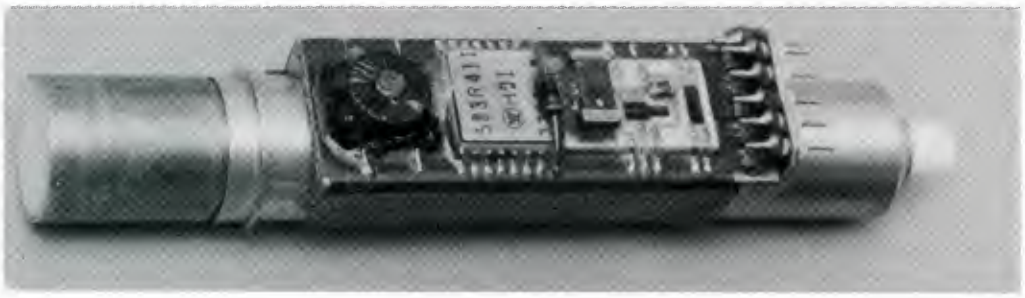

Figure 9. Phase Control Module - Radiating Element for EAR Array

AIRCRAFT ANTENNAS/CONFORMAL ANTENNAS
MISSILE ANTENNAS

by
Klaus Solbach
AEG, Radio & Radar Systems Division
Radar Subdivision A14 E101
D - 7900 Ulm
Germany

SUMMARY

The lecture covers three major areas of airborne microwave antennas, namely:

1) Missile conformal telemetry/telecommand and radar-fuze antennas
2) Missile and aircraft nose radar flatplate antennas and
3) Aircraft Electronic Warfare antennas.

In Section 1, the basic system environment for missile telemetry/telecommand and fuze functions is sketched and the basic antenna design together with practical examples are discussed.

In Section 2, the principle requirements of modern nose-radar flat plate antennas are shown to result from missile/aircraft system requirements.

Basic principles of slotted waveguide antenna arrays are sketched and practical antenna designs are discussed.

In Section 3, the present EW-system designs are sketched to point out requirements and performance of practical radar warning and jamming antennas (broadband spiral antennas and horn-radiators).

With respect to newer developments in the ECM scenario, some demonstrated and proposed antenna systems (lens-fed arrays, phased array, active array) are discussed.

1. CONFORMAL MISSILE ANTENNAS

In modern warfare missiles play important roles in attack and defence. An example mission is sketched in Fig. 1. Here, a surface-to-air missile is being fired against an air-target. During launch and during a good part of its travel (Fig. 1a) the missile keeps contact with the ground station to deliver status information (telemetry) and to receive course corrections (midcourse guidance). In order to maintain contact under any missile attitude relative to the ground station the missile employs an omni-directional antenna for its communication system.

The next phase of mission is depicted in Fig. 1b where the missile's own seeker takes over then guidance of the missile towards the target. Missiles can employ either active seeker heads (active radar with scanning antenna) or semi-active seeker heads (receive only with directional antennas) where the illumination of the targets is performed, e. g., by a ground based of airborne high-power slave illuminator. Basically, both types of seekers may use the same antenna technology as is used in fighter nose-radars. Many existing systems still use parabolic dish antennas on two-axis scannig mechanisms while later systems employ flatplate slotted array antennas. The terminal phase of the missiles mission is sketched in Fig. 1c. Here, the missile has sucessfully intercepted the target and crosses its track within only some meters.

In order that the missile's war-head is detonated at the best possible time a proximity-fuse system is used on board the missile. While optical sensors are often used for this application a microwave radar-fuze as known from ammunition and smaller

rockets is practical too. In this instance, an omni-directional (in roll-plane) antenna is needed with moderate gain into the forward direction. The return signals from the target are processed by the fuze radar processor and track-data concerning the relative motion of missile and target are extracted.

During the last phase the missile can report track-data to the ground station via its telemetry-antenna so that the probable outcome of the engagement may be assessed (kill assessment) even before the actual hit (or mishit).

Modern missiles can fly at extreme speeds (more than 3 Mach) which places priority on the aerodynamical characteristics of the missiles antennas. Some missiles use wing-mounted antennas, however, from the point of view of very low drag-effects but also with respect to the integrity of the missiles mechanical structure very thin antennas are desired wich can be wrapped around the cylindrical missile body (conformal antenna). These goals are nearly ideally attained by microstrip antennas on thin, fexible teflon-based substrates. These antennas are also quite inexpensive since they are manufactured in a standard printed circuit process. As will be shown in the following, both the radiating elements (patch) and the feed-structure (microstrip-line) are etched on the same surface of the copperclad substrate. The transmit/receive circuitry for the telemetry/telecomand or radar-fuze function can easily be placed inside the missile behind the wraparound antenna.

The radiating antenna surface can be protected against damage (weather, handling) by simply bonding another sheet of teflon-substrate to the antenna structure. This "Superstrate" creates a very low-loss and low profile radome for the antenna.

Before discussing omni-directional conformal missile antennas in detail a theoretical result concerning the realizability of ideal omnidirectional (isotropic) antennas in general shall be presented:

The term isotropic antenna basically means an omnidirectional antenna exhibiting radiation characteristics without any dependence on direction of radiation, neither in power density nor in polarisation. However, it has been shown /1/ that such an antenna is impossible. Either, such an antenna would have at least one null in its power pattern or it would exhibit all kinds of polarization over the radiation sphere; the latter have been called quasi-isotropic antennas. This result means that in a communication link with a quasi-isotropic radiator on one end the other end must use a polarization agile antenna (or a dual-polarization antenna if only receive is required). This problem does not arise in a fuze-system: here the omni-directional antenna may exhibit any polarization without serious loss of system gain, since hardly any practical target may exhibit extreme polarization dependence in its radar cross-section.

The first omni-directional conformal missile antenna was published by R. Munson /2/ in 1974. Fig. 2a shows its basic layout and physical attachment to a missile. The radiator used in this design is a broad patch (a ring when wrapped arround the missile) of half wavelength width. Currents flow under the patch in z-direction producing a standing wave field distribution in the substrate below the patch with equal phase fringing fields at the lower and upper patch ends (Fig. 2b). These fields can be assumed to be the sources of radiation in the antenna structure. The feed lines are designed in such a way that on the one hand the patch-radiator is excited with equal phase and amplitude along its periphery and on the other hand the input terminal leading to the transmit/receive circuit inside the missile is matched to a given impedance.

As the sketch of the radiating fringing field lines indicate, this antenna radiates only a single polarization. Thus, two nulls occure in the radiation pattern.

The nulls are located in the +/- z-direction and are due to the symmetry of the radiator, since in the z-axis direction all contributions of radiation from the circular radiator must superimpose distructively. In the roll-plane (x-y-plane), however, the radiation, ideally, is isotropic. Over the radiation sphere, the polarization of this antenna maintains the ϑ -direction.

A measured radiation pattern of such an antenna is given in Fig. 3, showing the deep null for the axial direction and the low ripple omni-directional property in the roll-plane.

Most practicle missile telemetry/command antennas are based on the original design, but the principle antenna structure was rigorously analyzed only recently in a paper by J. Ashkenazy et. al. /3/. It is shown that the null-width depends on the dielectric constant and thickness of the substate and gets narrower as the diameter of the cylinder (missile) increases. Fig. 4 presents some of their results; it is seen that the axial null width is reduced to very small values by use of thick dielectric substrates, rather than air-filled substrates of low dielectric constants (e. g. honeycomb).

For most practical cases of telemetry/telecommand systems the limiting factor will be the fraction of area on the radiation sphere over which the missile antenna pattern falls below a certain system-threshold value, e. g. - 10 dB_i. Since the axial null normally will be very narrow, the fractional area will be on the order of less than 1 %, i. e. the probability of system fade-out due to a pattern null is extremly low with this simple antenna design.

This argument deos not hold in a system where the axial direction of radiation has special significance. This is certainly so in the radar fuze system, where the head-on direction of intercept is the desired situation and a pattern null would possibly render the system blind.

The requirements for the fuze-antenna get even more difficult since, ideally, the antenna should exhibit an isotropic pattern only in the foreward half space while the back radiation should be suppressed. This would increase the antenna gain in the target direction and reduce possible clutter from an area without targets (back half space).

A solution to this antenna problem has to incorporate radiation elements of two orthogonal polarizations in order to avoid the null-condition experienced in single-polarization omni-directional antennas. Using the microstrip/patch-radiator technology many approaches may be taken, with one example shown in Fig. 5. Here a patch radiator with only quarter-wave width is short-circuited at one end. The effective sources of radiation are the fringing fields at the periphery of the patch showing x- and y-direction. A quasi-isotropic wraparound antenna can be constructed using this type of radiator in such a way that the pattern-null for one polarization can be filled up by radiation of the other polarization. Across the radiation sphere the polarization will vary between both polarziations going through clean linear states and all sorts of eliptical polarization.

A measured radiation pattern for such an antenna is shown in Fig. 6. In the measurement, the transmitting horn was rotated continually to change its direction of polarization, while the antenna under test was slowly rotated around its measurement axis. This leads to strongly oscillating pattern plots where the antenna is near-lineary polarized and constant plots where the antenna is near-circularly polarized.

It is seen that a null is avoided in the cylinder axis; gain in the forward direction is achieved by arraying two radiator elements in the axial direction, as is seen in Fig. 7. The gain into the foreward direction is accompanied by a reduction in the back direction which is similar as in conventional end-fire array antennas.

Antennas of the type described above for telemetry/telecommand and radar-fuze applications operate usually at L- to S-band frequencies (1 - 4 GHz) in narrow bands only a few MHz wide. For air-to-air or air-to-ground missiles often use is made of the aircraft radar to communicate with the missile, thus X-band frequencies are employed. Using dielectric substrates of 1 to 2 mm thickness such bands can be easily covered. Since the antennas cannot easily be frequency-tuned, in practice, the antennas have to be designed for considerably higher bandwidth in order to allow for the normal tolerances in dielectric constant/thickness encountered in the substrate materials. Wider bandwidth requirements, however, mainly create impedance match problems with the radiators which can be overcome only by developing new broad-band radiating elements and reactance compensating feed circuits.

In the future, apart from larger bandwidth, these systems may also require some form of electronic beam-switching or phased array properties. Such requirements would certainly be well within the present technological limits, but so far no major development has been pushed into this direction.

2. NOSE RADAR ANTENNAS (MISSILE & AIRCRAFT)

As mentioned in Section I, missiles often employ active/semi-active seeker heads with highly directive antennas to search and track their targets. Aircraft on the other hand carry nose radar systems for many more functions (multi-mode, multi-function) but use very similar antennas for these radars. As an example, Fig. 8 sketches some of the radar modes of a modern fighter aircraft. The spectrum of radar modes, and thus also the performance goals of the antennas, differ slightly depending on the aircrafts' missions but, generally, the antennas are required to yield simultaneously high gain, low sidelobes, high power-handling and monopulse capabilities. The antennas are mounted to two-dimensional scanning mechanisms (gimbal) which provide fast and accurate motion of the antennas over wide angular sectors (up to +/- 70° in both planes). Either electrical or hydraulical motors are used to drive the antennas and servo-to-digital interfaces connect the gimbal to the radar computer.

Differences of missile seeker antennas and aircraft nose radar antennas originate mainly from the different airframe size and radar concept: In a missile the nose diameter typically is smaller than in an aircraft and the system cost aspect leads to a cheaper high-peak power pulse radar (employing e. g. a magnetron transmitter of several tens of kW peak) for the missile as compared to the more flexible high mean-power multi-mode/multi-PRF pulsedoppler radars in modern military aircraft. This mainly leads to higher stress on the far-off sidelobe level and the r. m. s. level in aircraft antennas as compared to missile antennas. The low r.m.s. level requirement basically is caused by the medium PRF-modes (clutter limited system) of the aircraft radars. In both cases, however, the ultimate sidelobe performance of the antennas still is determined by the degradations through the conical radoms used in most cases. In high performance pulse doppler nose radars a radom which contains a pitot boom including the necessary connections and lighthing protection is not acceptable.

Missile and aircraft nose radars today operate in the X- to Ku-band frequency range with aircraft radar tending towards X-band frequencies (wider radar range in bad weather) and missile radar tending towards higher frequencies (low beamwidth with relatively small diameter). Antenna sizes (aperture diameter) range from more then 90 cm (fighter aircraft) to below 20 cm (smaller missiles), with typical beamwidths ranging from 1.5° to several degrees. Certain recent missile developments tend towards mm-wave active seeker technology which will push flat plate antenna technology well into the 35 GHz region.

Older nose radars still use parabolic dishes for the antenna, while most later nose radars employ flat plate antennas (slotted waveguide array). The reasons for this transition of technology have been the considerable improvement of the sidelobe level yielded by flat plate antennas over the conventional parabolic dish (there is no "spill-over" and no "blocking"-effect in slotted array antennas), the lower inertial moment and the freedom to realize optimized (e. g. maximum gain/minimum sidelobe level) aperture distributions in waveguide slot array antennas. However, this change has resulted in a drastic reduction in antenna bandwidth: While the dish antenna is limited in bandwidth only by the feed-horn characteristics and the monopulse-comparator, the slotted array antenna is a narrow-band resonant structure where the bandwidth decreases with increasing number of slots excited by each waveguide-section. Since the number of waveguides cannot be increased without increasing the complexity of the corporate feed network most practical flat plate antennas used in modern nose radars trade bandwidth against complexity (and cost) and thus exhibit only some few % bandwidth.

To allow these issues to be discussed more detailed, in the following, a short description of the design and manufacture of contemporary nose radar flat plate antennas is given.

Principally, slotted waveguide arrays may employ slots in the narrow wall as well as slots in the waveguide broadwall. Slots in the broad wall, as sketched in Fig. 9, are perferred, however, for two reasons: First, these slots have all the same inclination, which reduces the cross-polarized radiation to very low values (The cross-polarization pattern is most important for the monopulse accuracy and jammer rejection). Second, slots in the broad wall allow a very flat antenna design where the waveguide height may be reduced to far below a quarter wavelenght (The thickness of the antenna is most important for the over-all antenna weight which should be as low as possible to allow fast scanning). The slots in the waveguide walls are fed by the propagating modes inside the waveguides (transmitting antenna). Either travelling waves or standing waves may be employed, but the resonant (standing wave) excitation is preferred for two reasons: First, the travelling wave excitation produces a beam squint with frequency ("frequency scanning") while the resonant excitation produces a boresight beam across the complete frequency band. Second, in a travelling wave feed the incident power cannot be radiated completely since the waveguide is terminated in a matched load in order to suppress reflected waves. The resonant feed, on the other hand, uses the reflected wave from a short-circuit termination to radiate the incident power completely. The resonant array thus has a very high radiation efficiency which is most important with respect to the limited power resources in an airborne system.

As is implied by the term resonant array this type of antenna structure is narrow-band by its nature: While radiating slots can be used over bandwidths far above 10% (depending on the slot width-to-length ratio) the arraying of many slots in a standing wave feed waveguide creates a narrow-band structure with bandwidth decreasing proportional to increasing number of slots. A rough estimate could be e. g. a 5 % bandwidth for a 10-slot array (The frequency sensitivity of the resonant slot array is seen in an impedance mismatch at the feeding point and also in a deteriorating radiation pattern). Depending on the size of the antenna and the required bandwidth several tens to some hundreds of sub-arrays (resonant slotted waveguides) have to be employed. In order to feed these sub-array waveguides, a corporate feed network usually is totally impractical since it would have to split into so many exit ports. To relief this situation several sub-array waveguides can be fed through one external feed waveguide using standing wave excitation of coupling slots as sketched in Fig. 10. Here, a group of four sub-array waveguides, each containing four radiating slots are crossed by a feed waveguide, containing four slots, which couple to the subarray waveguides. This resulting slot module can again be fed by e. g. a single slot in the crossing feed waveguide (not shown in Fig. 10) or by feeding one of the ends of the

feeding waveguide. The latter choice was employed in the example antenna shown in Fig. 11, where the seven subarray waveguides of each quadrant are fed by one crossing feed waveguide; the ends of the four feed waveguides are bent to the array back to be excited by a monopulse comparator. The concept realized in the example antenna is only possible for relatively small and narrow-band antennas; it has to be noted that the additional resonant feed element (crossing waveguide) additionally reduces the bandwidth of the antenna. Thus, normally, the modules are fed by a corporate feed network which has to split into a few up to some 10 ports per antenna quadrant. Depending on the degree of division (a tree-like structure is normally employed) this can easily be realized using a discrete waveguide network containing straight and curved waveguides and matched (e. g. "magic tee") power splitters or reactive (unmatched) dividers. In order not to further reduce the antenna bandwidth the corporate feed has to maintain equal path length to all output ports. The antenna aperture amplitude and phase distribution are very critically dependent on the divider-ratios and effective path length balance realized with the corporate feed. The same is true for the monopulse comparator used to feed the four quadrants of the antenna. To achieve the required accuracy, there may be the need for tuning devices within the network.

With the modern trend towards low sidelobe antennas (first sidelobes and r.m.s.-sidelobes) theoretical design tools (CAD) and precision manufacturing employing CNC-machines have gained supreme importance. Early slotted waveguide arrays were designed using first- and second-order approximations for the fields inside the waveguides and across the radiating slots /e.g. 4 - 6/. The latest analytical models, however, now include nearly all of the effects encountered in practical antennas, like coupling from slot-to-slot outside and inside the waveguide, finite thickness of slotted plate, low height of the waveguides and large slot width-to-length ratio /7/ (still not included are diffraction effects at the array edges). Thus, using modern theory the required slot geometries can be reliably calculated to extreme accuracies on the order of µm which is more than the 10 ... 20 µm accuracy achieved in production programs employing CNC machines.

The achieved accuracy in the fabrication of the slotted plate, waveguides and feed network determines the degree to which the theoretical radiation-pattern is approached in the practical antenna; basically, systematic errors (e. g. symmetry errors) lead to higher near-in sidelobes while random variations (e. g. slot displacement variations) lead to increasing r.m.s.-sidelobe levels.

In modern slotted waveguide arrays high fabrication accuracies are supported by designing the antenna to consist of several flat plates sandwiched together, rather than consisting of many individual slotted waveguides bonded together, as was the case in Fig. 11. In this way optimum use can be made of the inherent accuracies of CNC-milling machines in the realization of the critical geometries. The principle construction method can be seen in the example antenna shown in Fig. 12. Here, the radiating slots are all milled in one single sheet of aluminum covering a double-sided waveguide plate. The waveguide plate contains all sub-array waveguides (feeding the radiating slots) on one side and all crossing feed waveguides on the other side; the coupling slots are produced as slots through this plate connecting sub-array waveguides and feed-waveguides. Also, the next level of power distibution (corporate feed) employs four milled waveguide structures for superior accuracy and reproducibility. In the example antenna the only conventional, soldered waveguide assembly is the monopulse comparator which consequently contains fine-tuning devices to compensate manufacturing tolerances. It is, however, feasible to use precision milling techniques for the realization of an equivalent comparator as is shown in Fig. 13. Here, four 3 dB short-slot hybrid couplers are milled together with connecting waveguides and phase compensating waveguide sections. The lower waveguide part and the upper cover plate are brazed together to form a highly reproduceable low-weight and low profile component.

These manufacturing techniques can be employed for other materials as well. For example, magnesium can be used in stead of aluminium for its lower specific weight. Recently, also metallized carbon fibre reinforced plastic was used to produce extra low weight slotted waveguide arrays /8/ but this material cannnot be processed in the same manner as metals. Due to greater wall thickness, weight reductions in carbon fibre based antennas are not as large as the reduction in the specific weight of carbon fibre versus magnesium promises.

Today, there is a trend back to higher system-bandwidths (ECCM improvement) which will have to be followed by the designers of flat plate antennas. The problems posed by broader-band resonant array antennas lie mainly in the construction and fabrication of the feeding networks, but modern CAD and precision manufacturing techniques will allow next generation flat plate antennas approaching the 10 % bandwidth order. This may, e. g., lead to highly complex corporate feed structures with waveguides milled into both sides of a metal plate, similar as the waveguide plate in Fig. 12. Also, more use of matched power dividers may be made in contrast to the present use of reactive divider sections.

If a nose radar system employs several modes demanding different beam shapes (e. g. pencil beam for ground mapping or air-to air modes and "spoiled" beam for terrain avoidance mode, see Fig. 8) either more than a single antenna may be used with each antenna optimized to one requirement, or one antenna can be used with integrated switches to change the power/phase distribution appropriate to each required beam shape.

If, on the other band, variable polarization is required there is no solution available besides the well-known polarizer grating structure which could be mounted in front of the array surface on a rotating mechanism. For acceptable speeds of the polarization changer the mechanism would, however, be to heavy to be fitted to the lightweight antenna/gimbal unit.

Some recent nose radar concepts require the IFF-antenna to be integrated with the primary radar antenna for radar-controlled interrogation etc.

There are two ways to achieve such an integrated IFF-antenna in a flat plate nose radar antenna: First, IFF-radiators (e.g. dipoles) can be arranged around the periphery of the slot-array in such a way that neither the antenna-to-radome spacing is reduced nor the primary radar antenna pattern is disturbed to an appreciable degree. Such an array of IFF-radiators will naturally be limited to a small number of elements and thus give only a small gain.

The other method for integrated IFF-antennas has only recently been developed /9/ and employs a dielectric/metal-strip grating structure sandwiched to the slot array surface. The grating structure is used to create a planar patch-radiator array for the IFF-frequency very similar to a microstrip antenna array. This structure may cover the complete slot antenna surface without seriously degrading the primary antenna performance since the structure is transparent ("invisible") at the primary radar frequency.

Just how far this new concept can be used in contemporary very-low-sidelobe flat plate antennas cannot be judged at this time since no full scale antenna development has used it so far.

Many of the mechanically scanned antennas for airborne radar may, in the future, be replaced by electronic scanned arrays, either passive (Phased Array) or active (Active Modules); this technology is discussed in another lecture.

Also, for certain low power, smaller diameter antennas printed circuit technology can be employed (microstrip etc.) rather than waveguide technology; this topic also is discussed in another lecture.

3. EW-ANTENNAS

Microwave EW-antennas are found basically in radar (threat) - warning receiving systems and radar jamming systems. These systems employ several isolated antennas or many antennas grouped in arrays or even several arrays, depending on the type and size of aircraft. E. g., Electronic Combat aircraft and stand-off jammer aircraft may carry high-power transmitters and high-directivity array antennas, while common fighter aircraft employ smaller power, lower gain jamming systems for self-defence only. In Fig. 14, a traditional fighter aircraft situation is shown, where the aircraft detects and analyzes hostile radar illumination mainly by its radar warning system. The ECM-system receives and retransmits the hostile radar signal or uses other jamming techniques for its transmission.

The radar warning system traditionally has been incorporated in the airframe with several small broadband antennas distributed over the wings or fins. Here, mostly spiral antennas of the type shown in Fig. 15 are used for their low volume, broad beamwidth and broad bandwidth. E.g., a typical spiral antenna exhibits 2 - 18 GHz or 6 - 18 GHz bandwidth with a constant broadside beamwidth of $\pm$ 40° in both principle planses. In these systems circular polarization is employed to cover all possible linear polarizations transmitted by hostile radar. In practice, the radiation pattern of a typical spiral antenna as shown in Fig. 16 can exhibit axial ratios of several dB over the beamwidth sector and over the frequency range.

With the increasing operating frequencies of threat radars (especially missile seekers) modern radar warning systems will have to cover at least up to 40 GHz which is hardly a problem with contemporary antenna technology.

Jamming systems are carried either as a pod under the aircraft's wing or as an integral part of the airframe. The latter solution is often desired by the EW-System designer since, in principle, optimum configuration of the antennas can be achieved; on the other hand, antenna placement on the airframe competes with other requirements and to a certain degree limits the airframe designer. The podding of ECM systems in many cases has been perferred because these systems can be mounted to the airplane only if mission requires it and can be repaired and even changed/upgraded more easily than aircraft integrated systems.

In present ECM-pods mostly broadband horn antennas are employed to receive hostile radar illumination and to transmit jamming power either coherently or incoherently. Typically, several horn antennas are mounted at the extremities of the pod in order to cover the fwd and aft azimuth sectors. The horns can be either switched to one or more transmit-amplifiers/receivers or each be driven by its own transmitter to achieve higher jamming power. In such systems e.g. four horns of $\pm$ 60° az-beamwidth are employed with elevation beamwidth on the order of $\pm$ 20°. A typical horn design is shown in Fig. 17: As in most ECM-horn designs this horn is fed by an input section with 45° twist-angle in order to split the waveguide mode into two orthogonal waves. The basic horn structure is strongly modified by the addition of several pieces of dielectric material of peculiar shape, which serve to balance the two orthogonal modes with 90° phase quadrature (circular polarization). A typical radiation characteristic is given in Fig. 18. It is seen that the pattern is very broad and that axial ratios of better than 3 dB are achieved over the full half-power-beamwidth. Horns of this type can be designed to operate over bands of 2 -3 octaves and can handle the 100 ... 200 W-CW-

power levels achievable with modern broadband TWT-amplifiers (pulsed power up to kW-level).

With the recent improvements of hostile radar technology especially in the field of ECCM-capabilities, and with other changes in the expected ECM scenario, new EW-systems are generally required to exhibit an order of magnitude higher Effective Radiated Power (ERP). While self protection jammers are required to produce 1 - 10 kW, stand-off and escort jammers may go well into the MW region. Taking into consideration the limited resources in an aircraft, it is obvious that there is no chance of achieving this goal by simply adding more transmitter-tubes. Instead, it has generally been accepted that the gain of the jammer antenna system has to be increased drastically while the produced RF-power is changed only little.

While a higher gain antenna increases ERP, it also reduces coverage due to the narrower beam. It thus turns out that in order to cover the usually required 120° fwd and aft angular sector in azimuth there is a need for either multi-beam capability or electronic beam scanning Consequently, many different antenna systems so far have been designed, tested and introduced exploiting either lens-fed radiator-arrays /10/ or conventional phased array technology /11/. Conceptual designs exist for extremely high ERP-Systems using large arrays of active modules distributed over large parts of the aircraft skin.

The basic design of a lens-array antenna system of the Rotman type /12/ is shown in Fig. 19. The lens has several beam-ports (1 - 7) which collect power from all connected array elements. In the figure, two distinct waves are shown incident to the antenna where in each case the full gain of the array is utilized for the output power at the corresponding beam-ports. A practical antenna assembly using a Rotman-lens connected to broadband horn radiators is shown in Fig. 20.

The shown antenna design can be used as reception array to locate a victim radar by either switching a single or several receivers to the output-ports in order to observe the beam-sectors simultaneously. Equally, a single transmitter could be switched to the appropriate beam-port in the transmit mode but usually the design is extended to include a separate transmitter behind each array element. Here, smaller tubes ("Mini TWT") are employed, producing power on the order of 40 W per tube. Thus, relatively small arrays can produce more power than an ordinary single high-power tube with much better reliability (graceful degradation). The principle Rotman lens-array is capable of beam-forming in one plane only.

Thus, either the radiating elements have to exhibit relatively broad coverage in the orthogonal plane (elevation) or a more complex two-dimensional lens-array structure has to be used with beams formed in both dimensions.

Circular polarization usually is achieved by placing a polarizer (strip or meander) in front of the antenna array. Bandwidths achieved for operationable systems seems to be slightly less than what can be achieved with broadband horn radiators. Dimensions (e.g. length of array) naturally are much larger than dimenions of single horn radiators, thus it is difficult to integrate the system in a relatively narrow pod environment. At least for higher numbers of beam-ports (or radiating elements) these antenna systems have to be integrated into the airframe, e.g. the wings or fins.

The other current alternative for high-ERP ECM systems employs the well-known phased-array principle, as discussed in another lecture. This leads to more complex systems but with the advantage of easy scanning in both principle planes. This approach has drawn considerable attention recently due to the development of solid state active array modules /13/. The resulting systems promise high ERP at low cost/low volume with

the added advantage of very high reliability. Polarization agility, too, will be more easily achieved in such arrays than in multi-beam antennas.

REFERENCES

/1/ H.F. Mathis, "A Short Proof, That An Isotropic Antenna Is Impossible", Proc. IRE 39, August 1951, p. 970

/2/ R. E. Munson, "Conformal Microstrip Antennas and Microstrip Phased Arrays", IEEE Trans. Antennas & Propagation, January 1974, pp. 74 - 78

/3/ J. Ashkenazy et al., "Electric Surface Current Model for the Analysis of Microstrip Antennas on Cylindrical Bodies", IEEE Trans. Antennas & Propagation, March 1985, pp. 295 - 300

/4/ S. Silver, Editor, "Microwave Antenna Theory and Design", Rad. Lab. Series, MC Graw-Hill Book Company, 1949

/5/ R. C. Hansen, Editor, "Microwave Scanning Antennas", vol. 2, Academic Press, 1966

/6/ R. S. Elliot, "Antenna Theory and Design", Englewood Cliffs, NJ, Prentice-Hall, 1981

/7/ R. S. Elliot, W. R O'Loughlin, "The Design of Slot Arrays Including Internal Mutual Coupling", IEEE Trans. Ant. & Prop. 1986, 1149 - 1154

/8/ S. Brunzell. H. Magnusson, "Lightweight CFRP Waveguide Array", MM 1984, Proceedings 305 - 309

/9/ M. Shelly, K. Bond, "Invisible antenna takes up less space", Microwaves & RF, June 1986, 93 - 95

/10/ D.H. Archer, A.A. Black, "Higher ERP with lens fed multibeam Arrays", Journal of Electronic Defence, March 1982, 51 - 59

/11/ M. Simpson, "High ERP Phased Array ECM Systems", JOED, March 1982, 41 - 49

/12/ D.H. Archer, "Lens-fed multiple beam arrays", Microwave Journal, Sept. 1984, 171 - 195

/13/ J. L. Armitage, "Electronic warfare solid-state phased array", Microwave Journal, Febr. 1986, 109 - 122

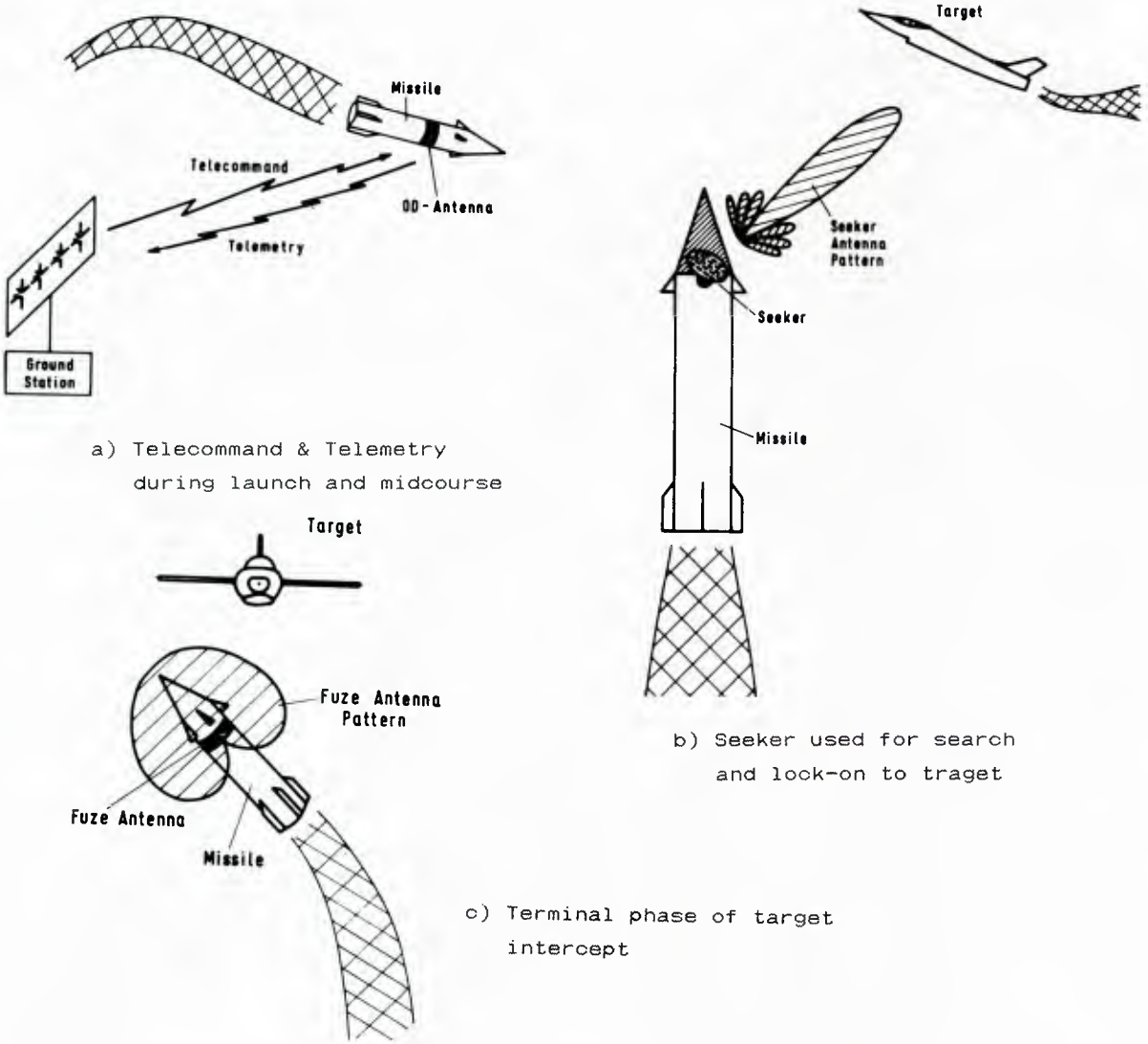

Fig. 1 Use of Microwave Antennas during a surface-to-air missile mission

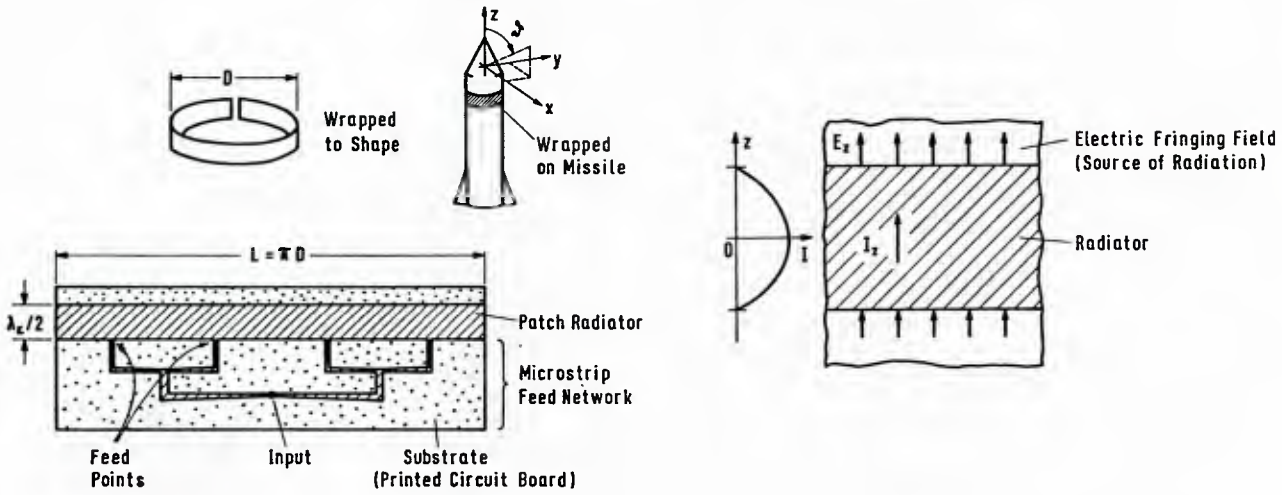

Fig. 2 Wraparound omni-directional missile antenna

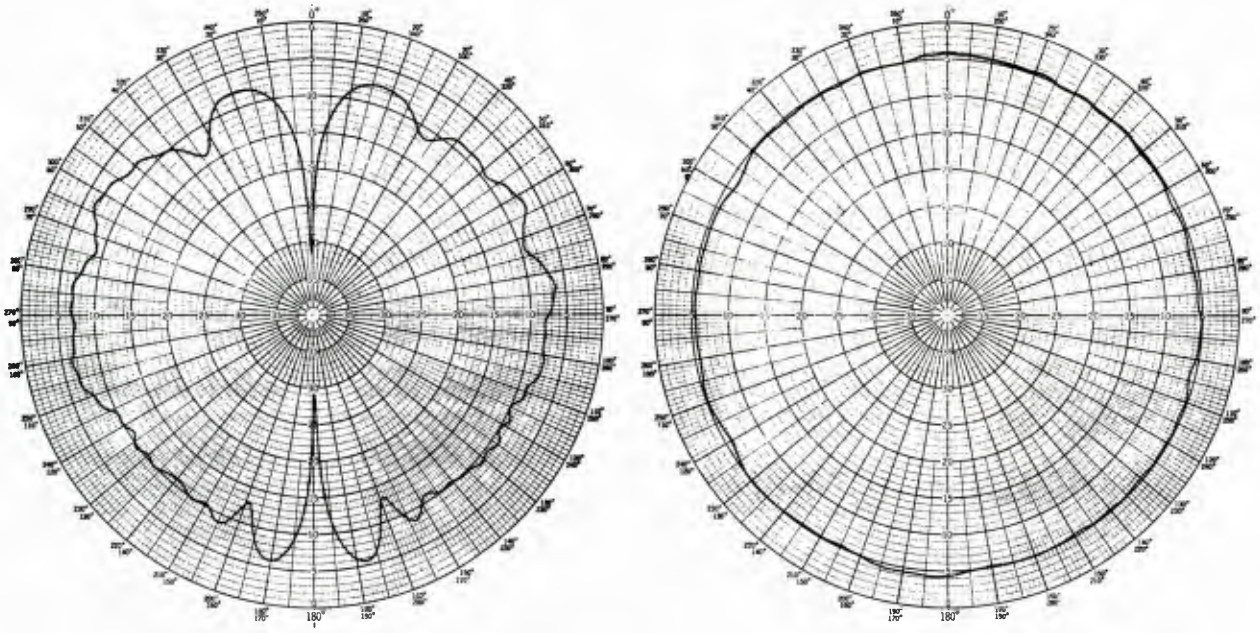

a) Axial cut b) Roll-plane cut

Fig. 3 Radiation pattern of practical wraparound, telemetry missile antenna

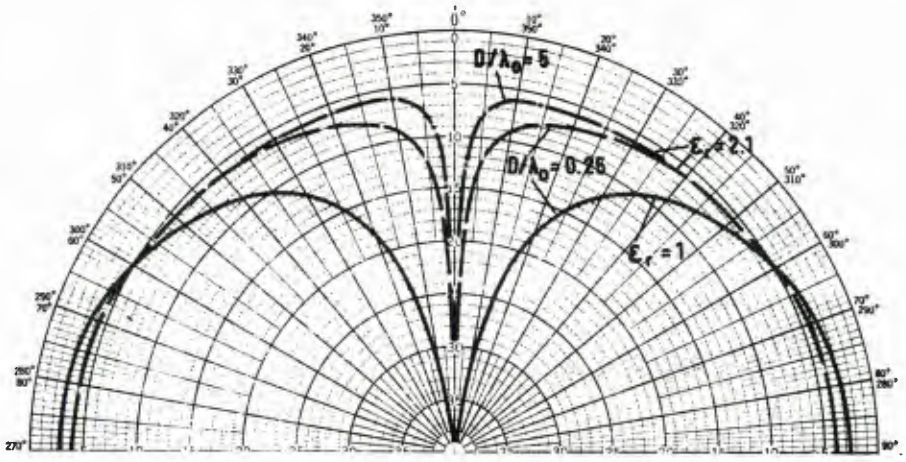

Fig. 4 Theoretical axial cut radiation pattern as a function of missile diameter D and substrate dielectic constant ε_r

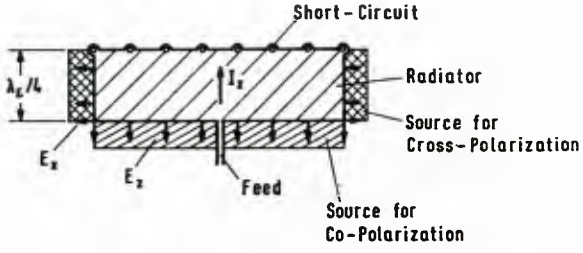

Fig. 5 Field distribution of quarter-wave shorted patch radiator

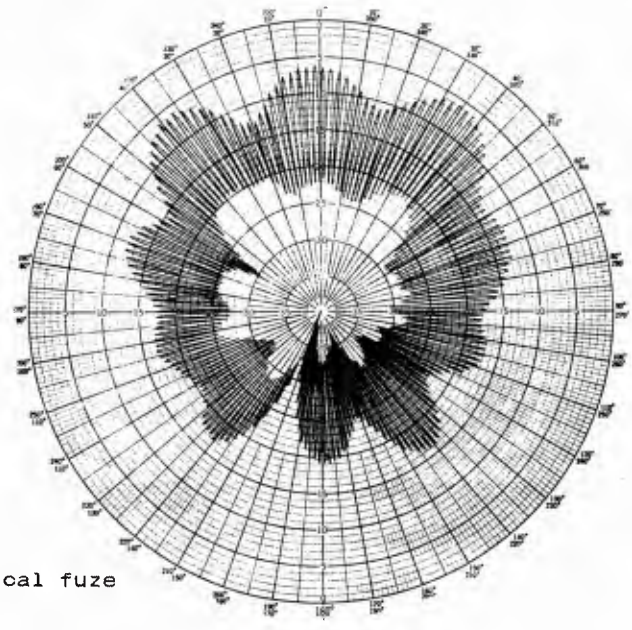

Fig. 6 Radiation pattern of practical fuze antenna (Axial cut)

Fig. 7 Photograph of fuze antenna

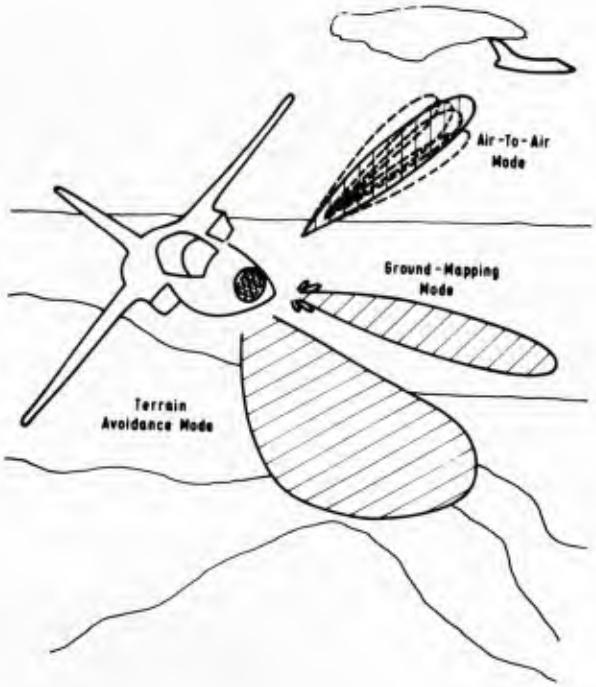

Fig. 8 Use of nose radar antenna in various radar modes of a fighter aircraft

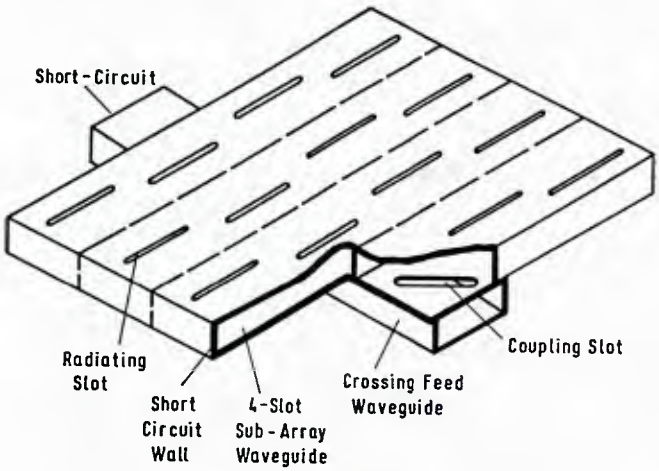

Fig. 10 Sketch of the waveguide configuration in resonant array modules

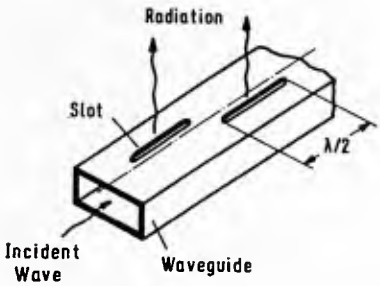

Fig. 9 Basic configuration of waveguide broadwall radiating slots

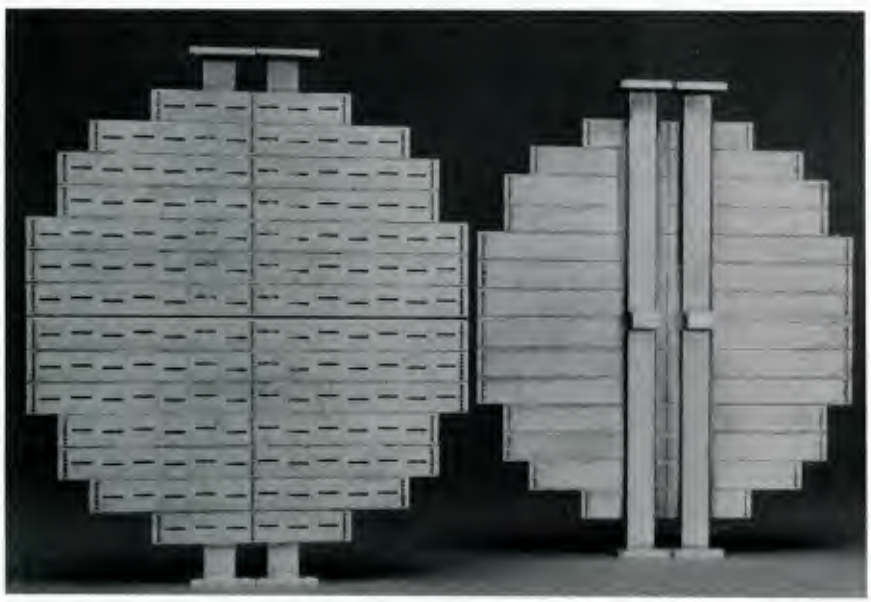

Fig. 11 Photograph of a small slotted waveguide array antenna (drawn waveguide dip-brazing technology)

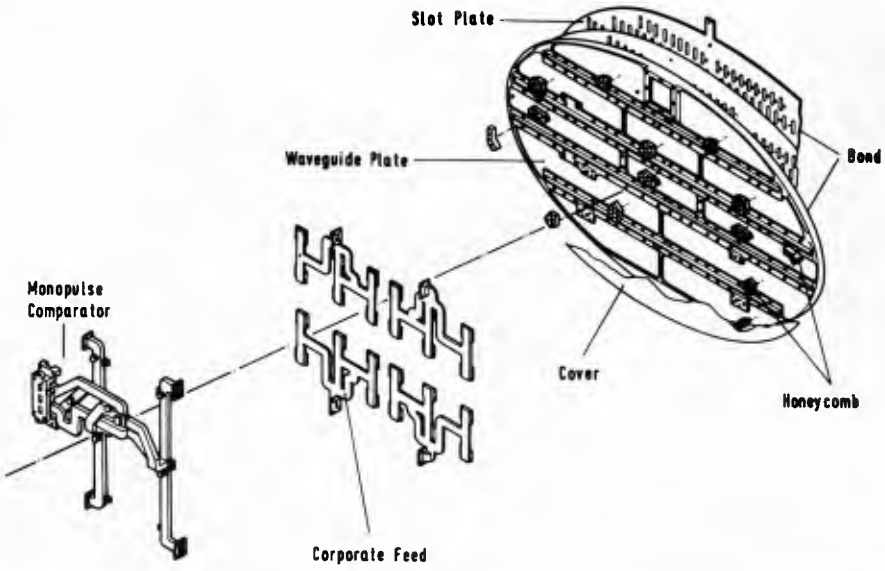

Fig. 12 Disassembled view of a large flat plate antenna (milled waveguide plate sandwich technology)

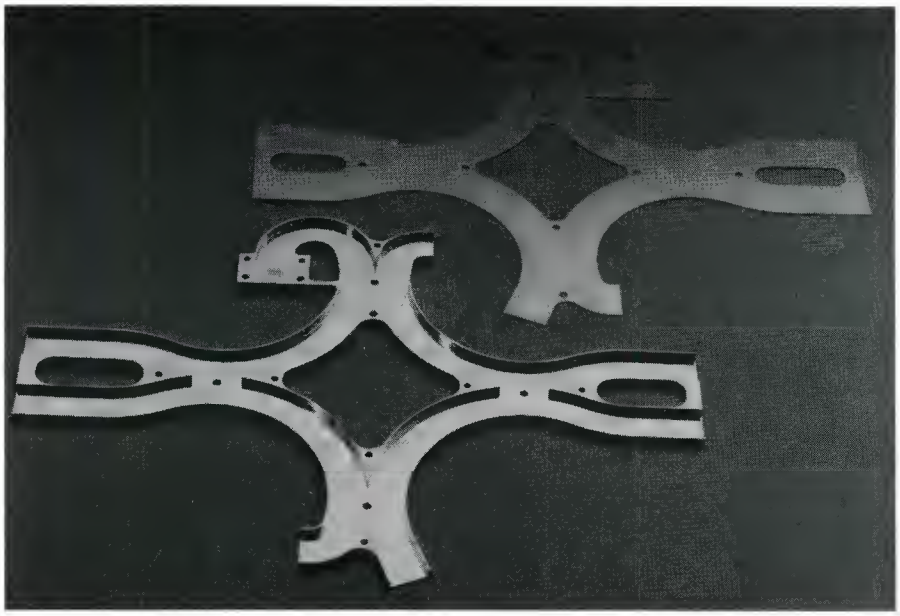

Fig. 13 Photograph of a planar monopulse comparator (milled waveguide technology)

Fig. 14 Use of EW-systems in fighter aircraft

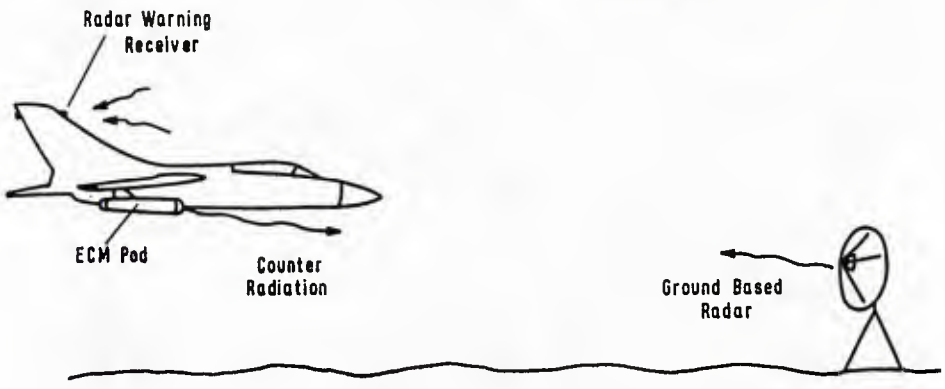

Fig. 15 Photograph of EW-receiver spiral antenna

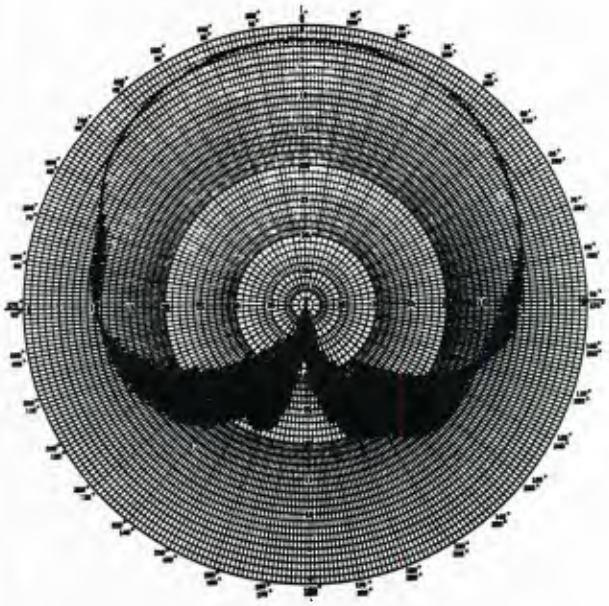

Fig. 16 Typical radiation pattern of a broadband spiral antenna

Fig. 17 Disassembled view of an ECM-horn radiator

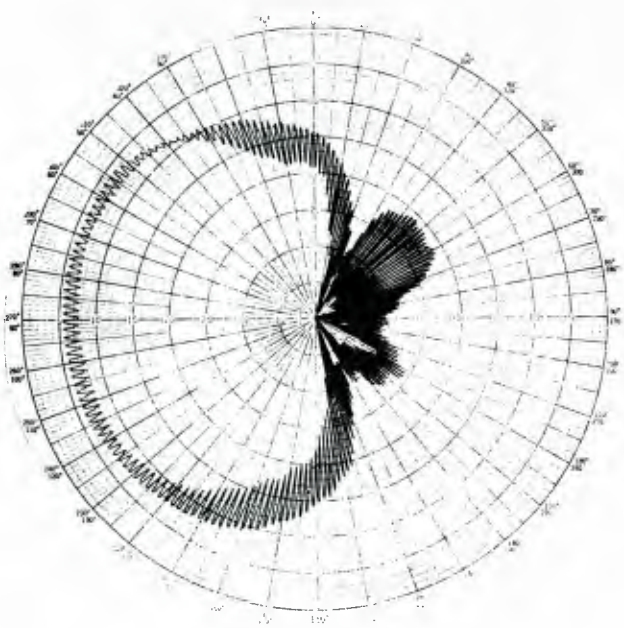

Fig. 18 Typical radiation pattern of a broadband horn radiator

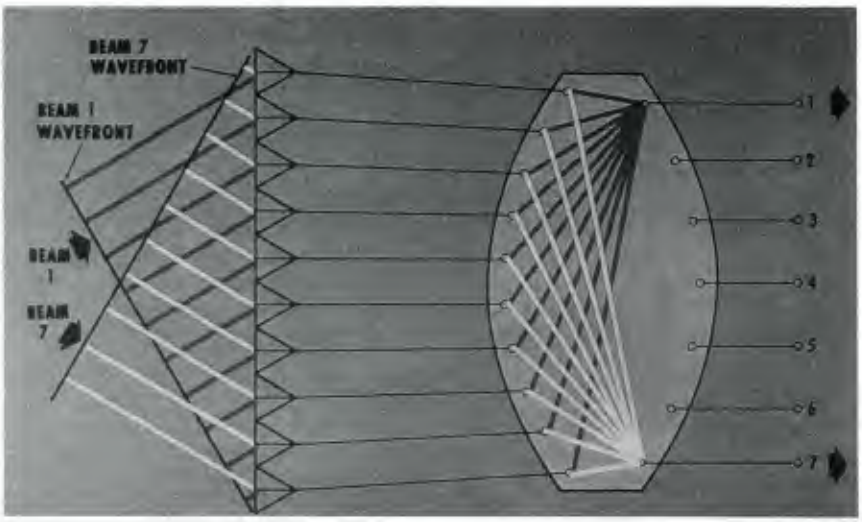

Fig. 19 Rotman-lens array antenna principle of operation

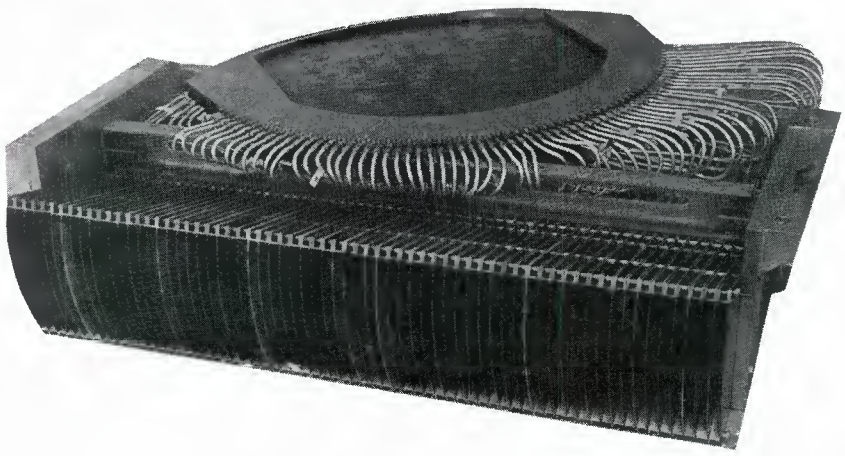

Fig. 20 Photograph of a practical Rotman-lens array antenna (Raytheon)

SPACECRAFT MULTI-BEAM AND CONTOURED-BEAM ANTENNAS

by
P. Balling
TICRA
Kronprinsensgade 13
DK-1114 Copenhagen K
Denmark

SUMMARY

High-gain spacecraft antennas with multiple beams and contoured beams are key components in satellite communications and direct broadcast systems. This is reflected on the latest generation of communications satellites, where the antenna subsystem is the largest subsystem with its weight of more than 300 kg. The antennas achieve a large communications capacity through multiple frequency re-uses and may be reconfigured to serve different coverage areas.

The paper overviews the current multi-beam and contoured-beam antenna technology. Different implementations, reflector or lens with feed array or direct radiating array, are considered. The emphasis is placed upon systems with offset paraboloidal reflectors. The limitations of the offset reflector with respect to beam scanning and cross polarization are reviewed. Computer-aided design procedures and design examples are presented.

1. INTRODUCTION

The antenna systems carried on board spacecraft have over the last 25 years undergone a rapid evolution which parallels that of the spacecraft themselves. In fact, the spacecraft system requirements have been and continue to be a main driving force behind the rejuvenation of antenna theory and technology which previously were considered to be mature disciplines. This evolution has been supported by the simultaneous advent of abundant computational facilities.

Early spacecraft were small, spin-stabilized satellites in low orbits. The antenna systems were simple, often with a low power in a narrow frequency band, typically in the VHF band. Current spacecraft have become large and highly specialized and often carry several antenna systems which are tailored to the role of the spacecraft. Most communications spacecraft are placed along the geostationary arc some 36,000 km above the surface of the Earth. The multi-beam and the contoured-beam antennas reviewed in this paper are examples of particularly complex antenna systems which significantly increase the capacity and flexibility of these satellite systems. By international agreement certain frequency bands have been allocated for the different satellites services and rules have been set to minimize the interference with other satellite systems and with earth-based systems [1]. Typically, the uplink signals from the Earth to the satellite and the downlink signals back to the Earth use different bands. Some of the most important frequency-band allocations for the fixed satellite services (communications satellites) are indicated in Table 1. The frequency allocations differ slightly for three CCIR regions of the world and various restrictions may apply so that the full bands cannot be used. Other bands are allocated for communication with mobile stations and for direct broadcast. Additional bands are allocated at higher frequencies. Initially, the lower bands have been the most popular as the technology has been better developed.

	Uplink	Downlink
C-band	5.925- 7.250 GHz	3.400- 4.200 and 4.500- 4.800 GHz
Ku-band	12.500-13.250 and 14.000-14.800 GHz	10.700-11.700 GHz
Ka-band	27.500-31.000 GHz	18.100-21.200 GHz

Table 1. CCIR allocations for the fixed-satellite service

1.1 Multi-Beam Antennas

The finite frequency spectrum available and the finite number of slots along the geostationary arc for satellites operating in the same frequency band are best utilized by a multi-beam antenna which illuminates the coverage area by a number of element beams. A hexagonal beam lattice is the most efficient for contiguous area coverage. If the antenna radiates N beams and the available frequency spectrum is divided into K bands or channels so that adjacent beams use different bands, the frequency spectrum can be re-used M=N/K times. Figure 1 shows different beam topologies where the number in each cell or beam foot print gives the channel number. The more channels the frequency band is divided into, the larger the spacing will be between the cells where the same frequency is re-used and the better the isolation will be between these beams. However, the number of times the frequency is re-used will be less. In practical systems, adjacent or overlapping beams may use orthogonal polarizations to improve the isolation or increase the number of frequency re-uses.

As an additional advantage of dividing the coverage area into smaller cells, the spacecraft antenna gain is drastically increased. If all the power radiated by the satellite were uniformly distributed over $\pm 8.7^{\circ}$ field-of-view subtended by the Earth, the ultimately achievable gain would be 22.4 dBi. This would require an infinitely large, lossless antenna. In practice less than 17 dBi is obtained towards the edge of the Earth using a horn antenna. With a multi-beam antenna, the upper limit on the achievable gain would be set by size of the element-beam foot print or by the acceptable size and complexity of the antenna system and the accuracy with which the antenna can be kept pointed towards the coverage area. This shift

from the early low-gain over medium-gain spacecraft antennas, which required huge earth-station antennas, to high-gain spacecraft antennas with small beam foot prints has in conjunction with improvements in satellite power and low-noise receivers lead to the introduction of comparatively cheap, small earth-station antennas. More aspects of multi-beam antennas are discussed in [2-4].

The simple beam topologies of Figure 1 carry some disadvantages. In real life, the communications requirements are not uniformly distributed over the field-of-view and a multi-beam antenna system with many beams requires many transponders and a large switch matrix to provide the inter-connectivity between the uplink and the downlink beams. Also, it has not yet been practical without the use of several antennas or excessive antenna losses to radiate element beams with the crossover levels down from the beam peak in the order of 3-4 dB needed for a contiguous coverage. These problems have lead to the concept of contoured-beam antennas where several of the element beams are combined in a cluster or a composite beam.

1.2 Contoured-Beam Antennas

A contoured-beam antenna provides one or more beams with foot prints on the Earth tailored to specific geographical areas. Sometimes these antennas are referred to as multi-beam antennas or shaped-beam antennas. The beam-contouring conserves the satellite power and reduces the interference both with adjacent frequency re-use coverage areas of the same satellite system and with other systems. Figure 2 illustrates the most common hardware used to generate a contoured beam: a feed array which illuminates an offset paraboloidal reflector. Each feed element, usually a small horn, generates a scanned pencil beam which is termed an element beam or a component beam. The foot prints of these element beams on the Earth are indicated by small circles on Figure 2. A contoured beam which provides service to coverage area A is obtained by adding the element beams radiated towards the coverage area with appropriate (complex) weight factors. These weights or feed excitations are generated by a beam-forming network (BFN) which often is a power divider tree with phase shifts provided by line length differences at the feed ports.

The feed array and in particular the BFN are the most critical parts of a contoured-beam reflector antenna as they must realize the desired feed excitations with acceptable amplitude and phase tolerances and low VSWRs at both the feed ports and the beam port over the operating frequency bandwidth. The antenna system is required to operate in a hostile space environment with temperature excursions in the order of -60 to 60 ^{o}C or more over the 7 to 10 year satellite lifetime. The BFNs of most current contoured-beam antennas consist of fixed power dividers and phase shifters. These BFNs are usually implemented in TEM-line in the 6/4 GHz bands and in waveguide in the 14/11 and 30/20 GHz bands. Waveguide BFNs have lower insertion loss, but are heavier and more bulky than TEM-line BFNs. The stringent matching requirements have lead to the almost exclusive use of hybrid couplers rather than simple 3-port TEEs or E-plane couplers in the power divider tree.

Advanced antenna systems include on international communications satellites switches to provide slowly reconfigurable beams to allow a satellite to operate from different locations along the geostationary arc and to accommodate traffic changes and on DSCS III fully reconfigurable BFNs with variable ferrite power dividers. Future systems are likely to include more variable power dividers and variable phase shifters in ferrite or solid-state technology. This will allow both a high degree of beam flexibility and the fast reconfigurability required for hopping and scanning beams with TDMA. Ultimately, BFNs are expected to include many active components to compensate for losses. This will provide very compact and flexible BFNs.

If the antenna system only is required to generate a single fixed contoured beam, a shaped reflector illuminated by a single feed is an attractive solution with respect to both performance and cost mainly because no BFN is required. This concept is reviewed in Section 5.

1.3 Choice of Reflector, Lens or Array?

The use of a focusing device such a reflector or a lens provides a one-to-one relation between the element beams and the feed horns. This relationship does not exist in the case of an array, where each array element contributes to all element beams, and an array with several independent beams operating at the same frequency and polarization would suffer from significant losses unless a Butler-matrix type BFN is used with orthogonal array illuminations for the different beams. In the cases of multi-beam antennas where each beam can be generated by a single feed and of contoured-beams antennas where only a few element beams are used to generate the contoured beam, the BFN is much simpler for a reflector and a lens. As a result, array antennas have found only little use as spacecraft multi-beam and contoured-beam antennas. Nevertheless, we will consider contoured-beam array antennas further in Section 7. A review of multi-beam arrays is given in [5].

The choice between reflector and lens is more difficult. In the past, most systems have used reflectors due to their low weight and cost, excellent bandwidth and polarization properties and the fact that they can be analyzed very accurately with the existing RF analysis methods. A main disadvantage of the reflector is the need to use an offset-fed reflector geometry to avoid blockage by the large feed array, BFN and support structure. The offset-fed reflector has significantly worse scan and cross-polarization performance and occupies a larger volume on the spacecraft than a similar center-fed reflector.

The lens is a focusing device with axial symmetry but without blockage. As furthermore the remaining dominant scan aberration, coma, may be removed by choosing the inner lens surface to be a sphere so that the Abbé sine condition is fulfilled, lens antennas have considerable attraction for multi-beam applications [6]. Dielectric lenses are far too heavy for use at microwave frequencies on a spacecraft, and new low-weight but also more complicated lenses such as the zoned waveguide lens and the printed-circuit bootlace or TEM-line lens outlined in Figure 3 have been devised. These lenses may be attractive in systems with somewhat less than 100 element beams where the number of waveguide or printed-circuit elements can be kept reasonably small. The DSCS III spacecraft in fact flies three multi-beam zoned waveguide lens antennas operating at about 8 GHz [4]. The bandwidth of a zoned waveguide

lens is not compatible with those stated in Table 1. The more broadbanded TEM-line lens has been investigated for use at C band [7]. However, its weight was considered to be so large that the receive and the transmit function would have to be combined in one antenna. The matching problem at the inner lens surface could not be solved over the combined frequency band and led to degradations of the element beams near the axis. Because of their complexity and the still unsolved problems, lens antennas are not considered further in this paper. It is expected that lens antennas will prove to be more useful at millimeter and submillimeter wavelengths.

Solid reflectors manufactured from carbon-fiber re-enforced plastic (CFRP) have become very popular due to their low weight and excellent thermal behavior. Surface accuracies in the order of 1/100 wavelength RMS are required to ensure low sidelobes. Solid offset reflectors provide excellent cross-polarization performance when used with circular polarization. However, many domestic systems use linear polarization. This has led to the development of gridded and dual gridded reflectors to reduce the cross polarization introduced by the offset configuration.

2. FUNDAMENTALS OF CONTOURED-BEAM REFLECTOR ANTENNAS

2.1. Basic Definitions

Contoured-beam reflector antenna systems have a unique set of performance parameters. Most other antenna systems, including earth station antennas, optimize the on-axis gain subject to certain sidelobe constraints often defined by an envelope. The driving system parameters are EIRP and G/T with sidelobe constraints added to minimize interference. Cross-polarization requirements often only apply near the beam axis. When an antenna is required to serve an area rather than just a single direction, the minimum coverage area gain and not the peak gain becomes the significant parameter. Hence, the standard definition of antenna efficiency does not apply to contoured-beam antennas. The efficiency η of a contoured beam antenna is defined as the ratio of the minimum coverage area gain MCAG to the gain G_{un} of a lossless antenna which distributes all the radiated power uniformly across the specified coverage area Ω (in steradians), i.e.,

$$\eta = MCAG/G_{un} \tag{1}$$

where

$$G_{un} = 4\pi/\Omega . \tag{2}$$

Alternatively, the gain*area product, MCAG×Ω, may be defined. Due to the finite satellite pointing accuracy, the gain slope must be controlled within the area of uncertainty for each earth station. The area of uncertainty is called the pointing-error box, sphere or ellipse dependent upon its actual shape which is determined by the satellite attitude control system. The coverage area Ω must include the pointing error.

A pencil beam with a circular foot print is the simplest example of a beam with an area coverage. If we assume a Gaussian beam shape and no losses, the power pattern

$$G(\theta) = 4\ \ln 10/\theta_{10}^2\ 10^{-(\theta/\theta_{10})^2} \tag{3}$$

gives the directivity. The polar angle θ is measured from the beam axis and θ_{10} is half the 10-dB beamwidth. The minimum coverage area gain occurs at the edge of the coverage area, $\theta = \theta_c$, and is maximized for $\theta_{10} = \theta_c\sqrt{\ln 10}$. This result also applies for Gaussian beams with elliptical foot prints. Thus, the minimum coverage area gain is about 4.3 dB below peak gain for circular and elliptical foot prints. The associated gain*area product is $4\pi\ 10^{-\ln 10}$ or 15176 degrees^2, which corresponds to a contoured-beam efficiency of only 36.8 per cent even though that all losses have been neglected. This efficiency, which accounts for the great gain difference between the ideal and the practical global-coverage antenna in Section 1.1, may be improved by a flatter gain over the coverage area and a steeper gain fall off at the edge of the coverage area.

When the antenna system provides multiple contoured beams, the driving antenna parameter becomes the isolation which can be achieved between beams which re-use the same frequency band either through spatially separated copolarized beams or through orthogonally polarized beams. Figure 4 illustrates the different definitions of inter-beam isolation which apply for receive and transmit satellite antennas. When the satellite antenna transmits, an earth station served by beam B may receive an interfering signal via a sidelobe of beam A. The transmit isolation is defined as the ratio of the desired signal from beam B to the undesired signal from beam A and depends on both the relative antenna gain and the relative transmit power, i.e., the relative EIRP. With the satellite antenna receiving, the interference occurs via the sidelobes of the beam itself from earth stations outside the service area. If all earth stations transmit with the same EIRP, the receive isolation is defined as the ratio of the antenna gain towards the earth station in the coverage area to the antenna gain in the direction of the interfering earth station at the highest sidelobe level. The receive isolation is considered to be the most difficult as a single high-level sidelobe which falls in a frequency re-use coverage, will destroy the isolation on all coverage-area stations.

The minimum spacing between adjacent copolarized frequency re-use coverages, measured in beamwidths of the element beams, determines the required aperture size or resolution of the antenna system. An antenna pointing error of ε will reduce the minimum coverage area spacing by 2ε. Thus, a large pointing error may require a significantly larger and more complex antenna system.

2.2. Overview of the Current State-of-the-Art

The INTELSAT communications satellites provide an important example of the practical use of reflector antenna systems with multiple contoured beams. The complexity of in particular the C-band antenna systems have grown significant for each new spacecraft series as illustrated by the increasing complexity of the coverages shown in Figure 5. INTELSAT IV A introduced two-fold frequency re-use through two spatially isolated hemispherical beams by means of an array-fed offset paraboloidal reflector antenna system [8]. This concept was further developed on INTELSAT V where four-fold frequency re-use was realized by the addition of two smaller zone beams in the opposite sense of circular polarization. These zone beams have one shape when the spacecraft operates over the Atlantic or the Pacific Ocean region and another over the Indian Ocean region [9, 10]. The trends towards both more frequency re-uses and more reconfigurability of the beam coverage contours continue on INTELSAT VI. Two hemispherical beams and four zone beams in opposite senses of circular polarization provide six frequency re-uses. The four zone beams are reconfigured for each of the three ocean regions providing a total of 14 coverage beams with six active in a given ocean region [11, 12]. The achievements and the limitations of this technology are summarized in Table 2 [13]. It is common practice to use separate antennas for the transmit and receive function to reduce both the bandwidth over which an antenna is required to operate and problems associated with passive intermodulation.

The increased number of frequency re-uses sets stringent sidelobe and cross-polarization requirements in the order of 27-30 dB over a field-of-view which extends approximately $\pm 10^{o}$ from the subsatellite point to accommodate both antenna pointing errors and the spacecraft pitch biasing used to maximize the minimum spacing between spatially isolated beams. As the spacecraft are placed above the middle of the oceans, the beam coverages fall near the maximum scan angle so that scan aberrations degrade the achievable sidelobe isolation. So far, however, the diameter of the spacecraft antenna, measured in wavelengths, has been moderate, and the number of beamwidths scanned less than 6-7 half-power beamwidths. This is demonstrated by the observation that for all satellites in the INTELSAT IVA, V to VI series the minimum separation between two copolarized coverages is about 1.5 element-beam beamwidths for 27 dB isolation [14]. This relationship may continue for significantly larger reflector diameters if longer f/D ratios or more complex feed arrays and BFNs can be accommodated to reduce the aberrations of the scanned element beams. Figure 6 shows the calculated contoured-beam efficiency versus coverage area size for INTELSAT VI. The two upper curves apply for a smaller feed element diameter of about 1.3 λ and in case of the uppermost curve also the effect of a slightly increased spacing between the coverage areas [15]. Other contoured-beam antennas also for domestic/regional and direct broadcast systems are reviewed in [16-20].

2.3. Analytic Model of Reflector Element Beams

A simple analytic model is presented for the element beams radiated by small circular or square feeds in an offset paraboloidal reflector with circular aperture. Effects due to the illumination taper and the spillover are included to provide an accurate assessment of the achievable minimum coverage area gain. The model neglects scan aberrations and cross-polarization and is therefore best suited for reasonably large f/D ratios and/or small scan angles. Even then we have found that the model may give surprisingly good predictions for the minimum coverage area gain and the average sidelobe level. The model cannot be used to determine the number of feeds or the feed excitations accurately. Therefore, the model is most useful in initial trade-off studies to determine approximately the antenna size and feed complexity given the coverage specifications. The detailed design optimization should be carried out using element beams calculated by an accurate reflector antenna analysis program such as GRASP [21].

Let the aperture distribution due to a single feed be approximated by

$$g(\rho) = \alpha_o + (1-\alpha_o)\left[1-(r/a)^2\right]^n, \tag{4}$$

where the radial variable $\rho < a$. The parameter α_o is the relative illumination at the reflector edge. Typical parameter values corresponding to an element beam would be $n = 1$ and $\alpha_o = 0.7$. We assume that this amplitude distribution applies for all element beams. As we neglect scan aberrations, the phase distributions caused by the lateral displacement of the feeds in the tilted focal plane only direct the wave fronts towards the positions in the beam grid. The element beams are approximated by the normalized patterns

$$f_j(\theta,\phi) = ka\left[\alpha\,\Lambda_1(kax_j) + \beta\Lambda_{n+1}(kax_j)\right]. \tag{5}$$

The functions $\Lambda_n(x)$ are given by Bessel functions $\Lambda_n(x) = 2^{n+1}\,(n+1)!\,J_{n+1}(x)/x^{n+1}$ so that $\Lambda_n(0) = 1$. The argument depends on the perimeter ka of the circular aperture in wavelengths and the distance

$$x_j = ((u-u_j)^2+(v-v_j)^2)^{1/2} \tag{6}$$

between the field direction (u,v) and the beam direction (u_j,v_j) in the uv-plane where $u = \sin\theta\cos\phi$ and $v = \sin\theta\sin\phi$. The angles θ and ϕ are the polar and the azimuthal angle in a standard spherical coordinate system directed along the antenna boresight. The pattern parameters α and β in (5) depend via the edge taper α_o upon the primary parameters

$\Delta\theta_3$ - the half-power element beam beamwidth, and
θ_B - the element beam spacing

as outlined below. In order to model the offset reflector and the feed element including spillover losses, the following secondary parameters

d_c/D - the relative offset height or clearance,
d_e - the feed element spacing in wavelengths, and

θ_{10} - half the 10-dB feed beamwidth

are specified. These parameters are indicated on Figure 7. Given the above primary and secondary parameters, the parabola focal length f and the reflector diameter D can be derived. The reflector clearance d_c, the distance from the parabola axis to the reflector edge, should be so large that no scanned beams are blocked by the feed array. The feed element spacing d_e and the feed beamwidth $2\theta_{10}$ are roughly inversely proportional for a given feed type.

Once the above parameters are given, an initial values of the reflector diameter D, the focal length f and subtended semi angle θ^* are calculated assuming a 3 dB edge taper by the approximate formulae:

$$D = 1.029\ (1 - 0.212\ \log_{10}\alpha_o)/\Delta\theta_3 \tag{7}$$

$$d_1 = (0.5 + d_c/D)D \tag{8}$$

$$f = (Kd_e/\theta_B + \sqrt{(Kd_e/\theta_B)^2 - d_1^2})/2 \tag{9}$$

$$\theta^* = \text{Arctg}\ d_1/f - \text{Arctg}\ d_c/2f \tag{10}$$

where K = 0.97. All angles are in radians an all lengths in wavelengths. Note that (9) has no solution if $\theta_B > Kd_e/d_1$. An improved value may now be calculated for the average aperture edge illumination using

$$\alpha_o = 10^{-(\theta^*/\theta_{10}^2)}\ /2/(1 + D^2/8(f^2+D^2)). \tag{11}$$

Given this value, the values for D, d_1, f and θ^* are updated using (7) through (10). The offset paraboloid is now completely determined, and the pattern coefficients are determined from

$$\alpha = \alpha_o/N\ L_{so} \tag{12}$$

$$\beta = (1-\alpha_o)/[(1+n)N]\ L_{so}, \tag{13}$$

$$N = [(1+n+2n\alpha_o+2n^2\alpha_o^2)/(1+3n+2n^2)]^{1/2} \tag{14}$$

where

$$L_{so} = 1-10^{-(\theta^*/\theta_{10})^2} \tag{15}$$

gives the element-beam spillover loss. The pattern coefficients are normalized so that the pattern (5) squared gives the directivity. This normalization is convenient for the normalization of the feed excitations discussed in Section 2.5. The effect of typical element-beam edge tapers on the directivity is very small, about 0.1 dB or less. The corresponding element-beam spillover loss is more significant as discussed in Section 2.7. A number of other beam models or simple design rules are available for initial contoured-beam reflector antenna trade-off and layout [22, 23].

2.4 Array Elements

The array element is a key element in determining the overall performance. The feed element must be chosen in accordance with the reflector geometry. For a specified beam-spacing/beamwidth ratio, $\theta_B/\Delta\theta_3$, a smaller feed requires a shorter f/D ratio of the parabola than a larger feed. The $\theta_B/\Delta\theta_3$ ratio is usually close to unity corresponding to an element-beam crossover level of about -3 dB. The feed diameters in the range from 1 to 1.6 λ match well f/D ratios in the range from 0.7 to 1.4. For small f/D ratios, the reflector subtended angle becomes larger and the spillover losses smaller. However, the scan losses increases. The spillover losses are minimized if the product $\theta_{10}d_e$ is kept small. This parameter plays the role of an array-element quality number and is relatively independent of the size of a particular type of element as already discussed in Section 2.3. For a small circular fundamental-mode horn the value of this parameter is about 1.00 while it is about 1.17 for a small dual-mode or Potter horn. Small corrugated horns are quite useless as array elements because of the large space taken up by the corrugations. From these considerations it would appear that small fundamental mode horn would be the most useful for contoured-beam antenna applications. However, the mutual coupling in the array environment will in practice annihilate the excellent theoretical performance of the small fundamental-mode radiator.

The circular waveguide feed elements discussed above and the square waveguide feed elements are used commonly in circularly polarized antenna systems. Many linearly polarized domestic/regional systems use rectangular feeds of different sizes with or without dielectric loading often illuminating a dual gridded reflector. The feed horn dimensions are optimized to match the image of the coverage area in the focal plane of the reflector. These systems may realize very respectable values of the minimum coverage area gain with a minimum of antenna hardware but are not dealt with in the paper [24, 25].

In a dual circularly polarized antenna, a feed element in conventional waveguide technology consists of a horn radiator, a polarizer and an orthomode transducer. In a large antenna system with many feeds, this may be a very bulky and mechanically fragile system. Therefore, microstrip patch radiators have recently received considerable attention as a potential very compact replacement .

2.5 Network Loss and Feed Excitation Normalization

When several feeds are excited simultaneously to generate a contoured beam, the overall edge illumination and spillover loss will in general decrease. On the other hand, the beam forming network (BFN) required to generate the optimized amplitude and phase distribution at the feed ports introduces Ohmic and mismatch losses. This BFN loss increases with the number of feeds ports as more layers of power dividers and longer line lengths are required in the power divider tree. Fully reconfigurable BFNs may have significantly higher losses than fixed BFNs.

The feed excitations a_j must be normalized by

$$P_{in} = 4\pi \sum_{j=1}^{N} |a_j|^2 = \begin{cases} 4\pi & \text{for directivity} \\ 4\pi 10^{-LBFN/10} & \text{for gain.} \end{cases} \quad (16)$$

Then, the directivity or the gain will be referred to the total incident power at either the feed apertures or at the BFN input port. The directivity referred to the total radiated power is derived if the excitation normalization is

$$P_{rad} = 4\pi \sum_{i=1}^{N} \sum_{j=1}^{N} r_{ij}\, a_i a_j^* = 4\pi, \quad (17)$$

where r_{ij} is the normalized mutual resistance and $r_{ii} = 1$.

2.6. Mutual Coupling

For a sufficiently large array element with a Gaussian pattern, the normalized mutual resistance is

$$r_{12} = e^{-(kd_{12}\theta_{10})^2/4\ln 10}. \quad (18)$$

This indicates that the mutual resistance depends with the approximations made only on the product $d_{12}\theta_{10}$, which for adjacent feeds is equal to the feed quality number. Thus, the requirements for low mutual coupling and for a small spillover loss are in conflict: A large value of $d_e\theta_{10}$ reduces the mutual coupling but increases the element beam spillover loss. In a study of feed-array directivity, $\cos^q\theta$-approximations to the feed element pattern have been used [26].

The mutual resistance given by (18) is derived from an idealized feed pattern and neglects higher-order modes and cross polarization. It relates to the small signal which appears at the port of a feed when an adjacent feed is excited. This effect is quite negligible for practical feed-array elements and (16) is a good approximation to the power radiated by the feed array. However, the effect of the array environment on the element pattern is much stronger. This effect, which may be termed mutual scattering, sets up the cross-polar mode and higher-order modes at the radiating aperture and has a pronounced effect on the cross-polar performance.

Much work has been carried out on mutual coupling in phased-array antenna systems using the concept of the active element pattern and the unit cell approach. These techniques do not apply to contoured-beam antenna feed arrays which have very non-uniform amplitude and phase distributions. The number of elements is typically smaller than in a phased array and the element size is larger. No electronic scanning takes place and the blindness effects of scanning phased arrays are of no concern. The concept of the embedded element pattern is more useful. The embedded feed pattern is defined as the pattern the feed radiates in the array environment with the feed element excited and all other elements terminated with their actual loads. Mismatches at the feed ports into the BFN have been noted to have a significant effect on the cross polarization - in particular for circular polarization.

A comprehensive study of mutual coupling in contoured-beam antenna feed arrays has been reported in [27]. The method of moments is used and the results apply to a finite number of circular waveguide feeds in a ground plane.

2.7. Spillover Loss Calculation

The spillover loss of a contoured beam will be lower than that of an element beam because of the array factor. The spillover loss is defined as the ratio of the feed power which hit the reflector to the total radiated feed power. The total power radiated by the feed array has been calculated (16). The element beams overlap and are usually not orthogonal. Therefore, the power intercepted and radiated by the reflector must be determined by integrating the total reflector far field. It is much simpler, however, to determine the power radiated by the reflector by integrating the Poynting vector across the reflector aperture A as proposed in [28]. We then obtain for the amplitude distribution in (4)

$$P_{rfl} = 4\pi \sum_{i=1}^{N} \sum_{j=1}^{N} a_i a_j^* \left[\alpha^2 \Lambda_1(kax_{ij}) + 2\alpha\beta\Lambda_{n+1}(kax_{ij}) + (n+1)^2\beta^2\Lambda_{2n+1}(kax_{ij})/(2n+1)\right], \quad (19)$$

where the pattern coefficients α and β are defined above. The parameter x_{ij}, similar to (6), is the spacing between the beam centers in the uv-plane. The "cross correlation" pattern in (19) is wider than the element-beam pattern except in the case of uniform illumination. If the element-beam positions coincide with the nulls of the "cross-correlation" pattern, the beams decouple and become orthogonal. It appear that "losses" due to non-orthogonal beams are of a fundamental nature and may be related to different mechanisms in different antenna systems, e.g., BFN losses, spillover losses in reflector and lens systems and grating-lobe losses in arrays [29].

Figure 8 shows the spillover losses for a single element beam and a cluster of seven element beams. The feed spacing is kept constant equal to 1.07 λ and the beam spacing is increased by decreasing the focal length. The angle subtended by the reflector increases with increasing beam spacing, and the element beam spillover loss decreases. The dotted curve is the element beam spillover loss calculated accurately by a reflector antenna analysis program. The spillover loss of the 7-element cluster is much lower than that of the element beam and almost independent of the beam spacing. For a fixed reflector geometry, the beam spacing (or the beam crossover level) may be varied by changing the feed spacing. Table 3 gives the approximate spillover losses of both single and uniformly excited 7-element clusters of circular fundamental-mode and dual-mode feeds. The table gives the calculated spillover losses for $\theta_B/\Delta\theta_3$ equal to 0.7, 1 and 1.3 corresponding to crossover levels of 1.5, 3, and 5 dB.

	Single feed			Cluster		
$\theta_B/\Delta\theta_3$	0.7	1.0	1.3	0.7	1.0	1.3
TE_{11}	5.7	3.1	-	1.5	1.3	-
$TE_{11}+TM_{11}$	6.8	4.1	2.3	2.6	2.4	2.1

Table 3. Spillover loss in dB.

A significant fraction of the large element-beam spillover for small beam spacings may be recovered by the array factor. For the dual-mode feed cluster, where the grating lobe losses are larger due to the larger feed size, the effect of the array factor on the spillover loss becomes very small for large beam spacings. A hexagonal array lattice will reduce the grating-lobe losses. For each feed type, a smaller feed spacing will slightly reduce the cluster spillover loss. The table indicates that there is a need for improved feed elements which utilize the focal-plane area more efficiently but without high mutual coupling. Another and probably more promising remedy might be to use improved reflector systems.

Even though the spillover loss of a contoured beam can be considerably reduced by the array factor, it can not be neglected. In the sense that this loss represents radiated power, it is very harmful in a frequency re-use antenna system if it is intercepted by the antenna or by other satellite structures and re-radiated as cross polarization back into the coverage or as high sidelobes into adjacent coverages. Such antenna-farm effects are difficult to predict as they depend upon the wide-angle radiation from the feed array and require special analysis software.

2.8. Scan Characteristics of Single Reflectors

Figure 9 shows isogain contours for the on-axis and some scanned element beams for a 3.2 m offset paraboloidal reflector at 4 GHz with an f/D ratio of 1.3. As a beam is scanned a way from boresight, a gain loss and a beam widening occur. These beam degradations depend for a given scan angle upon the D/λ ratio, the offset angle θ_o, the f/D ratio, and the aperture illumination. For the single offset paraboloidal reflector, where the scan degradation is due to astigmatism [30], the scan loss in dB for the scan angle θ_{sc} may be approximated by

$$L_{sc} = C(n,\alpha_o)\ (D/\lambda\ D/f\ \sin\theta_o\ \sin\theta_{sc})^2, \qquad (20)$$

with $C(n,\alpha)= 0.1116\left[(n+1)\alpha+6(1-\alpha)/(n+2)(n+3)\right]/(1+n\alpha)$. The parameters n and α_o are the exponent and the edge taper of the reflector aperture illumination (4). For scan losses larger than 5 dB, (20) predicts too large losses. The scan loss is not a loss in radiated power as the BFN loss and the spillover loss. It represents a loss in the resolution or the beam-contouring capability of the reflector due to the widening of the element beams for large scan angles. Some scan degradation may be compensated for by a more complex feed array.

The scan losses of the center-fed paraboloidal reflector are for the same aperture diameter, f/D ratio, scan angle and aperture illumination order of magnitude less than those of the offset-fed reflector. The dominant aberration is due to coma, which has a minor impact on scan loss and mainly degrades the sidelobe performance [31]. As the total scan loss is determined by a combination of coma, higher-order astigmatism and spherical aberration, no simple expression exists for the scan loss in the center-fed paraboloidal reflector.

2.9. Polarization Considerations

Circular polarization was initially chosen for use in the international communications satellite system because of the Faraday rotation. When a linearly polarized signal traverses the ionosphere, the polarization plane undergoes a rotation. At 4 and 6 GHz, the maximum Faraday rotation is approximately 9 and 4^o with opposite directions for transmit and receive (CCIR Report 551-1, Sect. 2.3.1). This choice of polarization was fortunate from the point-of-view of antenna technology. Circularly polarized offset reflectors do not generate cross polarization but exhibit a slight beam squint in the plane perpendicular to the plane of symmetry [32, 33]. The magnitude of this beam squint is given by the approximate formula

$$\Delta\beta = \mathrm{Arcsin}(\lambda\sin\theta_o/4\pi f). \qquad (21)$$

The direction of the beam movement depends upon the hand of the polarization. The Faraday rotation is inversely proportional to the square of the frequency and presents no problem above 10 GHz. Then, depolarization caused by rain becomes important and from the point-of-view of cross polarization, circular polarization becomes the worst possible choice. The shape of rain drops is generally spherical. However, the shape of falling rain drops becomes slightly elliptical due to the air resistance. The rain-induced attenuation and phase shift are maximum (minimum) for the polarization aligned with the major (minor) axis of the rain drop. No depolarization takes place for linear polarization aligned with the major or the minor axis of the rain drop. In practice, the depolarization is minimized for linear polarization aligned with local earth station vertical and horizontal (CCIR Report 564-2, Sect. 8.2). Thus for frequency re-use antenna systems in the 14/11 GHz bands and possibly even the 30/20 GHz bands, linear polarization should be used aligned with the average local vertical and horizontal within each coverage area [34]. However, this alignment will reduce the cross-polar isolation between adjacent coverage areas under clear-sky conditions as the polarizations then no longer are orthogonal.

In the single offset paraboloidal reflector, the feed axis is in general tilted to bisect the angle subtended at the focal point by the reflector in its plane of symmetry. This feed axis tilt generates two cross-polar lobes in a linearly polarized system [32, 35, 36]. The peak of the cross-polar lobes occurs in the plane perpendicular to the plane of symmetry. For a uniformly illuminated aperture, the peak cross-polar level relatively the peak copolar level is

$$E_{cross}/E_{co} = 0.36\ \theta^*\ \tan\theta_o/2, \qquad (22)$$

where θ^* (in radians) is the semi angle subtended by the reflector. A tapered aperture illumination will decrease the cross polarization slightly. Any significant reduction requires either a more complicated feed element, a more complex feed array design, or that a gridded reflector be used.

3 OPTIMIZATION OF CONTOURED-BEAM REFLECTOR ANTENNA SYSTEMS WITH FEED ARRAYS

The synthesis of a contoured-beam antenna system may be divided into steps. Initially the fundamental antenna performance requirements such as

- coverage area(s),
- minimum coverage-area gain,
- maximum coverage-area gain slope,
- sidelobe and cross-polar isolation and
- frequency band

must be specified. Next, the antenna designer may identify the range of a number of antenna parameters such as

- reflector aperture size, and
- feed-array complexity

and examine the performance trade-offs versus the antenna system size and complexity. These trade-off studies require that optimum feed excitations be determined and the resulting contoured beams be analyzed for several antenna configurations. If these studies are carried out with simple analytic element-beam models, large savings can be realized in both human effort and computer time.

When a viable solution has been identified by these initial optimizations, an element-beam layout with half-power element beam beamwidth $\Delta\theta_3$ and the element beam spacing θ_B will be known. Given this element-beam grid, the feed-element size and the orientation of antenna on the satellite, an initial reflector antenna and feed array layout may be determined ensuring that no blockage occurs. Then, the detailed optimizations are carried out using element-beam data determined by an accurate reflector antenna analysis program. It is desirable to include as many potential error sources as possible. Degrading effects not predicted by the software can be included by means of measured data, e.g., of the patterns of the feeds embedded in the array. In case the results of the optimizations indicate that the performance requirements can not be met, these requirements or the range of antenna parameters being considered must be revised.

3.1 Optimization Procedures

Many different, more or less rigorously based optimization procedures have been proposed to determine the feed excitations which provide the "best" contoured beam. It appears that no optimization procedure is complete. Usually the antenna designer specifies the reflector and the feed array geometry. Only then an optimization procedure determines the "best" feed excitations by optimization of the antenna performance, e.g., gain and isolation, over a finite number of pattern sample points. These sample points will be termed synthesis stations as they may not correspond to actual earth stations. A more complete optimization can be carried out by repeating the feed excitation optimization for a large number of antenna geometries. A general optimization procedure may optimize both element-beam grid and excitations but the usefulness of the results will be limited by the accuracy of the element-beam model. For practical antenna systems, it is still prohibitive and probably not desirable to include in the closed optimization loop a complete electromagnetic analysis with a.o. BFN tolerance analysis and feed-array mutual coupling analysis.

A contoured-beam synthesis is a power-pattern synthesis problem as opposed to a field-pattern synthesis problem. Furthermore, the power pattern are only specified in certain regions. The power pattern in the complementary regions of the far-field sphere and the phase pattern should be allowed to float in the optimization and take on any values which improve the power pattern in the regions of interest. Thus, even the apparently simple problem of determining the best feed excitations for a specified antenna geometry is a complex nonlinear problem and it can not be determined if a solution is a local or a global optimum. It appears often, however, that the optimum is quite flat so that small changes in antenna geometry, initial feed excitations input to the optimization procedure, stations locations, etc. may result in quite different feed excitations but very often only in small changes of the antenna performance. It is recommended to input different initial solutions to iterative optimization algorithms and to carry out sensitivity studies of the final solution with respect to excitation errors. The optimization is in general carried out on the copolar field only. In systems which implement frequency re-use by means of orthogonal polarizations, the required cross-polar performance is typically implemented by antenna designs which have low inherent cross polarization.

The following four sections describe a least-squares optimization procedure with a power constraint, the formulation of the minmax synthesis problem, a minmax optimization procedure which utilizes a general-purpose algorithm which recently has been extended to work more efficiently on contoured-beam synthesis problems, and recent progress with minmax or maxmin algorithms which have been developed specifically for contoured-beam reflector antenna synthesis. Many different approaches are described in the literature [e.g., 37-45].

3.2 Least-squares Synthesis

The method, also known as the regularization method, is explained below using a matrix notation [46]. We define the matrix $e = \{e_{ij}\}_{M\times N}$ where e_{ij} is the contribution of element beam j, j = 1,2,...,N, towards synthesis station i, i = 1,2,...,M. Two column vectors $a = \{a_j\}$ and $g = \{g_i\}$ contain the N excitations and the desired field on the M synthesis stations. The number of synthesis stations exceeds in general the

number of element beams and a solution can only be found in a least-squares sense. In order to optimize the minimum coverage area gain, the power input to the antenna must be constrained. Therefore we add the norm of the excitation vector a, which gives the incident power (16), to the least-squares pattern error by a Lagrange multiplier α. The expression to be minimized is then

$$J = (a^T e^T - g^T)W(ea - g) + \alpha a^T a, \tag{22}$$

where the weight matrix W is a diagonal matrix and the superscript "T" denotes conjugate transposition. This gives the following matrix equation for the unknown excitations a

$$(e^T We + \alpha)a = e^T Wg. \tag{23}$$

Initially, we only specify the amplitude of the desired field on the synthesis station by

$$g_i = (G_o p_i f_{oi})^{1/2}, \tag{24}$$

where G_o is a gain normalization constant, p_i the desired relative gain level, and f_{oi} a path length correction factor if flux density rather than gain shall be optimized. As gain normalization constant we can use the peak achievable minimum coverage area gain (1) with a back off. This requires that the angular area Ω of the coverage area be determined.

The relationship between the Lagrange multiplier α and the incident power is established by means of the eigenvalue equation corresponding to (23). The matrix $e^T We$ is Hermitian and the positive real eigenvalues and the eigenvectors may be determined by standard techniques. We expand the unknown excitation vector in the complete basis formed by the eigenvectors. The expansion coefficients are determined in terms of the Lagrange multiplier α which in turn is derived from the power constraint (16).

The specification of the desired field (24) implied a constant pattern phase. To remove this limitation in a heuristic way we include a phase factor $\exp(j\Phi_i^k)$ which is updated iteratively. At the kth step we determine the pattern phase from the excitations derived in the k-1th step by

$$\exp(j\Phi_i^k) = \sum_{j=1}^{N} a_j^{k-1} e_{ij} \Big/ \Big| \sum_{j=1}^{N} a_j^{k-1} e_{ij} \Big|. \tag{25}$$

A new right-hand side of (23) is calculated and a new value of α must be determined for each step in the phase iteration. However, the eigenvalues and the eigenvectors remain the same throughout the iteration. The iteration is terminated when the relative change of the least-squares error (22) decreases to a specified value.

3.3 Formulation of Minmax Synthesis Problem

The least-squares solution discussed above will in many cases be very good except, possibly, on a few critical synthesis stations. A minmax method may improve the performance on the these critical stations generally at the expense of the average performance over all stations. The minmax optimization problem consists of finding the feed excitations a_j so that the realized power gain

$$pw_i = \Big| \sum_{j=1}^{N} a_j e_{spj} \Big|^2 \tag{26}$$

minimizes the maximum value of the residual or pattern error

$$f_i = w_i \left| pw_i/(f_{os} G_o) - p_i \right| \tag{27}$$

over all pattern constraints i, i.e., synthesis stations s and polarizations components p. In (26) and (27), the following notation has been used

e_{spj}	field towards station s in polarization p from element beam j,
f_{os}	path length compensation factor towards station s if flux density is optimized,
p	polarization selector equal to 1 or 2,
p_i	desired relative power level for pattern constraint i. Often $p_i = 1$ for coverage-area constraints, $p_i = 0$ for isolation constraints and p_i equal to a specified gain roll-off function with a back off if a reference pattern shall be enforced,
s	synthesis station number, $s = 1,2,\ldots,M_s$, and
w_i	weight factor used to equalize coverage and isolation constraints.

The residuals for coverage area pattern constraints which exceed the gain goal are set equal to zero.

The minmax optimization problem consists of determining the feed excitation vector a which minimizes the maximum residual

$$F_{minmax} = \max_i f_i. \tag{28}$$

The corresponding least-squares error (22) minimizes the average deviation over all stations. The weight factors w_i and W_i are used to increase the magnitude of the residuals in isolation areas to correspond to the magnitude of the copolar residuals in the service area. If the minimum coverage area gain is MCAG, the maximum sidelobe (cross-polar) level is MSL and the coverage area weight factor is unity, the minmax sidelobe (cross-polar) weight factor

$$w = (G_o - MCAG)/MSL \tag{29}$$

will equalize the residuals. The weight factors behave slightly differently in the minmax and in the least-squares optimization. The best agreement between the two optimizations is obtained if $W_i = w_i^{1/2}$.

3.4 Synthesis by General Minmax Algorithm

The general minmax algorithm is an extension of the iterative method described in [47]. Let the column vector x_k represent the excitation vector at the kth step of the iteration, $f_i(x_k)$ the associated error or residual (27) at the ith pattern constraint, the column vector b_{ik} an approximation to the gradient of the residual with respect to the excitations and the column vector h an increment to the excitation vector. Then,

$$F_k(h) = \max_i (f_i(x_k)+b_{ik}{}^T h) \tag{30}$$

is a linear approximation of the minmax pattern error (28) for small values of $\| h \| = \max|hj|$. At each step of the iteration, the linear subproblem (30) is solved by linear programming subject to a bound on the solution, $\| h \| < \lambda_k$, giving the solution h_k. The vector x_k+h_k is accepted as the new approximate solution if the non-linear objective function has decreased. Otherwise the step is rejected and repeated with a smaller λ_k. The bound λ_k reflects the region near x_k where (30) is a reasonable approximation to the original non-linear problem and it is adjusted automatically during the iteration. The approximations to the gradients are updated using a rank-one formula by Broyden [48],

$$b_{ik+1} = b_{ik}+(f_i(x_k+h_k)-b_{ik}{}^T h_k)/(h_k{}^T h_k)h_k. \tag{31}$$

In a contoured-beam optimization, the number of synthesis stations can be large in particular when a global envelope constraint in enforced as in Section 4.2 or when several contoured beams with common excitations are optimized simultaneously as in Section 4.3. A significant amount of storage is needed for the derivative matrix and large linear programming problems must be solved at each step of the iteration. In practical problems, however, the number of stations where the pattern error (residual) attains the maximum value is small compared to the total number of stations. Therefore at each step, we identify the stations within a specified range of the largest residual. These stations define the overall pattern error F in a neighborhood about x_k and are called the active stations. Working mainly only with the stations within a range of the largest residual, we realize large savings in storage and computing time whereas the convergence properties remain the same. The derivative matrix is stored and updated only for the active stations - typically about 1/5 and less of all stations. The size of the linear programming sub problems are reduced by the same proportion. However, all stations are still checked at each step of the iteration and the active set is updated as required. The gradients of the residuals which are active at both x_k and x_k+h_k are updated by (31). For the newcomers we use a difference approximation since we have no estimate b_{ik} of the gradient at x_k.

In case of a singular problem, the iteration may become slow because the process is caught in a long valley with steep sides [49]. It is a characteristic of a singular problem that with N excitation variables, the number of worst stations where the residuals are equal to the maximum residual will be less than N+1. The number of worst stations is generally considerably less than the number of active stations used in the iteration and less than the number of excitation variables even in the final stages of the iteration. Thus, most contoured-beam synthesis problems appear to be singular. When we decide that the process has been caught, we apply a "special" non-descent iteration to bring the process out of the valley. It can be proven that the extended method theoretically has the same convergence properties as its precessor whereas in practice the new method is considerably faster and can handle much bigger problems within the same computer memory.

3.5 Specialized Minmax Algorithms

The general minmax algorithm provides the maximum degree of freedom in the design. We may choose to optimize only the amplitudes, only the phases or both the amplitudes and the phases of the excitations with only small changes of the software. Also, the location of the element beams may be optimized or degrading effects such as BFN frequency dispersion and BFN random errors could be accounted for. However, the general algorithm does not take advantage of the special properties of a specific contoured-beam synthesis problem as opposed to, e.g., microwave network synthesis problems. The general algorithm does not use the closed-form analytic derivative of residuals which are available in special cases but uses approximations derived by finite differences and Broyden's formula. These approximations are both more time consuming and more inaccurate. They may result in a reduced rate of convergence in the final stages of the iteration, where a large linear programming problem may have to be solved at each step.

A simple minmax algorithm has been proposed by in [50] to be applied in cases with amplitude only or both amplitude and phase excitation optimization. For the excitation normalization (16) with no loss, the derivative of the ith residual f_i (27) with respect to a_j is given by

$$f_i{}'_j = 2[(\sum_{j=1}^{N} e_{ij}a_j)e_{ij}^{\star} - |\sum_{j=1}^{N} e_{ij}a_j|^2 a_j]. \tag{32}$$

The factor $w_i/(f_{oi}G_o)$ has been suppressed. It is further shown in [50] that the gradients ∇f_i are perpendicular to the excitation vector. At each step in the iteration, the active stations are identified and a best search direction is found by solution of a system of linear equations. The length of the incremental vector Δa_k to be added to the excitation vector a_k in the kth step is determined very efficiently by a linear search.

We found that each step in the iteration proceeds extremely fast compared to the general minmax algorithm and that very often good results are obtained. The range of the residuals which define the active stations gradually decreases during the iteration. In our implementation, the method sometimes requires very many iterations to terminate. When the number of active stations becomes equal to the number of excitations, the linear system of equations used to determine the search direction becomes singular and the iteration is forced to terminate.

Recently, the convergence of the method has been considerably improved by determining the best search direction by solving a linear programming problem and improving the linear search [51]. Only the worst stations are considered in the search direction determination. The results indicate that order-of-magnitude saving in computer time may be realized when closed-form derivatives are used instead of

derivative approximations. A possible future extension may be to implement a hybrid algorithm which would use analytic derivatives whenever they are available and derivative approximations otherwise.

4 SYNTHESIS EXAMPLES

The optimization procedures described in Section 3 have been implemented in a synthesis software. This section gives three examples of results obtained with this software package. Other recent design examples includes dual-mode antenna optimization [52] and an offset side-fed Cassegrain antenna with ten contoured beams [53].

4.1 Antenna without Stringent Sidelobe Specifications

4.1.1 Contoured-beam antenna specifications

The optimization of a contoured-beam reflector antenna system for a European Communications Satellite coverage is provided to illustrate the design procedure. The antenna is a transmit antenna with the requirements outlined below:

Frequency band:	10.7-11.7 GHz
Polarization:	RHCP
Min. coverage area gain including BFN loss and spillover:	28 dBi
Max. pattern slope in coverage area:	5 dB/degree
Max. copolar sidelobe level:	-20 dB
Min. cross-polar isolation in coverage area:	30 dB

An area coverage including a 0.2° pointing error was specified. The number of feeds was anticipated to be between 20 and 30 and the antenna envelope should be compatible with the ECS platform and the Ariane launcher. The feed element was chosen to be a small conical horn placed in a hexagonal grid with an element spacing of 1.07 λ at the center frequency. The coverage was composed of four isolated stations and a large area specified by a piece-wise linear contour. The area specification was converted into discrete station specifications by adding synthesis stations inside the piece-wise linear contour. It was found that a spacing between the samples in the uv-plane of

$$\delta_{uv} = 0.01\ \Delta\theta_3, \tag{33}$$

with the element beam beamwidth $\Delta\theta_3$ in degrees, gave a reasonable trade off between accuracy and computation time. This corresponds to about 60 per cent of the maximum Nyquist sampling spacing λ/D and allows for truncation effects near the edge of the coverage, the tilt of the effective aperture plane along the plane of the reflector rim curve, etc. When a large range of element beam beamwidths is being considered, it becomes necessary to use more than one coverage sampling spacing. Figure 10 shows the 58 synthesis stations representing the ECS coverage for the half-power beamwidths 2° and 1.5°. The spacing (33) between the internal samples is 0.015 corresponding to 0.86°. For the half-power beamwidth equal to 1.2°, the sample spacing was reduced to 0.012 or 0.69°, and 81 synthesis stations were obtained.

4.1.2 Initial optimization with analytic element beams

The preliminary design trade-off was carried out with the analytic beam model for the beamwidths $\Delta\theta_3 = 2.0^{\circ}$, 1.5° and 1.2° to determine approximately the reflector size and the number of feed element. In each case, the beam spacings θ_B = 1.2, 1.1 and 1.0 $\Delta\theta 3$ were considered. The initial beam grids set up included all element beams with a distance less than Δ_{BS} from the nearest stations. With Δ_{BS} = 1.25, 1.00 and 0.80 θ_B, a total of 27 initial beam grids were considered. In each case, the flux densities on the Earth were optimized taking into account the path length differences between the satellite and the synthesis stations. An initial set of real excitations was obtained by the least-squares algorithm and used as starting point for the minmax algorithm which also varied the antenna pointing and the beam lattice orientation and spacing. All the excitations are real-valued because the element beams are real-valued.

The configuration with $\Delta\theta_3 = 1.5^{\circ}$, $\Delta_{BS} = 1.65^{\circ}$ and initial value $\theta_B = 1.65^{\circ}$ was found to give the best compromise between antenna complexity and performance. However, the optimum is quite flat. Figure 11 shows optimized the element-beam lay-out, which includes 24 element beams, and the isogain contours of theoptimized contoured beam 1, 2, 3, 5, 10, 15, 20, 25, and 30 dB below peak gain. The number of "active" stations in the minmax optimization is 17, which is well below 24, the number of element beams. This indicates that we are dealing with a singular problem. Only four least-squares residuals exceeded the minmax residual. The associated synthesis stations belonged to the set of "active" stations in the minmax solution. The analytic beam model provides an initial antenna geometry shown in Figure 12 as seen from the dish. The feed lay-out is the image of the element-beam lay-out in Figure 11.

4.1.3 Final optimization with PO/GTD element beams

The initial antenna geometry was further optimized using accurate element beam data determined by PO, GTD and Whittaker reconstruction. These beams are complex-valued so that both feed excitation amplitudes and phases were optimized. The initial least-squares feed excitations were determined using iterative updating of the pattern phase and used as starting point for the minmax excitation optimization. The optimized excitations were inspected for weakly excited feeds. These feed were eliminated and the excitations of the remaining feeds re-optimized. Table 4 summarizes the principal results with an assumed BFN loss of 1.4 dB.

	Least-squares	Minmax		
	Min flux	Min flux	Min gain	Spillover
Analytic beam model:				
all 24 beams	27.85	28.31	28.09	-1.02
PO/GTD beams from GRASP:				
all 24 beams	28.21	28.40	28.17	-1.21
-beams 18, 20 and 22	27.81	27.97	27.73	
-beams 20 and 22	28.15	28.26	28.02	

Table 4. Results of ECS optimizations. Levels in dB and dBi.

Several observations may be made. Firstly, the least-squares solution is in all cases quite good compared to the much more time consuming minmax solution. Secondly, the prediction obtained by analytic element-beam model is very close to the one obtained using a much more accurate element-beam model. The element-beam model is quite sensitive to the value assumed for the feed quality number $d_e\theta_{10}$. Thirdly, deleting feed or element beam 18 has a significant impact on the solution so that caution should be exercised when feeds are eliminated. The optimization should begin with a generous number of feeds which gradually are removed. Each time, the excitations of the remaining feeds must be re-optimized. Figure 13 and 14 show the element beam half-power contours and the contoured-beam isogain curves derived by means of PO, GTD and Whittaker reconstruction at 10.7 and 11.7 GHz. The decrease of element-beam half-power beamwidth with increasing frequency may be noted. The agreement with the analytic beam model in Figure 11 is good except for a slight widening of the low level contours in Figure 13 and 14 due to the scan aberrations neglected in the analytic element beam model.

The finite tolerances of the BFN, mismatches, frequency dispersion in the BFN and mutual coupling will cause the realized feed excitations to deviate from the optimum values determined by the synthesis software. Excitation errors not accounted for will degrade the antenna performance. Some of the degrading effects may be included in the pattern optimization. Thus, it has become common practice to carry out the excitation optimization simultaneously at both edges of the frequency band if the antenna is required to operate over any significant bandwidth. Table 5 summarizes the results of computer simulations of the effect of random excitation errors on the minimum coverage area gain. For the range of errors and the configuration considered, amplitude errors seem to be more serious than phase errors. For practical applications, the average excitation error should be less than a few tenth of a dB in amplitude and 5° in phase.

Peak excitation		Gain degradation due to		
amplitude error	phase error	amplitude only	phase only	amplitude and phase
0.3 dB	3°	0.19 dB	0.00 dB	0.17 dB
0.6 dB	6°	0.32 dB	0.09 dB	0.44 dB
0.9 dB	9°	0.61 dB	0.16 dB	0.66 dB
1.2 dB	12°	1.16 dB	0.24 dB	0.88 dB
1.5 dB	15°	1.12 dB	0.32 dB	-

Table 5. Degradation of the minimum coverage area gain as a function of random excitation amplitude and phase errors.

4.1.4 Measurements on array-fed contoured-beam antenna

In the European Space Agency's COBRA (contoured-beam reflector antenna) program, the prototype of the antenna described above was designed, manufactured, integrated and tested [54]. The rms deviation of the measured amplitude and phase excitations from the nominal values are indicated in Table 6 at the edges and the center of the frequency band.

Frequency	Amplitude	Phase
10.7 GHz	0.58 dB	5.6°
11.2 GHz	0.24 dB	5.9°
11.7 GHz	0.59 dB	6.5°

Table 6. Rms deviations of excitations at feed ports.

Figure 15 shows in full line the measured copolar contours 1, 3, 5, 10, 15 and 20 dB below peak gain at the edges and the center of the frequency band. The calculated contours 3 and 20 dB below peak gain are superimposed in dotted line. The agreement is fair apart from 11.7 GHz where strong mutual coupling effects between the small circularly polarized feeds not accounted for in the analysis are believed to degrade the minimum coverage area gain from 28.1 to 25.6 dBi at Barcelona. The cross-polar discrimination was better than 28 dB at the design frequency [55].

4.2 Impact of Global Sidelobe Constraint on Frequency Re-use Antenna System

The interference between the different satellite communications systems has in the past been controlled by coordination such that any new system would not obstruct the existing systems. In the future, it likely that communications satellite antennas must meet reference pattern specifications similar to those which already apply to earth-station antennas and direct-broadcast satellite antennas. This will conserve the finite available frequency bandwidth and geostationary arc. Such antenna reference patterns are difficult to define for a contoured beam, which may be of a complicated shape. They will complicate the antenna design process as many more synthesis stations must be considered. This example investigates the potential impact of a global pattern envelope constraint on an antenna similar to the Intelsat VI 4-GHz hemi/zone antenna already considered in Section 2.2. This antenna already meets stringent sidelobe requirements in the adjacent frequency re-use coverage areas.

4.2.1 Sidelobe envelopes of current antennas

Figure 16 shows the calculated isogain contours at MCAG (the minimum coverage area gain) and 27, 30 and 33 dB below MCAG for the Intelsat VI Indian Ocean region (IOR) zone 2 beam at the lower edge of the 4-GHz band where the problems with sidelobes and the roll-off of the pattern from the coverage area are the most severe. The four spatially isolated zone beam coverages are indicated by the four piece-wise linear composite coverages. We note that fairly high sidelobes extend from zone 2 towards zone 4. The figure also shows a number of linear segments which extend from about 1° inside the zone beam coverage to about 7° outside. Figure 17 shows the superimposed cuts along these gain roll-off pattern traces. The horizontal angular scale gives the distance from the point where a gain roll-off pattern trace intersects the MCAG contour. No traces away from the Earth are considered. In these directions, the sidelobes are much higher. The full (dotted) line near 0° represents the maximum (minimum) envelope of the pattern traces. The full (dotted) line further away indicates the envelope of most (all) of the traces. The dot/dash line indicates the additional degradation caused by the calculated line length dispersion in the beam-forming network. In a practical antenna, several other imperfections will degrade the performance.

4.2.2 Gain roll-off optimization

Figure 18 indicates the locations of the synthesis stations used in the optimization. Initially, no gain roll-off stations (indicated by 7) were used. The optimization then uses 176 stations and 36 beams. It is carried out at both band edges simultaneously so that the number of pattern constraints is twice the number of stations. Figure 19 shows the resulting gain contours at the lower edge of the band with isogain contours at the MCAG level and 27, 30 and 33 dB further down. The levels do not include losses and give directivity. The minmax solution is superior to the least-squares solution on the worst stations and improves in this case the MCAG level by 1.2 dB. The sidelobes are higher than in Figure 16 but the fit to the desired composite coverages is tighter.

Figure 20 shows the optimized gain contours obtained for carefully selected sets of gain roll-off stations. Initially, gain roll-off stations were set up from the edge of the composite coverage with a maximum tolerable field level calculated from a gain roll-off reference curve. This may lead to the specification of critical synthesis stations which with the minmax algorithm would destroy the overall antenna performance. With the gain roll-off curve used in the optimization, it was found that no gain roll-off station should be placed closer to the coverage area than 3° for this zone beam. Also, no stations should be placed in (the polar) regions where no feed is available for controlling the pattern. The resulting 265 synthesis stations are shown in Figure 18 with deleted gain roll-off stations marked by circles. The sidelobe performance has been considerably improved while the MCAG level has been reduced by only a few tenth of a dB. However, the gain slope of the edge of coverage has been degraded. Increasing the number of feeds slightly will improve the MCAG level and the gain slope but seem to have little impact on the sidelobe performance.

4.3 Reconfigurable Antennas with Shared Excitations

Increasing satellite lifetimes of 10 to 14 years have accelerated the need for the same spacecraft to be able to provide different services over different coverages at different times. The full range of possible future requirements to a spacecraft cannot be anticipated for such a long time and can probably only be met by a fully reconfigurable antenna system. Such antenna systems do not require any special synthesis software as the antenna may be optimized separately for each coverage requirement. However, they are excessively complex and expensive to implement, and in practice, less complex and more reliable systems with limited reconfigurability are implemented, e.g., as in the Intelsat C-band hemi/zone antenna systems by means of switches. Such a case is considered in this section. A set of shared excitations is optimized to meet the Intelsat VI Atlantic and Indian Ocean region zone 2 beam coverage requirements. The shared excitations would then by switches be combined with separate sets of unique excitations for each ocean region. In each ocean region, the sidelobe requirements in the adjacent zone beam coverages are included.

Figure 21 and 22 show the 185 synthesis stations used for the Indian Ocean region zone 2 beam optimization and the 218 synthesis stations used for the Atlantic Ocean region zone 2 beam optimization. The minimum coverage area gain is optimized subject to meeting a sidelobe isolation of more than 30 dB in the adjacent zone beam coverages. First, the two zone beams will be optimized independently of each other. Then, the two zone beams will be optimized simultaneously sharing many element beams with identical excitations.

4.3.1 Optimization with separate excitations

A initial optimization is carried out for each coverage separately. Figure 23 and 24 show the contour plots of the two optimized zone beams. The optimizations are carried out using the analytic element-beam model. Isogain contours are shown through the minimum coverage area gain level and 20, 25, 30 and 35 dB further down. The minmax pattern error is slightly larger for Indian Ocean region zone beam.

4.3.2 Optimization of shared excitations

At this stage, the two sets of excitations obtained by the optimization of each ocean region separately are inspected and each excitation is assigned to one of the following three BFNs:

BFN 1 generates the excitations only used by the Indian Ocean region zone beam,

BFN 2 which generates the excitations only used by the Atlantic Ocean region zone beam, and

BFN 3 which generates the excitations which are shared for the two zone beams.

The total number of element beams is 46. The breakdown of the element beams and the excitations between the two zone beams and the three BFNs is given in Figure 25. The combined synthesis problem consists of 61 different excitations and 403 synthesis stations. In this case, the synthesis is carried out so that the power division between BFN 1 and BFN 3 for the Indian Ocean region zone beam and between BFN 2 and BFN 3

for the Atlantic Ocean region zone beam are optimized by the program. Figure 26 and 27 show the contour plots of the two optimized zone beams with shared excitations for the analytic element-beam model. The minimum coverage area gain (or rather directivity) and the minimum sidelobe isolation are listed in Table 7 for the case with separate excitations and with shared excitations. The table gives data obtained both with the analytic element beams and with element beams calculated by an accurate reflector analysis program.

	Analytic element beams		PO/GTD element beams	
	Separate	Shared	Separate	Shared
Min. gain:				
Indian 2	26.18 dBi	26.19 dBi	25.91 dBi	26.00 dBi
Atlantic 2	25.58 dBi	25.36 dBi	25.32 dBi	25.17 dBi
Min. isolation				
Indian 2	33.09 dB	33.10 dB	32.29 dB	32.55 dB
Atlantic 2	33.81 dB	33.10 dB	33.09 dB	32.55 dB

Table 7. Performance with separate and with shared excitations.

Thus, no degradation has taken place for the Indian Ocean region zone beam which had the largest minmax residual. The performance of the Atlantic Ocean region zone beam has been "equalized" so that minmax residuals now are identical for the two zone beams. The agreement between the results obtained by analytic beams and PO/GTD beams is surprisingly good.

5 SHAPED CONTOURED-BEAM REFLECTOR ANTENNAS

In this Section we consider an alternative contoured-beam reflector antenna requiring only a single feed. The surface of the offset reflector is shaped so that the modified wavefront along the original reflector surface provides the desired wavefront. The deviation from the paraboloidal surface is so small that the amplitude distribution along the original reflector surface remains essentially undistorted and only negligible cross polarization is generated. The similar surface shaping technique has previously been utilized for a japanese experimental Ka-band communications satellite [56, 57].

5.1 Optimization of Aperture Phase Distribution

In our version of the synthesis technique, the phase of the aperture field is expanded into Zernike or circle polynomials, i.e.,

$$\Phi(\rho,\phi) = \sum_{n=1}^{N} \sum_{m=-n}^{n} c_{mn} e^{jm\phi} R_{mn}(\rho), \tag{34}$$

where ρ and ϕ are the polar aperture coordinates and $c_{-mn} = c_{mn}^{*}$. The Zernike or circle polynomials find use in optics for orthogonal expansions in circular apertures. The polynomials are simply related to the scan aberrations such as spherical aberrations, astigmatism, coma, etc. [59]. Rapid calculation of circle polynomials is possible by recursion. The expansion coefficients c_{mn} take the role of the feed excitations in the array-fed reflector. For a particular set of expansion coefficients, the field is calculated on all stations by a simplified and fast physical-optics integration across the deformed reflector surface. The general minmax routine described in [47] is used to determine an set of expansion coefficients which optimize the gain on all synthesis stations. The procedure has also been utilized to synthesize elliptical beams with very low sidelobes [58].

When an optimum phase distribution has been determined, the shaped reflector is derived by a ray-tracing procedure from the offset paraboloid used as initial solution. The optimization of the phase expansion coefficients is numerically more difficult than feed excitation optimization. The element beams are almost orthogonal and varying one feed excitation affects only few stations. The phase expansion coefficients, on the other hand, interact nonlinearly and varying one coefficient will affect all stations but by very small amounts.

The reflector shaping procedure has been applied to the ECS coverage already considered in Section 4.1. The design was carried out at 11.2 GHz using the offset paraboloidal reflector similar to the one considered in Section 4.1 as starting point. An optimized surface deformation which generates the contoured beam is indicated by the three-dimensional plot in Figure 28. The optimized shaped reflector antenna system was analyzed by physical optics. Figure 29 shows the calculated copolar isogain contours at the edges of the frequency band 1, 2, 3, 5, 10, 19, 20, 21 and 30 dB below peak gain. The calculated minimum coverage area directivity of 28.81, 29.21 and 28.84 dBi at 10.7, 11.2 and 11.7 GHz compare favorably with the corresponding minimum coverage area gain values of 27.93, 28.18 and 28.10 dBi of the array-fed reflector. No attempt was made to suppress the sidelobes. The antenna was assumed to be circularly polarized. The cross-polar performance was found to be very sensitive to the cross-polar performance of the feed. Even low levels of feed cross polarization would generate "hot spots" of cross polarization in the reflector far field.

5.2 Measurements on Shaped Contoured-beam Reflector

The shaped reflector contoured-beam reflector was re-optimized with a smaller offset angle θ_o to allow the use of a linearly polarized feed horn which was available. A modified aperture phase expansion was determined with significantly lower sidelobes at the cost of a reduced minimum coverage area gain. The shaped reflector was manufactured for the scaled frequency band 16.4 - 18 GHz in order to reduce the reflector size to be within the limitations set by the surface machining equipment available. The antenna measurements were carried out at the spherical near-field test range at the Technical University of Denmark. During the antenna measurements, the feed horn was found to move and it was necessary to

strengthen the feed support structure. Figure 30 compares over an extended angular range the measured and the calculated co- and cross-polar pattern cuts along the planes of maximum and of minimum beamwidth. The agreement is excellent apart from the angular region $7^{\circ} < \theta < 14^{\circ}$ in the plane of the narrow beamwidth, where scattering from the enlarged feed support structure appears. The measured minimum coverage area directivity of 27.3 dBi occurs at the high end of the band where the predicted value is 28.1 dB. The shaped reflector antenna holds significant advantages over the array-fed reflector antenna for applications where no reconfigurability and only a single beam is required. No BFN is required and complicated mutual coupling effects in the feed array are avoided. The BFN and the spillover losses are absent or drastically reduced so that the gain delivered can be higher. Shaped reflector antenna systems are in rapid development and major future progress is likely with the recent advent of rigorous methods [60]. Work is also being carried out on dual reflectors [61].

6 DUAL REFLECTOR SYSTEMS WITH SMALL SCAN DEGRADATIONS

The dual offset Cassegrain or Gregorian reflector systems permit cancellation of the cross polarization for a linearly polarized on-axis beam [62]. This is achieved if the axes of the feed, the subreflector and the main reflector are adjusted according to the condition

$$\tan \gamma/2 = 1/M \tan \phi/2 \qquad (35)$$

where γ is the angle from the main reflector axis to the subreflector axis and ϕ the angle from the subreflector axis to the feed axis (see Figure 31). The value of the subreflector "magnification" M determines the subreflector type:

(1) $M > 1$: The subreflector is the convex branch of a hyperboloid with the eccentricity
$e = (M + 1)/(M - 1)$.
This is a conventional dual offset Cassegrain.

(2) $0 < M < 1$: The subreflector is the concave branch of a hyperboloid with
$e = (1 + M)/(1 - M)$.
This is either the front-fed or the side-fed dual offset Cassegrain discussed below.

(3) $M < -1$: The subreflector is an ellipsoid with
$e = (M + 1)/(M - 1)$.
This is a conventional dual offset Gregorian.

Dual offset reflector configurations which fulfil the condition (35) has no first-order astigmatism which otherwise is the dominant scan aberration in offset reflector antennas [30]. Conventional compensated dual offset Cassegrain and Gregorian antennas, $M > 1$ and $M < -1$ above, are difficult to design with no blockage for large scan angles, and the feed array is larger than in the case where the main reflector is used as single reflector. These problems are reduced when $0 < M < 1$ for the two different configurations in Figure 32, which both are designed for a $\pm 10^{\circ}$ scan. In Figure 32a, the feed array is located in front of both the subreflector and the main reflector and the system has been termed it the front-fed offset Cassegrain (FFOC) antenna system [63]. In the second configuration in Figure 32b the feed array and the subreflector are placed on either side of the main reflector. This system has been termed the side-fed offset Cassegrain (SFOC) antenna system [53]. Both the FFOC and the SFOC have unique scan properties over the full $\pm 10^{\circ}$ field-of-view due to the large focal length of the main reflector. The large field-of-view requires that the subreflector size be comparable to the main reflector size. For contiguous Earth coverage, the feed array size is excessive and the systems may not be competitive to an array antenna. However, the inherent property of a reflector antenna system of associating single feeds with high-gain spot beams makes the configurations shown in Figure 32 very attractive candidates for meeting partial Earth coverage requirements with many high-gain beams.

6.1. Scan Properties of the FFOC and the SFOC

Figures 33 and 34 show the calculated principal co- and cross-polar pattern cuts for secondary beams radiated by small linearly polarized conical horns placed at the locations which are corresponds to beams on axis and with 10° downward scan, 10° upward scan and 10° lateral scan. The diameters of the feeds are $1.8\ \lambda$ (FFOC) and $2.2\ \lambda$ (SFOC) and correspond to a beam spacing of 92 per cent of the beam width. This is close to the spacing which gives the highest gain at the cross-over level for multi-beam applications where each beam is radiated by a single horn. In each case, the feed location is optimized to minimize the phase errors and the feed axis is aligned so that the central ray hits the center of the main reflector surface. For both the FFOC and the SFOC, the diameter D of the projected aperture is $120\ \lambda$. The small feeds provide only a slight aperture taper. This situation exhibits both the highest sidelobes and the largest scan losses. The calculated peak directivity, peak sidelobe level and peak sidelobe level for the two configurations are given in Table 8. The peak directivity is broken up into a number of efficiencies

$$G_{sc} = \eta_{sp}\, \eta_{ar}\, \eta_{ap}\, G_o \qquad (36)$$

where

η_{sp} is the spillover efficiency, (the fraction of the feed power which hits the main reflector),
η_{ar} is the relative projected area (the ratio of the areas obtained by projecting the main reflector rim into a plane perpendicular to the direction of the scanned beam and into a plane perpendicular to the direction of the on-axis beam),
η_{ap} is the aperture efficiency including loss due to phase errors, amplitude taper and cross polarization. (This loss in dominated by the phase errors associated with the scan as the aperture illumination is almost uniform), and
G_o is the peak achievable directivity $\pi D/\lambda$ (51.53 dBi for $D = 120\ \lambda$).

Beam direction	η_{sp} dB	η_{ar} dB	η_{ap} dB	Directivity dBi	Sidelobe dB	Cross-pol dB
FFOC:						
on axis	-4.62	0	-0.03	46.88	-28.38	-48.68
10^{o} downward	-3.48	+0.75	-2.28	46.52	-39.63	-38.06
10^{o} upward	-5.87	-1.07	-1.55	43.04	-23.14	-35.52
10^{o} sideward	-4.78	-0.07	-0.63	46.05	-33.63	-37.40
SFOC:						
on axis	-5.09	0	-0.02	46.42	-28.01	-54.78
10^{o} downward	-4.68	+0.34	-0.36	46.83	-33.28	-40.20
10^{o} upward	-5.72	-0.52	-0.24	45.05	-29.88	-37.49
10^{o} sideward	-5.29	-0.07	+0.03	46.20	-30.25	-41.56

Table 8. Peak directivity budget and peak sidelobe level of FFOC and SFOC.

Due to the relatively small feed size and small angle subtended by the subreflector rim, the feed spillover is large. The large scan causes a significant change of the relative projected area. As the main reflector is closer to vertical for the SFOC than for the FFOC, the area loss for upwards scan is smaller for the SFOC. The aperture efficiency is, except for the on-axis beam, dominated by phase errors, i.e., scan aberrations. We see that the effect of these phase errors is smaller for the SFOC. The smaller scan aberrations of the SFOC also follow from the pattern in Figures 33 and 34. The sidelobes and the cross polarization are lower for the SFOC than for the FFOC. As the aperture diameter increases, e.g., to 240λ, the superiority of the SFOC with respect to electric performance is accentuated. For both configurations, the scan losses are higher for beam scanning in the plane of symmetry than in the perpendicular plane. In the plane of symmetry, the scan losses due to phase errors are slightly higher for downward scan, but they are compensated by reduced spillover and area losses. In a practical design, the antenna axis should be repointed to equalize the overall scan loss in all directions or give preference to critical areas in the coverage. Comparisons with the single offset paraboloidal reflectors show that the FFOC achieves similar scan performance as a single offset parabola with an f/D ratio equal to about 2.6. The SFOC is comparable to a single offset parabola with an f/D of about 5.6.

More details including the initial design of a feed array to generate 10 contoured beams out of the SFOC are given in [53].

7 CONTOURED-BEAM ARRAY ANTENNAS

Table 2 indicated the significant growth of the feed array size for each new INTELSAT spacecraft series. If the trend towards larger and radiating apertures and f/D ratios continues, the feed array size will ultimately exceed the reflector size and the antenna mass and volume requirements will have a tremendous impact on spacecraft design and launch cost. Thus, it may become advantageous to "discard the reflector and turn the feed array towards the Earth" and use it as a directly radiating array.

7.1 Array Excitation Optimization with Pencil Element Beams

We consider the planar array configuration in Figure 35. It consists of N_e elements in a hexagonal lattice. We define N_b element beams radiated by the array in a hexagonal lattice over the field-of view shown in Figure 36. The half-power beamwidth of the element beams is determined by the array diameter D and is for a uniform array illumination approximately $\Delta\theta_3 = \lambda/D$. The optimization of the array excitations to meet specified coverage and isolation requirements is carried out by the algorithms discussed in Section 3 but indirectly by optimizing the excitations of the element beams. Then, the array excitations are calculated from the element-beam excitations. The optimization via the element beams is much more efficient than a direct optimization of the array excitations because

(1) the number of element beam is in general much less then the number of array elements, and
(2) the element beam are almost orthogonal to each other over the far-field pattern in the sense their pattern only overlap little as opposed to the array element patterns, which overlap completely. As a result, the optimization is a more well behaved problem.

The number of array elements for a given aperture size is determined by the requirement that no grating lobes fall in the field-of-view. The antenna designer may choose the element-beam positions independently for each coverage area of a multi-beam array antenna. This is not possible for a reflector antenna. The aperture size in wavelengths and the angular extent of the coverage area determines the number of the degrees of freedom of the synthesis problem [64]. In most cases, the beam spacing can be chosen a little larger than the beam width as in the case of a reflector antenna. No advantages are gained by choosing the beam spacing significantly smaller than the beam width.

Figure 37 shows an optimized contoured beam for an array consisting of 169 conical horns with a diameter of 2.84 λ. The array diameter is identical to the size of the INTELSAT VI hemi/zone reflector. By gradual removal of weakly excited array elements followed by re-optimization of the remaining excitations, the number of array elements can be reduced significantly. A full account of the design procedure and many design cases have been given in [65].

8. ACKNOWLEDGEMENTS

This paper is based on work performed, in part, for the European Space Technology and Research Centre (ESTEC) of the European Space Agency and, in part, under the sponsorship and technical direction of the International Telecommunications Satellite Organization (INTELSAT). Any views expressed are not necessarily those of INTELSAT. The author wishes to thank R Jorgensen, TICRA, K Pontoppidan, TICRA, PE Frandsen, TUD, and Antoine Roederer, ESTEC. The author is grateful to former colleagues at INTELSAT in particular to DK McCarthy, W Bornemann and WJ English.

9 REFERENCES

[1] "Radio Regulations", ITU, Geneva, 1982

[2] KG Schroeder (1972), "Characteristics and applications of multi-beam spacecraft antennas", 4th AIAA Comm. Sat. Syst. Conf., Washington, D.C., paper No. 72-530

[3] P Foldes (1982), "Recent advances in multibeam antennas", 11th European Microwave Conf., Amsterdam, 59-72

[4] LJ Ricardi (1982), "Multiple beam antennas", Ch. 6 in AW Rudge, K Milne, AD Olver and P Knight (Eds.), "The Handbook of Antenna Design. Volume 1". London: Peter Peregrinus Ltd.

[5] JL Butler (1966), "Digital, matrix and intermediate-frequency scanning", Ch. 3 in RC Hansen (Ed.), "Microwave Scanning Antennas. Volume 3". New York: Academic Press, 241-268

[6] AR Dion (1982), "Lens antennas", Sect. 3.7 in AW Rudge, K Milne, AD Olver and P Knight (Eds.), "The Handbook of Antenna Design. Volume 1". London: Peter Peregrinus Ltd.

[7] HHS Luh, TM Smith and WG Scott (1982), "A dual-band TEM lens for a multiple beam antenna", IEEE Trans. Antennas Propagat., Vol. AP-30, 224-229

[8] F Taormina, DK McCarty, T Crail and D Nakatani (1976), "INTELSAT IVA communications antenna - frequency re-use through spatial isolation", Intl. Conf. on Communications, Philadelphia, 4.10-4.14

[9] CC Han, AE Smoll, HW Bilenko, CA Chuang and CA Klein (1976), "A beam-shaping multifeed offset reflector antenna", 6th AIAA/CASI Comm. Sat. Syst. Conf., Montreal, 245-249

[10] EW Matthews, CL Cuccia and MD Rubin (1979), "Technology considerations for the use of multiple beam antenna systems in communications satellites", IEEE Trans. Microwave Theory Tech., Vol. MTT-27, 998-1004

[11] MF Caulfield, FA Taormina, BM Flynn, SO Lane, TM Paige and VE Cascia (1982) "INTELSAT VI antenna system design and development", Conf. Large Space Antenna Syst. Tech., NASA Langley, 743-765

[12] SO Lane, MF Caulfield and FA Taormina (1984), "INTELSAT VI antenna system overview", 10th AIAA/CASI Comm. Sat. Syst. Conf., Orlando

[13] WJ English (1980), "Improving future communications satellite antenna designs", 8th AIAA/CASI Comm. Sat. Syst. Conf., Orlando, 464-470

[14] DF DiFonzo (1982), "Evolution of satellite antennas", IEEE Intl. Symp. Antennas Propagat., Albuquerque, 358-361

[15] P Neyret (1984), "Antenna technology at INTELSAT", Journées Internationales de Nice sur les Antennes, Nice, pp. 69-90.

[16] WVT Rusch (1982), "Reflectors with contoured beams", Sect. 3.5 in AW Rudge, K Milne, AD Olver and P Knight, "The Handbook of Antenna Design. Volume 1". London: Peter Peregrinus Ltd.

[17] B Vidal Saint Andre and P Neyret (1980), "The application of single reflector multi-feed antennas to direct T.V. satellites", 10th European Microwave Conf., Warszaw, 90-94

[18] A Roederer(1984), "Antennes pour satellite de télévision directe", Journées Internationales de Nice sur les Antennes, Nice, 154-167

[19] H Soule, J Rosen, J MacGahan, J Dumas and C Profera (1984), "Shaped-beam antenna for direct broadcast satellites", 10th AIAA/CASI Comm. Sat. Syst. Conf., Orlando

[20] V Galindo-Israel, Y Rahmat-Samii, W Imbriale, H Cohen and R Cagnon (1984), "A CONUS time zone DBS antenna system with single polarization", IEEE Intl. Symp. Antennas Propagat., Boston, 143-146

[21] K Pontoppidan (1979), "Pattern prediction methods for high performance single and dual reflector antennas", Final Report S-101-02 on ESTEC Contract 3629/78/NL/AK, TICRA A/S, Copenhagen, Denmark

[22] SW Lee and Y Rahmat-Samii (1981), "Simple design formulas for designing an offset multibeam parabolic reflector", IEEE Trans. Antennas Propagat., Vol. AP-29, 472-478

[23] A Saitto (1981), "Gain-bandwidth product and other reflector antenna relationships", ESA Journal, Vol. 5, 249-258

[24] GAE Crone, A Jorgensen and AG Roederer (1984), "Comparison of contoured beam reflector antenna designs for improved European coverage", IEEE Intl. Symp. Antennas Propagat., Boston, 792-795

[25] PD Patel and KK Chan (1985), "Optimization of contoured beams for satellite antennas", Proc. IEE, Vol. 132, Pt. H, 400-406

[26] Y Rahmat-Samii and SW Lee (1983), "Directivity of planar array feeds for satellite reflector applications", IEEE Trans. Antennas Propagat., Vol. AP-31, 463-470. See also correction in Vol. AP-32, 762

[27] PJB Clarricoats, SM Tun and CG Parini (1984), "Effects of mutual coupling in conical horn arrays", Proc. IEE, Vol. 131, Pt. H, 165-171

[28] L Lewin (1975), "Expression for decoupling in multiple-beam antennas", Electr. Ltrs., Vol. 11, 420-421

[29] PJ Wood (1986), "Some extensions of the beam orthogonality concept for multi-beam antennas", IEEE Montech '86 Conf. Antennas & Comm., 310-313

[30] C Dragone (1982), "A first-order treatment of aberrations in Cassegrainian and Gregorian antennas", IEEE Trans. Antennas Propagat., Vol. AP-30, 331-339

[31] J Ruze (1965), "Lateral-feed displacement in a paraboloid", IEEE Trans. Antennas Propagat., Vol. AP-13, 660-665

[32] TS Chu and RH Turrin (1973), "Depolarization properties of offset reflector antennas", IEEE Trans. Antennas Propagat., Vol. AP-21, 339-345

[33] NA Adatia and AW Rudge (1975), "Beam-squint in circularly polarised offset reflector antennas", Electr. Ltrs, Vol. 11, 513-515

[34] EA Ohm (1979), "Multibeam satellite antenna with optimized polarization distribution and full U.S. coverage", IEEE Intl. Symp. Antennas Propagat., Seattle, 266-269

[35] J Jacobsen (1977), "On the cross polarization of asymmetric reflector antennas for satellite applications", IEEE Trans. Antennas Propagat., Vol. AP-25, 276-283

[36] MJ Gans and RA Semplak (1975), "Some far field studies of an offset launcher", BELL Syst. Tech. J., Vol. 54, 1319-1340

[37] TS Bird (1982), "Contoured-beam synthesis for array reflector antennas by field correlation", Proc. IEE, Vol. 129, Pt. H, 293-298

[38] JF Bull, P Kalata and CE Profera (1982), "Application of the method of steepest descent optimization to the design of shaped beam antennas", IEEE Intl. Symp. Antennas Propagat., Albuquerque, 600-603

[39] C Dedeban, M Minoux and P Brachat (1984), "Un logiciel pour l'optimisation du diagramme de rayonnement d'une antenne à faisceau conforme", Journées Internationales de Nice sur les Antennes, Nice, 56-63

[40] S Mano, T Katagi and T Tsutsumi (1984), "Pattern synthesis of array fed reflector antennas", Electronics and Communications in Japan, vol. 67-B, No. 7, 38-45
[41] K Shamsaifar and M Calvo (1986), "Contoured beam synthesis for a small number of feeds by optimizing their position and excitation", IEEE Intl. Symp. Antennas Propagat., Philadelphia, 727-730
[42] RFE Guy (1985), "A synthesis technique for array antennas of general shape with various aperture constraints", 4. Intl. Conf. Antennas Propagat., Warwick, 35-39
[43] GT Poulton (1986), "Antenna power pattern synthesis using method of successive projections", Electr. Ltrs., Vol. 22, 1042-1043
[44] AI Zaghloul and DK Freeman (1986), "Phased array synthesis for shaped beams using power matrix method", IEEE Intl. Symp. Antennas Propagat., Philadelphia, 177-180
[45] D Kawabata, M Ueno, T Morroka, T Chiba, R Kawashima, W Bornemann and WJ English (1986), "Synthesis of spacecraft antennas by use of Fourier transform method", IEEE Intl. Symp. Antennas Propagat., Philadelphia, 719-722
[46] JR Mautz and RF Harrington (1975), "Computational methods for antenna pattern synthesis", IEEE Trans. Antennas Propagat., Vol. AP-23, 507-512
[47] K Madsen (1975), "Minimax solution of non-linear equations without calculating derivatives," Math. Prog. Study, Vol. 3, 110-126
[48] CG Broyden (1965), "A class of methods for solving non-linear simultaneous equations", Mat. of Comp., Vol. 19, 577
[49] K Madsen and H Schaer-Jacobsen (1976), "Singularities in minimax optimization of networks", IEEE Trans. Circuits and Systems, Vol. CAS-23, 456-460
[50] CA Klein (1984), "Design of shaped-beam antennas through minimax gain optimization", IEEE Trans. Antennas Propagat., Vol. AP-32, 963-968
[51] L Daemen (1986), "Etude d'optimisation d'antennes multisources", M.Sc.EE Thesis, Faculté des Sciences Appliquées, Université de Liège
[52] P Foldes, F Rispoli and R Jorgensen (1986), "Antenna design for the Eutelsat program", IEEE Intl. Symp. Antennas Propagat., Philadelphia, 165-168
[53] R Jorgensen, P Balling and WJ English (1985), "Dual offset reflector multi-beam antenna for international communications satellite applications", IEEE Trans. Antennas Propag., Vol. AP-33, 1304-1312.
[54] S Adatia, P Balling, B Claydon, P Ingvarson and A Roederer (1980), "A European contoured beam reflector antenna development", 10th European Microwave Conf., Warsaw, 95-99
[55] DJ Brain, A Brunt, WT Costello, Y Kol, MS Sidat and R Waugh (1985), "A circularly-polarised antenna for contoured beam coverage of Europe", 4th Intl. Conf. Antennas Propagat., Norwich, 536-540
[56] T Katagi and Y Takeichi (1975), "Shaped-beam horn reflector antenna", IEEE Trans. Antennas Propagat., Vol. AP-23, 756-763
[57] H Kumasawa, T Katagi and T Ebisui (1983), "Shaped-beam horn reflector antennas with aperture phase distribution modified by a plane wave", IEEE Intl. Symp. Antennas Propagat., Houston, 338-341
[58] R Jorgensen (1980), "Coverage shaping of contoured-beam antennas by aperture field synthesis", Proc. IEE, Vol. 127, Pt. H, 201-208
[59] S Cornbleet (1976), "Microwave Optics". London: Academic Press, 380-383
[60] BS Westcott (1983), "Shaped Reflector Antenna Design". Letchworth, Hertfordshire, England: Research Studies Press Ltd.
[61] N Adatia and S Tun (1986), "Shaped dual offset reflector antennas for contoured beam spacecraft applications", Journées Internationales de Nice sur les Antennes, Nice, 148-153
[62] H Tanaka and M Mizusawa (1975), "Elimination of cross-polarization in offset dual-reflector antennas", Electronics and Communications in Japan, Vol. 58-B, No. 12, 71-78
[63] S Makino, Y Kobayashi, S Urasaki and T Katagi (1984), "Front fed offset Cassegrain type multibeam antenna", National Convention of IECEJ
[64] JT Mayhan (1976), "Nulling limitations for a multiple beam antenna", IEEE Trans. Antennas, Propagat., Vol. AP-24, 769-779
[65] W Bornemann, P Balling and WJ English (1985), "Synthesis of spacecraft array antennas for Intelsat frequency reuse multiple contoured beams", IEEE Trans. Antennas Propagat., Vol. AP-33, 1186-1193

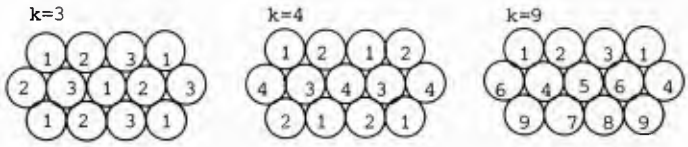

Figure 1 Multi-beam beam topologies for frequency re-use.

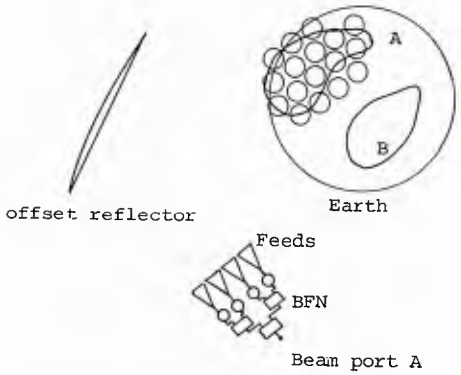

Figure 2 Contoured beam from offset reflector with feed array and BFN

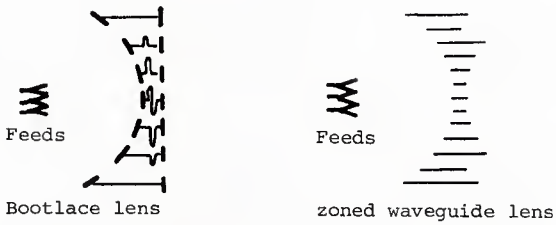

Figure 3 Microwave multi-beam lens antennas

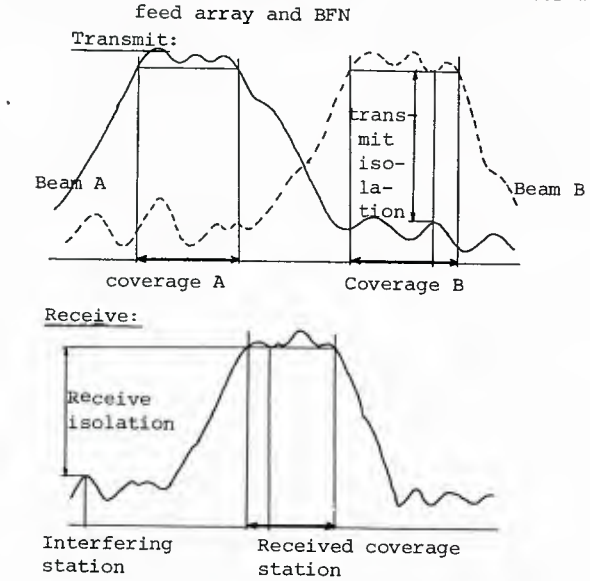

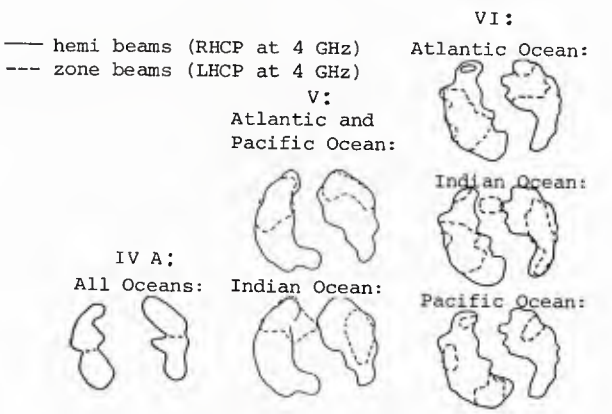

Figure 5 Growth in the complexity of the INTELSAT spacecraft hemi/zone coverages

Figure 4 Definition of isolation for transmit and receive contoured-beam antennas.

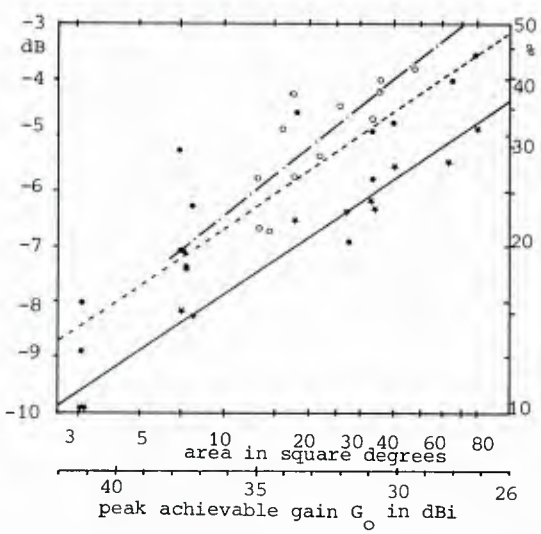

Figure 6 Contoured-beam efficiencies versus coverage area size for 3.2 m reflector at 4 GHz. The lines are determined by linear reqression for the following three cases:
—— INTELSAT VI antenna (**)
---- similar but with 1.3λ feeds (●●)
-.-. similar but with 1.3 feeds and relaxed coverage area specs. (oo)

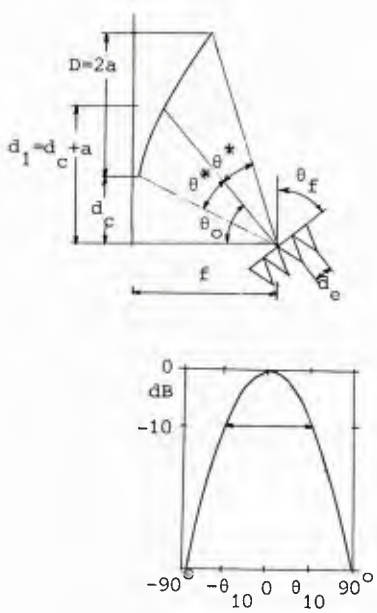

Figure 7 Reflector and feed parameters used in the simple analytic beam model.

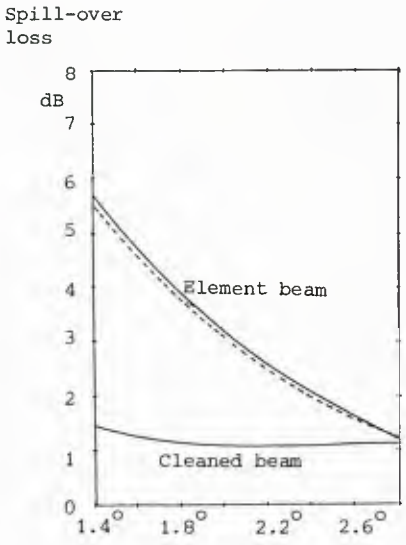

Figure 8 Spillover loss vs. spacing of component beams.
—— simple analytic beam model
---- reflector antenna analysis program

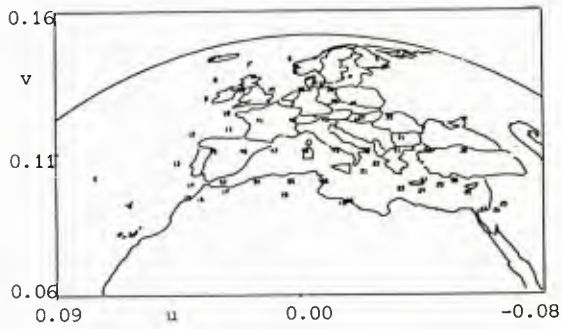

Figure 10 Examples of discrete stations (or sampling points) representing coverage-area specifications.

Figure 11 Contour plots for best analytical beam configuration →

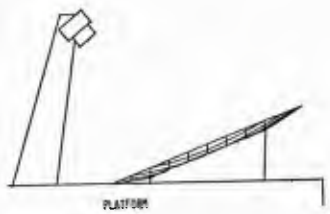

Aperture diameter = 1.101 m
Focal length = 0.845 m
Offset angle = 39.2°
24 feed elements

Sideview of array-fed offset reflector

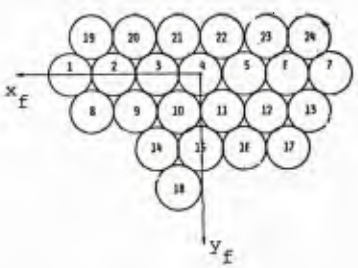

Figure 12 Initial ECS contoured beam reflector and feed array

Figure 13 PO/GTD element beams and contoured beam at 10.7 GHz →

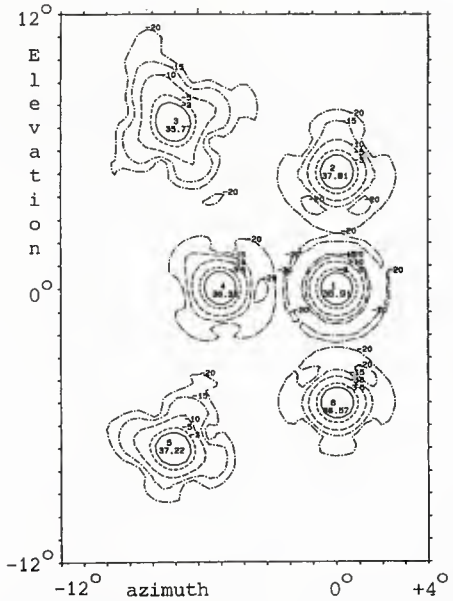

Figure 9 Gain contours 1, 3, 5, 10, 15 and 20 dB below peak gain level for on-axis and scanned element beams in a 43λ diameter offset-fed paraboloid.

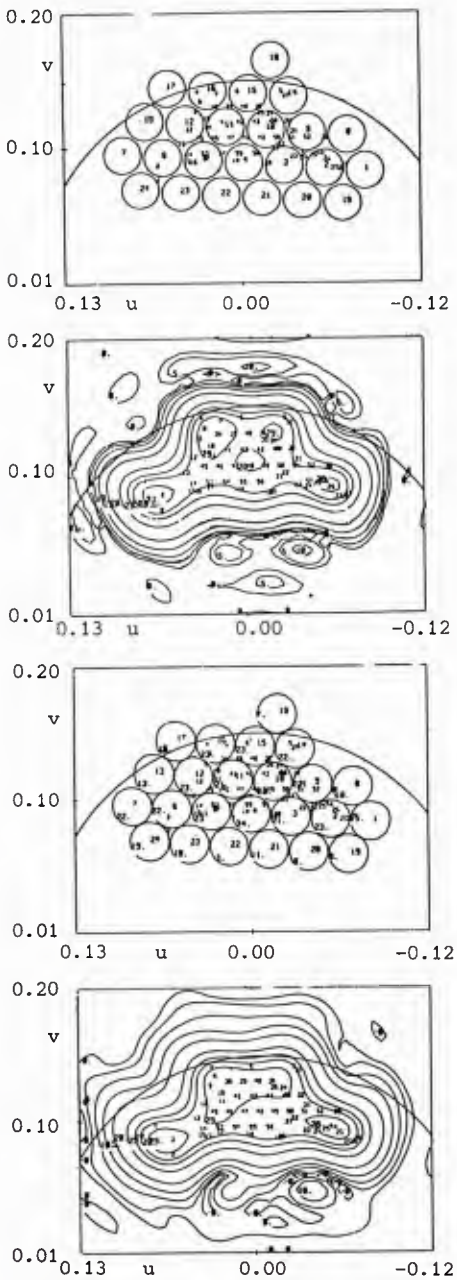

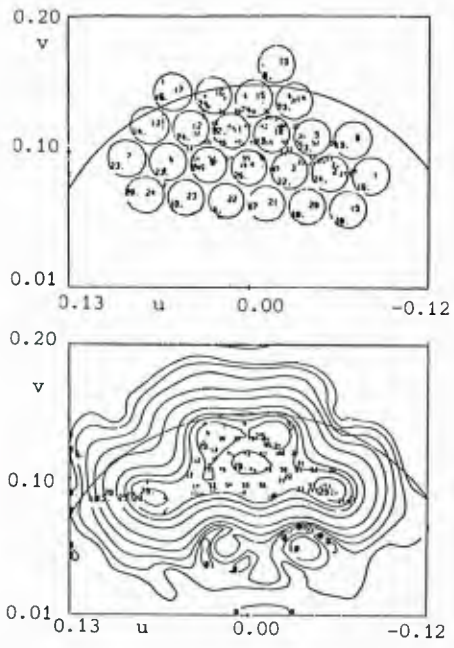

Figure 14 PO/GTD element beams and contoured beam at 11.7 GHz

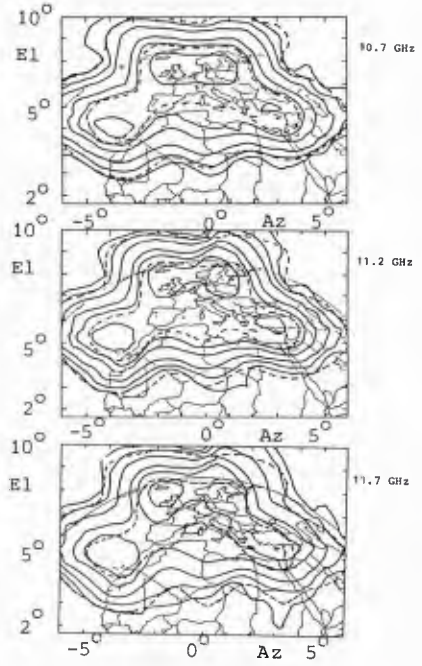

Figure 15 Measured gain contours 1, 3, 5, 10, 15 and 20 dB and calculated gain contours 3 and 20 dB below peak gain for ECS coverage array-fed contoured-beam reflector antenna
——— measurements (ERA)
----- calculation

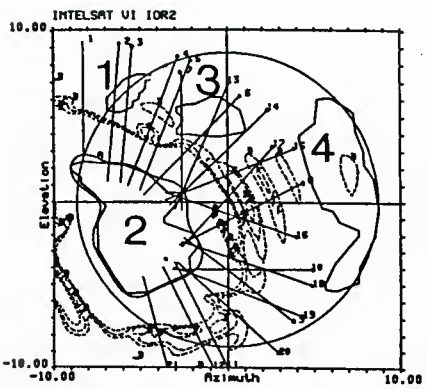

Figure 16
Nominal I-6 IOR zone 2 contours

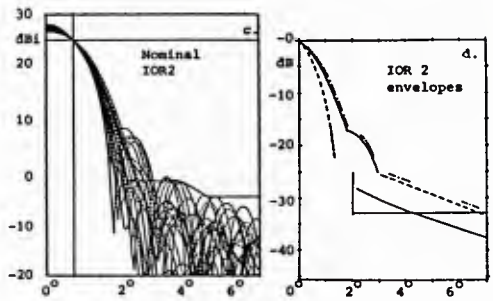

Figure 17 Gain roll-off patterns traces and envelopes ofr I-6 IOR zone 2.

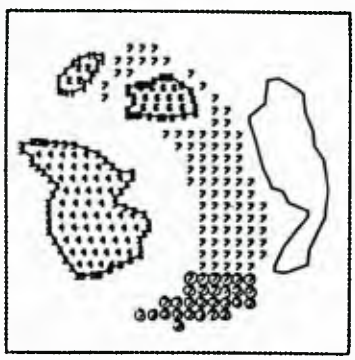

Figure 18
IOR 2 synthesis stations

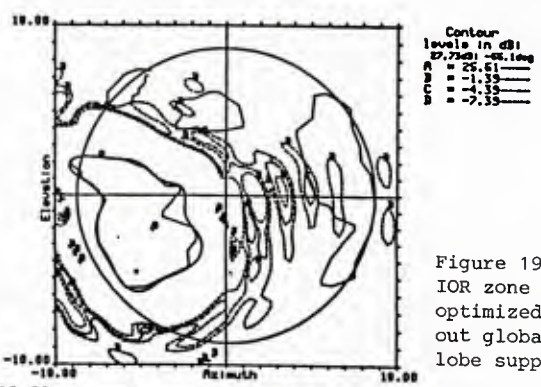

Figure 19
IOR zone 2 beam optimized without global sidelobe suppression

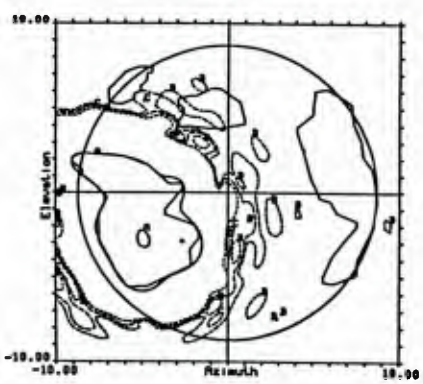

Figure 20
IOR zone 2 beam optimized with global sidelobe suppression

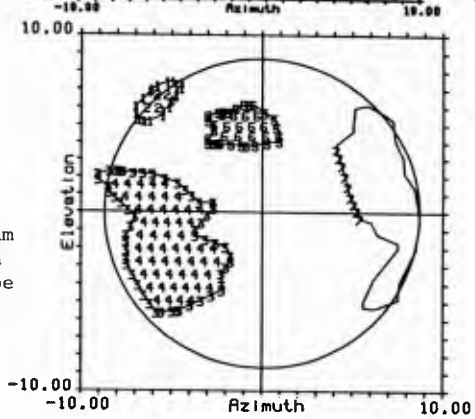

Figure 21
Synthesis stations for Indian Ocean region zone 2 beam

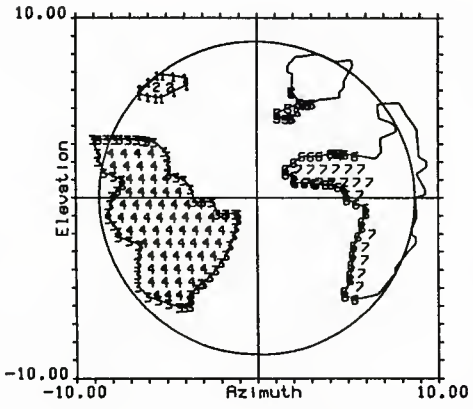

Figure 22 Synthesis stations for Atlantic Ocean region zone 2 beam

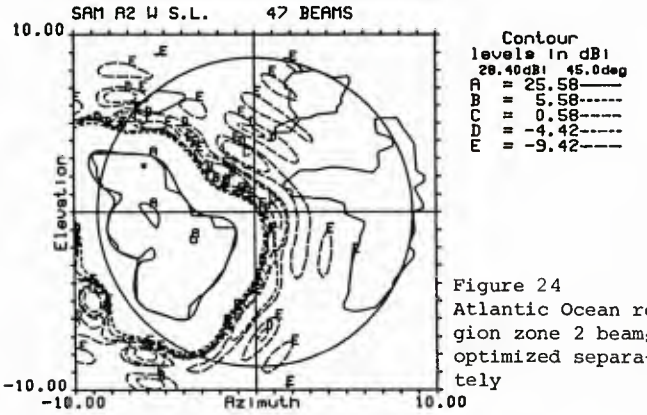

Figure 24 Atlantic Ocean region zone 2 beams optimized separately

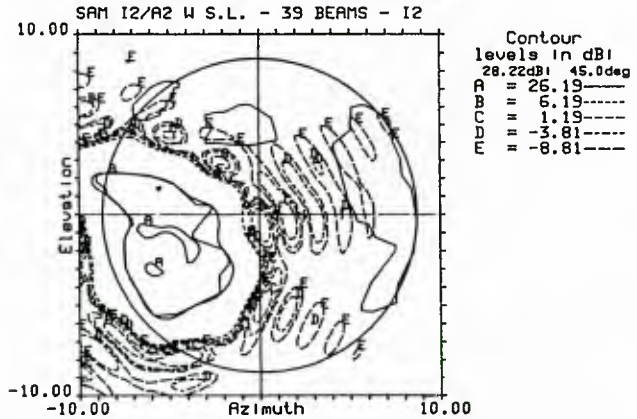

Figure 26 Indian Ocean region zone 2 beam optimized with 23 feeds common with Atlantic Ocean region zone beam

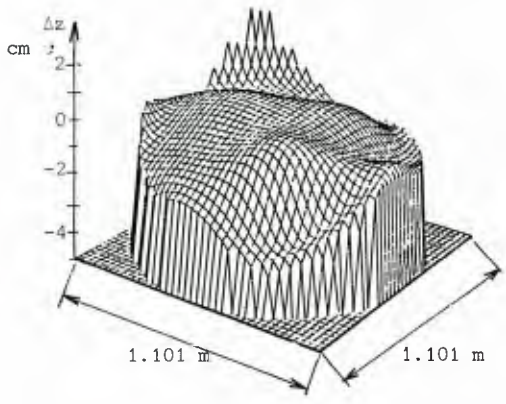

Figure 28 Deviations Δz of shaped reflector surface from paraboloid.

Figure 29 Isodirectivity curves for shaped reflector at edges of frequency band. →

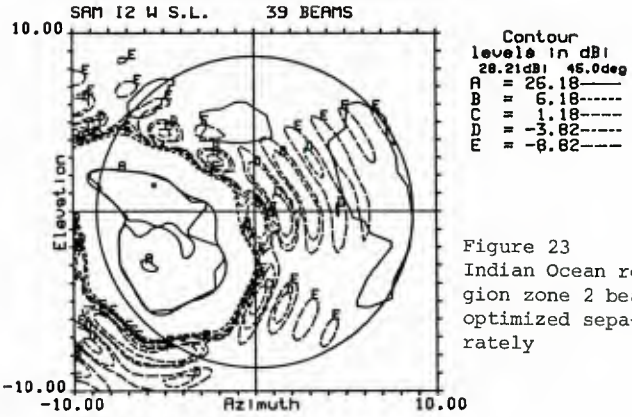

Figure 23 Indian Ocean region zone 2 beams optimized separately

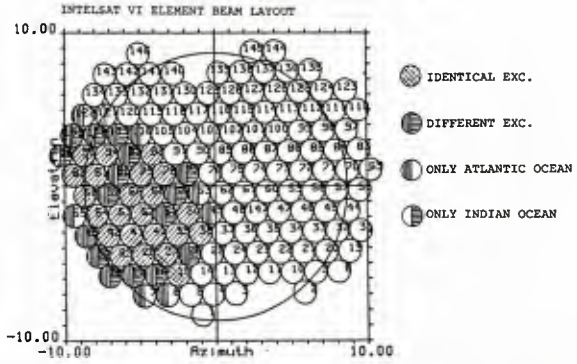

Figure 25 Shared and separate excitations for Indian and Atlantic Ocean region 2 beams

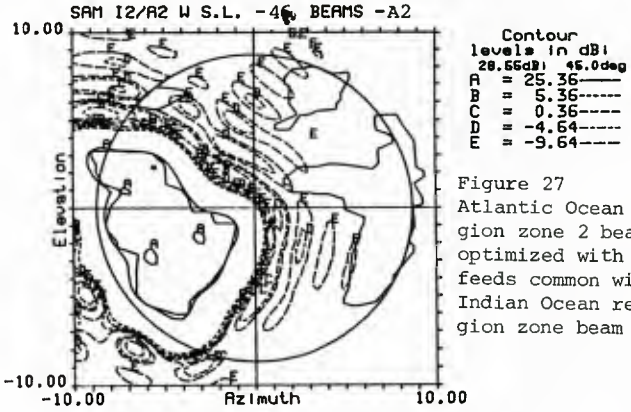

Figure 27 Atlantic Ocean region zone 2 beam optimized with 23 feeds common with Indian Ocean region zone beam

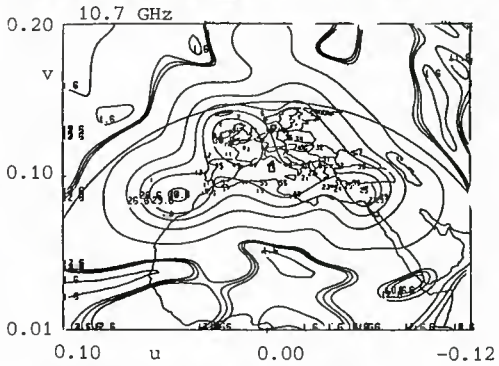

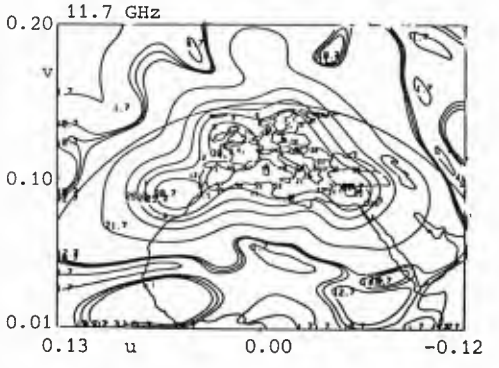

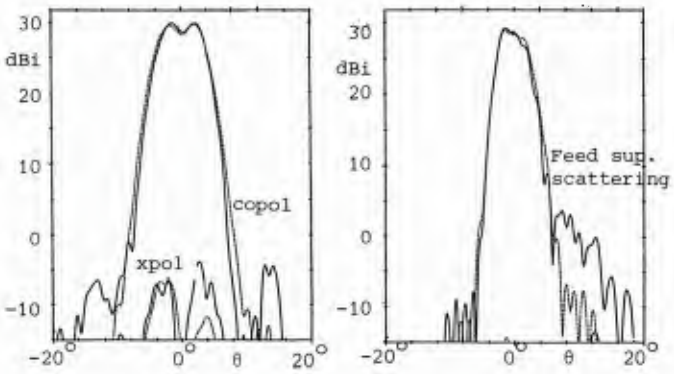

Figure 30 Measured and calculated principal pattern cuts at 11.7 GHz for shaped contoured-beam reflector.
——— measurement (TUD)
----- calculation

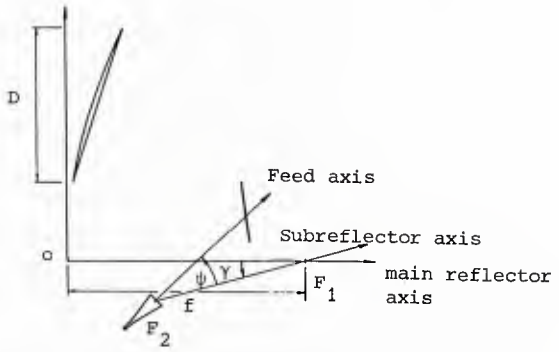

Figure 31 Conventional dual offset Cassegrain compensated for cross polarization and astigmatism

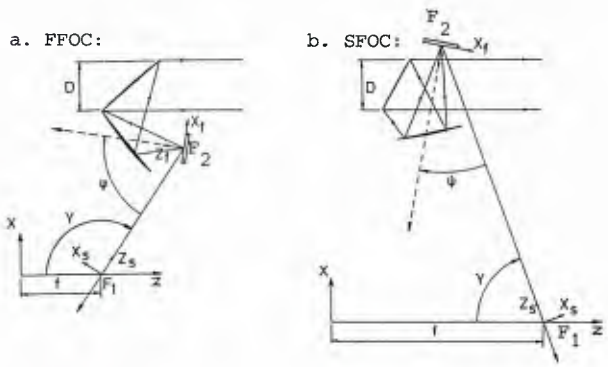

Figure 32 Alternative dual offset Cassegrain antennas compensated for cross polarization and astigmatism

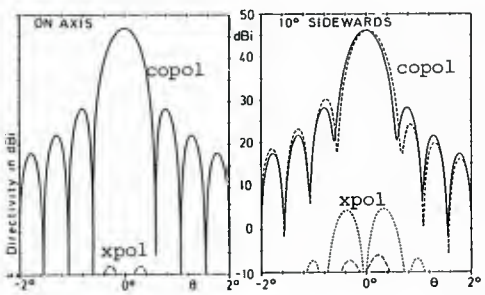

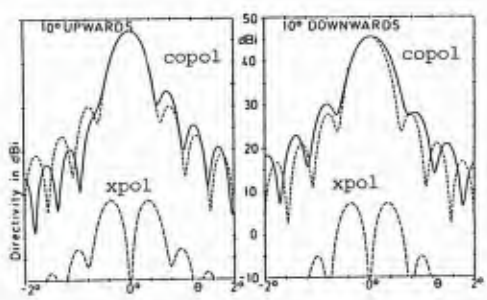

Figure 34 Principal pattern cuts for element beams for 120λ SFOC.

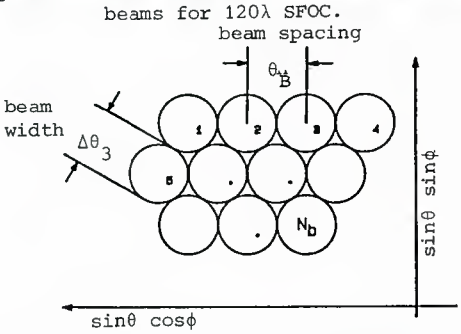

Figure 36 Array antenna element beams

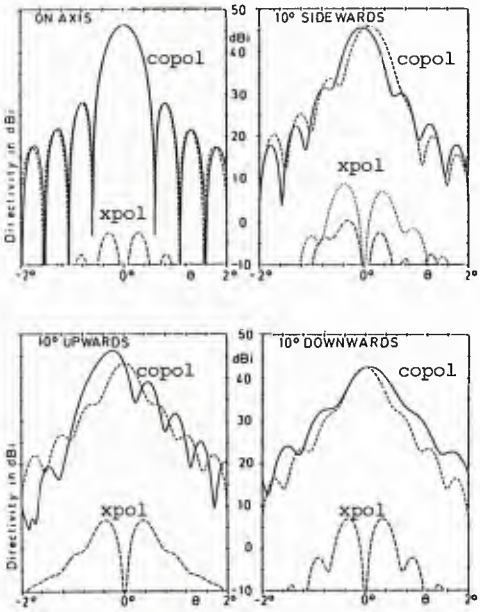

Figure 33 Principal pattern cuts for element beams in 120λ FFOC.

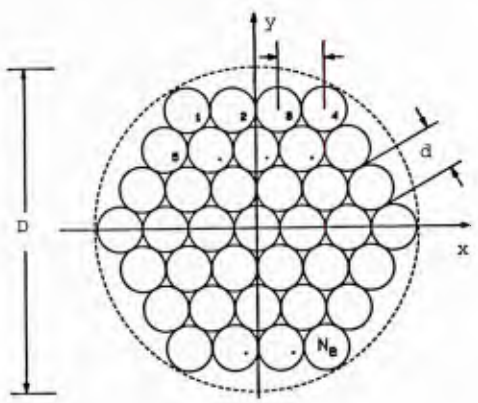

Figure 35 Array antenna element configuration

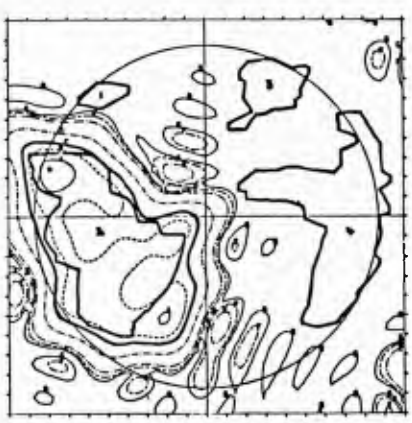

Figure 37 Optimized INTELSAT VI Atlantic zone 2 beam radiated by a direct radiating array.

MILLIMETER WAVE ANTENNAS FOR AVIONICS

by

FELIX K. SCHWERING

US ARMY CECOM
Center for Comm/ADP
Fort Monmouth, NJ 07703
USA

SUMMARY:

An overview over the area of mm-wave antennas is presented with emphasis on possible avionics applications. For the purpose of the review, mm-wave radiating structures are grouped into two classes, i.e., antennas of conventional configuration and antennas based on new design concepts.

The first class is composed of well known antennas such as reflector, lens, horn and slotted waveguide antennas. The design principles and performance characteristics of these antennas are well established at microwave and lower frequencies and scaling into the mm-wave region is straightforward in most cases. The reduction in size and the tighter fabrication tolerances associated with the mm-wave region suggest certain modifications in the design and application of these antennas. But, in principle, they can be regarded as well understood. Most mm-wave antennas which are currently in use belong to this class of "conventional" antennas.

The second class, consisting of antennas with significant features that are peculiar to the mm-wave region, is still under study. It includes radiating structures such as printed circuit mm-wave antennas; antennas derived from open mm-waveguides; and integrated antennas. Some of these antennas have microwave counterparts. Others are new with no microwave heritage.

Millimeter wave antennas are usually of very reasonable size and weight, and some of these antennas are suitable for rapid mechanical scanning. Furthermore, there is a large group of mm-wave antennas that are useful for conformal installation, for pattern shaping, for multibeam operation and/or for electronic scanning. Most of these antennas are narrow beam, highly directive radiators; others are useful for fan-beam or omnidirectional operation. Millimeter wave antennas should be sufficiently versatile to satisfy most avionics requirements.

Atmospheric propagation conditions vary strongly throughout the mm-wave band and have to be taken into account in the design of mm-wave systems and their antennas. A brief summary of these effects is included in the paper.

I. INTRODUCTION:

The mm-wave region, commonly defined as the 30-300 GHz or the 1 cm - 1 mm wavelength band, is well suited for avionics uses such as communication, radar, guidance and remote sensing. The advantages of this frequency region are well known:

- The very large bandwidth resolves the spectrum crowding problem and permits the design of communication systems of very high data rates and radar systems of high range resolution.

- The short wvelength allows the design of antennas of high directivity but reasonable size so that radar and radiometric systems of high angular resolution and communication systems of high transmission security are obtained.

- The use of integrated and monolithic techniques in the design of transmitters and receivers will result in terminals that are rugged, compact, reproducible and inexpensive.

Propagation effects have a strong influence on the performance of mm-wave systems and must be taken into account in the design of these systems. As a general rule, mm-wave transmission requires unobstructed line-of-sight paths and, for such paths, absorption by atmospheric gases and by rain are the dominant propagation effects. Furthermore, in the case of operation near ground level, the line-of-sight may pass through vegetation, and foliage absorption and scatter may contribute significantly to the path loss.

Absorption by atmospheric oxygen and water vapor: The attenuation due to these gases varies strongly throughout the mm-wave band. Large transmission distances can be achieved in the low attenuation windows at 35, 94, 140, 220 and 340 GHz. On the other hand, operation near one of the steep absorption lines as, for example, the O_2-line at 60 GHz will allow to control the transmission distance by adjusting the frequency. In this way, a degree of covertness can be obtained or excess path losses due to heavy rain may be compensated adaptively. Furthermore, the utilization of increased atmospheric attenuation in conjunction with highly directive antennas will allow to operate several systems in the same band and at close range without interference. The attenuation rate due to atmospheric gases decreases with increasing height above ground. The effect is strong, in particular, near the low-attenuation windows and aircraft flying at heights above 5 km may achieve large transmission ranges.

Absorption by rain: Rain attenuation increases with frequency in the lower mm-wave region up to about 100 GHz and for higher frequences remains fairly constant. Typical attenuation rates are 0.5 dB/km at 30 GHz and 2 dB/km at 100 GHz for a light rain of 2.5 mm/hr. For a heavy rain of 50 mm/hr, the corresponding values are 10 dB/km and 20 dB/km.

Vegetation effects: Millimeter wave attenuation by vegetation depends strongly on vegetation type and density and tends to increase with frequency. A recent study has shown, moreover, that the attenuation rate decreases from a high value at short distances into a forest to a lower value at large distances, with substantial beam broadening occuring in the transition region. From the avionics viewpoint, however, vegetation effects will be a concern only in the case of ground-to-air communication with low-flying helicopters. In the case of high-flying aircraft, any vegetation path as seen from a ground station will be very short, although a path through trees will cross the canopy region where foliage attenuation and scattering is strongest.

Through fog, smoke and dust, mm-waves travel with little attenuation, and mm-wave systems are superior here to infrared and optical systems whose signals are strongly absorbed and scattered by such media.

A wide variety of antennas has been designed or is currently under investigation for the mm-wave region. For the purpose of this article, two classes of these antennas are distinguished, i.e., antennas of conventional configuration and antennas based on new design concepts.

Antennas of both classes should be useful for avionics uses because of their small size and weight, which is an important consideration, in particular, for helicopter application where available space is at a premium. Moreover, most antennas of the second class are amenable to conformal installation, or they may be flush-mounted with the aircraft skin, so that they are useful for high performance aircraft.

Antennas of conventional configuration: This class is composed of well known antennas such as reflector, lens and horn antennas. The design principles and performance characteristics of these antennas are well established at microwave and lower frequencies, and scaling into the mm-wave region is straightforward in most cases. From the applications viewpoint, there may be certain differences between the microwave and mm-wave versions of these antennas; but concerning basic design and performance, they can be regarded as well understood. Most mm-wave antennas which are currently in use belong to this class.

Antennas based on new design concepts: This class which consists of antennas with significant features that are peculiar to the mm-wave region, is still under study and is more heterogeneous than the first class. It includes radiating structures such as microstrip mm-wave antennas; antennas derived from the open mm-waveguides; and integrated antennas.

Microstrip antennas and printed circuit antennas in general have many practical advantages and, for this reason, have found numerous applications in the UHF through microwave bands. They have been studied extensively during the past decade. Recently several efforts have been made to extend these antennas into the mm-wave region. But his extension is not simply a matter of straightforward wavelength scaling; new problems as well as new opportunities appear.

Antennas derived from open mm-waveguides are typically traveling wave antennas, i.e., surface wave or leaky wave antennas. Some of these antennas (tapered dielectric rod antennas and periodic dielectric antennas) have been known for many years, But they have found renewed interest in the mm-wave region, and periodic antennas have been studied systematically only in this context. Other antennas of this subgroup, which may be described as uniform waveguide leaky wave antennas, are new developments with no microwave heritage.

Integrated antennas, where components such as phase shifters and power amplifiers or low-noise detectors are integrated with the radiating elements on the same substrate, are a new and very interesting group of mm-wave antennas which holds substantial promise for the design of low profile, low cost, lightweight, conformal antennas that are mechanically rugged and electrically highly versatile. These antennas are currently under study. Design guidelines are not as yet available on any systematic basis; but a number of interesting experimental models have recently been developed and described in the literature.

In the following, design principles for mm-wave antennas are briefly reviewed. For some of the antennas discussed here, avionics uses may not be obvious but they are included in the review for completeness.

II. MILLIMETER WAVE ANTENNAS OF CONVENTIONAL CONFIGURATION:

As mentioned above, these antennas are very similar to their microwave counterparts and their characteristics can be regarded as well understood. But there are also differences which are due primarily to the much smaller size and weight of mm-wave antennas and to their tighter fabrication tolerances. The question which antenna type should be used for a given application may be answered differently in the microwave and mm-wave regions.

A typical case here are mechanically scanned reflector antennas which, when dimensioned for the mm-wave region, have small size and weight, and are suitable for rapid beam scanning. These antennas can be used for applications where in the microwave region one would have to consider frequency scanned or phased arrays which are much more expensive [1]. Of particular interest are designs where the reflector moves while the feed remains stationary so that no rotary joint is needed in the feedline. A simple antenna of this type is sketched in Fig. 1. It consists of a horn-fed parabolic dish, which is stationary, and a planar reflector which rotates about the antenna axis and scans the beam in the azimuth

plane. An antenna designed for the 94 GHz band and a beamwidth of 0.7° operated at a scan rate of 600 RPM [2]. The scan rate is determined primarily by the purpose for which the device is used, and designing for higher scan rates should not be a major problem. In cases where a conical scan of moderate aperture angle is required, the rotary mirror may be replaced by a scanned dielectric wedge.

For the same reason of reduced size and weight, dielectric lens antennas become much more practical in the mm-wave region than at lower frequencies where their weight is often a limiting factor while otherwise they show very good electrical performance. For given performance, volume and weight of a dielectric lens decrease with the third power of wavelength and are usually very reasonable in the mm-wave region.

Recently lens shaping techniques have been developed for mm-wave lens antennas. Fig. 2 shows the cross section profile of a shaped rexolite lens designed by Lee [3] for operation as a multibeam antenna in the 44 GHz band at a gain of 33 dB. The antenna is not only shaped but zoned. In the case of microwave lenses, a main purpose of zoning is the reduction of dielectric weight while here it is used for the reduction of coma aberrations [3] (pattern distortions of off-axis beams).

A different type of lens antennas, which becomes attractive in the mm-wave region because of its very simple shape, are spherically symmetric lenses, i.e., lenses which have the shape of a full sphere [4]. The interesting point here is that simple homogeneous spheres made, for example, from teflon or rexolite yield already very good performance; and two-layer lenses which consist of a homogeneous spherical core surrounded by a concentric shell of different refractive index can be sufficiently well corrected to satisfy most practical requirements including a gain of up to 50 dB and good pattern quality with sidelobes below -25 dB. In addition, such spherically symmetric lenses allow wide angle beam scanning without pattern degradation.

Millimeter wave horn antennas are well developed and in general are very similar to their microwave counterparts [1]. Moreover, dielectric horns have characteristics that make them attractive for mm-wave applications. These horns have less critical tolerances and are easier to machine than metallic horns. When made from materials of low permittivity (1.5 to 2.5) they are useful as array elements and as primary feeds for reflector or lens antennas [5].

Millimeter wave array antennas of conventional configuration (slotted waveguide arrays) are not widely used up to now in the mm-wave region [1]. The probable reason is that these antennas and, in particular, large phased arrays would require highly precise fabrication techniques and are likely to be expensive. The trend seems to be more toward microstrip antennas and printed circuit arrays in general. These antennas can be conveniently and precisely fabricated by etching techniques and they allow integrated designs with the inherent advantages of compactness, reliability and reproducibility.

On the other hand, the technology for slotted waveguide arrays is available and several interesting linear and planar (flat plate) arrays have been designed and tested recently with encouraging results [6]. It was shown, in particular, that with these arrays a high directivity gain (>30 dB) can be achieved at good efficiency, which makes them superior to passive microstrip arrays whose feed system losses can be substantial and are not easily reduced when the array size is large. Furthermore, slotted waveguide arrays have the capability of providing extremely low sidelobes (edge slot arrays) and a very low cross polarization level (broad wall slot arrays). With these advantages, they should be a good choice also for the mm-wave region when high electrical performance is required.

Recent studies [6, 7] have demonstrated, moreover, that mm-wave slot arrays can be fabricated from standard metal waveguide by the use of high resolution photolithographic and chemical etching techniques which are precise and relatively inexpenxive. These techniques appear useful, in particular, for the fabrication of antennas designed for the 60 GHz band and above.

III. MILLIMETER WAVE ANTENNAS INVOLVING NEW DESIGN CONCEPTS:

1. Microstrip Millimeter Wave Antennas.

Microstrip antennas and, in particular, patch resonator antennas (which are commonly associated with the term microstrip antennas) have numerous practical advantages including low profile, ruggedness, ease of fabrication and reproducibility by etching techniques, lightweight, low cost. In addition, these antennas are well suited for conformal installation and integrated design approaches. They have been studied extensively during the past decade, at microwave frequencies, and can be regarded as well understood by now, though papers on this subject are still appearing quite frequently in the literature. Also, this antenna technique has been used very successfully for the design of a wide variety of antenna arrays for the microwave region and into the UHF band. The only problem with microstrip patch antennas is their narrow bandwidth, in the order of a few percent, which would not allow their use in broad band systems.

Because of the many advantages, extension of the microstrip antenna technique into the mm-wave region appears desirable and a number of studies with this objective has been conducted in recent years. But, as mentioned above, this extension is not simply a matter of straightforward wavelength scaling. New problems, as well as new opportunities, appear.

There are, in particular, two problems: fabrication tolerances and feedline losses. Both problems are associated primarily with the feed systems of mm-wave microstrip arrays rather than with the radiating patches themselves. For ease of fabrication, the feed system is usually printed with the radiating elements on the same substrate. The feedlines have a very small width, typically in the order of 0.1-0.2 mm for an array operating at a frequency in the 30-100 GHz band, and required tolerances are by an order of magnitude tigher. Thus, highly precise etching techniques are needed. Furthermore, microstrip lines are not low loss lines, and in large arrays, which are needed to obtain high directivity gain, feedline losses can be substantial, in particular, when a corporate feed system is used with long runs of mirostrip lines.

In recent design studies, various methods have been investigated to overcome these problems. The results lead to the conclusion that microstrip patch arrays will be useful antennas for the lower mm-wave band up to a frequency of 100 GHz and, possibly, 140 GHz [8]. For this band, it should be possible to design microstrip patch arrays of reasonably high gain which show good electrical performance including acceptable efficiency.

Note that good efficiency for printed circuit array antennas of any size can be achieved by the use of distributed sources and detectors placed near the array elements or at an appropriate subarray level. Printed antennas are well suited for integrated designs and, if Si or GaAs substrates are used, monolithic solid state amplifiers or mixers could be integrated with the radiating elements on the same substrate (which may consist of several layers if more complex functions are to be accommodated). Work on such integrated arrays is currently in progress. Feedline runs in these antennas will be short and feedsystem losses low. Additional advantages of integrated arrays include that they permit achieving a high output power in the transmit case through space-combination of many low power sources (thus overcoming the power limitation problem of mm-wave solid state sources); that the aperture illumination profile can be easily and precisely controlled; and that graceful degradation will occur if some of the amplifiers or detectors should fail. Moreover, such arrays may be designed in a modular fashion which would simplify fabrication and enhance design versatility.

Returning to passive microstrip antennas, it was mentioned earlier that the extension of these antennas into the mm-wave region also provides new opportunities. Specifically, the bandwidth limitation of these antennas may be overcome by the use of electrically thick substrates. This leads from microstrip patch resonator antennas to microstrip dipole antennas which may be useful not only for the lower but also for the upper mm-wave band above 100 GHz.

In the microwave region, the substrate thickness is, by necessity, a small fraction of a wavelength only. Thin substrates imply the use of resonator antennas of high Q in order to raise the radiation resistance to reasonable values. This, in turn, leads to a narrow bandwidth. In the mm-wave region, on the other hand, a substrate which is physically thin, can still have an electrical thickness of $\lambda/4$ or more. Hence, there is no need for the use of high-Q resonator antennas, but one can use other antenna configurations which provide much broader bandwidth as, for example, printed dipole or loop antennas of large width.

There is, however, one problem with antennas on thick substrates: the excitation of surface waves. These surface waves carry power away from the antennas but do not radiate so that their power must be regarded as antenna loss. The design problem is to obtain a large bandwidth while maintaining good efficiency. This problem has been investigated recently by Alexopoulos and his associates in a very thorough and interesting study which also has resulted in detailed guidelines for the optimum design of microstrip antennas on thick substrates. The antennas considered here were printed dipole antennas. For details, we refer to the literature [9].

Recent studies by the Alexopoulos group have been concerned with feed systems for large printed dipole arrays on thick substrates [10] - a critical problem for these arrays - and the use of a superstrate in addition to a substrate which can enhance antenna performance considerably [11].

2. Traveling Wave Antennas Derived from Open Millimeter Waveguides.

Most mm waveguides are open guiding structures which do not enclose the guided fields on all sides by metal walls. Hence, if the uniformity of the guiding structure is perturbed or if the guide is not excited in the appropriate mode, radiation will occur and part of the guided power will be leaked away from the waveguide. This leakage effect may be used to advantage for the design of antennas, by intentionally introducing perturbations in an open waveguide such that radiation occurs in a controlled manner.

Antenna types which belong to this class include tapered dielectric rod antennas, periodic dielectic antennas, and a number of novel radiating structures which may be grouped together under the name "uniform waveguide leaky wave antennas." The antenna configurations are sketched in Fig. 3. The first two antennas are both derived from dielectric waveguide. Tapered dielectric rod antennas, Fig. 3(a), are well known; they consist of a dielectric waveguide whose cross section decreases monotonically in the forward direction. A surface wave incident from a feedguide will be gradually transformed, as it travels along the tapered section, from a purely bound mode to a free space wave. The antenna is a typical surface wave antenna whose phase velocity is $<c$ so that it radiates in the forward (endfire) direction.

The remaining antennas of Fig. 3 are leaky wave antennas. Their phase velocity exceeds c and they radiate under an angle against the forward direction. The radiation angle varies with frequency, so that these antennas are useful for frequency scanning. Periodic antennas, Fig. 3(b), consist of a uniform dielectric waveguide with a periodic surface perturbation. The surface perturbation may take the form of a dielectric grating, as indicated in the figure, or one may use a grating of metal strips. Diffraction at this grating will transform a guided mode into a leaky wave and, hence, the waveguide into an antenna. Such grating antennas can be designed for radiation under any angle from backfire over broadside to endfire.

The antennas sketched in Fig. 3(c) are derived from grooveguide and NRD guide (non-radiative dielectric guide). The method used here to obtain radiation is the introduction of a perturbation which is uniform in the forward direction. In the case of the grooveguide antenna, it is the small metal strip which is asymmetrically placed in the upper waveguide arm; in the case of the NRD guide antenna, it is the foreshortening of the metal walls of this waveguide arm. These perturbations cause the fundamental mode to become a leaky wave and the waveguide will radiate. Radiation occurs under an angle; but as opposed to periodic antennas, the radiation angle is confined to the forward quadrant. This also applies to the antennas of Fig. 3(d).

In the case of these antennas, which are derived from microstrip and grooveguide, the guiding structure is not perturbed at all, which means that the fundamental mode remains a bounded wave. But a higher mode of these waveguides may be leaky. The waveguide dimensions are then chosen such that this mode is above cutoff, and by the use of an appropriate feed arrangement, it is insured that only this mode is excited.

The antennas of Figs. 3(c) and 3(d) have the outward appearance of uniform open waveguides; but these waveguides are modified/operated such that they are leaky and act as antennas. These antennas are an interesting new group of mm-wave radiating structures which, as mentioned above, may be called uniform waveguide leaky wave antennas. Suggested by Oliner and his co-workers, they are currently investigated by these authors; some interesting results have recently been published in the literature [12-15].

In contrast to these novel mm-wave antennas, the dielectric antennas of Figs. 3(a) and 3(b) have been known for some time. Tapered rod antennas, in particular, have been known for many years and have been used, on a limited scale, in the microwave region, for example as polyrod antennas. But dielectric antennas have found renewed interest in the mm-wave range; and periodic dielectric antennas have been studied systematically only in this context. By now, these grating antennas - specifically those with dielectric gratings - can be regarded as well understood [16].

Some mm-waveguides, notably fin-line and metal waveguide , are shielded rather than open guiding structures and the design of antennas which are directly compatible with these guides, takes a somewhat different approach. As an example, Fig. 4 shows three versions of an antenna recently suggested and studied by Yngvessen, et al [17] which would be useful as fin-line antennas although, originally, they have been investigated for operation with metal waveguide. But when used as fin-line antennas, they may be described by saying that the printed guiding structure of the line is extended by several wavelengths past the shielded enclosure; and, in this open region, the guiding structure is gradually tapered out so that a guided mode is transformed into a free-space wave as it travels along the antenna. Alternatively, the antennas may be described as "rudimentary horns." The structure sketched in Fig. 4(a) employs an exponential taper leading to a so called Vivaldi antenna; in Fig. 4(b) the taper is linear, while the structure of Fig. 4(c) includes a section of constant width. All of these antennas are traveling wave antennas which radiate in the endfire direction. Experiments [17] have shown that the antennas, when correctly designed, can provide good electrical performance including a moderately high gain of 10-17 dB, relatively low sidelobes, a circularly symmetric mainbeam, and a practically constant impedance over a wide band of frequencies. A theoretical study of these antennas is currently in progress [17].

3. Integrated Millimeter Wave Antennas:

A novel and very promising class of mm-wave antennas are those where components such as phase-shifters, mixers, variable reactors or amplifiers are integrated with the radiating elements on the same substrate. Such antennas are of interest not only for the lower mm-wave region but are well suited also for the so-called near mm-wave range above 100 GHz.

The design of these antennas, evidently, involves new problems and requires new approaches. Most of the problems should be well known to IC designers. But there are also difficulties peculiar to integrated antennas. For example, the radiating patches and feedlines of a microstrip array, though physically small, are large from an IC viewpoint and take up a substantial portion of the substrate surface so that the space available for integrated components and circuits is limited. Furthermore, a certain clearance is required between the radiating elements/feedlines and any integrated devices to avoid pattern distortions and undesired radiation coupling into active and passive components. Additional difficulties include heat sinking in transmit arrays and design problems caused by the high permittivity of silicon or GaAs, the preferred materials for monolithic integration. Because of these and similar constraints, it is likely that the electrical performance of integrated antennas will remain somewhat below the performance achieved with more conventional antennas. But this will be traded against substantial improvements in compactness, reliability and cost. To indicate some of the current developments in this area, Figs. 5 and 6 show two integrated antennas which have been investigated recently. As with all integrated antennas, the critical parts of these structures are the monolithically integrated solid state components.

Fig. 5 shows an integrated receiving antenna designed by Fetterman, et al, for the 140 GHz band. The following discussion draws from a recent paper by these authors [18]. The device, a twin-dipole with an integrated beam lead Schottky mixer diode, is fabricated in planar printed circuit technology on a quartz substrate. The Schottky diode, located at the feed point of the antenna, is monolithically created in a small, very thin GaAs plate which is bonded to the quartz substrate. This hybrid approach allows one to minimize excitation of surface waves in the substrate and maximize efficiency (which increases with decreasing ε) while maintaining a reasonable substrate thickness. The substrate is backed by a metal ground plane which enhances the directivity of the antenna in the forward direction and insures a large front-to-back ratio.

The antenna consists of two parallel full wave dipoles spaced one half wavelength apart and interconnected by a two-wire transmission line. The feedpoint is midway between the two dipoles so that they are driven in-phase. In this way, a pattern of nearly rotational symmetry about the broadside direction is obtained, which has a null in the plane of the substrate and is advantageous for receiving both the desired incident signal and the (quasi-optically coupled) LO signal. The spacing of the dipoles at $\lambda/2$ has the additional advantage that the high input imedance of the full-wave radiators is transformed into a much lower value at the feedpoint halfway between the dipoles.

The IF signal generated by the mixer diode is coupled out of the antenna through a printed balanced two-wire transmission line containing a low pass filter of cascaded quarter wavelength design (wide portion of feedline) to block out the high frequency mm-wave signals.

An experimental model of the antennas has shown optimum performance at 132 GHz. A half power beamwidth of 40°, a sidelobe level of -8 dB and a bandwidth of approximately 3% was measured [18]. Twin-dipole integrated antenas of this type should be well suited as array elements for planar monolithic mm-wave receive arrays and, when such arrays are placed in the focal plan of large reflecter or lens antennas, for mm-wave imaging. The authors estimate that, within the presently available technology, extension of the antenna design to frequencies up to 700 GHz is feasible [18].

The second integrated antenna to be discussed here functions as a beamsteering reflector. The antenna has been proposed and is currently studied by Rutledge, Luhman and their associates; the following discussion is based on a recent paper by these authors [19]. The essential part of the device is a planar diode grid which permits electronic control of the phase distribution of the reflected wave across the reflector aperture. The diode grid is a square mesh of metal strips printed on a GaAs substrate; see Fig. 6(a). The diodes are located on the vertical strips; they are Schottky type varactor diodes that are monolithically implanted in the substrate. The E-vector of the incident wave is assumed to be parallel to the vertical strips which have the effect of an inductive reactance; this reactance is in series with and subtracts from the capacitive reactance of the diodes. The horizontal strips of the mesh provide the bias, and the reactance of each row of diodes can be adjusted independently. In this way, the phase distribution of the reflected wave can be controlled across the mesh surface in the vertical direction and beamsteering becomes possible in the plane normal to the horizontal lines. The grid dimensions shown in Fig. 6(a) apply to a frequency of 90 GHz.

A cross section view of a beam steering reflector [19] using such diode grids is shown in Fig. 6(b). The reflector consists of a metal ground plane, two diode grids at a quarter wavelength spacing, and a quartz cover. The quartz cover acts as an anti-reflection layer; the permittivity of quartz is in good approximation equal to the geometric mean of the permittivities of GaAs and air, and the thickness of the layer is equal to a quarter wavelength in quartz. The ground plane serves as mounting block and heatsink. Its electric function is to prevent energy from escaping and to invert the impedance of the second grid as seen from the plane of the first grid. The use of two grids instead of one, at quarter wave spacings (in the substrate material), has the advantage that a phase variation over the entire range of 0° to 360° can be accomplished by varying the varactor capacitance over a convenient finite range only. Details may be found in Ref. [19] where a transmission line model of the structure is presented. It is shown here that for the example of the grid of Fig. 6(a) the inductive reactance of the grid wires is 160° at 90 GHz and that a variation of the diode capacitance over the range from 7 fF to 35 fF will be sufficient to produce a full 360° cycle of the reflection phase in the structure of Fig. 6(b). Such capacitance variations can be achieved with hyperabrupt Schottky varactors [19]. Computer evaluations have shown, moreover, that the reflection phase varies with the bias voltage in a nearly linear fashion. If, in this way, a progressive phaseshift is introduced in the reflected wave, beam steering is accomplished electronically. Assuming a series resistance of the diodes of 10Ω, the reflection loss has been estimated at 3 dB.

The present design will permit one-dimensional beam steering. To obtain two-dimensional beam steering, the varactor diodes would have to be controlled individually rather than on a row-by-row basis.

Varactor diode grids of the type shown in Fig. 6(a) may also be used as frequency multipliers by utilizing the non-linear characteristics of the diodes to produce outgoing waves at harmonic frequencies [19]. In this case, the grid would be used in conjunction with planar filters to separate the various harmonic component waves. A particular advantage of this type of harmonic generation is that the power of the outgoing wave is that of many distributed diodes combined, which overcomes the power limitation of single diode multipliers.

References:

[1] R. B. Dybdal, Millimeter Wave Antenna Development, Proceedings 1982 Antenna Appl. Symposium, Univ. of Illinois, 22-24 Sep 1982.

[2] K. Solbach, Various mm-Wave Antennas for Radar and Communication, Intern Workshop on mm-Waves, University of Rome, Italy, 2-4 Apr 1986.

[3] J. J. Lee, Dielectric Lens Shaping and Coma Correction Zoning, Part 1: Analysis, IEEE Trans. on Antennas and Propagation., Vol. AP-31, pp. 216-220, Jan 1983.

[4] T. L. Ap Rhys, The Design of Radially Symmetric Lenses, IEEE Trans. on Antennas and Prop., Vol. AP-18, pp. 497-506, Jul 1970.

[5] T. Ohtera and H. Uhje, Radiation Performance of a Modified Rhombic Dielectric Plate Antenna, IEEE Trans. on Antennas and Prop., Vol. AP-29, pp. 660-662, Jul 1981.

[6] K. Solbach, Some Millimeter-Wave Slotted Array Antennas, Proceedings of 14th European Microwave Conference, 1984.

[7] B. R. Rao, 94 GHz Slotted Waveguide Array Fabricated by Photolithographic Techniques, Digest of 1983 International IEEE-APS/URSI Meeting, pp. 688-689, Houston, TX, 23-26 May 1983.

[8] J. R. James and C. M. Hall, Investigation of New Concepts for Designing Millimeter Wave Antennas, Final Techn. Report on Contract DAJA37-80-C-0183, U.S.Army European Research Office, Sep 1983.

[9] N. G. Alexopoulos, P. B. Katehi and D. B. Rutledge, Substrate Optimization for Integrated Circuit Antennas, IEEE Trans. on Microwave Theory and Techniques, Vol. MIT-31, pp. 550-557, Jul 1983.

[10] P. B. Katehi and N. G. Alexopoulos, On the Coupling of Electromagnetically Coupled Microstrip Antennas - The Printed Strip Dipole, IEEE Transactions on Antennas and Prop, Vol. AP-32, pp. 1179-1186, Nov 1984.

[11] N. G. Alexopoulos and D. R. Jackson, Fundamental Superstrate (Cover) Effects on Printed Circuit Antennas, IEEE Transactions on Antennas and Prop., Vol. AP-32, pp. 809-816, Aug 1984

[12] P. Lampariello and A. A. Oliner, A New Leaky Wave Antenna for Millimeter Waves Using An Asymmetric Strip in Groove Guide, Part I: Theory; Part II: Design Considerations, IEEE Trans. Antennas and Prop., Vol AP-33, pp. 1285-1303, Dec 1985

[13] A. Sanchez and A. A. Oliner, Microwave Network Analysis of a Leaky Wave Structure in Nonradiative Dielectric Waveguide, Digest IEEE MIT-S International Microwave Symposium, pp. 118-120, San Francisco, CA, 30 May - 1 Jun 1984.

[14] P. Lampariello and A. A. Oliner, Bound and Leaky Modes in Symmetrical Open Groove Guide, Alta Frequenca, Vol LII, No. 3, pp. 164-166, 1983.

[15] A. A. Oliner and K. S. Lee, Microstrip Leaky Wave Strip Antennas, Digest 1986 IEEE AP-S International Symposium, pp. 443-446, Philadelphia, PA, 8-13 Jun 1986

[16] F. Schwering and S. T. Peng, Design of Dielectric Grating Antennas for Millimeter Wave Applications, IEEE Trans. on Microwave Theory and Technique, Vol. MIT-31, pp. 199-209, Feb 1983.

[17] K. S. Yngvessen, D. H. Schaubert, T. L. Korzeniowski, E. L. Kollberg, T. Thungren and J. F. Johansson, Endfire Tapered Slot Antennas on Dielectric Substrates, IEEE Transactions on Antennas and Prop, Vol. AP-33, pp. 1392-1400, Dec 1985.

[18] H. R. Fetterman, T. C. L. G. Sollner, P. T. Parrish, C. D. Parker, R. H. Mathews, and P. E. Tannenwald, Printed Dipole Millimeter Wave Antenna for Imaging Array Applications, Electromagnetics, Vol. 3, pp. 209-215, 1983.

[19] W. W. Lam, C. F. Jou, N. C. Luhman and D. B. Rutledge, Diode Grids for Electronic Beam Steering and Frequency Multiplication, International Journal of Infrared and Millimeter Waves, Vol. 7, pp. 27-41, Jan 1986.

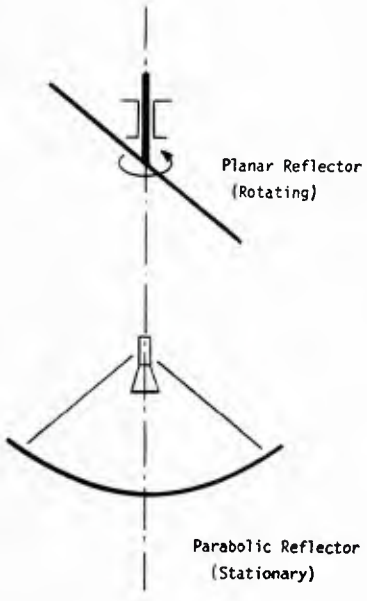

Fig. 1 Mechanically Scanned Reflector Antenna

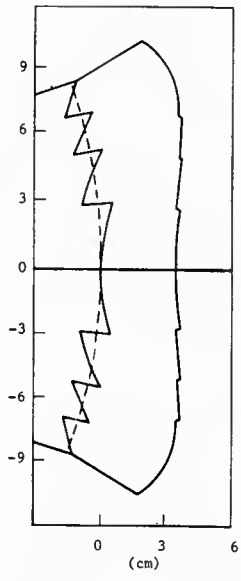

Fig. 2 Coma-Reduced, Shaped Lens Antenna for Multibeam Operation at 44 GHz (From Lee [3]).

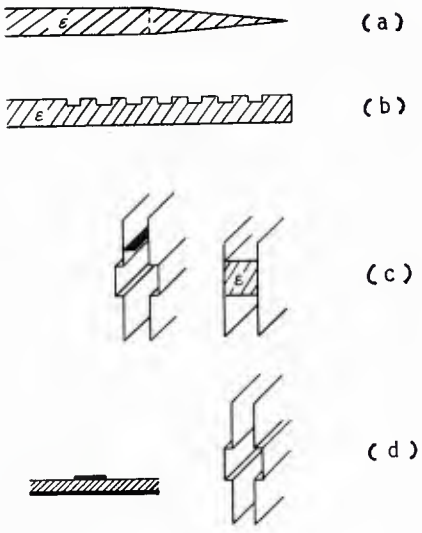

Fig. 3 Traveling Wave Antennas Derived from Open Millimeter Waveguides
(a) Tapered Dielectric Rod Antenna
(b) Periodic Dielectric Antenna
(c) and (d) Uniform Waveguide Leaky Wave Antennas

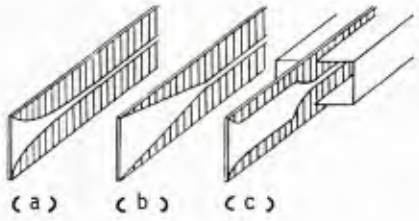

Fig. 4 Printed Traveling Wave Antennas Compatible with Shielded Millimeter Waveguides
(a) Vivaldi Antenna (Exponential Taper)
(b) Linear Taper Antenna
(c) Antenna with Constant-Width Section
(After Yngvessen, et al [17])

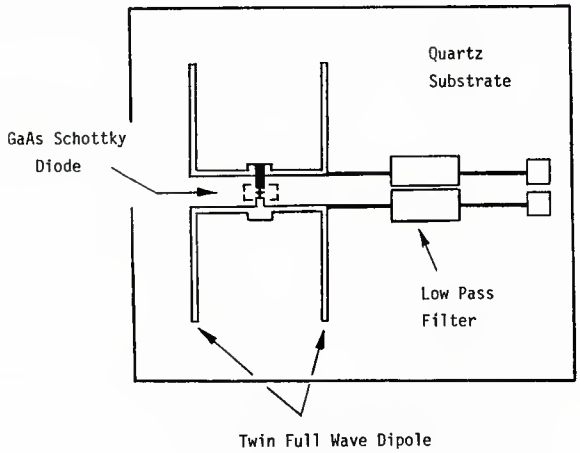

Fig. 5 Printed Twin-Dipole Antenna with Integrated Schottky GaAs Diode on Quartz Substrate
(After Fetterman, et al [18])

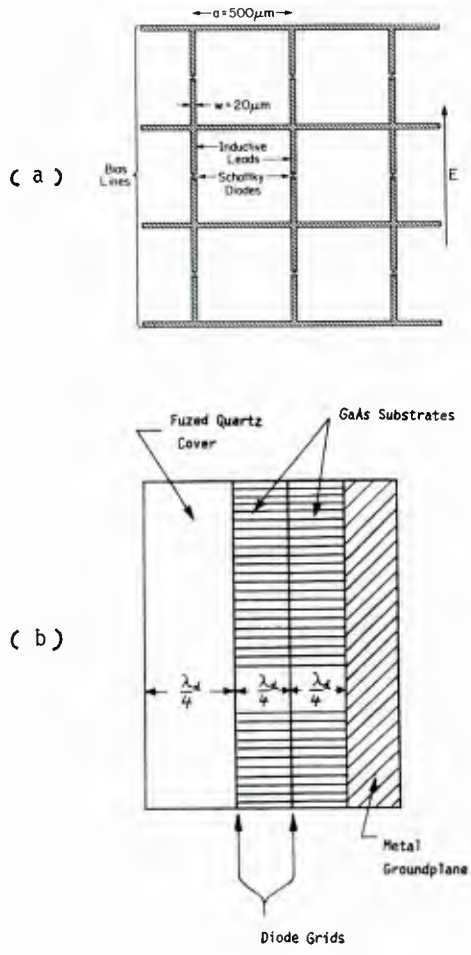

Fig. 6 Reflector Antenna for Electronic Beam Steering
(a) Metal Grid with Monolithic Varactor Diodes on GaAs Substrate (90 GHz)
(b) Cross Section View of Beam Steering Reflector with Two Diode-Loaded Grids
(From Lam, et al [19])

ADAPTIVE ANTENNAS

by
P.Barton
STC Defence Systems
Paignton, Devon, UK

0. Abstract

1. Introduction
1.1 Background
1.2 Basic Principles
1.3 Wanted Signal Discrimination

2. Adaptive Weight Control
2.1 Correlation Loop Approach
2.2 Weight Perturbation Approach
2.3 Direct Solution Methods
2.4 Circuit Considerations

3. Sidelobe Cancellation
3.1 Outline
3.2 Performance Limitations

4. Adaptive Array Configurations
4.1 Array Space Adaption
4.2 Beam Space Adaption
4.3 Circular Arrays

5. Partial Adaptivity
5.1 Thinned Arrays
5.2 Sub-array Adaption
5.3 Partial Adaption in Beam Space

6. Concluding Comments

7. Bibliography

ABSTRACT

The basic principles of adaptive antennas are outlined in terms of the Wiener-Hopf expression for maximising signal to noise ratio in an arbitrary noise environment; the analogy with generalised matched filter theory provides a useful aid to understanding. For many applications, there is insufficient information to achieve the above solution and thus non-optimum constrained null steering algorithms are also described, together with a summary of methods for preventing wanted signals being nulled by the adaptive system.

The three generic approaches to adaptive weight control are then discussed; correlation steepest descent, weight perturbation and direct solutions based on sample matrix conversion. The tradeoffs between hardware complexity and performance in terms of null depth and convergence rate are outlined.

The sidelobe cancellor technique is described, concentrating on large aperture main antennas associated with a small number of auxiliary antennas. Performance variation with jammer power and angular distribution is summarised and the key performance limitations identified.

Array antennas are increasingly being applied to avionics systems because of their high potential performance. Depending on whether the array process is considered at the focal plan or directly on the antenna face, arrays can be categorised into multiple beam or phase scan types. The configuration and performance characteristics of both will be covered, with a brief discussion of performance factors.

Attention is given in the last section of the lecture to partial adaptivity, since there can be a large cost penalty in implementing the optimum solution, especially for large apertures. The key parameters of number of degrees of freedom, angular sector coverage, number ofjammers and aperture size are examined and general performance trends outlined.

1. INTRODUCTION

1.1 Background

An adaptive antenna is one which reacts to the signal environment in which it is placed. The general objective is to increase the signal to noise ratio at the output of the antenna by optimising the directional pattern in some automatic way.

Many non-adaptive antennas are directive, especially those constructed from large apertures. A high gain beam can be formed surrounded by sidelobes at a significantly lower gain level. With the beam steered towards the signal, interfering signals received via the sidelobes will be suppressed and the signal to

noise ratio enhanced. In the case of dish antennas, the steering function will be mechanical. For phased arrays and multiple beam antennas, the beam can be directed electronically without the constraints of mechanical inertia.

It is possible with some non-adaptive design approaches to provide substantial suppression of jamming or interference signals which are angularly well separated from the wanted signal. Precisely applied tapered illumination functions across reasonably large apertures can allow -40dB sidelobes to be achieved. This level of performance is more readily obtained with single beam mechanically scanned antennas than with phased array or multiple beam types. Inevitably, the tapering action mismatches the antenna from the wanted signal spatial distribution but this modest loss is more than made up for by the lowering of sidelobe levels, for situations where external noise and interference dominate system performance.

The major limitations arising from use of non-adaptive antennas in severe interference environments are:

1) fairly large electrical apertures (i.e. in terms of wavelength) are required for low sidelobes to be achieved.

2) with a small electrical aperture a broad antenna beam is formed. Consequently a relatively large angular separation between interfering and wanted signals is required for significant discrimination to be obtained

3) very accurate and high resolution phase-shifters will be needed to maintain low sidelobes in a phased array and mutual coupling effects may well have to be accounted for in the beam scan programme.

4) scattering, multipath and obscuration effects from the platform on which the array is mounted or the land or sea environment can degrade the effective sidelobe level significantly.

In the light of these limitations, the adaptive technique promises a better capability to achieve high discrimination between wanted and unwanted if the available aperture is small and situated on a cluttered platform, or if extreme discrimination is required.

One of the earliest examples of an adaptive antenna is the self-cohering array the objective with this technique being to automatically phase the array to maximise gain towards a received signal. The other early application area (over 20 years ago) was sidelobe cancellation (a subject to which we will return) which is a device to reduce the sidelobe level of a large aperture array in specific directions to minimise effects of interference. These first sidelobe cancellors suffered major limitations in performance and it was commented in retrospect that these early failures set adaptive antenna technology back by several years. With the benefit of hindsight, what was missing was a good theoretical understanding of the adaptive process to account for apparently anomalous convergence, instability, null degradation, multipath degradation and other affects.

During the late 60's and early 70's a substantial amount of ground was gained in an improved understanding of both theoretical and experimental aspects of adaptive antennas, culminating in a special issue by IEEE in 1976 devoted entirely to this technology. Key papers by Applebaum, Widrow, Compton, Brennen & Reed and others were included, and the guest editor was William Gabriel.

From the mid 70's onwards to today, major research and development teams in the US and Europe have taken this technology to a point where it can be exploited cost effectively in the new generation of radars, communication and navigation systems. The advance of microwave integrated circuits and digital VLSI is key to practical implementation, allowing relatively complicated electronic functions to be implemented in a small volume and with low power consumption.

1.2 Basic Principles

The generally known concept of the matched filter (in frequency space) in Communication Theory provides an appropriate starting point. For the classical case of a signal spectrum S(f) embedded in white noise, it is shown that a filter having a frequency characteristic S*(f) provides the maximum signal to ratio at its output. Literally, this filter has an amplitude characteristic having the same shape as the signal and a phase characteristic which is conjugate to the signal; it "unwinds" the signal phase so that the filter output is due to cophasal signal elements.

Now take the case of maximising SNR when a signal is embedded in a coloured (i.e. non-uniform) noise background. Maximisation in this situation can be viewed as a two-part process; firstly, the frequency spectrum is weighted by a filter function A(f) which yields a uniform noise spectrum and secondly a modified matched filter is then incorporated to optimally integrate the now distorted signal A(f) s(f). Thus the modified matched filter has a characteristic A*(f) S*(f). Combining these two stages, we see as illustrated in fig. 1 that the overall filtering

function is given by A(f) A*(f) S(f). In effect, the information on noise distribution embedded in A(f) has been used to modify the shape of the original matched filter function s(f) for a uniform noise environment.

By analogy, optimum reception of a signal by for example an n element linear array antenna in an isotropic noise background is achieved by using phase weights to compensate for the phase differences between elements. Thus (referring to Fig. 2) if the space vector describing the signal direction is S, the signal waveform is s(t) and the noise from the n receiver channels is N, then the total signal can be described as

$$s(t)\ S\ +\ N$$

where $S^T = [1, \exp(j u), \ldots\ldots \exp(j (n-1) u)]$

$u = \frac{2\pi d}{\lambda} \sin\theta$

d = element spacing

θ = angle of arrival from beresight

λ = operating wavelength

and $N^T = [n_1(t),\ n_2(t), \ldots\ldots n_n(t)]$

The above example implies a uniform amplitude response across the array as well as a constant phase increment between elements. Since uncorrelated noise components sum together on a power basis regardless of their relative phase, whereas the signal will clearly be maximised if the combining phases unwind the space vector element phases, it is easy to show that the maximum SNR is obtained when the weight W with which the signal elements are combined is given by

$$W = kS^*$$

Now consider the case when the noise background is not isotropic but includes external sources of noise received from discrete angular directions added to the uncorrelated receiver noise components of the array receivers. The noise outputs N from the various receivers will now be correlated and the noise output from the array combiners will clearly not be independent of the weights as was the case previously. In concept, a matrix transformation A at the output of the array elements can be incorporated to uncouple the noise components, thereby producing n uncorrelated unit power noise components at its output.
With this assumption we write

$$E\left\{(AN)^*\ (AN)\right\}^T = I$$

where $E\{\ \}$ is the expectation operator and I is the identity matrix.

This can be rewritten as

$$A^*\ E\left\{N^*\ N^T\right\}\ A^T = I$$

where $E\{N^*\ N^T\}$ is the covariance matrix of the noise at the array output, which we will define as M. It follows directly that

$$M = (A^T\ A^*)^{-1}$$

Going back to the figure and remembering the analogy with matched filter theory we can now visualise that the optimum way to combine the modified signal at the output of the transformation A is by a cascade of A* and S* (see fig. 3)

$$\text{ie output } y = (A\ X)^T\ A^*\ S^*$$
$$= X^T\ A^T\ A^*\ S^*$$
$$= X^T\ M^{-1}\ S^*$$

that is with the input signal X weighted by weights given by

$$W_{\text{optimum}} = k\ M^{-1}\ S^* \qquad (1)$$

This is a form of the Weiner-Hopf equation for maximising signal to noise ratio in a network and is the basis for adaptive antenna operation. It can be visualised as a set of weight values which produce a beam towards the wanted signal and if necessary spatial nulls against external noise in other directions (fig.4) With an n element array, there are sufficient degreees of freedom to steer up to (n - 1) independent spatial nulls.

It is straightforward to check that (1) is consistent with the uncorrelated noise case, since then the covariance matrix M takes the form $P_N I$ where P_n is the noise power in each channel. Thus M^{-1} is $P_N^{-1} I$ and the optimum weight becomes

$$W_{optimum} = k P_N^{-1} I \quad S^*$$

$$\propto S^*$$

A position has been reached from which a conceptual adaptive procesor based on the Weiner-Hopf equation can be outlined. As shown in Fig. 5 the total signals received by the array are applied to a processor which first estimates M by self and cross correlating several snapshots of noise and averaging the result. The estimate of M is then inverted and multiplied by the steering vector S* to yield weight values W which are applied to a following beamformer.

The principal a priori requirement for this process to work is knowledge of S, the signal direction. M can be estimated fairly readily given sufficient averaging in the processor, but we cannot apparently do without S to obtain the optimum solution. Adding to this conceptual problem is the high accuracy with which S must be known in many circumstances, largely when signal to thermal noise ratios are high. Without sufficient accuracy the signal is treated as interference and will be nulled.

As will be described later, there are some situations where knowledge of the signal direction can be implicitly obtained if the processor has information relating to the structure of the signal waveform allowing it to generate a reference or training signal. For many cases however, there is insufficient knowledge of the signal and we are faced with developing sub-optimum adaptive processes and/or wanted signal discrimination methods for solving the problem.

1.3 Wanted Signal Discrimination

Preservation of gain in the signal direction is a key challenge for practical adaptive antenna designs. If the SNR is low, as it is for instance in spread spectrum systems such as the satellite-based GPS, then small errors in the direction assumed for S will not degrade signal gain. At high signal to noise ratios however, even small directional errors will result in the signal being treated as a jammer and a null may be formed against it. For many practical applications, palliative measures must be taken to prevent the processor "adapting out" the signals. In pulsed radars for example the mean SNR from small narrow pulse target returns will be much lower than that from continuous jamming waveforms spanning the pulse repetition interval. The mean sensitivity of the processor can then be adjusted so that it is inoperative against the target pulse but responsive to the jamming. Heavy clutter returns at short range, which can be suppressed by the radar's MTI and which therefore should not require an adaptively placed spatial null can be timegated out from the adaptive processor. Operation in frequency hopping radio systems provides another example: if at least the frequency hopping sequence is known, then the adaptive processor can be controlled so that it operates "one step ahead" and can therefore form weights in a "no signal" environment.

In general we may categorise signal discriminant techniques into the following.

(i) Precise knowledge of S (either explicitly or implicitly via a reference signal approach) enables the optimum solution.

(ii) Approximate knowledge of S allows signal preservation of an angular sector by constraining the growth of adaptive weights in non-linear fashion.

(iii) Establishing a threshold for adaption, from estimation of wanted signal received power. This will be effective against strong jamming.

(iv) Time-gating the adaption process ie inhibiting adaption during the known time of signal reception. Both gated radar operation and one step ahead adaption in a frequency hopped system as exemplified above fall into this category.

(v) Operating frequency and bandwidth control. In systems where the jamming spectrum differs from that of the desired signal, a window in the frequency domain for the adaptive processor can be provided which does not contain significant desired signal components. In many situations, the interference power spectrum will be significantly wider than the desired spectrum, in which case an offset sampling window may be used.

(vi) Adjusting the number of degrees of freedom. If a particular interference environment consists of N_i discrete sources which are stronger than the desired signal then no more than N_i degrees of freedom need be used to produce a substantial SNR improvement.

2. ADAPTIVE WEIGHT CONTROL

Having outlined the derivation of the optimum weights for a conceptual adaptive antenna, various practical forms of adaptive processor will now be described. Two types of closed loop processors, in which the array output is sensed in order to

provide drives to weight networks, are outlined to start with. The first of these, the closed loop correlation technique, requires sensing of both the individual element signals and the variable combiner output. The Weight Perturbation technique is the second type and relies only on measurement of signal power at the output of the variable combiner to control the variation of the weights. This is followed by a discussion of practical implementations of the direct class of solutions, which are directly aligned to the conceptual solution used in the introduction.

2.1 Correlation Loop Approach (fig. 6)

This is the best known type of adaptive antenna; both the Applebaum loop and the Widrow LMS configuration fall into this category. As part of the following description, the techniques of steering vectors, reference signals and sub- optimum null steering will also be covered.

In the correlation loop approach, adaptive weight control is provided by feedback loops driven by signals proportional to the correlation between the array output and the signals in individual channels. The loops enact a process of steepest descent either towards a maximum SNR or towards a minimum interference output, depending on how the circuit is controlled. In doing so, the 'error' signals from the correlators will be driven towards zero, indicating an absence of correlation between the input signals of the array and the variable combiner output. This condition manifests itself in the sense that the weights in the variable combiner produce spatial nulls towards interference sources in the antenna directional pattern.

The steady state solution for the weights can be straight forwardly obtained. As shown in fig. 6, a complex signal x_k in the kth channel of an n-element array is weighted by w_k. In steady state, the output of the kth correlator plus a bias or "steering" voltage s_k provides the drive to the loop amplifier; thus

$$G \left[s_k^* - E \left\{ x_k^* \sum (w_i x_i) \right\} \right] = w_k$$

or $$G \left[s_k^* - \sum E \left\{ x_k x_i \right\} W_i \right] = w_k$$

or $$G \left[s_k^* - \sum m_{ki} w_i \right] = w_k$$

Where G is the amplifier gain and m_{ki} is an element of the signal plus noise covariance matrix . Using matrix notation, with X being the column vector of n signal components and W being the weight vector, the solution for the whole array can be written as

$$G \left[S^* - M W \right] = W$$

If G is large, then

$$M W \simeq S^*, \text{ or } W = M^{-1} S^*$$

which has the same form as the Weiner-Hopf expression for the optimum weights derive in Section 1. As has been mentioned in section 1, the knowledge of S is a prime requirement for achieving the optimum adaptive solution. As well as providing it explicitly as in Fig. 6, we may provide a reference signal which, if it correlates with the wanted signal, will implicitly generate the correct steering vector. Fig. 7 shows the provision of such a signal y(t) and we can write for the kth channel:

$$G \; E \left\{ x_k^* \left[y(t) - \sum w_i x_i \right] \right\} = w_k$$

For the complete circuit therefore:

$$G \left[E \left\{ y(t) X^* \right\} - M W \right] = W$$

which, if G is large, becomes

$$W \simeq M^{-1} E \left\{ y(t) X^* \right\}$$

as long as the reference signal correlates with the wanted signal but not with any of the interfering signals. If correlation does not occur with the wanted signal, then the weights will decay to zero, as indicated in the equation, and the processor will be ineffective.

With no knowledge of either the signal waveform or space vector, the optimum solution is not achievable. Nevertheless, a useful type of adaptive antenna can still be realised, one in which an omnidirectional pattern takes the place of a beam steered towards the signal and in which therefore nulls are formed to suppress

interference in a pattern which is otherwise approximately omnidirectional. Fig. 8 is an outline schematic for such an array in which there are no steering vectors or reference signal applied; instead one of the channel weights (W_j) is held constant at unity. It will be shown that this configuration will minimise noise power at the array output subject to the constraint of the clamped weight. Referring to Fig. 8 we can write for the kth channel

$(K \neq j)$

$$- G \; E \left\{ x_k^* \sum w_i \; x_i \right\} = w_k$$

For the whole array, this becomes

$$(I + G M) \; W = \alpha C$$

$$\text{ie.} \qquad W = \alpha (I + G M)^{-1} C$$

where C is a column vector with all elements equal to zero except for the jth which has the value 1. The condition that the jth weight is unity demands

$C^+ W = 1$, from which we can determine α above.

We can write

$$C^+ W = C^+ (I + G M)^{-1} C = 1$$

or

$$\alpha = \frac{1}{C^+ (I + G M)^{-1} C}$$

Thus

$$W = \frac{(I + G M)^{-1} C}{C^+ (I + G M)^{-1} C}$$

If G is very large, then W can be written as

$$W \simeq \frac{M^{-1} C}{C^+ M^{-1} C}$$

$C^+ M^{-1} C$ is a scalar factor and the above equation can therefore be interpreted as $W \propto M^{-1} C$, ie a solution which can be considered optimum if the signal itself were isotropic. This is clearly not the case, but it does cause the adaptive procesor to assume that it can arrive from any direction. The solution obtained minimises the interference but does not maximise the signal and is therefore not an optimum solution. Nevertheless, especially for small arrays where the number of channels is low and therefore for which the maximum gain towards the signal is modest, the performance obtained is not grossly sub-optimum and, for severe ECM environments, can still provide a substantial improvement in system performance.

There are limits on the rate at which a correlation loop adaptive antenna can converge towards the optimum weight solution, dependent on the power and angular distribution of the external noise environment. The formal approach taken to analysise dynamic behaviour is to determine the eigen-structure of the noise covariance matrix and to show that the noise when decomposed into different independent components by means of an eigen vector transformation, exhibits a spread of power corresponding to the eigen values of the covariance matrix. It then follows, from the control law determining covergence, that the time constant of adaption to individual noise components (eigen values) is inversely proportional to the power in that component. When jamming sources are separated in angle by an amount exceeding the "natural" beamwidth of the array, the particular eigen values can be associated directly with individual jammers, and thus the spread of received jamming power will in this case determine the range of time constants involved in the covergence process.

The theoretical behaviour determines practical limits to the time constant in a hardware solution. In particular, the minimum time constant of adaption should not be less than 10/B where B is the interference bandwidth. Thus for a single jammer scenario, the correlation loop should for instance be capable of providing a deep null (say 40dB) after about 5 time constants have elapsed i.e. after 50/B seconds. For the case of a 1MHz bandwidth this corresponds to 50 μs. If however the array is confronted by a number of interference sources and is required to direct nulls towards each of them, then the response can be much more sluggish. The combined interference will be present all the time in individual channels; thus the strong jamming sources will limit the high frequency gain that can be applied in the feedback loops in order that weight noise is minimised and much slower responses to weak jamming components will be inevitable, the range of time constants being equivalent to the range of eigen values associated with external sources in the covariance matrix.

For instance, if 40dB net suppression was required and the jamming comprised a 0dBW and a -32dBW component, then the time constant of response towards the weaker component would be 1600 times longer than that towards the strong component. This

imbalance would only be partially compensated by the requirement for 5 time constants to elapse for adequate suppression of the stronger source, compared with one time constant for the weaker. If a 1MHz bandwidth is again considered, the time to covergence in this second situation is approximately 16ms.

2.2 Weight Perturbation Approach

A significant part of the cost of an adaptive antenna employing correlation loops is concerned with the high gain receiver channels needed in each element channel. A way of avoiding this is to perform the weighting and combining functions directly "behind" the antenna and to estimate the path of steepest descent by perturbing weights about a mean value and measuring the variation of power at the variable combiner output. The outline schematic of such an array is shown in fig. 9. An algorithm is considered which takes each weight in turn and perturbs it positively and then negatively for a time during which the mean power in the two conditions are measured. Thus for the kth channel the weight W_k is varied between $W_k + \delta W_k$ and $W_k - \delta W_k$.

An estimate of the power variation with weight value, the gradient G, is given by

$$G_k = \frac{P_k (W_k + \delta W_k) - P_k (W_k - \delta W_k)}{2 \delta W_k}$$

The perturbation step δW_k is chosen as a compromise between a relatively large step for accurate gradient measurement and a small one to minimise the introduction of additional output noise due to the perturbations. A perturbation step size given by

$$\delta W_k = \sqrt{\frac{P}{P_e}}$$

where P_e is the power level at an array element, leads to an excess noise power due to the perturbations of 3dB. Thus as the array adapts, P and consequently the perturbation size reduces.

The complete weight perturbation steepest descent algorithms for an I or Q component of a weight can be written as

$$W_{k+1} = W_k - \mu \sqrt{P_e} \left[\sqrt{P_k (W_k + \delta W_k)} - \sqrt{P_k (W_k - \delta W_k)} \right]$$

A major difference between weight perturbation and correlations processors is that the former needs to monitor signals at the array output and one antenna element only in a sequential manner. In addition, one of the weights is always perturbed from its nominal setting giving rise to "spikes" of interference power on the antenna output often referred to as perturbation noise. The technique retains feedback from the array output to correct hardware imperfections.

Fundamentally the weight perturbation approach is somewhat inferior to correlation because of perturbation noise and the necessity of having at least two Nyquist samples per gradient estimate. However the simplicity of the approach has lead to most system implementations being based on microprocessor technology in order to realise low cost. It is the use of microprocessors rather than dedicated logic which really slows down a perturbation processor's adaptation rate.

A typical microprocessor implementation including all the I/O operations to the weights and power meter, can consume 500 instruction cycles per iteration. For microprocessors with a 1 μs instruction time, the minimum time constant of adaptation would be around 20 ms. When derated by the variation in signal levels in complex jamming environment a maximum time constant of 20s is to be expected. Such time constants are not consistent with a high performance airborne adaptive antenna. However, it must be remembered that this is largely due to the microprocessor implementation and could be improved significantly by using customized digital control circuitry.

2.3 Direct Solution Methods

In section 1, following the derivation of the matrix form for the optimum weight solution, a conceptual approach for realising an adaptive antenna was suggested which does not rely on correlation loops; instead (fig.5) a mathematical processor is used first to estimate covariance, then to invert this estimate and multiply the inverse by a loop direction or constraint vector, and lastly to apply the weights to a digital beamforming circuit. It has been shown by several authors, notably Brennen & Reed (10) that this type of approach has the advantage of requiring only limited input data to accurately describe the external environment and provide an antenna pattern which can suppress a wide dynamic range of jamming signals. For an n element array, it can be shown that 2n "snapshots" of the array signal are sufficient for adequate performance.

For adverse interference environments, having a wide power spread in the jamming sources, the direct solution can be several orders faster than the correlation loop

approach. In practice, the major price to be paid is one of processing complexity. Both covariance matrix estimation and forming the inverse (essentially solving a set of linear equations) involve a high arithmetic operation count, each requiring of the order of N^3 multiply/add operations for an N element array. Further, it can be shown that the explicit formation of a covariance matrix doubles the logarithmic dynamic range of the data since its dimension is power and also that many of the candidate algorithms, eg Gauss Jordan elimination, give rise to reciprocals of small differences and are sensitive to the processing wordlength. In a paper by Ward et al (30) these performance characteristics are illustrated by a simulation of a particular case. A six element linear array receives four jamming signals at 0, -10, -20 and -40dB relative power levels against a background of -50dB thermal noise. Even though 22-bit floating point wordlength is employed within the processor partitioned into a 16-bit mantissa and a 6-bit exponent there is clear evidence from the variation in the thermal noise residual (fig.10a) of an unstable weight solution being obtained. Mainly as a result of these above limitations, together with the extreme complexity of realising a real time processor from existing MSI and LSI digital devices, the practical application of direct solution methods has lagged far behind the correlation loop technique.

Over recent years a new impetus to implement direct solutions has emerged with the development of systolic array processing techniques (ref 15) . Signal processing algorithms which can be partitioned into relatively simple elementary operations operating in parallel and involving time lags or data skew can be realised in a parallel pipeline form in which computing elements need only be connected to their 'nearest neighbours'. Digital VLSI elements can be designed to perform the individual cell operations and by use of several such chips in a highly parallel array, complex realtime processing can be realised at a very high throughput rate.

For the specific case of a direct solution adaptive processor, new algorithms have been developed which can exploit the regularity and parallelism outlined above and which do not require explicit evaluation of the signal covariance matrix. The process of adapting the weights of an adaptive with one weight held constant can be considered a least squares minimisation problem, in which the (n-1) adaptive channels are summed in such array as to minimise the difference between that signal and the one received by the non-adapting element channel.

Thus we can write

$$e_N = X_N W_N - y_N$$

where X_N is matrix comprising rows corresponding to N independent data snapshots received across all but one element of the array, W_N is a weight vector, y_N is a vector describing the data sequence received at the clamped element and e_N is a vector of residuals obtained over the sequence of N data snapshots. Rather than minimising e_N by a squaring process leading to direct evaluation of sample covariance, we may instead premultiply each side of the above equation by a unitary transformation say Q_N which does not affect the size (or norm) of the residual and does not square the data. Thus

$$Q_N e_N = Q_N X_N W_N + Q_N y_N$$

By choosing Q_N to give

$$Q_N X_N = \begin{bmatrix} R_N \\ 0 \end{bmatrix} \quad \text{and} \quad Q_N y_N = \begin{bmatrix} b_n^{(1)} \\ b_n^{(2)} \end{bmatrix}$$

(Rn being an (N-1) (N-1) upper triangular matrix, 0 a null matrix), the minimum norm condition for e_n can be obtained by inspection as

$$R_N W_N + b_N^{(1)} = 0$$

This equation therefore defines the least squares solution for the adaptive array and can be easily solved by back substitution.

The method adopted by Ward et al for the transformation process is the Givens rotation and for a detailed description of their method refer to (30)

To verify the numerical superiority of this method, the same example scenario of 4 unequal power jammers for a six element array was modelled using the Q-R decomposition technique outlined above. In fig. 10b we can see that, although the rate of adaption is rapid as for sample matrix inversion, the method shows no signs of numerical instability.

2.4 Circuit Considerations

Receiver Channels Balance

For the optimum solutions employing steering vectors, the signal space vector as perceived by the adaptive processor has to be accurately known so that the steering

vector can be closely matched and hence prevent signal cancellation. The degree of match required depends on the SNR. For example, a six channel array receiving at 20dB SNR in each channel requires the match to be closer than 2 degrees in phase and 0.5dB in amplitude. This is a tight requirement not only on the phase/amplitude balance between receiver channels but on the antenna array geometry and mutual coupling characteristics.

By contrast, there is no first order requirement on absolute phase and amplitude balance between loop direction vector formation via the reference signal approach channels with respect to interference nulling, or implicit look-direction, vector-formation via the reference signal approach, since any such ofsets are automatically accounted for in the solution for the weights. For example, consider the sub-optimum adaptive null steering configuration of Fig. 8 having phase and amplitude offsets in the channels represented by the diagonal matrix

$$E = \text{dia}\ (e_1\ \ e_2\ \ \ldots\ldots\ e_N)$$

The circuit will now adapt to yield weights given by

$$W = E^{-1}\ M^{-1}\ (E^*)^{-1}\ C^*$$
$$= K\ E^{-1}\ M^{-1}\ C^*$$

where C is the constraint vector $c_k^* = 1$, $c_j^*\ (j \neq k) = 0$. It can be seen that the adaptive weights have been modified by the factor E^{-1} which precisely compensates for the initial channel errors E. The compensation effect which is such a robust feature of adaptive antenna operation remains valid when E is not diagonal as caused by for example mutual coupling between array elements.

Although to a first order, adaptive weight control algorithms can compensate for channel offsets, the existence of frequency dispersion between channels can limit performance significantly. If amplitude and phase responses do not track between say two channels then a single valued amplitude and phase weight cannot provide optimum suppression of an interfering signal (fig. 11). Suppose interchannel variation in phase and amplitude increase linearly from the bandcentre to the bandedge, ie

phase between channels = $\alpha - \delta$ at lower bandedge
= $\alpha + \delta$ at upper bandedge

amplitude balance = 1 - a at lower bandedge
= 1 + a at upper bandedge

then the total interference residual ΔP (relative to the level at each individual element) will be given by

$$P = \frac{1}{3}\ (\delta^2 + a^2)$$

Errors of $\pm$ 0.05 rad (3 degrees) and $\pm$ 5% amplitude at the bandedges for example will thus give rise to residuals of approximately -28dB.

Weighting Circuit Accuracy

For the closed loop methods, there is no first order requirement on weighting circuit accuracy regarding null steering or reference signal generation since the adaptive loops compensate for these errors. (In contrast, a steering vector configuration will require tight absolute control on weights values in order that an accurate steering vector is applied to the system). The essential properties required for the closed loop approaches are

(i) effectively continuous control of the weight values.

(ii) monotonic transfer characteristics (to prevent unstable operation)

(iii) low frequency dispersion

For direct solutions, the optimum weights must be applied exactly since errors in the applied weights are not accounted for in their derivation. This leads in practice to the need for digital beamforming.

Other Requirements

Provision of a directive antenna pattern by combination of a number of signals in multiple channels of an array requires a high degre of linearity in the channels and combining networks as well as close matching of their frequency dispersion characteristic. It can be noted that a null depth of 40dB implies phase and amplitude balances across the aray of the order of 0.1dB and 0.5 degrees; thus even minor mismatching due to either dispersion or to different degrees of

non-linearity in the different channels can significantly degrade performance.

A further requirement in the case of the correlation loop approach is an adequate balance in the group delay between the two legs of the correlator. Unless this is sufficiently good to keep the phase delay of all signal and noise components matched to less than 90 degrees, poor convergence and possibly instability will arise.

3. SIDELOBE CANCELLATION

3.1 Outline

For a number of radar and communication systems employing large aperture receiving dishes, strong interference received via the antenna sidelobes can disrupt system operation especially near the main beam where sidelobe levels are not very low. The principle of sidelobe cancellation is to augment the antenna system with a number of auxiliary low gain antenna elements each with a separate receiver channel and to combine these signals adaptively with the main receiver output, the objective being to cancel the sidelobe response in specific directions. Fig. 12 shows an outline schematic.

The operation of this system can be described in similar fashion to the null steering array with a clamped element channel. For the sidelobe cancellation case, the main antenna output will be connected to the clamped channel and the auxiliaries will be variably weighted. The signal vector X now describes the relative phase and amplitude response of the signals received. M is the signal covariance between these channels and the weight solution is given by

$$W = \eta M^{-1} C$$

where η is a complex scalar quantity.

Take a simple example with one narrowband interference source and one auxiliary channel. If the output of the main receiver and auxiliary channel (each comprising signal and noise components) are respectively

$$v_1 = Am \quad \exp j\,[(wt + \alpha m)] + n_1(t) \exp jwt$$

and

$$v_2 = Aa \quad \exp j\,[(wt + \alpha a)] + n_2(t) \exp jwt$$

then the covariance matrix is given by

$$M = \begin{bmatrix} Am^2 + P_1 & Am\ Aa \exp j\,(\alpha a - \alpha m) \\ Am\ Aa \exp j\,(\alpha m - \alpha a) & Aa^2 + P_2 \end{bmatrix}$$

where P_1 and P_2 are the receiver noise powers in the two channels, we have to solve $MW = C$, from which we find that

$$W_1 = 1$$

and

$$W_2 = \frac{-Am\ Aa \exp j\,(\alpha m - \alpha a)}{Aa^2 + P_2}$$

These weights cause the external signal to be virtually cancelled and the output residual comprises mostly thermal noise from the main and auxiliary channels.

The more gain that the auxiliary channel has the smaller the noise contribution it makes to the output (since it reduces the scale required of the weight W2). The influence of the auxiliary on the total antenna pattern is illustrated in Fig. 3. Since the weighted gain of the auxiliary must be equal to that of the sidelobe to be cancelled, it may well degrade the overall antenna pattern away from the null should the cancelled sidelobe have been a relatively large one. Further, if the auxiliary gain does not aproximately match the envelope of the main antenna's sidelobe response then the far out sidelobe levels can be degraded considerably.

3.2 Performance limitations

Apart from the tendency to worsen the general sidelobe characteristics, there are a number of other potential limitations of the technique including

- Convergence rate limitations with a scanning antenna
- Aperture dispersion
- Multipath propagation

For surveillance radar applications, the sidelobe cancellor circuit has to be able to track the change in phase delay between the main dish and the phase centre of the auxiliary antenna as it scans, as well as the cyclic amplitude variation in the main dish sidelobe characteristic. If the scanning rate is Ω rads/sec, the main

dish aperture is L_m and the distance between main and auxiliary phase centres is L_p we may write for the near boresight case:

sidelobe period $\simeq \frac{\lambda}{L_m \Omega}$ seconds

and rate of phase delay variation $\simeq \frac{\Omega L_p}{\lambda}$ cycles/sec

For a typical example $\Omega = 1$, $L_m = 3m$, $L_p = 2m$ and $\lambda = 0.03m$ yielding a sidelobe period of 10ms and a phase rate of 67Hz.

In order that cancellation is maintained, the convergence rate of the cancellor must be sufficiently rapid so that its effective delay is very much smaller than the figures above.

Aperture dispersion effects can be another major shortcoming in this technique because of large distances between antenna phase centres, and the frequency dependence of the sidelobe pattern of the main antenna. Suppose sidelobe cancellation is to be effective over a signal bandwidth B, that the signal to be nulled covers that bandwidth and is received at an angle θ with respect to the normal of the line joining the phase centres of the main and auxiliary antennas. Then, the total relative signal phase dispersion across that bandwidth will be

$$\frac{2\pi \text{ Bd sin } \theta}{c} \text{ rads}$$

For small amounts of phase dispersion (less than 1 rad) this corresponds to a residual power, averaged across the bandwidth, of approximately

$$\frac{1}{12}\left(\frac{2\pi \text{ Bd sin } \theta}{c}\right)^2$$

relative to the uncancelled sidelobe level. As an example, for B = 20MHz, d = 2m and θ = 30 degrees, this residual level is -19dB.

Frequency dispersion between the main and auxiliary apertures can be even more of a problem than outlined above, if the main aperture itself includes a highly dispersive feed network such as a Serpentine feed for frequency scan antennas. For some types of frequency scan antenna, the delay between the feed point and the antenna phase centre can be as much as 10 times that implied by the physical distance involved.

For most antenna types, the sidelobe amplitude pattern will be frequency dependent as well as the phase difference between the main and auxiliary antenna. The forward sidelobes well away from the main beam are controlled largely by the step change in current density at the extremes of the aperture, the kth sidelobe null being at an angle θ_k off boresight given approximately by

$$\theta_k = \sin^{-1}\left(\frac{ck}{fL}\right)$$

where L is the distance between aperture extremes and f is the operating frequency.

If a bandwidth B centred at f is now considered, then the position of θ_k and θ_{k+1} at the bottom and top of the bandwidth are given by

$$\theta_k \text{ (lower)} = \sin^{-1}\left(\frac{ck}{(f - \tfrac{1}{2}B)L}\right)$$

$$\theta_k \text{ (higher)} = \sin^{-1}\left(\frac{ck}{(f + \tfrac{1}{2}B)L}\right)$$

$$\theta_{k+1} \text{ (lower)} = \sin^{-1}\left(\frac{c(k+1)}{(f - \tfrac{1}{2}B)L}\right)$$

$$\theta_{k+1} \text{ (higher)} = \sin^{-1}\left(\frac{c(k+1)}{(f + \tfrac{1}{2}B)L}\right)$$

Taking an example with L = 2m, k = 30, f = 10GHz and B = 40MHz, we find that the sidelobe null positions shift by approximately 0.1 degrees, a significant proportion of the nominal sidelobe width of approximately 1 degree.

Both amplitude and phase dispersion effects can be lessened by either having more than one auxiliary channel available for each broad band interference source or by incorporating an adaptive filter network in each auxiliary channel. The first method is wasteful in its use of auxiliaries and thus the second is to be preferred even though the number of adaptive weights to be controlled by the processor become relatively large.

The principle of adaptive frequency filters is covered quite extensively in the literature but it can be described in outline as follows. Suppose the bandwidth B is covered by a parallel bank of b filters each of bandwidth B. Adaptive phase and amplitude weights at the output of each filter can now be optimised independently to minimise the residual in that sub-band and the extent of dispersion in any one channel is thus reduced. Going back to the example of -19dB residual power across a 20MHz bandwidth using a single co plex weight, if the band were divided into 4 sub-bands and the weights individually optimised in each sub-band, the residual power would be reduced to about -31dB. An alternative implementation which allows a comparable improvement to be achieved is a tapped delay line filter with variable weights, the tap spacing being of the order of 1/B sec. (fig 14).

A further cause of performance degradation is multipath propagation. If a jammer signal is received via one direct and a number of indirect paths then, if the delay on each path is different, good cancellation may require a number of auxiliary antennas. Differential delays of the order of the reciprocal of the filter bandwidth or greater lead to the multipaths appearing as independent signals, thus requiring multiple sidelobe nulls to be formed. The situation is further complicated by cross-polar effects; multipath scattering may exhibit a significantly different polarisation than the direct path signal and may require separately weighted co- and cross-polar auxiliary channels to be optimally suppressed.

4. ADAPTIVE ARRAY CONFIGURATIONS

The logical development of the sidelobe cancellor is the completely adaptive array in which beams can be steered electronically and all sidelobes are optimised. The outline of adaptive antennas has already been given in terms of such an array and in this section we consider the broad implications of their realisation in both array and beam space.

4.1 Array Space Adaption

The principle characteristic of any fully implemented array antenna with a wide scan angle capability is the need for elements at approximately half wavelength intervals for both planes of scan. We may relate the number of elements N (and hence channels in a fully adaptive receiving array) to the antenna solid angle beamwidth Ω_o (rads ^{2}) approximately as follows

$$N \simeq \frac{4}{\Omega_o}$$

Take the example of 10 deg x 10 deg beamwidth, ($\Omega_o = .03$); then N is approxmately 130. Even for such a relatively broad beamwidth example, the current cost of implementation can be very high assuming the provision of a front end receiver channel for every element and the use of a correlation loop processor driving analogue weights. What advantages will this configuration offer over a non-adaptive phased array, to offset its higher cost? The two major benefits have to be firstly the provision of significantly lower sidelobes towards interfering signals and secondly the ability to reject jamming which is closer to the beam scan direction. A brief discussion follows, regarding what sidelobe performance is to be aimed for and the implications on convergence time of the correlation loops. A non-adaptive phased array might achieve -25dB sidelobes and hence an improvement in SJR of 25dB, whereas the target set for an adaptive implementation might be a 40dB SJR improvement. In order to cope with a worst case spread of 40dB in jamming powers (or more properly eigen value spread in the covariance matrix) the loops must be able to respond to the weakest significant jammer during the requisite beam dwell time. Thus the minimum time constant will be some 10,000 times shorter than this.

At an even higher cost the digital direct solution could be implemented with N = 130. Not only is a complete receiver required with digitised baseband outputs for each element channel, but a digital processor having some 4000 parallel processing "nodes" for the optimum dynamic performance. For wide band signals (several MHz), one VLSI chip will be required for every node, whereas narrow band signals may be processed with each VLSI chip functioning as a number of processing nodes. The key advantage of the direct solution is that the convergence of the processor towards the optimum set of weight will be extremely rapid and should allow performance improvements of 40dB or more to be obtained in the most demanding interference scenarios. A more cost effective digital processor can be envisaged in which optimum weights are computed off-line and applied to a digital beamformer; for many applications, especially with wide band waveform, the ability to completely adapt in 2N Nyquist intervals is broadly speaking around 100 channels of

adaptivity in a wideband system is a probable upper band in affordability for some years to come. We can conclude that for the time being a fully adaptive pencil beam array having a beamwidth less than 10 x 10 degrees is not a practical proposition. If scanning/adaptive beamforming is confined to one plane, then a fan beam of about 1 degree beamwidth with complete adaptivity can be achieved with approximately 100 channels.

4.2 Beam Space Adaption (Fig. 15)

Consider a line array of n elements which is connected to a multiple beamformer yielding n orthogonal outputs. An adaptive processor having n channels should be able to operate either directly on the element signals or on the derived beam outputs and produce the same optimised output. Thus for practical antenna systems using say microwave lenses in which the natural output of the antenna subsystem is on beam space, adaptive processing an in theory be applied with equal effect as in the array case.

The dynamic behaviour of a correlation loop processor can be different in the two cases, depending on the angular distribution of the interference. Suppose first that strong jamming is received from one direction at the same time as a weak jammer is received from another, separated from the first by an amount exceeding the natural beamwidth of the antenna aperture. Adaption in array space will be relatively sluggish since the stronger jammer will determine the loop bandwidth, with the consequent time constant of response against the weaker component being extended. Adaption in beam space can be more rapid than this because of the angular decoupling provided by the beamforming process. The beam pointing towards the weak jammer will have a relative low residual response to the strong jammer (depending of course on the beam sidelobe characteristics) and the correlation loop gain for that beam channel can be adjusted nearer to that required for optimum response to the weak interference source.

Now take a second example in which a cluster ofjamming sources are emitting in a confined angular region somewhat less than the receiving antenna beamwidth. The close spacing of the sources results in a relatively wide eigen value spread in the array case because of the intrinsic angular coupling and this will again lead to a relatively extended convergence characteristic. Adaption in beam space will now also tend to be sluggish, particularly so because a number of beam channel outputs have to be combined with probably only one or two having an appropriately positioned main beam.

Circular Arrays

An interesting type of array is a circle of elements in the plane of scan, for example monopoles mounted on a relatively large ground plane in the form of a disc. Beams or nulls can be formed by suitable phasing of the elements so that signals from a particular direction are combined in or out of phase. Because of the geometry, such beams or nulls an be steered in any direction in the plane of scan.

An adaptive null steering circular array can be constructed either by incorporating an additional element at the centre of the circle connected to a clamped weight, or by selecting one of the elements around the circle for the weight clamped channel. Whereas a central clamped element gives rise to a fairly constant null width with respect to null angle, the null width varies considerably with angle if the clamped element is part of the circle. For source, directions at right angles to the radial from the clamped element, relatively sharp nulls are obtained; when the direction is in-line with the radial then broader nulls will be produced.

A method for producing uniformly narrow nulls in every scan direction is to excite the array with phase modes, for instance using a Butler Matrix. In this way, a number of array patterns are created, all nominally omnidirectional, but with increasingly variable phase. The lowest order mode has a nominally constant phase response with angle since it is produced by an in-phase combination of all the elements. First order phase modes are produced if the successive elements are combined with a phase difference of 2π /N radians, where N is the number of array elements resulting in a far-field phase pattern varying by 2π radians over the entire circle. For the Butler Matrix this will be the case for the "$\pm$ 1" drive points. In principle, N phase modes can be generated, the mth mode requiring an incremental phase shift of $2\pi m/N$ radians between successive elements and producing a far-field phase variation of 2π m radians over the circle. A signal received from a direction θ will give rise to a signal distribution at the Butler Matrix output of the form

$$\ldots a e^{j}, \; a e^{j\theta}, \; a e^{j2\theta} \ldots, \; a e^{jm\theta} \ldots\ldots$$

This phase distribution is equivalent to that in a linear array of elements spaced by d receiving a signal at an angle β off boresight related to θ by

$$\theta = \frac{2\pi d}{\lambda} \sin\beta$$

Thus by analogy with the linear array for which end element clamping provides the sharpest null pattern, clamping the lowest (or highest) phase mode in a circular aray system and causing the other modes to be adaptively combined should result in a relatively sharp null pattern being produced, the width now being independent of θ.

5. PARTIAL ADAPTIVITY

It has already been shown that, even for modestly directive antenna beamwidths, fully adaptive beamforming over wide angles requires a large number of adaptive channels and a complex processor. For many situations, it will not be necessary to completely optimise the antenna pattern; sidelobe or mainbeam optimisation in a number of discrete directions will be sufficient to provide adequate system performance. Sidelobe cancellors are designed to provide such performance, but their implementation with auxiliary omni antennas as described in section 3 leads to a number of limitations, particularly the degradation in the general level of sidelobes. A number of partially adaptive configurations with better performance can be employed: thinned arrays, adaptive sub arrays and switched beam space adaption.

5.1 Thinned Arrays

This can be a useful technique for null steering applications, affording a useful trade-off between null width and constancy of gain away from nulls. On airborne platforms, multipath and shadowing effects cause significant variations of gain from a nominally omnidirectional antenna and these effects are usually factored into the system's power budget. Thus, some variation in an airborne-mounted adaptive antenna can usually be accommodated. Some authors have used the concept of retro-directive ("retro") beams in explaining the operation of an adaptive antenna and the concept is useful at this stage in assessing the gain ripple from a thinned adaptive array. In forming a null at a particular angle in an otherwise omnidirectional pattern, the array is effectively forming a beam in that direction and subtracting it from the omni response. Such a "retro" beam formed from a thinned array will have higher sidelobes than from a filled array of the same aperture and it is these relatively high sidelobes which cause pattern variations away from the null when the retro beam is subtracted from the main response. If the thinned array has N elements, then a single retro beam will have an average sidelobe power level of about 1/N. The sidelobes then combine with the quiescent omnidirectional pattern in various phases, the worst cases being in or out of phase. A typical pattern variation from a thinned array, measured experimentally, is shown in Fig. 16.

Sub-Array Adaption

There are various configurations which can be suggested, falling into two basic categories (a) sub-arrays steered in common with the main beam and (b) those which can be steered independently of the main beam; these are illustrated in Fig. 17.

For (a) the look direction of all the sub-arrays is aligned with that of the main beam and thus adaption is nominally confined to an angular region centred at the look direction. This enables good performance against jamming close to the main beam and does not disturb the far-out sidelobe pattern excessively. However, in attempting to cope with jamming outside the sector covered by the sub-array beams, unpredictable performance will arise as the system will attempt to provide a spatial null by adaptively combining the response in the sub-array sidelobes.

The unpredictable behaviour outlined above can be avoided by configuration (b) in which sub-arrays can be steered independently in different directions. Following a scanning programme by the main pencil to establish the approximate angular distribution of the jamming, sub-arrays are assigned various look directions to cope with the various jamming clusters.

Partial Adaption in Beam Space

The implementation of the sidelobe cancellation function in beam space leads to a potential better performance than that obtainable by auxiliary omnidirectional antennas. This can be seen from Fig. 18 in which the auxiliary channel is first switched to the beam which is aligned closest to the jammer direction and then allowed to adaptively combine with the "main" beam. Because of the directive nature of the auxiliary beam, the general sidelobe structure after adaption is scarcely degraded in this approach. Further, since the effective phase centres of the various beams can in principle be the same, the effects of frequency dispersion are lessened.

A multiple canceller system will require that m of the n beams can be switched into auxiliary channels. The control of this switching process requires that the jammer distribution is first estimated by switching successively between all the beams and noting the received power variation. A decision then has to be made as to how to distribute the m adaptive channels. In some limiting cases, some iteration may be required to optimise the assignment of the channels.

6. CONCLUDING COMMENTS

From the descriptions given of a variety of adaptive antenna configurations, it should be clear that there are many useful applications of the technique, particularly when radar, communication and navigation systems have to operate in a severe ECM environment.

A number of processing methods for adaptive weight control are possible, with an inevitable tradeoff between performance and complexity of realisation. However, the continuing rapid advance of digital VLSI technology indicates that very high performance in terms of null depth and speed of convergence will soon be available at relatively low cost.

The other major cost factor is the number of adaptive channels employed. The more channels, the greater the ECCM capability since in principle each additional channel enables a further jamming source to be suppressed. Small fully adaptive arrays (with say 10 elements or less) can already be implemented cost effectively. As the array size increases, a compromise will have to be taken when the required number of channels for a fully adaptive solution becomes too large. Partial adaptivity of one sort or another has then to be considered; various forms (including the sidelobe cancellor) have been outlined in the lecture. The development of microwave monolithic integrated circuits is important in this respect so that the cost of each receiver channel can be reduced.

Given the availability of high performance adaptive processors and cost-effective receiver technology, there remains the challenge of wanted signal discrimination. A very detailed knowledge of the signal structure or angle of arrival is required for the optimum adaptive solution to be implemented in practice. Failing this, some knowledge of say signal frequency or time of arrival will enable useful but sub-optimum solutions to be provided, in which null formation against the wanted signal is inhibited. There is a clear lesson here for future system designs. When a new system is to be developed which requires an adaptive antenna capability, then the signal format must be formulated with the requirements of wanted signal discrimination very much in mind.

Acknowledgements are given to UK-MOD and STC PLC for permission to publish this paper.

7. BIBLIOGRAPHY

1. J.E. Hudson "Adaptive Array Principles", IEE Electromagnetic Waves Series 11, Peter Peregrinus Limited, 1981.

2. R.A. Monzingo and T.W. Miller "Introduction to Adaptive Arrays", Wiley and Sons, 1980.

3. IEEE Transactions on Antennas and Propagation, Special Issue on Adaptive Antennas, 1976. Volume AP-24, Number 5.

4. S.P. Applebaum, "Adaptive Arrays", IEEE Trans. 1976, AP-24, pp 585-598.

5. R.T. Compton jr., "An Adaptive Array in a spread-spectrum communication system", Proc. IEEE, 1978, 66 pp 289-298.

6. C.R. Ward and P.J. Hargrave: "The application of sub-optimal control methods to adaptive antennas for airborne communication systems", IEE Conf. Publ. 195, Part 1, 1981, pp 174-178.

7. B. Widrow and J.M. McCool: "A comparison of adaptive algorithms based on the methods of steepest descent and random seach", IEEE Trans, 1976, AP-24, pp 585-598

8. C.R. Ward and P.J. Hargrave: "Problems associated with correlation loop adaptive antennas employing hard limiting", IEE Proc. F. Commun., Radar & Signal Process. 1983, 130, (1), pp 60-66

9. J.G. Searle and C.R. Ward: "Multifunction adaptive processor for small antenna arrays", IEE Proc. F. Commun., Radar & Signal Process. 1983, 130 (1), pp 57-62

10. I.S. Reed, J.D. Mallett and L.E. Brennen: "Rapid convergence rate in adaptive arrays", IEEE Trans. 1974, AES-10, pp 853-863.

11. G.H. Golub: "Numerical methods for solving linear least-squares problems:, Num. Math., 1965, 7, pp 206-216.

12. W. Givens: "Computation of plane unitary rotations transforming a general matrix to triangular form", J.Soc. Ind. Appl. Math., 1958, 6, pp 26-50.

13. S. Hammarling: "A note on modifications to the Givens plane rotation", J. Inst. Maths, Applics. 1974 13, pp 215-218.

14. J.G. McWhirter: "Recursive least-squares minimization using a systolic array", Proc. SPIE, 1983, 431, Real-Time Signal Processing V1, 2983.

15. H.T. Kung and W.M. Gentleman: "Matrix triangularization by systolic arrays", Proc. SPIE, 1981, 298, Real-time Signal Processing IV.

16. C. Mead and L. Conway: "Introduction to VLSI systems", (Addison-Wesley, 1980).

17. O.L. Frost: "An algorithm for linearly constrained adaptive array processing", Proc. IEEE, 1972, 60, pp 926-935.

18. G.W. Lank: "Effect of single bit digitization in adaptive array control loops", IEEE Trans. 1972, AES-8, pp 547-549

19. B. Widrow, P. Mantey, L. Griffiths and B. Goode: "Adaptive antenna system", 1967, Proc. IEEE, 55, 2143-2159.

20. D.E.N. Davies,: 1965 "A transformation between the phasing techniques required for linear and circular aerial arrays", Proc. IEE, 112, No. 11.

21. J.L. Butler: in R.C. Hansen, (ed.) "Microwave scanning antennas" (Academic Press, 1966).

22. P.W. Howells: "Explorations in fixed and adaptive resolution at GE and SURC", ibid., AP-24, pp 575-584.

23. B. Widrow, B.E. Mantey, L.J. Griffiths and B.B. Goode: "Adaptive antenna systems", Proc. IEEE, 1967, 55, pp 2143-2159.

24. J.E. Hudson and A.S. Ratner: "Adaptive arrays for h.f. communications", IEE Colloquium on Adaptive Antennas, February 1980, IEE Digest No. 1980/8.

25. A. Cantoni: "Application of orthogonal perturbation sequences to adaptive beam-forming", IEE Conf. Publ. 169, "Antennas and propagation", 1978, pp 398-402.

26. W. Rotman and R.F. Turner: "Wide-Angle Microwave Lens for Line Source Applications", Institute of Electrical and Electronics Engineers Transactions on Antennas and Propagation, November 1963, volume AP-11, No.6, pp 623-632.

27. R.J. Mailloux: "Progress in Phased Array Technology", Military Microwaves '80 Conference Proceedings, London, 22-24 October 1980, pp 303-308.

28. P. Barton: "Digital Beam Forming for Radar", Institution of Electrical Engineers Proceedings Part F, Communications, Radar and Signal Processing, August 1980, volume 127, No.4 pp 266-277.

29. P. Barton: "Factors in the Design of Adaptive Antennas" Military Microwaves '82 Conference Proceedings, London, pp 555-562

30. C.R. Ward, A.J. Robson, P.J. Hargrave and J.G. McWhirter: "Application of a systolic array to adaptive beamforming" IEE Proceedings, Vol. 131, Pt. F, No.6, October 1984.

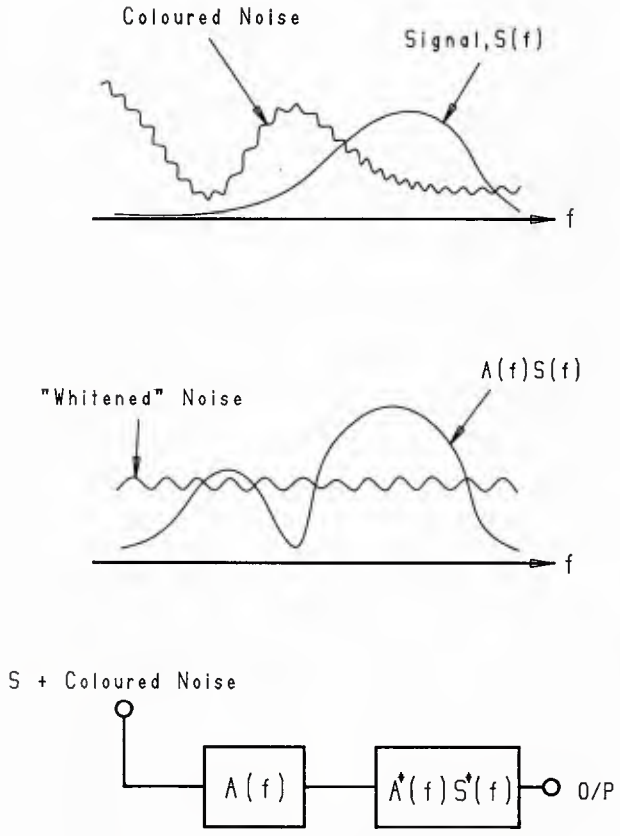

FIG 1. GENERALISED MATCHED FILTER

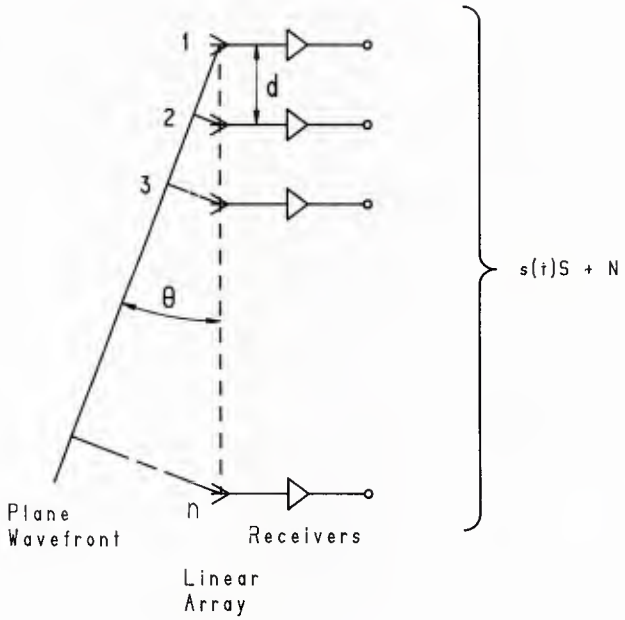

FIG 2. LINEAR ARRAY RECEIVING AN EXTERNAL SIGNAL

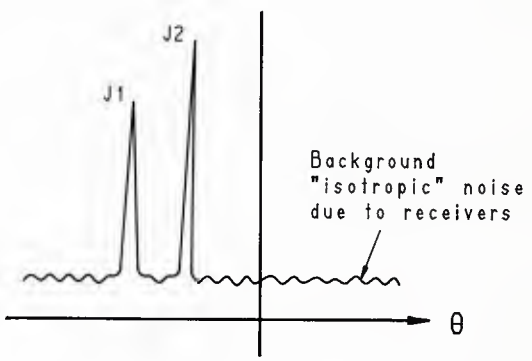

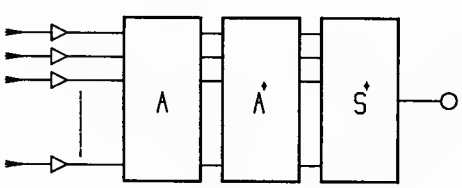

FIG 3. CASCADE OF MATRICES TO PRODUCE AN OPTIMUM ANTENNA RESPONSE

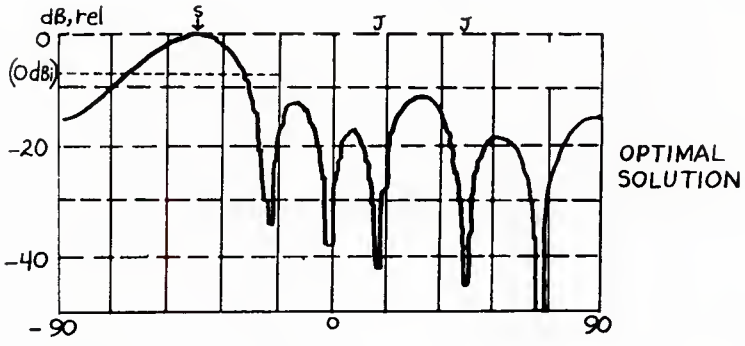

FIG. 4 DIRECTIONAL RESPONSE OF AN OPTIMUM ADAPTIVE ANTENNA IN A JAMMING ENVIRONMENT.

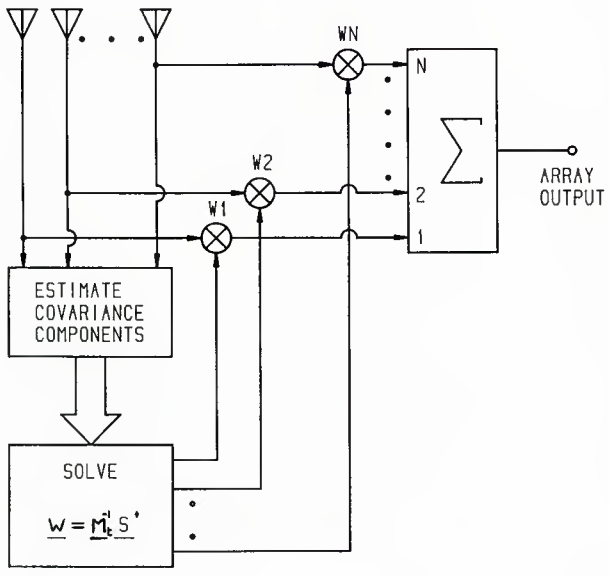

FIG. 5 CONCEPTUAL ADAPTIVE ARRAY

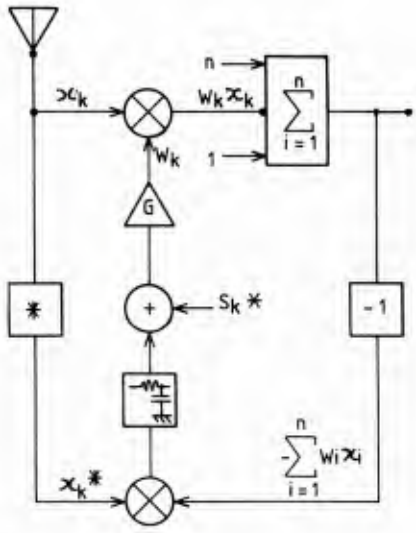

FIG. 6 CORRELATION LOOP ADAPTIVE ANTENNA WITH STEERING VECTORS

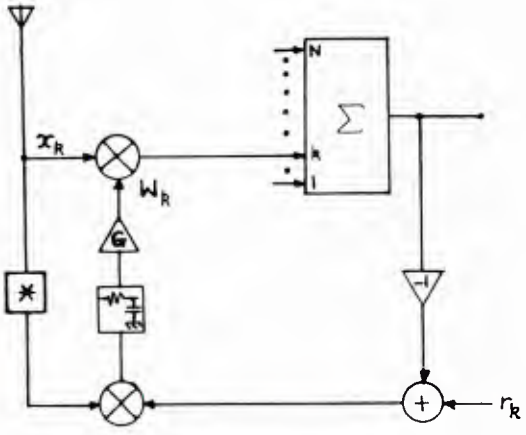

FIG. 7 A REFERENCE SIGNAL ADAPTIVE ARRAY

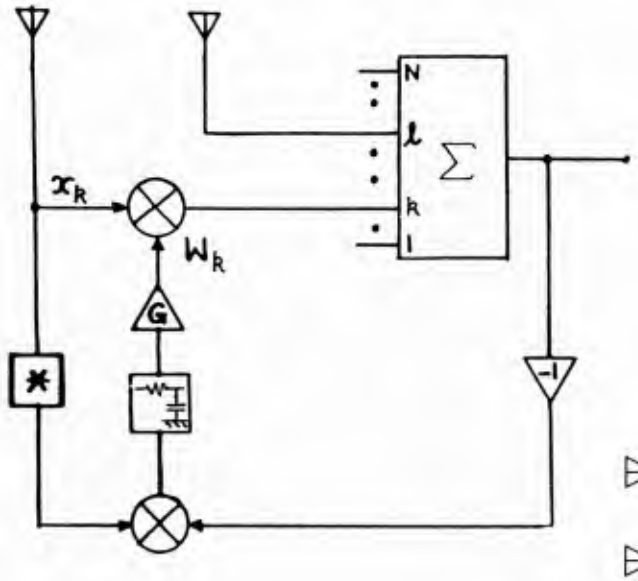

FIG. 8 SUB-OPTIMUM ADAPTIVE ARRAY

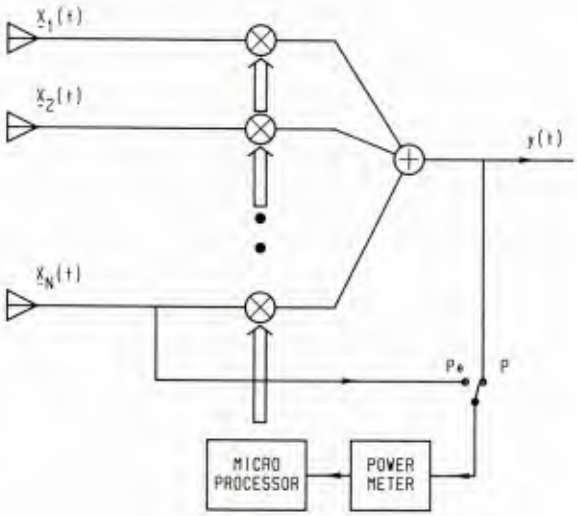

FIG. 9 WEIGHT PERTURBATION PROCESSOR

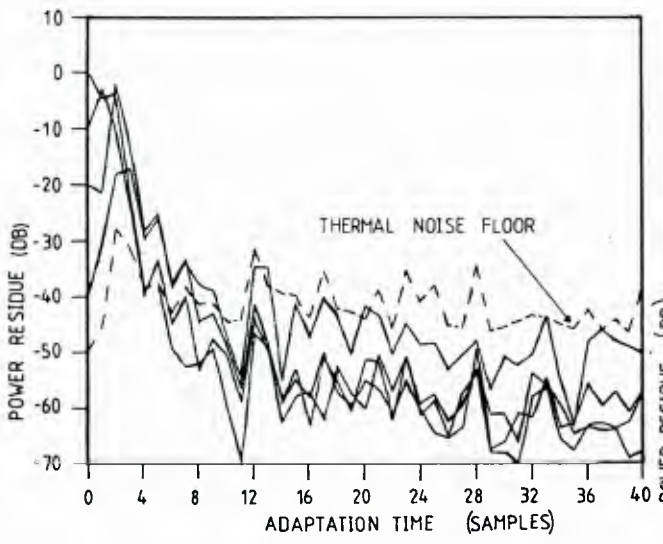

(a) Sample Matrix Inversion

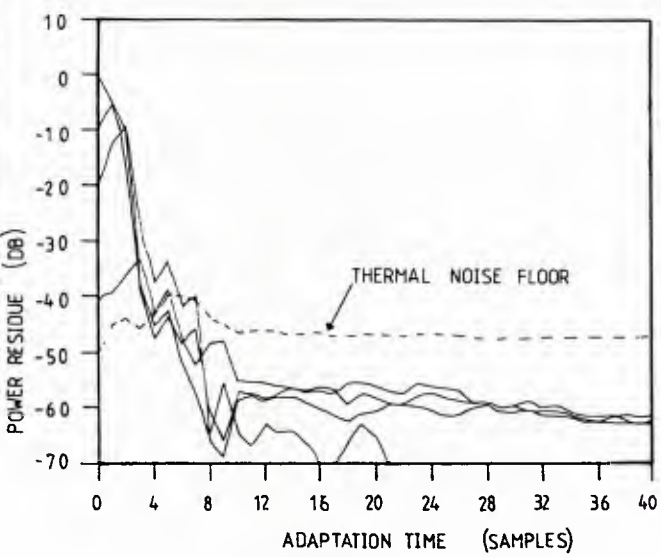

(b) Data Domain Q-R

FIG. 10 SIMULATIONS OF FINITE PRECISION ARITHMETIC

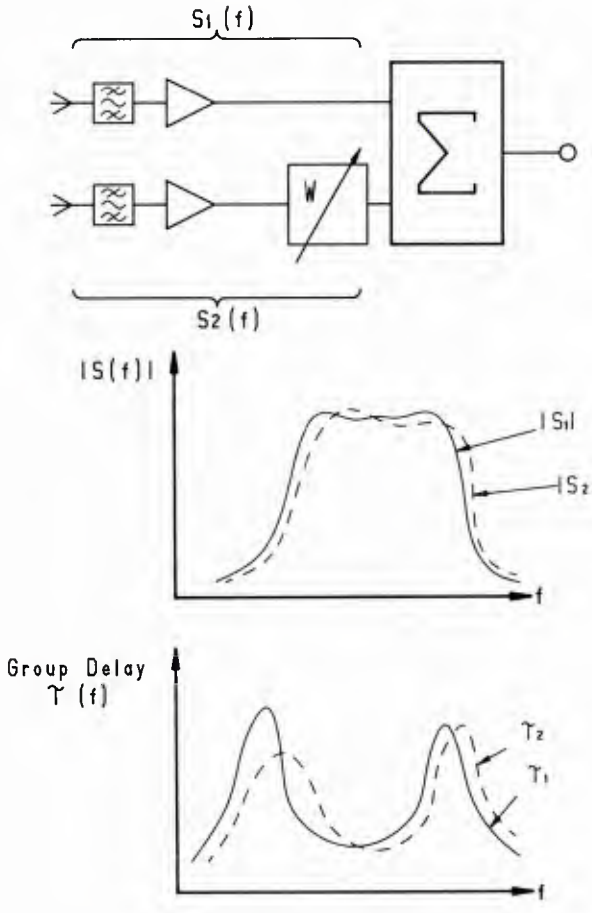

FIG 11. FREQUENCY DISPERSION BETWEEN CHANNELS

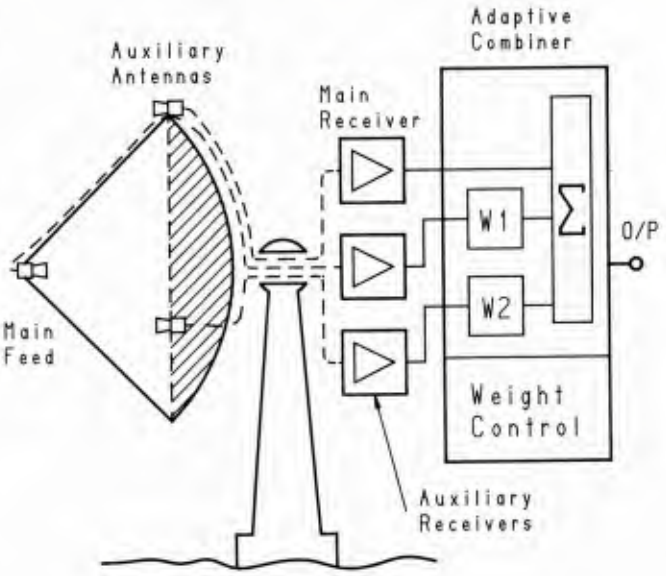

FIG 12. OUTLINE SCHEMATIC OF SIDELOBE CANCELLOR

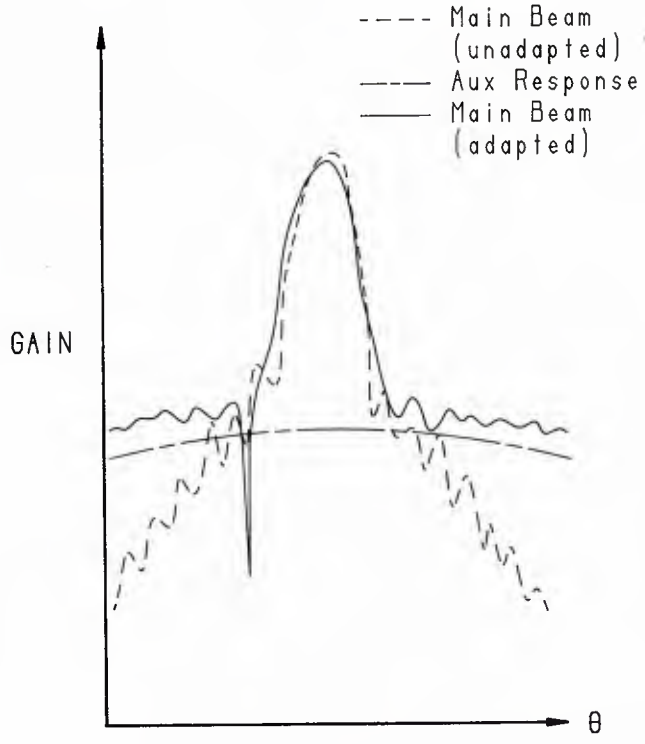

FIG 13. SIDELOBE CANCELLOR BEAM PATTERNS

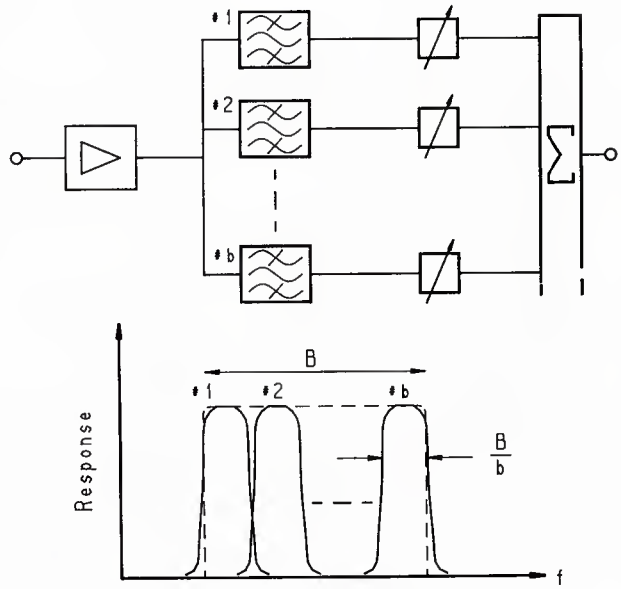

(a) Parallel Filter Bank

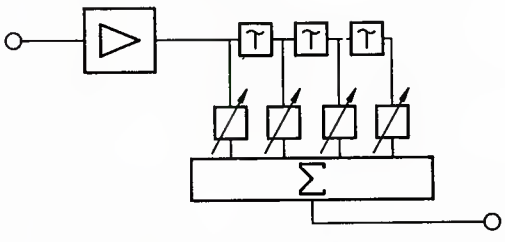

(b) Tapped Delay Line Filter

FIG 14. ADAPTIVE FILTER CONFIGURATIONS

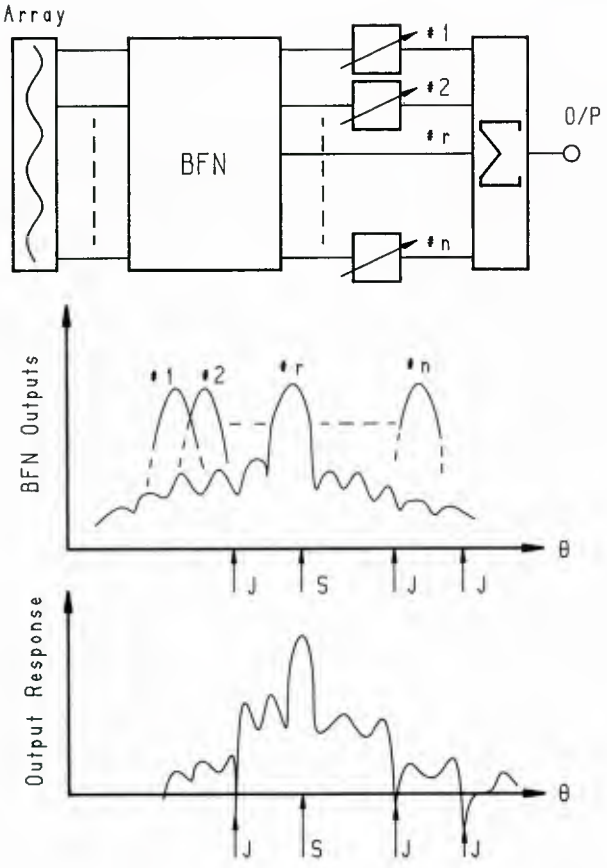

FIG 15. BEAM SPACE ADAPTION

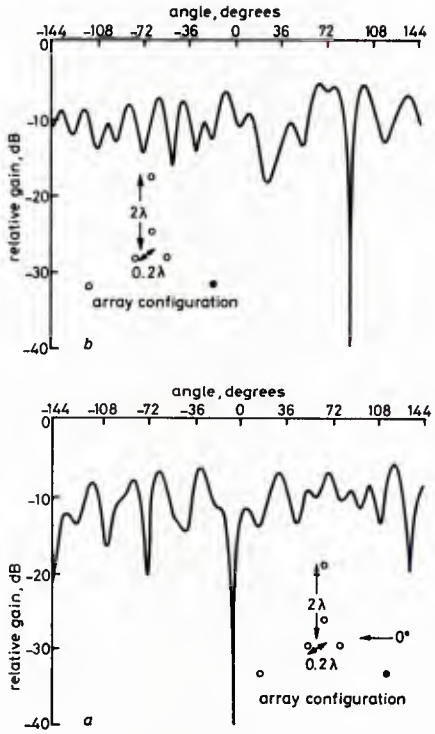

FIG. 16 ANTENNA PATTERNS FROM THINNED ADAPTIVE ARRAY

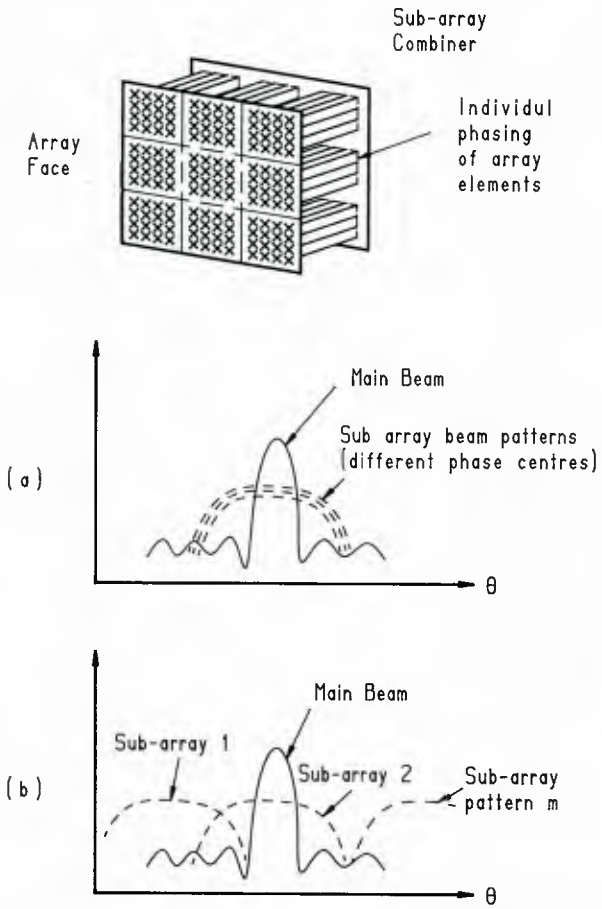

FIG 17. PARTIAL ADAPTIVITY IN BEAM SPACE

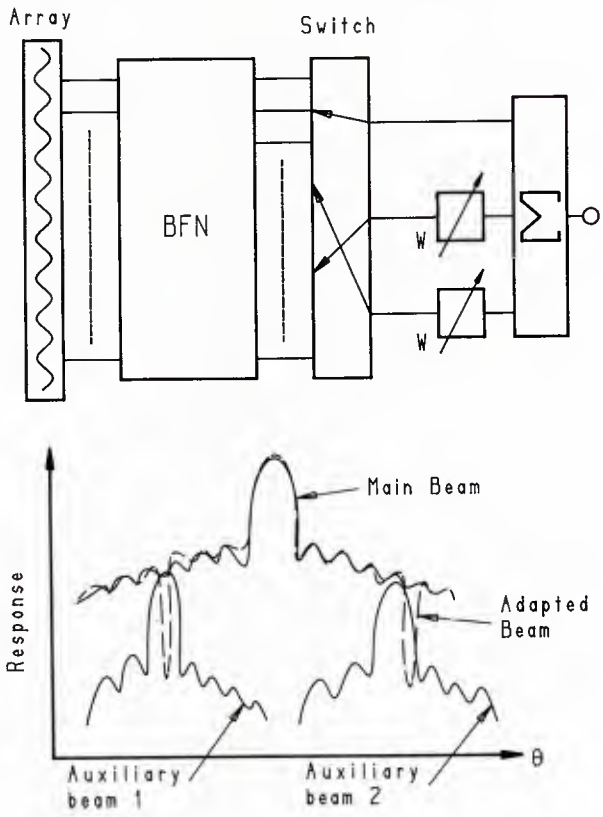

FIG 18. PARTIAL ADAPTIVITY IN BEAM SPACE

MIC TECHNOLOGY FOR PHASED ARRAYS

R. Douville
Communications Research Centre
Ottawa, Ontario, Canada

1.0 INTRODUCTION

The evolution of microwave integrated circuits (MICs) during the 60's and 70's permitted the consideration of active aperture phased array antennas. Several such systems have in fact, been realized and demonstrated. An early example of this was the Molecular Electronics Radar Array (MERA) system developed in the late 60's by Texas Instruments. However, such systems continued to be expensive and impractical, in most cases due to the high cost and lack of reproducibility of the microwave components required. More recently, phased arrays such as the PAVE/PAWS, COBRA/DANE and the AEGIS have been deployed. However, they are very large and expensive and "one-of-a-kind" in nature. The rapid evolution of monolithic (MMIC) and miniature MICs (MHMIC) during the 70's and 80's and their potential for overcoming these limitations has resulted in renewed interest in the development and deployment of phased array antennas for many applications, until now considered totally impractical.

Phased array requirements differ greatly depending on the application. They may be for radars or for communications, and they may be for airborne, terrestrial, or space application. Table I lists several types of systems, each placing different general demands on the required phased array T/R module. As may be seen, the requirements vary greatly in frequency of operation, bandwidth, need for conformal structure, necessity of combined transmit and receive functions, importance of weight and size, and total power consumption.

TABLE I - TYPICAL SYSTEMS REQUIREMENTS FOR PHASED ARRAY MODULES

REQUIREMENT	EHF MILSTAR = SATELLITE	EHF MILSTAR = AIRCRAFT	ADVANCED TACTICAL RADAR	ADVANCED AIRBORNE SURVEILLANCE RADAR	SPACE BASED RADAR	ADVANCED LOW-LEVEL SHIP DEFENSE RADAR	ADVANCED RADAR ESM
FREQUENCY OF OPERATION	Rx 44 GHz Technology Still Immature Tx Power @20 GHz	Tx Power @44 GHz Very Difficult	SHF Moderate Difficulty	UHF Requires Large MMICs & Elements	UHF Requires Large MMICs & Elements	SHF Moderate Difficulty	All Bands required 2-40 GHz
COMPLEXITY	Moderate if Separate Rx & Tx CW Operation	Moderate if Separate Rx & Tx CW Operation	Full Complexity T/R Capability Pulsed Operation	Full Complexity T/R Capability Pulsed Operation	Full Complexity T/R Capability Pulsed Operation	Possibly Simplest With IF or Baseband Phase Shiftomg	Receive Only Tight Phase Spec.
ENVIRONMENTAL	Spaceborne Radiation Long-Life, Unattended	Airborne Reparability Radiation	Portable	Airborne Reparability Radiation	Spaceborne Radiation Long-life, Unattended	Shipborne	Shipborne Airborne Reparability
NUMBER OF ELEMENTS	Hundreds	Hundreds	Hundreds	Thousands	Many Thousands	Tens to Hundreds	Thousands
STRUCTURAL	Conformal, Light, Compact Integrated Module & Antenna Element?	Conformal, Light Integrated Module & Antenna Element?	Rugged	Conformal Lightweight	Spaceborne Ultra-Lightweight Compact	Light Compact	Shipborne-Compact Airborne-Conformal Lightweight
TRANSMIT MODULE POWER	Moderate Power, CW Efficient, Thermal Load on Satellite	High Power, CW Efficiency for Better Time-on-Station	Very High Power, Pulsed Efficiency for Better Portability	High Power, Pulsed Efficiency for Better Time-on-Station	High Power, Pulsed Very High Efficiency Low Thermal Load	Moderate Pulsed	Not required
BANDWIDTH	CW Narrowband Hopped 5-10%	CW Narrowband Hopped 5-10%	Pulsed Very Narrowband Agile 20%	Pulsed Very Narrowband Agile 10-15%	Pulsed Very Narrowband Agile ≈10%	Pulsed Single Frequency Agile ≈10%	Very Wide Multi-Octave

The block diagram of typical transmit/receive (T/R) modules is shown in Fig. 1. In some cases, the module may be required only to receive or transmit but not both; it may require active phase or amplitude control in the MIC, or these functions may be carried out at IF or baseband following up- and downconversion. In general, the basic elements include a phase-shifter, a low-noise amplifier, and a high power amplifier. This paper will concentrate on the technology and performance of these. In complete T/R modules, switches are of course used and, in some applications where IF or baseband phase shifting and processing is used, mixers and oscillators may be required. However, these latter will not be addressed here in detail. Since many potential applications require wide bandwidths, this parameter will also be discussed. In all cases, the size of the T/R module is important; in some cases to ensure the module size is compatible with the phased array antenna element spacing, in others, to meet the requirements of airborne or spaceborne systems.

The successful realization of an active aperture phased array antenna obviously requires several unique circuit-oriented problems to be addressed. These might include the choice of radiating antenna element, microwave signal distribution and coupling to the antenna elements, control of the active functions, and heatsinking and DC power distribution as well as the realization of the various microwave circuit functions normally associated with phased array antennas. Of necessity, this paper will focus on the latter item, the microwave circuit functions, although some of the techniques to be discussed will certainly have potential for addressing others in this list. Some of these issues will be addressed in other papers in this lecture series. However, the very strong interdependency of the various circuit oriented problems will likely require a closer working relationship between system, antenna, circuit and device designers than ever before.

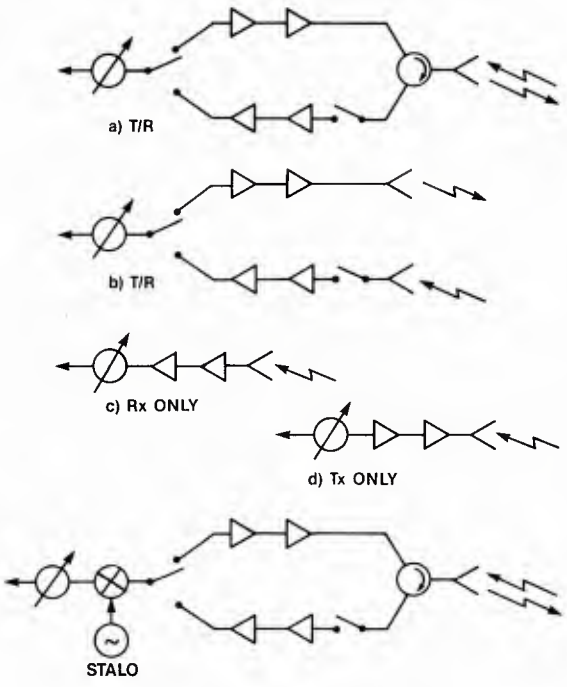

Fig. 1. Typical Phased Array Module Types.

This paper is intended to give an overview of MIC technology with respect to its use in phased array systems for military applications. Historically, the term MIC has been used to refer to planar microwave circuits using one or more different forms of printed transmission lines, all characterized by their ability to be photoetched on a suitable dielectric substrate. Active and passive discrete components such as transistors, chip capacitors and resistors are then attached. This technology is more precisely referred to as "hybrid" MIC (HMIC). The field of MIC design is currently undergoing a major revolution due to the rapid emergence of "monolithic" MIC (MMIC) design. In this latter, all components, including the active devices, are fabricated using deposition and etching processes, thereby eliminating the need for attachment of discrete components. This paper discusses these technologies with respect to their potential in phased array antennas.

Section 2.0 will address some of the types of planar transmission lines available to the MIC designer, and will explain some of the factors which must be considered and traded-off. Section 3.0 will describe some of the fabrication technologies of the various forms of MICs. It will also address some of the packaging and testing problems of MICs for military phased arrays. Section 4.0 will review the current performance capabilities of MICs with respect to several parameters of interest to the phased array requirements of possible military systems.

2.0 CIRCUIT TYPES AND SOFTWARE SUPPORT

2.1 Planar Transmission-line Types

Table II shows four of the more common planar transmission line and passive matching circuit types currently used for MICs. Each consists of a double or single-sided transmission medium whose performance may be determined by the dimensions on a single plane. Thus all are characterized by their inherent amenability to fabrication using photo-masking and etching procedures. Table II also lists and compares several important characteristics each of which must be considered when selecting a configuration for a specific MIC.

Microstrip is easily the most popular largely due to its simplicity, relative ease of tuning, and extensive supporting analysis and software. Much work has been done to characterize, analyze, understand and document the various electrical parameters of microstrip. The result is that modern microstrip circuit design practices have become well established and standardized and have been incorporated as a standard element in all major microwave circuit design packages. At higher EHF frequencies, microstrip becomes increasingly difficult to fabricate controllably and its loss and radiation characteristics begin to deteriorate.

At these frequencies, alternatives such as fin-line often provide solutions[1]. They give good loss and shielding characteristics at EHF and are very compatible with many other mediums including waveguide. The past decade has seen a substantial maturing of supporting analytical information for these.

Slot-line has the advantage that both the ground and circuit elements are on the same side of the substrate. In addition, this unique characteristic finds application where coupling through a substrate from one circuit to another is desired such as is often encountered in signal distribution networks in planar arrays. However, slot-line is limited to a range of high impedance values.

TABLE II - PLANAR CIRCUIT TYPES

CIRCUIT TYPE \ FACTOR	FREQUENCY RANGE (GHz)	LOSSES	IMPEDANCE RANGE (OHMS)	FABRICATION TOLERANCES	PACKAGING & INTERFACES	MINIATURIZATION	SUPPORTING ANALYSIS & SOFTWARE
MICROSTRIP	1 ~ 40	High at EHF	10~140	Tight at EHF	Coax - Good W/G - Poor Box Modes	Good - Very small at EHF	Good
SLOT LINE	1 ~40	High at EHF	45 ~ 250	Tight at EHF	Coax - Medium W/G - Medium Box Modes	Medium	Medium
FIN LINES	Extended W/G Bands eg 18-40	Medium	10 ~ 800	Low - Medium	Coax - Poor W/G - Good Other planar - Good	Medium Good size at EHF	Medium
PRINTED LUMPED ELEMENTS	1 ~ 30	High	L<50 nH C≲0.2 pF	Tight at EHF	Other Planar - Good	Excellent	Medium to Poor

Often, several of these structures are combined into one circuit in order to take advantage of the specific topological and electrical features. Fig. 2 shows an E-plane mixer which uses a combination of fin-line, microstrip and coplanar waveguide.

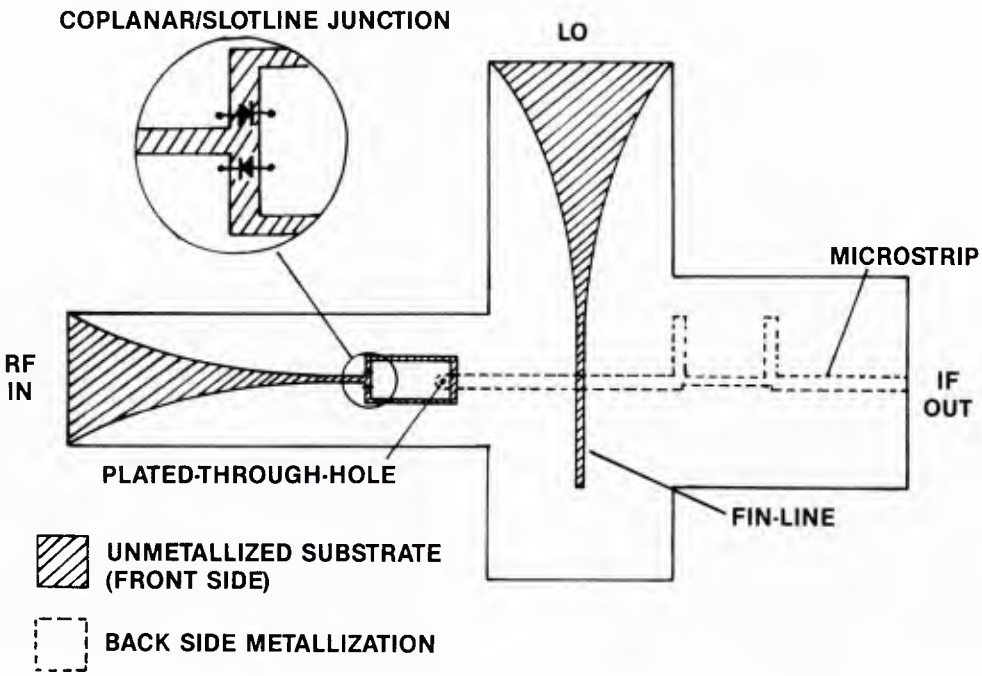

Fig. 2. 19/4 GHz E-Plane Mixer Using Several Planar Transmission Line Structures.

Also included in Table II are printed lumped element components. Typically limited to applications at lower microwave frequencies, the development of MMICs has resulted in renewed interest in these components with the added complexity of multilayer lumped elements such as thin-film capacitors[2]. However, they are not yet well supported by good analytical models and typically do not have low losses.

2.2 Software and Design Problems

Substantial software exists at present for the support of conventional MIC design. Routines such as Super-Compact, CADEC, Touchstone and Microwave SPICE permit moderately complex networks to be analyzed and optimized. Combined with routines such as Auto-art and MICAD, they even assist in the layout of the resultant masks. Software packages are also available to analyze and provide the dimensions of many of the structures used in MICs such as shown in Table II [3]. Where better known structures such as microstrip are used, agreement between predicted and measured performance is quite good. In addition, where agreement is not good, it is often possible to fine tune or "tweak" the performance of the circuit manually.

For the design of MMICs or, as described later, printed batch processable HMICs, final tuning or "tweaking" of the performance is impossible or highly undesirable. It therefore becomes important to have much more accurate software. Models used for active and passive elements must, of necessity, become very complex particularly where wideband performance is required. Software requirements begin to exceed the capabilities of the above mentioned commercially available routines.

A simple example may be used to illustrate this problem. A typical configuration is given in Fig. 3 based on use of lumped element matching circuits for a simple single-stage microwave amplifier. However, since the physical size of the lumped elements may be an appreciable fraction of a wavelength, become quite complex. Once the parasitic elements for each of the inductors and capacitors are introduced and lengths of transmission line are added to account for the interconnects, this circuit expands to that shown in Fig. 3b. Of course the field-effect-transistor would also be replaced by an equivalent circuit, possibly created using a modelling program such as SPICE. The result of course, is a complex circuit requiring sophisticated software for analysis. Optimization of the element values now becomes tedious and essentially manual, since variation of any one of the original lumped elements results in an often analytically unpredictable variation in the parasitic elements. Extension of the problem to a sophisticated component such as a complete receive or transmit module is virtually impossible.

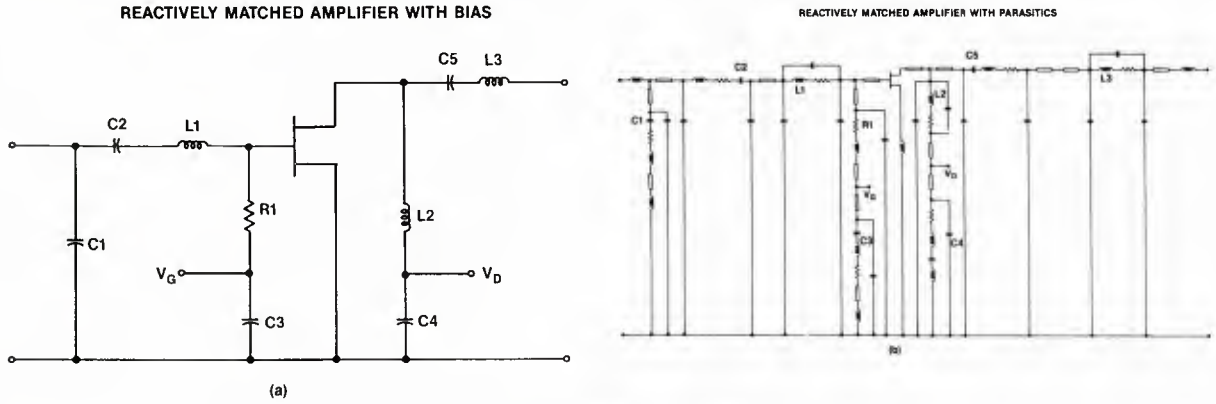

Fig. 3. Single-stage Amplifier Diagram with Lumped Element Matching Circuits: a) without parasitics; b) with parasitics.

The need for improved software and techniques to handle MMICs is thus apparent. Fig. 4 shows three of the many different forms of lumped element inductors. Each of these has substantially different parasitics and therefore requires a different model. Present models are still insufficiently developed and understood to permit complete flexibility of their application particularly where wideband performance is required. Recently, software has been developed which permits the performance of complex structures such as these to be anlayzed using more direct electromagnetic analysis routines[4]. The same method may be applied to more complex structures as well consisting for example of several inductors and capacitors.

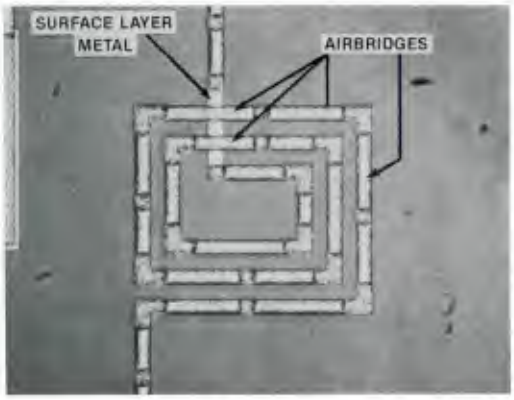

(a) TRIQUINT

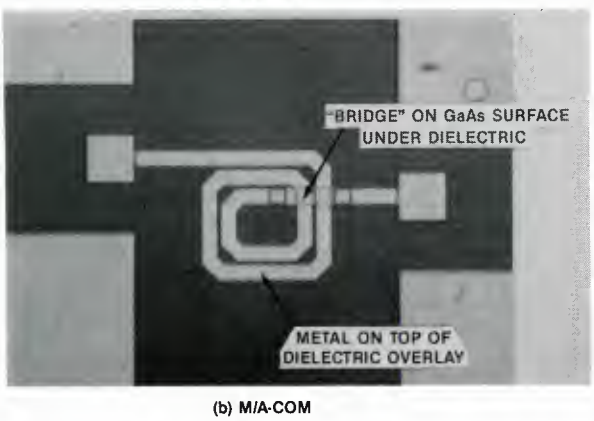

(b) M/A-COM

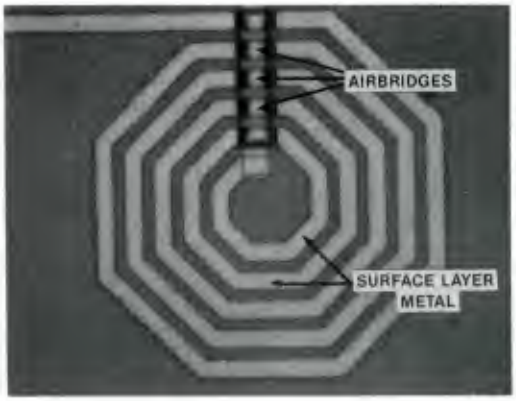

(c) ADAMS-RUSSELL

Fig. 4. MMIC Lumped Inductor Structures: a) TriQuint; b) M/A COM: c) Adams-Russell

Another problem the MMIC designer is faced with is that of anticipating the effects of process variations [5]. Fabrication processes are not 100% controlled and predictable and designs must be assessed in advance for sensitivity to any consequent variations. Appropriate statistical analysis capabilities such as those provided in Super-Compact are necessary.

3.0 FABRICATION TECHNOLOGIES

3.1 Hybrid MIC Technology

Fig. 5 shows a typical HMIC which uses microstrip and consists of several ceramic substrate sections on which are etched specific circuit patterns. In such a circuit both the thickness and the dielectric constant are of fundamental importance to the functioning of the circuit. Patterns are created using thin-film or thick-film photomasking and etching techniques. Resolutions required on linewidths and gaps are generally greater than 0.1 mils, somewhat less demanding than that of semiconductor device fabrication. Typically only one such masking and etching cycle is required.

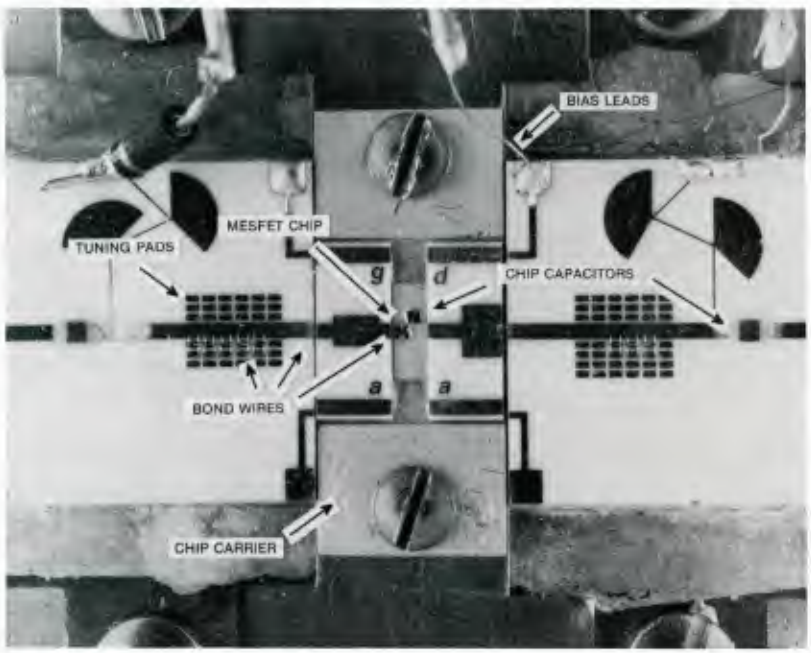

Fig. 5. Conventional Hybrid MIC (HMIC) Structure using Alumina Substrate.

The circuit illustrates several of the typical features of HMICs. The use of separate substrate sections permits the HMIC design to be iterated more readily. Use of a chip carrier permits some of the repeatability and re-usability features of packaged devices to be realized. Special attention can also be paid to device heatsinking. This approach is particularly attractive in custom applications requiring limited numbers and where optimum performance over narrow bandwidths is desired.

Also illustrated in Fig. 5 is the use of wire-bonding and device and chip capacitor die attachment. Each of these requires specific, typically manual, processing steps and adds to the complexity and cost of the fabrication process and facility needed. In addition, each represents a failure prone step in the processing cycle as well as representing a potential variability factor in the RF performance, the overall effect being a reduction in the yield and consequent increase in cost.

Some of these drawbacks are partially overcome by the ability to perform on-circuit tuning or "tweaking". This permits performance to be optimized and yields to be improved. The matrices of tuning pads shown on the input and output sections of the amplifier in Fig. 5 demonstrate this feature. Often, the tuning is achieved by moving metallized or unmetallized tuning chips about on the microstrip circuits. Later, these chips may be attached using epoxy or, as in the case shown here, replaced with wire-bonds.

Fig. 6 shows another form of HMIC. The primary difference from that shown earlier is the use of soft substrate material, in this case a teflon-fibre based material known as RT Duroid. Such circuits generally offer lower cost alternatives to ceramic substrates, but are typically not capable of achieving the same linewidth resolutions. In addition, some processes such as wirebonding, while not impossible, are less reliable. Often such circuits may be fabricated in large numbers on substrates which may be 100's of cm square or may contain other elements such as phased array antenna elements.

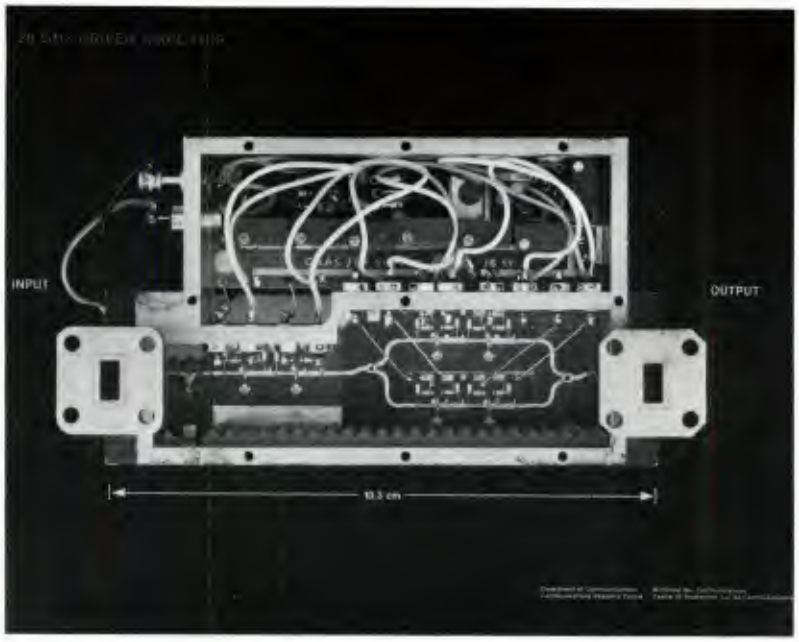

Fig. 6. Conventional HMIC Using Soft Substrate Material (RT Duroid).

3.2 Miniature Hybrid MIC

The past few years has seen an increasing effort to eliminate the use of chip resistors and capacitors as well as wire-bonds from HMIC fabrication. The resultant components, which may be referred to as Miniature HMICs (MHMIC), often use printed lumped element matching networks and aim at batch processing of multicircuits to which active devices are later attached [6,7]. An excellent example of this is the Fujitsu CASPAC approach shown in Fig. 7 [8]. This unit uses metal-oxide-metal (MOM) capacitors, spiral inductors and tantalum nitride thin-film resistors. In place of wire-bonds, airbridges are fabricated as part of the overall process. FETs are then die attached to the package and wire-bonded to the circuit. Another example which uses several similar process steps is the miniature beryllia circuit concept developed at RCA [9]. In this technique, by creating a metallic septum through the substrate to ground, the FET may be flip-chip bonded to the surface of the circuit thus virtually eliminating all wire-bonding. Beryllia is used for its excellent thermal heatsinking properties.

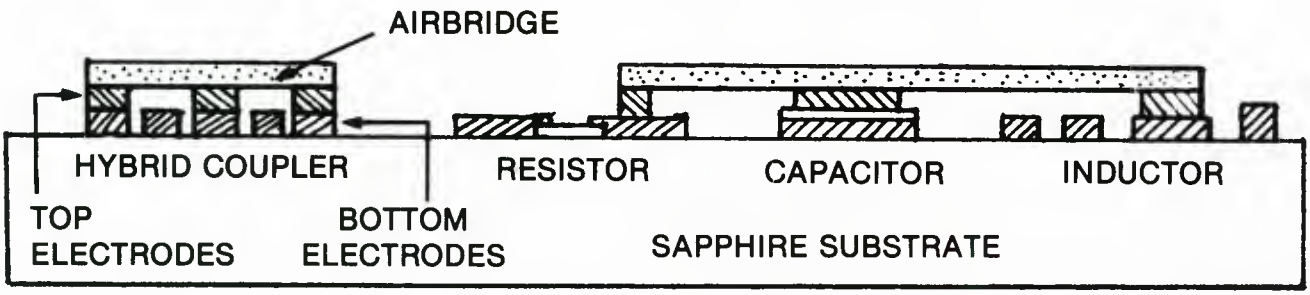

Fig. 7. Typical Miniature Hybrid MIC (MHMIC) Structure.

These examples demonstrate the batch fabrication, small size and light weight potential for MHMICs. They retain much of the flexibility of conventional HMICs and can be used with off-circuit, possibly pre-screened chip or packaged devices. This approach eliminates many of the labour intensive and potentially unreliable and unreproducible steps of the conventional HMIC. A penalty of course is the more complex sequence of photo-masking, etching and deposition steps. A facility for oxide deposition is now required in addition to photo-etching. Although a total of five or more mask cycles is necessary, the mask quality and resolution required are somewhat more relaxed from that needed for semiconductor device fabrication.

3.3 Monolithic MIC Technology

3.3.1 Semiconductor Processing

Fig. 8 illustrates the basic structure of a monolithic MIC (MMIC). As may be seen, the matching circuits are now processed onto the same substrate as the active device. The substrate material is typically high purity GaAs although Si is finding significant use for UHF applications.

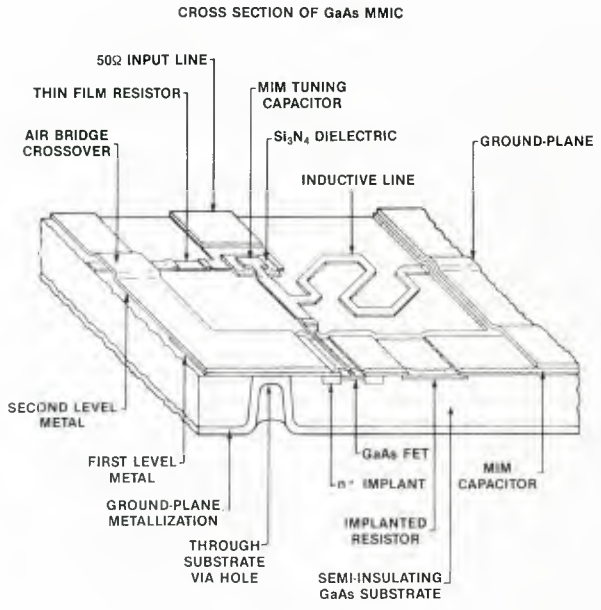

Fig. 8. Cross Section of GaAs MMIC Structure.

The active devices used are most commonly MESFETs and require the deposition of a high mobility semiconducting layer on the surface of the substrate. This is commonly done using Vapour Phase Epitaxial (VPE) growth or selective ion implantation techniques. Historically, VPE has given better device noise and power performance where low gate to source resistance is important. However, improvements in selective ion implantation show promise of matching the performance of VPE while providing greater uniformity over the wafer and eliminating the need for step changes in height due to mesa etching processes [10].

Two other approaches gaining attention are Molecular Beam Epitaxy (MBE) and Metallo-Organic Chemical Vapour Deposition (MOCVD). Both of these provide better control of the epitaxial layer thickness and the doping levels. In addition, both are capable of growing complex epitaxial profiles and can therefore be used to create sophisticated heterojunction structures as might be required in digital ICs and in newly emerging microwave devices [11]. For most MMICs where such structures are not yet generally used, the process steps for both MOCVD and MBE are essentially the same as for VPE but more expensive and slower.

3.3.2 Circuit Fabrication

As seen in Fig. 8, the typical MMIC may contain capacitors, resistors, inductors, airbridges, and microstrip or other transmission line structures. Each of these requires at least one deposition and pattern definition step and thus at least one masking cycle. In addition, the capacitors require the deposition or creation of oxide or nitride layers, a process which is somewhat more difficult than that for Si ICs due to the absence of a usable native oxide of GaAs. The resistors are typically formed in the epitaxial layer of the GaAs although thin film resistors may also be used. The creation of the airbridges may also require the deposition and etching of further dielectric layers. As a result of the high cost of processing a wafer, every effort is taken to minimize the surface area required by the various elements. This results in a limitation on the range of possible values for the various passive elements as well as a constraint on achievable Q-factors [12].

Fabrication of the MESFET requires the definition of metallization in patterns with dimensions as small as 0.2-0.3 μm. This represents esentially the limit of current photolithographic processes and results in the generation of costs of MMICs typically an order of magnitude greater even than for MHMICs as discussed earlier. Electron Beam (EB) lithographic techniques show promise of improving this as well as providing improved reproducibility.

Fig. 9 illustrates the basic steps required in the fabrication of an MMIC on previously doped semiconductor. As may be seen, several masking, deposition and etching steps are required. In order to realize low inductance grounds, via holes are also often used. This as well as the desire for better heatsinking requires thinning of the wafer to ≈100 μm or less. The via holes are then etched and the backside is metallized. Fig. 10 shows a typical MMIC containing several of the features discussed above.

3.3.3 Process Yield

Of great importance to the effective use of MMICs is the realization of the highest yield possible from each substrate wafer. Several factors including process variability, intolerant circuit designs, intolerant specifications, and complexity of component function contribute to reduction in yields.

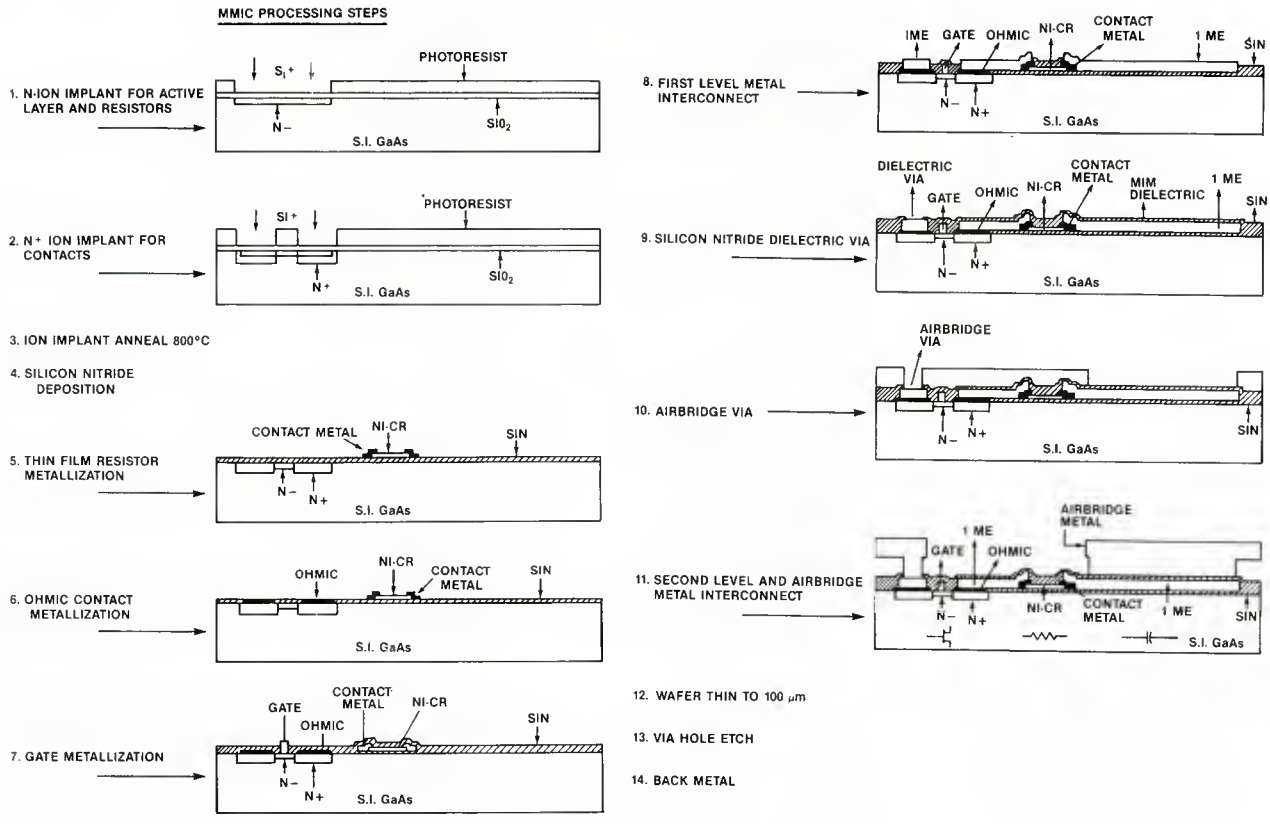

Fig. 9. Processing Steps for MMIC.

The inability to precisely control MMIC fabrication processes results in variations in the various element values as illustrated earlier in Section 2.2. As seen in Fig. 9, up to 14 steps may be required to realize an MMIC. Even if each step has a yield of 95%, this still results in an overall wafer yield of only 50%. Packaging, assembly and test steps following this would of course further reduce this yield. In practice, step yields are not all the same. One major contributor is the FET gate definition step due to the very small dimensions encountered. These dimensions directly affect several of the FET parameters including the transconductance, input match and noise figure. In addition, the total power achievable by a single FET is a function of the total realizable gate periphery. As a rule of thumb, a yield figure of 90% per millimeter of gate periphery is a practical limit for gate lengths greater than 1 μm. Of course, for gate lengths less than this, as would be encountered above X-band, yields would degrade.

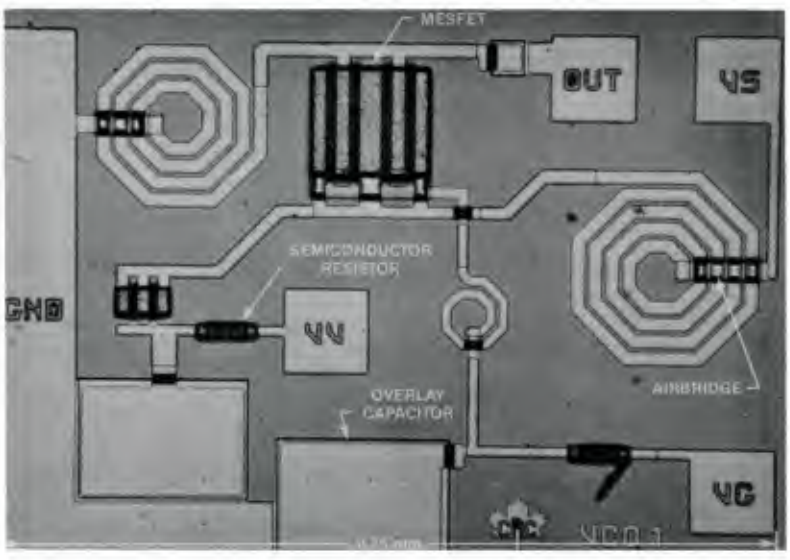

Fig. 10. Simple MMIC Showing Basic Structures.

A second very significant contributor is the capacitor dielectric deposition step. Precise control of capacitance values translates into the need for precise control of the thickness of the thin dielectric layer. For matching into the low impedances typically encountered with power FETs, large capacitance values are often encountered, and this translates into thinner and larger area thin-film cap also in greater probability of dielectric breakdown due to pin holes in the dielectric layer. Again, as a rule of thumb, a yield figure of 90% per 20 pF of capacitance is a practical limit. In order to offset this, the larger capacitors are sometimes placed off the wafer.

Another factor important to the yield realized is the size of the wafer used. Typically, yields are less near the outer edges of any given wafer due to optical effects in these areas. Assuming a 50% yield, a 5 cm wafer would produce about one thousand 1 mm^2 chips. Larger wafers such as the 7.5 to 10 cm wafers now being worked with would be expected therefore to produce a larger percentage of successful chips [2]. Alternatively, assuming the processing costs are not increased by the larger wafer, larger more complex chips may now be produced for the same cost.

In order to maximize the yield, design approaches which may not offer the best performance but are less sensitive to process variations, must be traded off against the need for more circuitry to achieve the same overall performance and functional complexity. Furthermore, unlike HMIC techniques where some tuning or tweaking may be possible, the designer must establish much better device and component models and must have the ability to assess the statistical characteristics of his designs.

Fig. 11 illustrates the statistical gain variation of a simple single stage amplifier as a result of anticipated variations in the transconductance and capacitance due to tolerances in process control. As may be seen in the figure, a total gain variance of about 1 dB must be anticipated and, depending on the specification tolerance, could translate into a reduction in yield. For a multistage amplifier, this would of course result in a much larger overall gain variation. For a single wafer, the variance would be expected to be less as is shown in the figure. In practice, the mean for any specific wafer might not be the same as that for the overall process. To accommodate this, some electronic gain adjustment might be incorporated.

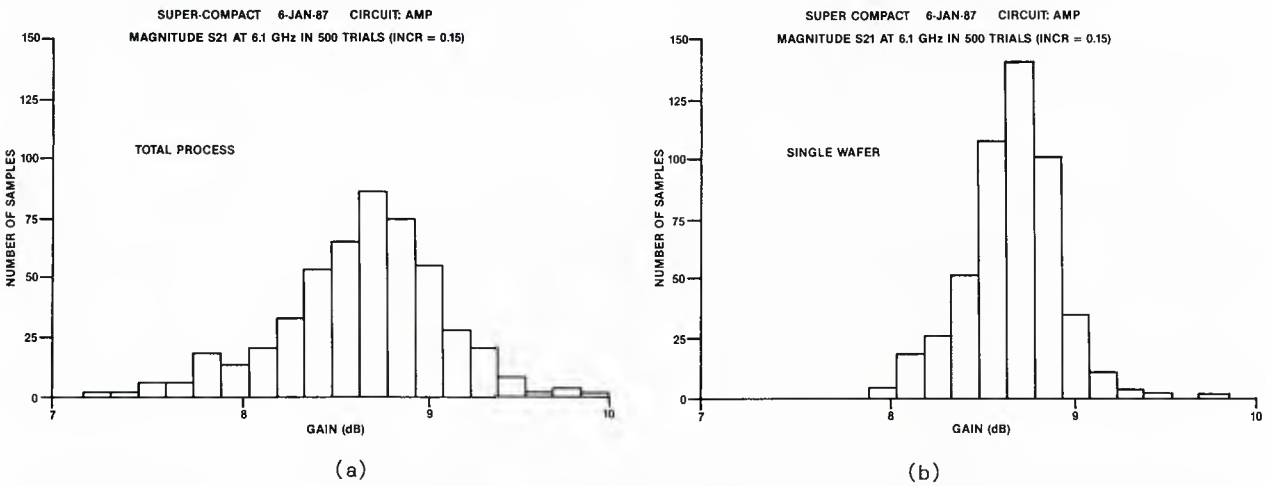

Fig. 11. Statistical Gain Variation for a Single-stage Amplifier based a) Overall foundry estimated process variation; b) Estimated process variation over single wafer.

This example also indicates the importance of avoiding overly tight tolerances on specifications. For the example shown, a gain specification of 8.25 dB ±0.5 dB would result in a projected yield of about 86% whereas specification tolerance of ±0.1 dB would reduce this to about 34%. For a six stage amplifier based on the same device, this translates to a specification tolerance of ±3.0 dB rather than ±0.6 dB.

3.4 Comparison of HMIC and MMIC Technology

Table III compares some of the features of a typical conventional hybrid implementation of a high gain amplifier with the equivalent MMIC version [12]. In terms of performance, the MMIC is generally able to achieve wider bandwidth and slightly more gain than its HMIC equivalent. However, in terms of noise figure or power output, the hybrid is generally able to provide some improvement since the key input or output devices may be preselected and some on-circuit tuning is possible. This will be expanded later.

TABLE III - COMPARISON OF HYBRID AND MONOLITHIC AMPLIFIERS

	Hybrid	Monolithic
Frequency (GHz)	8 - 18	7.5 - 18.5
Noise Figure (db)	4.5	5.2
Gain (dB)	40 ± 2	57 ± 1.5
Wire Bonds	400	14
Number of FETs	16	16
Number of Substrates	16	5
Number of Carriers	8	1
Number of Discrete Passive Chips	72	--
Volume (mm^3)	2048 (unpackaged)	926(packaged)

Of more importance in Table III is the large number of discrete components, wirebonds and individual substrates required for the HMIC. This suggests a large number of manual and labour intensive assembly steps. Such steps not only add to the cost, but are sources of unreliability and unreproducibility. The MMIC reduces this to essentially one substrate and a very small number of wirebonds to attach to the outside world. Miniature HMIC obviously falls between these two since the majority of wirebonds and discrete passive chips are eliminated.

Not shown in Table III is the number of masking, deposition, pattern definition, and etching steps required to process the two amplifiers. As seen earlier, an MMIC requires 10-14 such steps while an MHMIC might require 5-10 such steps. The conventional HMIC requires only 1 or 2 although this process may have to be repeated once for each substrate carrier (16 in the example shown). In addition, the quality and line definition requirements of masks necessary for the HMICs are generally not demanding or expensive while purchase of complete mask sets for MMICs may cost upwards of $15000 per iteration. Also, due to the need for specialized equipment to produce them, these latter often contribute substantially to overall MMIC design iteration times of 3-6 months compared to about 1 month for conventional HMICs. These factors underline the previously mentioned importance of accurate device electrical models and sophisticated computer analysis and optimization routines for MMICs. At the completion of the various fabrication steps, however, the MMIC may yield several thousand complete amplifiers while the HMIC would yield only one. The MMIC would also have a substantial size advantage over the HMIC.

Obviously, the approach selected is volume dependent and sensitive to the exact performance required and achievable by the various technologies. In addition, in order to benefit from the more expensive MMIC process, it is very important to realize the highest yield possible. In some applications such as spacecraft transponders, the volume may not be as important as the size, weight and performance advantages of MMICs. Lastly, it is expected that optimum cost vs performance will be realized in many cases by taking advantage of the relative benefits of each technology based on the application.

3.5 Packaging, Assembly and Test

There is general agreement that 75 to 80 percent of the cost of T/R modules will lie in the packaging, assembly and testing rather than the cost of the circuit or wafer production itself [13,14]. The main advantages of MMICs or MHMICs will be realized in reducing these costs by reducing the number of chips and therefore chip-related assembly costs. However, the costs of both packaging and testing of such circuits are highly volume sensitive and therefore new approaches must be developed.

3.5.1 Packaging

Conventional HMICs have typically used mechanical housings with standard SMA or equivalent input and output connectors. The evolution of MHMICs and MMICs has initiated significant activity into the development of more suitable packages. Such packages must be small and compatible with planar circuit structures with provision for multiple DC connections. They must also have low loss controlled impedance input and output (I/O) ports with good I/O isolation up to high microwave frequencies. They often must provide low thermal impedance and, in most applications, must be capable of being hermetically sealed. Lastly, they must be capable of being attached readily into subsystems and of being automatically tested in production fixtures. Above all, they must not contribute substantially to the cost of the component.

Several packaging concepts have been developed to date. One of the simplest approaches has been to insert the MIC into variations of the conventional MESFET stripline packages. This of course is limited to simple components which require only one set of RF and DC I/Os. An example of this is the M-FET amplifier package developed at AT&T [15]. Such packages are examples of a more generalized structure known as multilayer ceramic packages which, in their basic form, use a metal sealing ring between the lid (which may also be metal) and the ceramic walls. This ring often results in the existence of a package resonance which can reduce the useful frequency range.

Fig. 12 shows an example of this package concept recently developed by M/A-COM [16]. Several features are worth noting here that address the problems highlighted earlier. First of all, a coplanar ground-signal-ground configuration is used to provide a totally planar I/O capability. To insure low inductance transitions and reduce the coupling to the sealing ring, the ground portion of these I/Os is wrapped from the top to bottom of the ceramic substrate and via-holes are provided internal to the package. A total of eight coplanar DC lines are provided by use of standard lead-frame technology. A copper plug is brazed into a hole in the kovar base to provide a low thermal resistance path. Once the MMIC, mounted and pretested on a molybdenum carrier, is soldered into the package, the lid is attached using tin-silver alloy to provide an overall hermetic unit. The package is 12.5 x 12.5 mm outside dimensions and offers about 4 x 4 mm of useful area for the chip. It provides useful performance up to 20 GHz and has built-in capability for I/O DC decoupling. The CASPAC amplifier package used by Fujitsu [8] and the MICPAC used by Texas Instruments [12] are other examples of this type of package.

Much effort has been expended to develop surface mount packaging techniques for lower frequency and digital circuits. Such packages offer high packing densities, automated assembly and light weight. Avantek has developed a form of this package for MIC applications referred to as the Planar Pak [17]. In this package, all components are fabricated or assembled on one side of an alumina or beryllia ceramic substrate. RF and DC contact is made through plated via holes to leads on the opposite side of the substrate. These may be trimmed flush with the edge of the substrate for maximum packing density. The package lid is then brazed to the substrate to give a hermetic seal. Measurements have shown useful performance to 20 GHz.

To date, most effort has been concentrated on realizing packages which may be of general usefulness and commercial value. The phased array antenna problem presents a unique situation in that the choice of array topology may be highly dependent on the package configurations available. This implies that the optimization of antenna arrays will likely require a much closer relationship between the circuit, package and antenna designer than ever before.

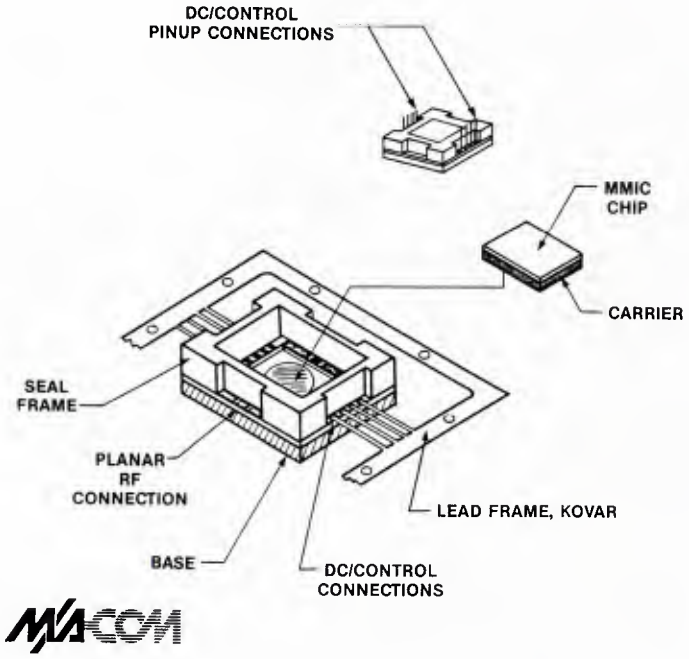

Fig. 12. M/A-COM MMIC Package

3.5.2 Testing

In practice, testing is carried out at many stages during the development of sophisticated modules such as those typically encountered in phased arrays. During the fabrication cycles, process monitors and controls are used to reject wafers early during the processing stages. Once the wafer is completed, DC probing is normally carried out before the wafer is diced into chips. More recently, with the development of RF wafer probing techniques, it has also become possible to carry out some microwave evaluation on the individual circuits prior to dicing. This avoids the costly step of packaging or mounting the chip only to determined that its RF performance is unacceptable. These probing steps can readily be automated but are typically incapable of properly assessing all of the necessary parameters, particularly where pulsed measurements are required. At this point the chip may be packaged either into an individual package or with several other chips.

For military applications, performance evaluations are typically extensive and exhaustive. Table IV [18] illustrates this point. The table is a matrix of tests required to completely evaluate a T/R module. For example, complete evaluation of the output power performance of the module over 12 frequencies, 3 input power levels, 16 phase states, 3 duty cycles, 3 load matches, 3 voltage states and at 3 temperatures requires a total of 2880 different data points be generated. Extending this over all the parameters listed results in a total of 87528 test points. This number underlines the complexity and costliness of the testing problem and emphasizes the need for development of new test methods and philosophies.

TABLE IV - T/R MODULE TESTING CHART [18]

	NUMBER FREQUENCIES	PHASE STATES	INPUT POWER	DUTY CYCLES	LOAD MISMATCHES	VOLTAGES SENSITIVITY	TEMPERATURES	TOTAL DATA POINTS
OUTPUT POWER	12	16	3	3	3	3	3	2880
PHASE Tx/Rx	24	32	6	6	6	6	6	23040
GAIN Tx/Rx	24	32	6	6	6	6	6	23040
I/P SWR Tx/Rx	24	16	2	2	2	6	6	6912
O/P SWR Tx/Rx	24	16	1	2	2	6	6	6528
PHASE LIN Tx/Rx	24	32	6	6	6	6	6	23040
AM/PM Tx/Rx	6	2	10	2	2	6	6	312
INTRA PULSE Tx GAIN & PHASE	3	16	3	3	3	3	3	720
PULSE/PULSE Tx GAIN & PHASE	3	16	3	3	3	3	3	720
NOISE FIGURE	12	4	1	1	1	3	3	336
							TOTAL =	87528

First of all, since rejection of a module at this point could prove very costly, it is important every effort be made to evaluate the quality of the wafer prior to dicing. This will require development of improved and automated wafer probing techniques and improved ability to interpret wafer quality from DC measurements. It may prove more realistic to simply reject entire wafers rather than require any significant testing between the wafer dicing and final assembly. A sampling statistical approach to electrical qualification as is frequently used now at the device level may be necessary [14].

Much effort is underway to define and develop sophisticated automated module level testing systems [19,20]. Even with such systems, for major phased arrays which may require 1 to 100 thousand modules, the total testing time may prove excessive. In addition, the problem arises of the interpretation and use of the data. New correlative techniques and possibly some form of expert system may be required for this. Development of methods of phased array antenna testing which are capable of identifying faulty modules may prove to be most cost effective.

4.0 PERFORMANCE CAPABILITIES

MIC performance is closely tied to that of microwave active devices of which the GaAs MESFET is the most common. This section reviews and compares the noise figure, power, bandwidth and phase shifting capabilities of MMICs and HMICs based on use of MESFETs.

4.1 Noise Performance

4.1.1 Device Capabilities

The noise figure achievable with either HMICs or MMICs is ultimately limited by the achievable performance of discrete MESFETs. The current state-of-the-art is illustrated in Fig. 13. The useful frequency range of operation of a MESFET as a low-noise amplifier is directly dependent on the narrower dimension of the gate stripe, which corresponds to the length of the gate, and on the gate-to-source spacing. Conventional photolithographic techniques are typically limited to about 0.5 μm. Using direct write electron beam lithography, gate lengths of 0.2-0.3 μm are achievable with good reproducibility.

The results reported by Hughes [21] and included in Fig. 13, were achieved in this manner. As the gate-to-source length is increased, the gate-to-source resistance increases and this results in an increase in noise figure. As the frequency increases, phase delay along the gate stripe begins to occur. Both factors combine to limit the achievable noise figure for a given frequency. By dividing the gate stripe into segments or by using an airbridge gate contacting approach to offset some of these effects, an improvement in the performance of MESFETs has been demonstrated [22].

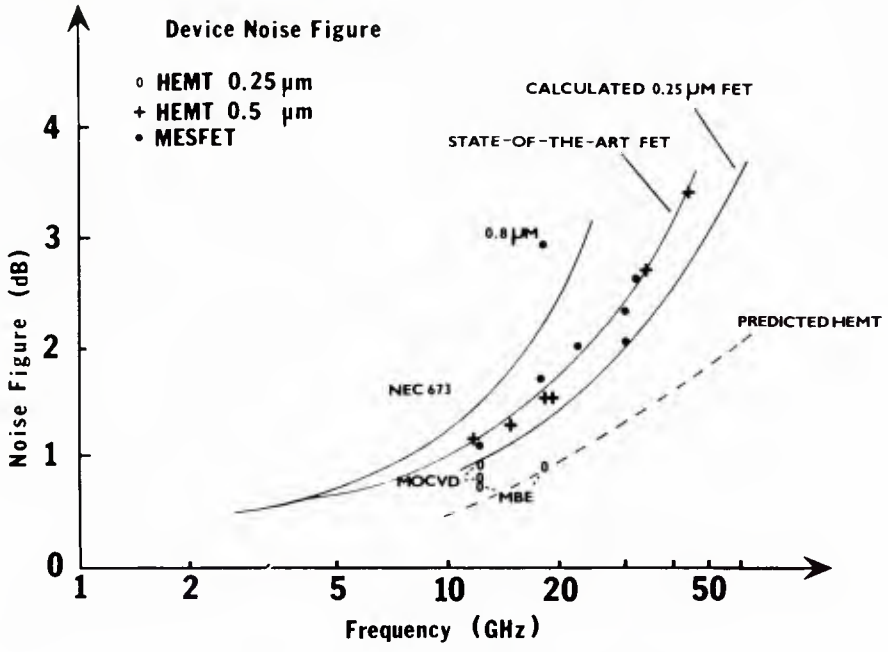

Fig. 13. State-of-the-Art MESFET Noise Figures.

Much attention is currently being given to a new MESFET device technology which uses heterojunction structures consisting of GaAlAs and GaAs. These devices, known as High Electron Mobility Transistors (HEMTs) have the potential for doubling the speed of operation of a typical MESFET for similar dimensional parameters [11]. As may be seen from the figure, significant noise figure performance has already been demonstratred and further improvements may be expected. The technology is still in its infancy. Most results to date have been obtained using the expensive and slow MBE process and this remains a drawback to its practical exploitation particularly for MMICs. In Fig. 13 is shown some promising recent results for HEMTs fabricated using the potentially lower cost MOCVD process [23].

A similar device to the HEMT and known as a Heterojunction Bipolar Transistor (HBT) is also under development and shows great promise of improving the 1/f noise performance of microwave and millimeter-wave oscillators [24].

4.1.2 Amplifier Noise Performance

Fig. 14 illustrates the current state-of-the-art performance reported for low-noise amplifiers. The results are typically for narrowband amplifiers, defined here as less than an octave bandwidth. For the MMICs, due to their inherently wideband nature, this is not necessarily meaningful. It will be noted that the noise figure of HMICs continues to surpass that of MMICs. This may be attributed to the ability to provide high Q on-circuit tuning and to pre-screen for the best devices. In addition, the requirement to use much thinner metal thickness for the matching elements in MMICs results in a slight degradation. Design procedures for optimizing the performance of discrete FETs are now well established. In contrast, development of MMIC compatible MESFET designs for incorporation in more complex MMICs is still underway [25,26].

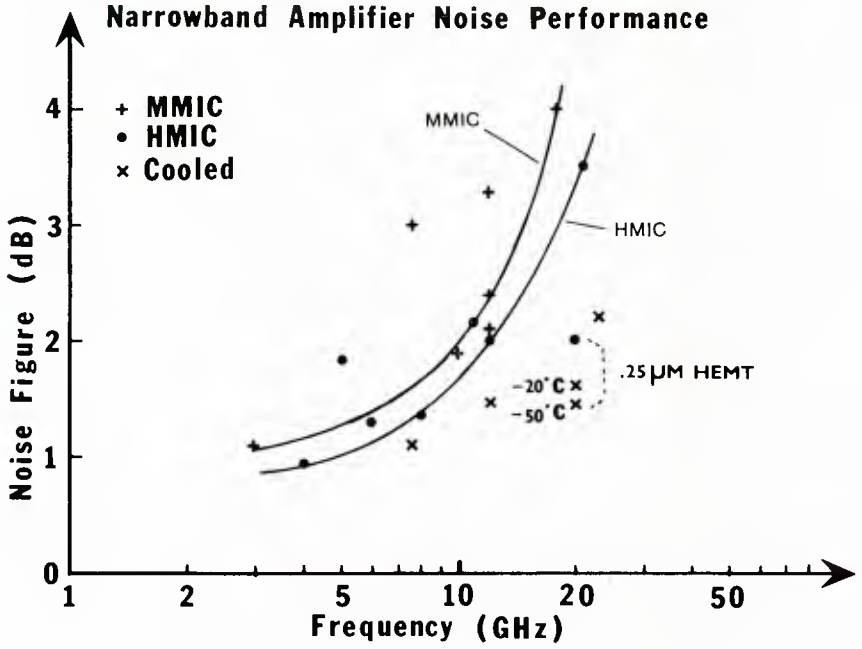

Fig. 14. State-of-the-Art Narrowband Amplifier Noise Figure Performance.

As the frequency of operation increases, matching circuit losses typically begin to increase and it becomes more important to keep the physical size of the input circuit small. Use of small lumped element matching circuits essentially colocated with the active device meets this requirement in MMICs. In addition, bondwires are eliminated. By use of series feedback, simultaneous noise matching and good return loss characteristics have been demonstrated on an MMIC [27]. Similar techniques are difficult to employ with HMICs due primarily to the positioning of matching structures. Miniature HMICs may be expected to realize some of these advantages but the need to bond to the MESFETs will prove to be a limitation.

It is generally desirable whenever possible to avoid the use of isolators for reasons of both size and cost. In HMIC multistage amplifiers, the relatively long distances between devices and the mismatches which occur between them, due possibly to the use of wirebonds, often result in gain ripples unless isolators are used. This problem is not as severe for MMICs since the distances are generally much smaller thus avoiding the need for isolators.

4.2 Power Performance

4.2.1 Device Capabilities

Fig. 15 illustrates the state-of-the-art in discrete MESFET power performance. Factors which affect the power capabilities of MESFETs include the overall gate periphery, source inductance and resistance and the ability to distribute and eliminate device heat. To achieve the first, several electrodes are used. As the overall width of the device "cell" becomes large, it becomes increasingly difficult to maintain phase and amplitude balance over the device. At this point, several MESFET cells each containing a number of gate stripes are typically combined. This not only requires good uniformity between cells but also well balanced combining structures.

Various approaches are being examined to reduce the source inductance including the development of "flip-chip" designs and the use of "via" holes combined with airbridges for cell interconnection. These latter approaches are also aimed at reduction of thermal impedance. In addition, as mentioned earlier, the GaAs device or MMIC wafers are thinned to about 100 μm or less, again to reduce thermal resistance to ground.

New device structures are also being developed to give higher power capabilities. Included in Fig. 15 are some recently reported results for new HEMT structures which use double and quadruple heterojunctions [28,29]. The performance of these devices in terms of power per unit length of gate periphery is very promising. The HBT also shows great promise and, although significant results have not yet been published, analysis suggests power levels up to twice that of conventional MESFETs [24].

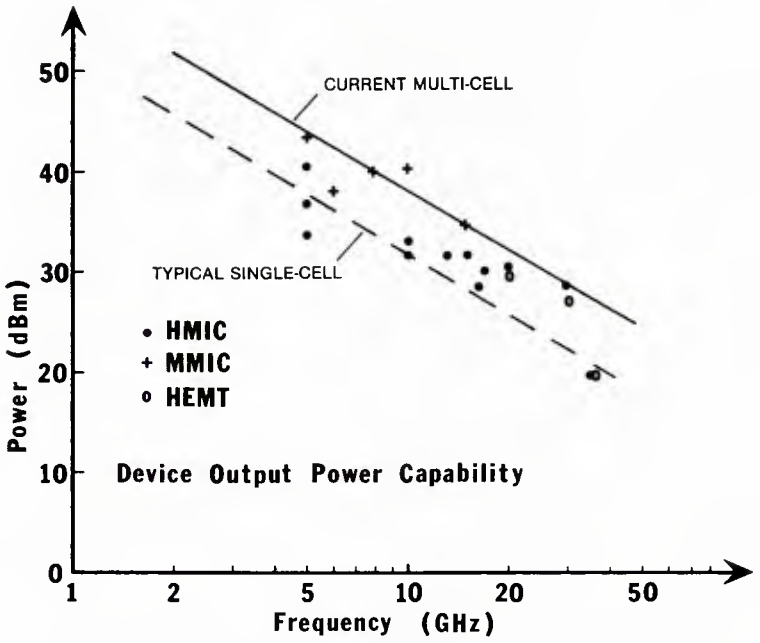

Fig. 15. State-of-the-Art MESFET Power Capabilities.

4.2.2 Amplifier Power Performance

Fig. 16 summarizes the amplifier output power performance demonstrated by HMICs and MMICs to date. The complexity, large chip size and the need for exceptional uniformity and control of process steps for power MESFET fabrication is comparable to that used for many MMICs. Many multi-cell devices are in fact implemented using MMIC or MHMIC techiques internal to the device package. This is reflected in the fact that the $1/f^2$ curve shown in Fig. 16 is identical to that shown in Fig. 15 for the multi-cell device. To achieve powers higher than on these curves, conventional HMIC or waveguide or coax combining techniques may be used. Some examples are included in Fig. 16. Such techniques are typically quite narrowband.

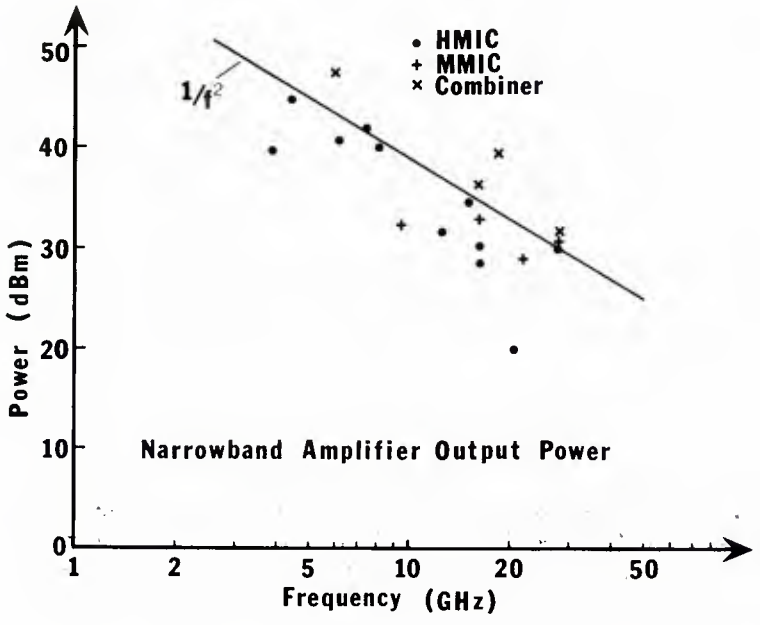

Fig. 16. State-of-the-Art Power Amplifier Performances.

A consequence of the paralleling of cells in a power FET is a decrease in the device impedance to the point where it becomes very difficult to match. Since impedance levels for microstrip are typically in the range 10 to 140 ohms, matching into power FETs becomes very difficult in conventional HMICs particularly when bandwidth is important. In MMICs, thin-film capacitors are more typically used. However, the low device impedances result in the need for large values of capacitances and this translates into large areas and very thin dielectric layers, both highly undesirable. In these cases, MHMIC techniques may prove to be of particular value in permitting off-circuit capacitors to be produced independently of the power FET.

Power amplifiers using MESFETs are capable of achieving power-added efficiencies over 40%. Even this result leaves over 60% of the DC power to be dissipated largely through the FET. This underlines the importance of good heatsinking for power amplifiers. Typically, MMIC power amplifiers have not achieved the same efficiency as HMIC units. However, by using the distributed amplifier approach described later, the thermal heatsinking problem is somewhat eased. This approach is essentially limited to MMIC implementation. Another technique used in pulsed amplifier operation to improve efficiency is to turn the drain bias on only when transmitting. This of course, requires implementation of a timing circuit. Although this does not substantially ease the FET heatsinking problem due to the fast thermal time constants of typical FETs, it does reduce the overall DC power consumption and thermal load on the system.

4.3 Bandwidth Performance

Although the bandwidth achievable by MICs is a function of various factors, the most significant are the MESFET cutoff frequency, and the physical size of the matching circuits. Factors affecting the cutoff frequency of MESFETs are very similar to those noted in 4.2 as affecting the noise performance and are primarily related to the dimensions of the gate structure.

Fig. 17 illustrates the state-of-the-art in bandwidth performance of MICs. HMIC amplifiers achieving much more than octave bandwidths are not common. In practice, the performance of HMIC amplifiers both conventional and miniature, is limited by the ability to both position the MESFET chip and to wirebond it reproducibly. The phase error resulting from inaccuracies in either of these parameters typically results in excessive gain ripple and, particularly at high microwave frequencies or where large numbers of stages are cascaded, may result in significant gain degradation. In addition to its inherent control of these variables, the small physical size of the MMIC approach lends itself to application of feedback techniques which show great promise for bandwidth improvement [30].

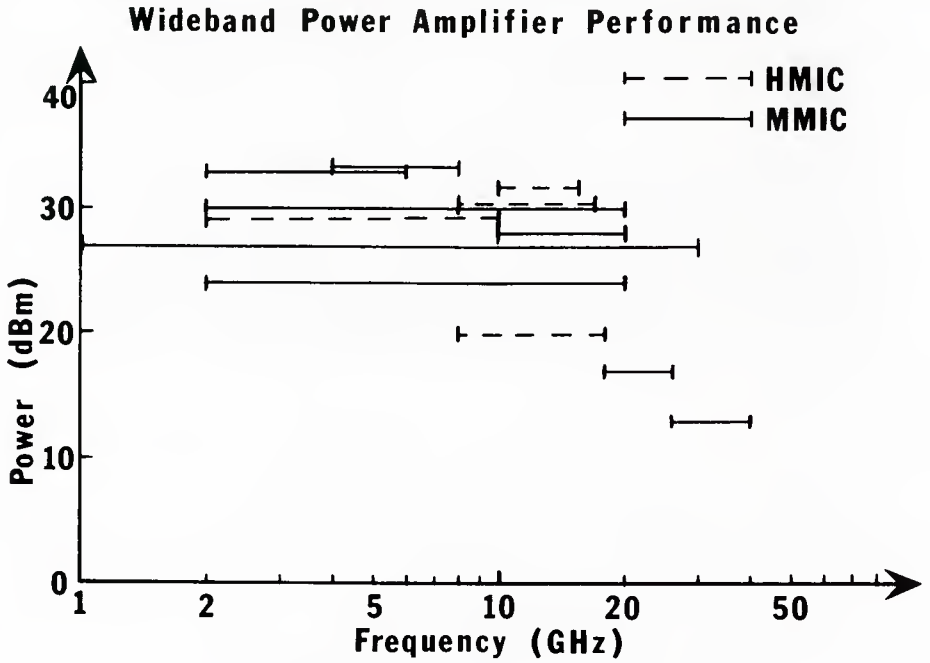

Fig. 17. MESFET Amplifier Bandwidth Capabilities.

A very significant recent development made possible by the small size of MMICs is the distributed amplifier approach [30,31]. This technique, which makes use of the MESFET parasitic elements to effectively realize a transmission line structure, has demonstrated remarkable performance as shown by the 1 Watt 2-20 GHz amplifier development by Raytheon [31] and the 0.5 Watt 1-30 GHz amplifiers developed by Hughes and Avantek [32]. The approach does not give high gain for the number of FETs used and is not particularly efficient with respect to DC power or chip area consumption. However, its exceptionally wide band operation and distributed thermal loading make it attractive. To date, such amplifiers have demonstrated noise figures equal to or better than HMIC wideband amplifiers. Aitchison [33] has analytically demonstrated the potential for distributed amplifiers to achieve noise performance similar to that of a MESFET resonantly tuned for optimum noise figure.

4.4 Phase Shifters

It is somewhat more difficult to provide a generalized assessment of the performance capabilities of phase shifters. However, some generalization is possible in many of the desirable characteristics. Typically, 4 to 7-bit phase shifters are required, often with an additional requirement for some fine control or adjustment. Increasingly, and partly due to the promise of MMICs, modern phased arrays are demanding small size and weight and good uniformity of performance over relatively large numbers of array elements. HMIC phase shifting techniques have generally proven unable to effectively meet all of these requirements at low enough cost. MMICs and to some extent, MHMICs show promise of overcoming this. However, their ability to fulfil this promise will depend on the realization of good wafer yields. The phase shifter is still considered to be one of the greatest contributors to low yields in T/R modules. Much attention is therefore being placed on developing new area-efficient designs which minimize overall gate periphery and capacitance. The following will briefly review some of the techniques currently being examined.

Several of the basic forms of phase shifters have already been demonstrated in MMIC form. At frequencies below Ku-band, many distributed circuit structures such as hybrid couplers and power combiners as well as simple switched segments of transmission line may occupy large amounts of chip area and so become impractical. To overcome this, various lumped element structures are used. Often these result in frequency constraints on the performance. In some cases, particularly at low frequencies, the lumped element equivalents may contain large capacitances and these may compromise the wafer yield and phase shifter reproducibility.

A popular technique for digital MMIC phase shifters is the switched-line type in which lengths of line differing in overall phase length by the desired phase delay are switched in or out of the signal path by an active device, typically a MESFET. At higher frequencies, these lengths are physically quite small and make reasonably efficient use of chip real estate [34,35]. At lower frequencies, the switched-line lengths are replaced by lumped element low-pass and high-pass filters. An interesting approach to this type of phase shifter implemented by Raytheon is shown in Fig. 18 [36]. Here, MESFET switches are incorporated directly into the high-pass/low-pass filter sections. This permits the MESFET parasitics to be included as elements of the filter thus resulting in wider bandwidth operation. The MESFET parameters are adjusted to ensure the appropriate values for the parasitic elements. The unit shown is a 3-bit phase shifter which gave good performance over the 6-18 GHz frequency range and was realized on a 1.25 x 2.2 mm chip.

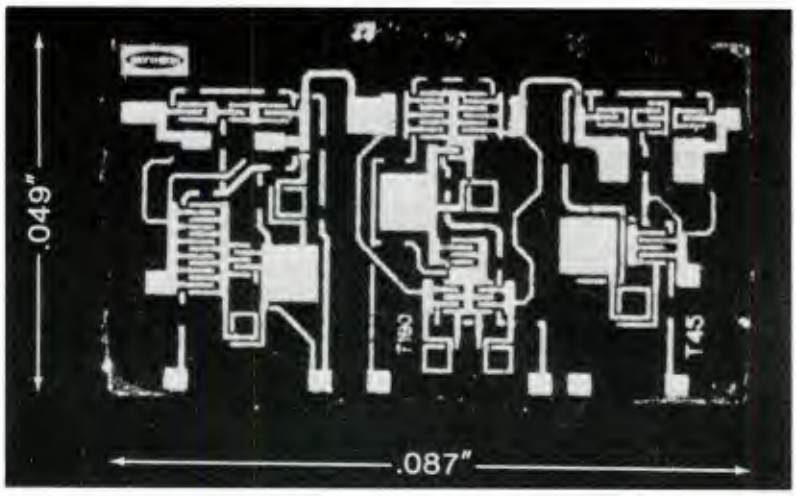

Fig. 18. A 3-Bit Phase Shifter using High-Pass/Low-pass Filters.

A variation on this type has been described by Plessey [37]. In this case, the MESFET parasitics are incorporated into a 90° high-pass/low-pass phase shifter. Two such phase bits are then used to realize the 180° bit, a third in the 90° bit and a fourth in a 0-90° variable phase bit. The variable phase bit uses a technique known as vector modulation. In this technique, two signals in phase quadrature are combined in the ratio sine/cosine of any desired phase angle. The resultant output is a vector of constant amplitude and with the desired phase angle. The vector modulator is realized using novel MMIC compatible splitters, combiners and variable attenuators all realized using lumped element components and MESFETs. The 22.5° phase steps for a 4-bit shifter are then realized by setting the MESFET attenuator bias to preset values. Raytheon has implemented a 5-bit unit which is similar to this and gives improved phase accuracy [38].

More recently, General Electric has implemented a digitally controllable sine/cosine attenuator [39] in which the resultant attenuation settings correspond to that required to realize the various 11.5° resolution steps in a 5-bit phase shifter. In this design, five paralleled dual-gate MESFETs with gate lengths scaled appropriately are simply switched ON or OFF. An X-Band version of a complete 5-bit phase shifter occupies only 1.1 x 3.3 mm and uses a minimum of gate periphery.

Another popular type of phase shifter for HMIC realization has been the reflection type. These typically use some form of 90° coupler terminated in switchable lengths of line and are generally practical only at frequencies above X-Band. A recently developed variation of this type consists of a Lange coupler terminated in a transmission line along which are 16 shunt Schottky diode switches [40]. Each switch corresponds to one phase state. The result was an 8-12 GHz 4-bit phase shifter on a chip 3.7 x 2.3 mm. This type of phase shifter gives, more correctly, a delay shift as is ideal for steering of a phased array.

A C-Band implementation which uses 90 and 180° reflection type phase shifters combined with 11.25, 22.5 and 45° loaded line phase shifters has also recently been described [41]. In this approach, the good return loss characteristcs of the reflection type were used to moderate the poor return losses of the loaded line sections. A sixth analog bit and was used to fine tune the overall phase. It was implemented as a second 11.5° bit whose load was variable by varying the impedance of MESFETs. The size of the overall unit was 4.19 x 9.3 mm.

5.0 CONCLUSIONS

Fig. 19 illustrates a complete T/R module developed at Raytheon [42] and represents essentially the state-of-the-art in integrated T/R module technology. The unit contains all the components in Fig. 12a except for the circulator. Several points are worth noting. First of all, the module consists of several separate chips. At present, integration beyond this level is not consistent with realization of acceptable yields. The package shown has several of the features discussed earlier for multi-layer ceramic packages. Several leads are provided for the DC biassing, phase shifter control, switch activation as well as the RF input and output.

Fig. 19. A Complete T/R Module.

In summary, MIC technology is rapidly demonstrating its ability to meet the very stringent performance, size and weight requirements necessary to the successful realization of phased array antennas. This is being achieved both through improvements in HMIC techniques as well as the development of MMIC technology. Optimum systems will likely make use of combinations of the two. The degree to which the technology has advanced is particularly dependent on the required frequency of operation. Table V illustrates this [18].

TABLE V-CURRENT STATUS OF MODULE TECHNOLOGY

MATERIAL	30+ GHz TECHNOLOGY	
DEVICES		10-20 GHz MODULE TECHNOLOGY
CIRCUITS		
MODULES		
MODULE TO MODULE TRACKING (PHASE & AMPLITUDE)		MODULE VALIDATION 10 GHz
RELIABILITY		
THERMAL-MODULE / SYSTEM		
ELECTRICAL INTERFACE		
RADIATION / EMP		
COST-CHIP / PACKAGE / TEST		
CONTROL-PHASE SETTING-ADAPTIVE OPERATION IN AN ARRAY		

The exploitation of these improved technologies will require development of improved methods of design, packaging and testing and, possibly more importantly, will require a re-examination of the traditional separations between the device, circuit, antenna and system designers.

ACKNOWLEDGMENTS

The cooperation of R. Mailloux and H. Chilton of the Rome Air Development Center is gratefully acknowledged. Also, the author acknowledges the ready support of Dr. M. Stubbs in preparing some of the information.

REFERENCES

1. H. Stolze et.al., "Material and Circuit Evaluation for Millimeter Wave Applications", ESA Contract Report, Contract 4044/79/NL/DG/(SC), NTIS N82-20455, February 1981.

2. R.S. Pengelly, D.C. Rickard, "Design Measurement and Application of Lumped Elements Up to J-Band", 7th EMC, 5-8 Sept., 1977, Copenhagen, p. 460.

3. "Microstrip Computer Programs", Verlag Henning Wolff, Aachen, W.-Germany.

4. Y.L. Chow, X.Y. She, G. Howard, M.G. Stubbs, M. Gaudreault, "A Modified Moment Method for the Computation of Complex MMIC Circuits", EMC 1986, Dublin, Ireland, p. 625-630.

5. C.W. Suckling, "Procedures Examined for Successful GaAs MMIC Design", MSN&CT, March 1986, p.79-87.

6. R. Douville, "MIC Technology - Current Status and Future Trends", AGARD Workshop on Future Technology for Airborne Systems, The Haag, October 1985.

7. E.F. Belohoubek, "Miniature Hybrid Circuits - Alternatives to Monolithic Circuits", RCA Review, Vol. 46, December 1985.

8. J. Browne, "Miniature Amplifier Meets Transistor Size Requirements", Microwaves & RF, July 1983, p. 114-119.

9. F.N. Sechi, H.C. Johnson, J.E. Denlinger, R. Brown, "New Miniature Beryllia Circuit Technology", Microwave Journal, March 1985, p. 117-124.

10. G. Gibbons, "Status of GaAs Component Technology for Low-Cost Microwave Systems", MSAT '83, Washington, D.C., March 1983, p. 336-342.

11. J. Berenz, "High Electron Mobility Transistors", IEEE MTT Newsletter, Summer 1984, p. 43-52.

12. R.S. Pengelly, "Hybrid vs Monolithic Microwave Circuits - A Matter of Cost", MSN, January 1983, p. 77-114.

13. B. Berson, "GaAs MMICs - The Solution for Phased Arrays?", MSN&CT, November 1985, p.54.

14. T. Harper, W. Kennan, N.K. Osbrink, "In Search of the $300 T/R Module", Microwave Journal, March 1986, p. 48-57.

15. F.M. Magalhaes, J.P. Beccone, J.C. Irvin, S.J. Perelli, W.O. Schlosser, "A Microwave GaAs FET Power Module with GaAs Matching Circuits", Microwave Journal, May 1985, p. 205-224.

16. B.A. Ziegner, "High Performance MMIC Hermetic Packaging", Microwave Journal, November 1986, p. 133-139.

17. N.A. Osbrink, R.B. Levitsky, S.B. Moghe, "Surface-Mounted MICs and MMICs Play Vital Role in Military Communications", MSN&CT, January 1985, p. 72-84.

18. H. Chilton, E. Jones, RADC, Private Communication.

19. T.R. Gheewala, "Requirements and Interim Solutions for High-Speed Testing of GaAs ICs", GaAs IC Symposium, 1985, p.143-146.

20. E.J. Jones, "T/R Module Evaluation Test System", Automatic RF Techniques Group Fall 82 Conference, Boulder, CO., November 1982.

21. L.C.T. Liu, E.T. Watkins, "GaAs Integrated Circuits for Microwave Communications", IEEE MILCOM '84, October 21-24, 1984, p.3.4.1-3.4.4.

22. R.M. Malbon, N.K. Osbrink, "Small-Signal, Low-Noise Active Devices", Microwave Journal, February 1985, p.121-137.

23. K. Tanaka, M. Ogawa, K. Togashi, H. Takakuwa, H. Ohke, M. Kanazawa, Y. Kato, S. Watanabe, "Low-Noise HEMT Using MOCVD", IEEE Trans. MTT, Vol. MTT-34, No. 12, December 1986, p. 1522-1526.

24. C.A. Liechti, "Heterostructure Transistor Technology - A New Frontier in Microwave Electronics", EMC 1985, Paris, France, p. 21-30.

25. E.T. Watkins, J.M. Schellenberg, H. Yamasaki, "A Low-Noise FET Amplifier", 1985 MTT Symposium, St. Louis, MO., p.321-323.

26. A.K. Gupta, D.P. Siu, K.T. Ip, W.C. Peterson, "Low-Noise MESFETs for Ion-Implanted GaAs MMICs", IEEE Trans. MTT, Vol. MTT-31, No. 12, Dec. 1983, p. 1072.

27. R.E. Lehmann, D.D. Heston, "X-Band Monolithic Series Feedback LNA", IEEE 1985 Microwave and Millimeter Wave Monolithic Circuits Symposium, St. Louis, MO., June 3-4, 1985, p. 54.

28. K. Hikosaka, Y. Hirachi, M. Abe, "Microwave Power Double Heterojunction HEMTs", IEEE Trans. Electron Devices, Vol. ED-33, No. 5, May 1986, p. 583-589.

31. Y. Ayasli, "Decade Bandwidth Amplification at Microwave Frequencies", Microwave Journal, April 1984, p. 71-79.

32. J. Goel, S. Yuan, "Transmitters Using Power Amplifiers", IEEE MILCOM '84, October 21-24, 1984, p.10.4.1-10.4.6.

33. C.S. Aitchison, "The Intrinsic Noise Figure of the MESFET Distributed Amplifier", IEEE Trans. MTT, Vol. MTT-33, No. 6, June 1985, p. 460-466.

34. A. Gupta, G. Kaelin, R. Stein, S. Huston, K. Ip, W. Peterson, M. Mikasa, I. Petroff, "A 20 GHz 5-Bit Phase Shift Transmit Module with 16 dB Gain", 1984 GaAs IC Symposium, p. 197-200.

35. V. Sokolov, J.J. Geddes, A. Contolatis, P.E. Bauhahn, C. Chao, "A Ka-Band GaAs Monolithic Phase Shifter", IEEE Trans. MTT, Vol. MTT-31, No. 12, December 1983, p. 1077-1082.

36. M.J. Schindler, Y. Ayasli, A.M. Morris, L.K. Hanes, "Monolithic 6-18 GHz 3 Bit Phase Shifter", 1985 GaAs IC Symposium, p. 129-132.

37. C.W. Suckling, P.N. Rigby, T. Bambridge, R.S. Pengelly, R.S. Butlin, "The Performance of GaAs Lumped Element Phase Shifters at S- and C-Bands", EMC '83, Nuremburg, W. Germany, p. 374-379.

38. P. Maloney, J. Selin, G. Jones, "Continuously Variable L-Band Monolithic Phase Shifters Using GaAs", 1986 GaAs IC Symposium, p. 78-81.

39. Y.K. Chen, Y.C. Hwang, R.J. Naster, L.J. Ragonese, R.F. Wang, "A GaAs Multi-Band Digitally-Controlled 0-360 Phase Shifter", 1985 GaAs IC Symposium, p. 125-128.

40. K. Wilson, J.M.C. Nicholas, G. McDermott, "A Novel MMIC, X-Band, Phase-Shifter", 1985 Microwave Monolithic Circuits Symposium, p. 10-14.

41. C. Andricos, I. Bahl, E. Griffin, "C-Band 6-Bit GaAs Monolithic Phase Shifter", 1985 Microwave Monolithic Circuits Symposium, p. 8-9.

PRINTED CIRCUIT ANTENNA TECHNOLOGY

Daniel H. Schaubert
Department of Electrical and Computer Engineering
University of Massachusetts
Amherst, MA 01003
U.S.A.

ABSTRACT

Printed circuit antennas are being used on a variety of spacecraft, aircraft, and projectiles where their low profile and conformability minimize interference with the structural and aerodynamic properties of the vehicle. The basic microstrip antenna has been studied extensively, but some important aspects of its performance are not yet characterized by the analyses that are available to the designer. Furthermore, new applications in millimeter wave monolithic phased arrays are forcing the designer to use substrates that are electrically thick and that may have a high permittivity. This paper describes several characteristics of microstrip antennas and identifies some that are being studied with the aim of improving antenna performance. A brief description of analysis techniques available to the designer and researcher will be presented. Finally, several aspects of monolithic and integrated phased arrays will be considered. General properties of these arrays will be discussed, and then several architectures and their associated printed circuit radiators will be presented.

1.0 INTRODUCTION

Printed circuit antennas have been in for a variety of applications ranging from marine buoys [1] to space-born synthetic aperture radars [2]. Antennas utilizing stripline circuits and radiating slots comprise one class of printed circuit antennas. Stripline fed slots like those in Figure 1 have been used individually and in arrays for conformal, low-profile antennas. The element has a broadside radiation pattern with nearly uniform radiation in the E-plane and a moderately wide beamwidth in the H-plane. If the ground plane of the antenna is sufficiently large, then little radiation is observed in the region $z < 0$. Variations on the basic element design such as [3] have improved the bandwidth of the antenna.

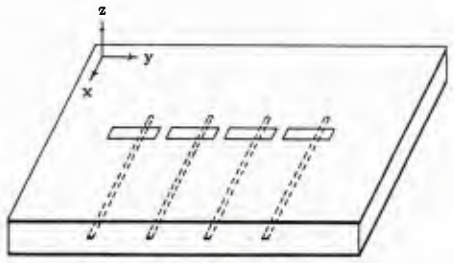

Figure 1. Stripline-fed slot array. Mode suppression posts are usually required to prevent parallel-plate mode coupling between elements

An alternative to the use of stripline to feed the radiating slot is to use microstripline as shown in Figure 2. This element is bidirectional, but it can be backed by a plane reflector spaced $\lambda_o/4$ in order to obtain a unidirectional pattern. Such a configuration has been used for a small broadside array [4], but it cannot be used for scanning arrays due to the existence of parallel plate mode coupling [5].

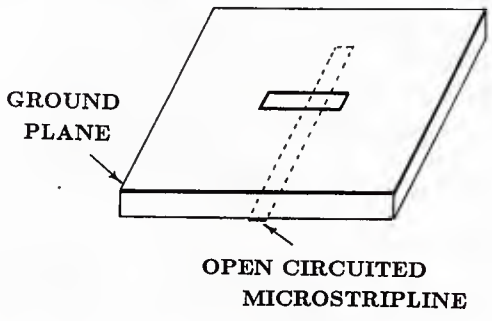

Figure 2. Microstripline fed slot element.

Another major class of printed circuit antennas that has received considerable attention in recent years is microstrip radiators. These antennas consist of a somewhat arbitrarily shaped patch of thin metal on the upper surface of a dielectric slab that has a ground plane on its lower surface. The dielectric slab, which may also have magnetic properties, can be somewhat arbitrary consisting of one or several layers, but it should be low loss in

order to maintain good efficiency. Also, it is generally uniform in the directions parallel to the ground plane, although this is not necessary. Some typical configurations of microstrip antennas are depicted in Figures 3 and 4. These antennas have the advantages normally associated with printed circuit antennas: thin, inexpensive to fabricate by photolithographic techniques, rugged, conformable, lightweight (compared to waveguides). In addition, microstrip structures appear to be better for integration than stripline. Most microwave integrated circuits are fabricated in microstripline, and similar techniques are being employed for the lower millimeter wave frequencies. The major disadvantages of microstrip radiators are their small bandwidth (typically only a few percent) and their efficiency. The total efficiency is reduced by two different mechanisms; circuit losses due to imperfect conductors and dielectrics and losses to surface waves guided along the dielectric substrate. Circuit losses are inherent in all microstripline circuits, but they can become more important in large arrays where feedlines may be several wavelengths long. Surface wave losses are not encountered in most other kinds of radiators, and they can have a profound effect on antenna performance. This topic will be discussed in more detail in section 3.

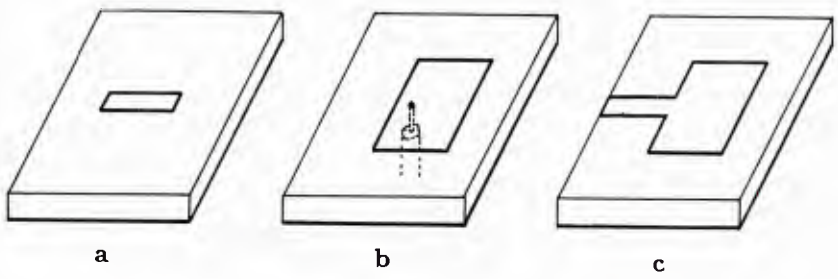

Figure 3. Some typical single-layer microstrip elements. (a) Microstrip dipole, (b) Coaxial-fed patch, (c) Microstripline-fed patch.

In the sections that follow, several aspects of microstrip antenna technology will be discussed. Among the topics of current interest are computer aided design (CAD) techniques for elements and arrays, elements and architectures for integrated and monolithic arrays at millimeter wavelengths, increased operating bandwidths, and circular or dual-polarized elements. Section 2 describes the analytical models that are currently in use for CAD of microstrip antennas and discusses their relative strengths and weaknesses. It also contains a brief discussion of the basic characteristics of microstrip antennas. Section 3 presents some considerations for monolithic and integrated phased arrays. These lead to various architectures for arrays of printed circuit radiators and these lead to different element designs. Section 3 also contains several element designs that have been developed to meet various requirements.

2.0 MODELS FOR DESIGN AND ANALYSIS OF MICROSTRIP ANTENNAS

Early explanations of the performance of microstrip antennas were based on a transmission line model [6], which also provided a starting estimate for the design of an antenna for a specific frequency. However, the predicted resonant frequencies obtained from this model were frequently in error by 3 to 5 percent, which exceeded the usable bandwidth of the antenna. Consequently, better models were needed for CAD of microstrip antennas and these were developed based first upon a cavity model for the resonant antenna and later upon a moment method model.

The major parameter of interest in CAD programs is input impedance. This is because the impedance is a key design parameter and it is often difficult to obtain good predictions of antenna impedance. Radiation patterns are also important, but the pattern of a microstrip antenna can be approximated quite well by using simple formulas based on two radiating slots. Mutual impedance is of interest in array applications, and it can

be obtained by using moment method techniques, or some approximate techniques based on transmission line models.

2.1 Transmission Line Model

The simplest explanation of the operation of a rectangular microstrip antenna comes from the transmission line model. The voltage distribution on a resonant section of microstripline is depicted in Figure 5a. If the line is shortened to include only one half cycle of the standing wave, voltage and current distributions similar to those in Figure 5b result.

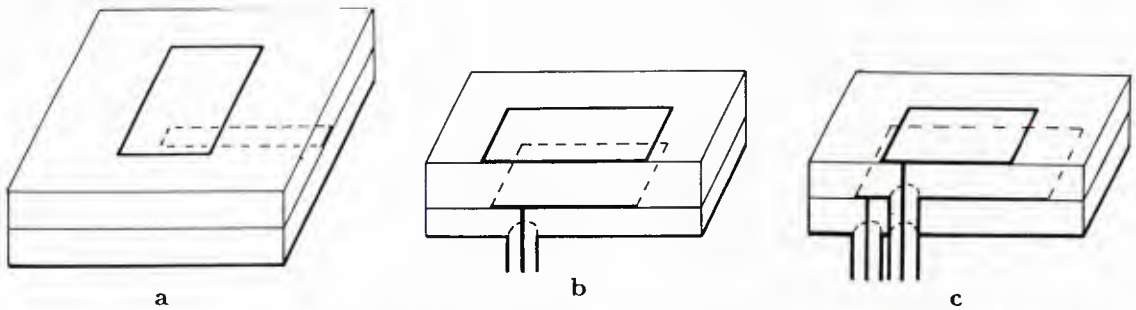

Figure 4. Some typical, two-layer microstrip elements. (a) Patch coupled electromagnetically to microstripline, (b) Stacked patches with upper patch coupled electromagnetically to lower patch (cut away view), (c) Stacked patches with independent feeds (cut away view).

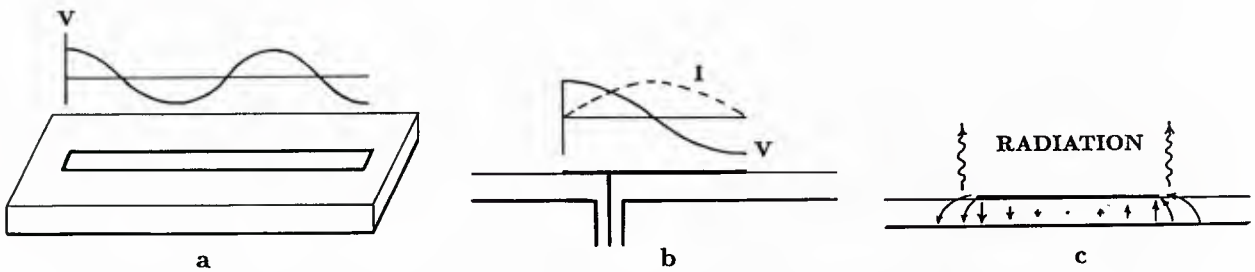

Figure 5. Transmission line model of microstrip antenna. (a) Resonant length of microstripline, (b) One-half wavelength resonant line fed by coaxial probe, (c) Electric field under line and fringing out at open-circuited ends.

The fringing electric fields can be considered as equivalent sources, that radiate maximum strength broadside to the plane of the antenna (Figure 5c). A typical radiation pattern is depicted in Figure 6, showing the wide broadside pattern that makes the microstrip antenna an attractive element for conformal arrays. The input impedance of the microstrip antenna can be adjusted easily by moving the feed location until the desired ratio of voltage to current is obtained (*cf*, Figure 5b).

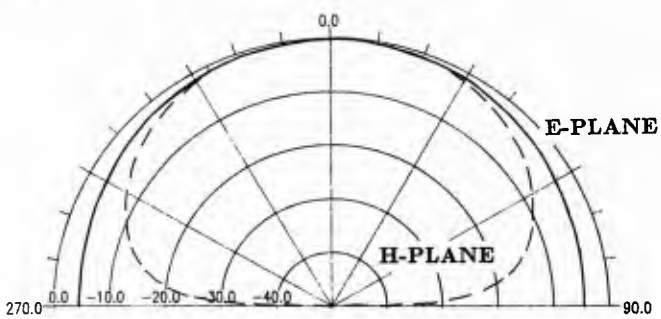

Figure 6. Typical radiation pattern of microstrip antenna.

The radiation from a simple rectangular patch antenna is polarized linearly with the electric field along the resonant length of the antenna (parallel to the current flow on the conducting patch). A rectangular patch can be resonated in both the horizontal and vertical directions at frequencies f_H and f_V where the dimensions L_H and L_V (see Figure 7) are approximately one half the wavelength in the substrate at the respective frequencies. By making $L_H = L_V$ and feeding the two inputs 90° out of phase, a circularly polarized radiator can be obtained.

Shapes other than rectangular can also be used for the microstrip radiator. Many examples can be found in the literature and in two recent books [7, 8]. In all cases, efficient radiation with reasonably good impedance values can be obtained when the structure is resonant and large fringing fields are present. The cavity models discussed below often are useful in interpreting the resonances of microstrip antennas.

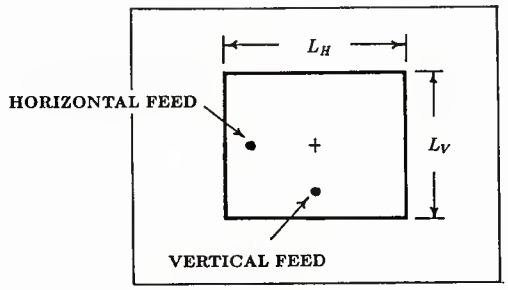

Figure 7. Rectangular patch antenna with feeds for horizontal and vertical polarization at different frequencies.

2.2 Cavity Models

Cavity models for microstrip antennas are based on the premise that the field distribution in the dielectric region between the patch radiator and the ground plane (Figure 8) is nearly the same as that in a cavity enclosed by perfect electric conducting walls top and bottom and perfect, or nearly perfect, magnetic conducting walls around all the sides. For thin substrates that result in narrow-band, high-Q antennas (antennas that have large internal field strengths relative to the amount of power radiated) this premise is valid and it forms the basis of the cavity models developed by Lo and Richards [9, 10] and Carver [11, 12]. These models differ in their means of incorporating the power lost to radiation, but both have proven to be useful for designing antennas and for interpreting the behavior of antennas.

The Lo/Richards model [10] evaluates the cavity field assuming perfect magnetic conducting side walls and a vertical strip of electric current as the feed. The radiated fields are calculated by removing the conducting walls and allowing the tangential electric fields on the side walls to radiate into *free space* above the ground plane. The power lost to this radiation is added to that lost to conductors and dielectric and is used to calculate the input impedance. A comparison of calculated and measured results from [10] is shown in Figure 9. This example shows the capability of the method to analyze antennas with multiple feeds. This capability has been exploited to analyze antennas that are tuned by shorting posts [13] or reactive loads [14, 15] as shown in Figure 10.

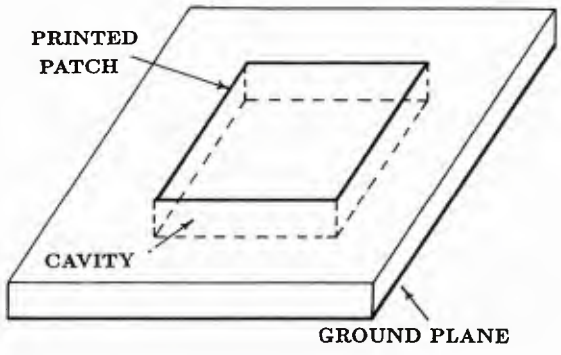

Figure 8. Cavity region between printed patch and ground plane.

The cavity model of Carver [11] incorporates the effects of fringing and radiation at the side walls of the cavity region by using a finite wall admittance on a cavity of length L and width W. Simple formulas based on parallel plate radiation and microstrip open circuit susceptance are used to estimate the wall admittance.

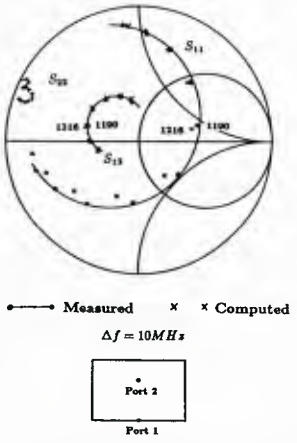

Figure 9. Two-port S parameters of rectangular microstrip antenna comparing measurement and calculation by cavity model. [after 10]

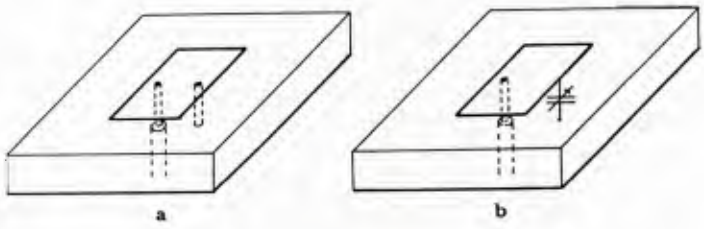

Figure 10. Frequency tuning by reactive loads, (a) Shorting post, (b) Capacitor.

Cavity models always assume no field variations in the direction perpendicular to the ground plane, which restricts the substrate to be electrically thin. In practice, it is found that the input impedance cannot be predicted accurately for substrates thicker than $0.02-0.03\lambda_0(\lambda_0$=free space wavelength). For substrates having relative permittivity $\epsilon_r \lesssim 10$, the range of validity may be restricted to even thinner substrates. Also, the accuracy of the predicted resonant frequency is not as good as one would like, but a quantitative evaluation of this parameter is difficult because typical variations in substrate permittivity lead to errors that are nearly as large as those observed. Despite these shortcomings, the cavity models are very useful for design and interpretation of experimental results and they are computationally efficient to use compared to moment method techniques.

2.3 Moment Method Models

The currents that flow on the conducting patch of a microstrip antenna satisfy an integral equation that can be derived by enforcing Maxwell's equations and the appropriate boundary conditions. This integral equation has a kernel function that is the electric field due to an infinitesimally small current element on a grounded dielectric slab. Obtaining an expression for this field is straightforward, but it involves infinite integrals that must be evaluated numerically. Several researchers [16-20] have done this and obtained solutions to the integral equation for the current on a microstrip radiator by using the method of moments. These solutions are quite rigorous in that they use the Green's function for the grounded dielectric slab and they include radiation, surface wave effects of the grounded substrate, and mutual coupling. The principal approximations involve the choice of basis and testing functions, which must be chosen judiciously in order to obtain accurate solutions within a reasonable computation time.

The example in Figure 11, taken from [19], shows the agreement that can be achieved between the calculated and measured input impedance of an antenna built on a thin substrate (thickness $\approx 0.01\lambda_0$) with a moderate dielectric constant ($\epsilon_r = 2.55$). The computation time required to obtain such a solution by the moment method is approximately 10 minutes per frequency point on a DEC VAX 11/750 running in a multiple user environment. The long computation time is the primary disadvantage of the moment method solution. Another problem with existing cavity models is related to the way in which the feedline or feed probe interacts with the currents on the resonant patch. For thin (thickness $\lesssim 0.02\lambda_0$), low permittivity ($\epsilon_r \lesssim 4$) substrates, a simple feed model often suffices. However, for thicker substrates with higher permittivity, feed models that are generally applicable do not yet exist. As a result, reliable predictions of microstrip element performance for many cases of practical importance cannot yet be obtained for many cases of practical importance, such as moderately wide bandwidth antennas and millimeter wave antennas on GaAs. Nevertheless, some characteristics of arrays can be predicted and these will be discussed in section 3. (The feed problem has not been adequately treated by cavity models, either.)

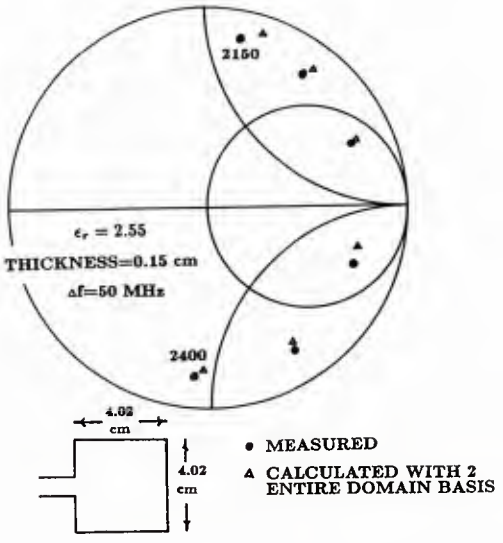

Figure 11. Comparison of input impedance, measured and calculated by moment method. [after 19]

The moment method can be readily adapted to compute the mutual impedance between two or more microstrip antennas. Pozar has illustrated this [19, 21].

3.0 ELEMENTS AND ARCHITECTURES FOR INTEGRATED PHASED ARRAYS

Integrated phased array antennas consisting of a large number of elements and operating at millimeter wavelengths have motivated many antenna developments in recent years. Reduced cost, increased reliability, and performance are some of the reasons for investigating monolithic and integrated structures, and the high level of integration of active and passive components in these structures makes them different from most systems that have been developed to date. The coexistence of these components requires the use of substrates, transmission lines, and circuit designs that have not been necessary in modular units at lower frequencies.

This section addresses some of the issues pertinent to the design of monolithic and integrated arrays. Surface wave effects due to printed antenna substrates are studied to determine their impact on array performance and to motivate a consideration of several array architectures and element designs. Using criteria such as scan range, bandwidth, substrate real estate, polarization, and feed line radiation, monolithic array designs are compared to some multiple-layer and two-sided designs. Broadside radiating elements such as microstrip dipoles and patches are considered as well as end-fire radiating slots.

3.1 Design Considerations for Integrated Arrays

In addition to the usual electrical requirements such as bandwidth, scan range, polarization, and sidelobe level, integrated arrays are subject to many other requirements, which can be referred to as mechanical requirements. Many of these are a consequence of the large number of elements that may be required ($10^3 - 10^5$) or the high level of integration that is desired. Grating lobe considerations limit element spacing to be approximately $\lambda_0/2$ so the radiating element and all of its circuitry (phase shifters, switches, amplifiers, bias lines, etc.) must fit within a cell having a surface area on the order of $0.25\lambda_0^2$. This can be a severe constraint if a truly monolithic

array (*i.e.*, everything on one surface) is desired. Heat can be a problem because the density of active devices in a millimeter wave array, their efficiency and the thermal conductivity of GaAs can lead to unacceptably high temperatures in an integrated array. Some attractive electrical designs must be discarded because they cannot adequately dissipate heat. Also, the fragility of thin GaAs substrates places a strict requirement on the strength and rigidity of the array structure. Finally, the manufacturability and electrical reliability of the array must be considered. Transitions from board to board or from wafer to wafer should avoid difficult via connections whenever possible, and the economies of photolithographic fabrication must be utilized, which implies that the array should be as monolithic as possible.

3.2 Antenna Substrate Effects

A straightforward integration of radiating elements and active circuits on a GaAs substrate offers the best use of photolithographic techniques, but it is not optimum for antenna performance. Microstrip and tapered slot antennas perform better on low-ϵ_r substrates. Microstrip antenna arrays exhibit scan blindness due to a resonance of the surface wave modes of the dielectric sheet that occurs when the propagation constant of the surface wave coincides with the propagation constant of a Floquet mode [22, 23]. The typical plot of the calculated reflection coefficient versus scan angle in Figure 12 shows the blindness at about 45° from broadside [23]. The usable scan range can be increased by decreasing the substrate thickness, but this also reduces the antenna's bandwidth. The curves in Figure 13 illustrate the trade-off that must be made between bandwidth and scan range. In order to obtain 10% bandwidth on GaAs, the substrate must be about $0.05\lambda_0$ thick. But, the array will then be blind at 60° and the usable scan range (for which a reasonable impedance match is obtained) will be limited to about 45° from broadside. The effects of substrate permittivity and thickness and of element spacing are shown in Figure 14 [24]. This figure shows that lower permittivity substrates provide a wider scan range. Also, the bandwidth of microstrip elements is greater on lower permittivity substrates [25]. However, active devices cannot be fabricated on low-ϵ_r substrates, so alternative element designs and array architectures must be developed. Some examples are presented below. In addition to scan blindness, surface waves on microstrip arrays can diffract from substrate boundaries to degrade the antenna's polarization and side lobes. They could also provide a coupling path to circuit elements on the substrate.

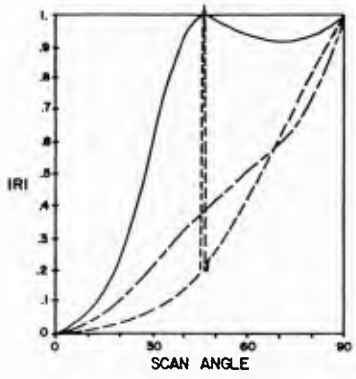

Figure 12. Reflection coefficient magnitude for infinite microstrip patch array. Square grid spacing is 0.5λ, substrate is 0.06λ, ϵ_r=12.8.

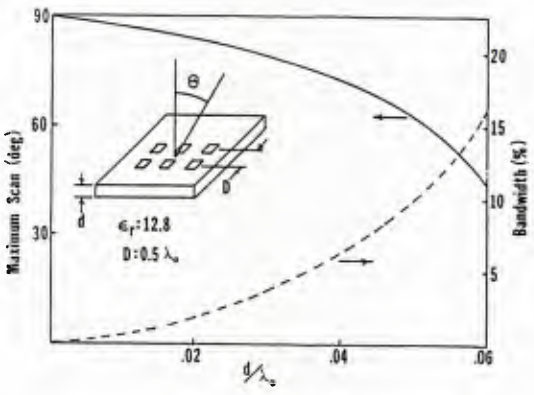

Figure 13. Angle of scan blindness and bandwidth of patch antennas on GaAs.

3.3 Some Elements for Integrated Arrays

Some advantages and disadvantages of microstrip dipoles and patches on GaAs were noted above. Arrays built on low-ϵ_r substrate and fed by means of a via connection from a monolithic circuit on GaAs below the ground plane are possible, but the via connections are not as reliable as one would like and the input impedance of millimeter-wave, probe-fed microstrip patches is difficult to predict. Some alternative designs are considered here, with emphasis on alleviating one or more of the problems noted above.

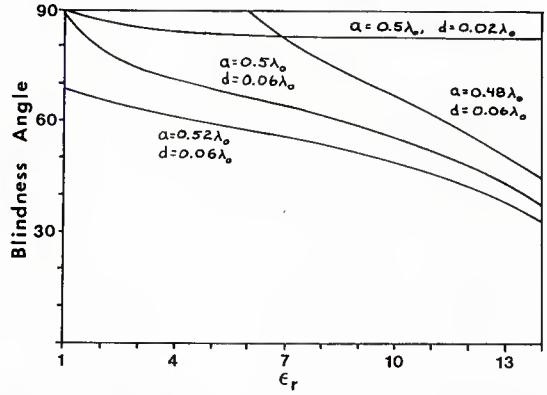

Figure 14. Scan blindness angle for various element spacings, (a) and substrate thickness (d).

3.3.1 Two-Layer Microstrip Patch

A two-layer antenna design based on the approach of Oltman and Huebner [26] could be useful for integrated arrays. A lower substrate of GaAs can support microstrip feed circuits with active devices. An upper substrate of low-ϵ_r material supports a patch antenna that is electromagnetically coupled to the feed circuit (see Figure 15). The patch radiator will behave as if it is on a substrate that is thicker than the GaAs and has a lower ϵ_r. This will increase the bandwidth and scan range of the antenna. However, at millimeter wavelengths, the GaAs may be a few hundredths of a wavelength thick and scan blindness may still occur at angles closer to broadside than would be allowed for some applications. Also, spurious radiation from the feed network and unintentional coupling from the radiating patches to various components on the lower substrate could affect array performance.

The use of electromagnetic coupling provides additional degrees of freedom in the size and shape of the feed circuit that couples power to the patch. This can be used to control the input impedance and should permit some increase in operating bandwidth.

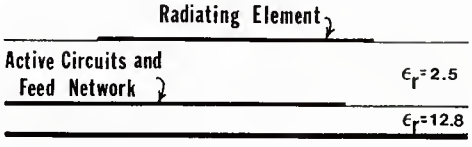

Figure 15. Microstrip radiator electromagnetically coupled to microstrip feed network on GaAs in two-layer configuration.

3.3.2 Two-Sided Microstrip Patch Array

A standard architecture for microwave arrays of microstrip patches utilizes a microstrip feed network below the ground plane of a radiating array. The microwave power is transferred from the feed lines to the radiating elements by a small probe that penetrates the common ground plane (Figure 16). This technique allows different substrates to be used for the radiating elements and the feed network and it works well when the substrates are thin and made of low-permittivity material. However, excess inductance of the probes and difficulties in fabricating the feed-through probes make this technique undesirable for integrated arrays at millimeter wavelengths.

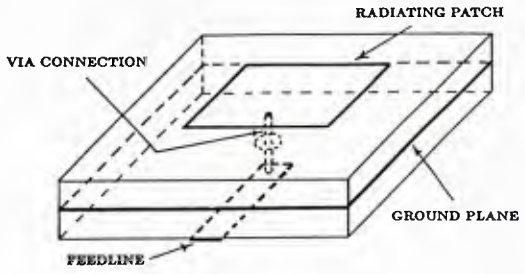

Figure 16. Two-sided element design with via connection between feed line and radiating patch.

3.3.3 Aperture-Coupled Patch Antenna

The aperture-coupled patch antenna resembles a traditional microstrip array element with a microstrip patch antenna on a substrate with relative permittivity ϵ_r^a and a feed network on a substrate with relative permittivity ϵ_r^f. These are separated by a common ground plane. In the traditional configuration, a via connection carries power from the feed network to the radiating patch. In the new design [27], the via connection is replaced by an electrically small aperture (Figure 17) that couples power efficiently to the patch and is easy to manufacture. An open-circuited length of the microstripline extending beyond the aperture provides an additional degree of freedom to be used for impedance matching and bandwidth enhancement. This stub together with the aperture length can be used to control the input impedance over a wide range of values, as illustrated in Figure 18. These results were calculated by using a moment method technique [28] and have been found to be in good agreement with measured results. The bandwidth and radiation patterns of the patch antenna are essentially the same as those of a probe-fed antenna on the same substrate. The peak radiation from the aperture on

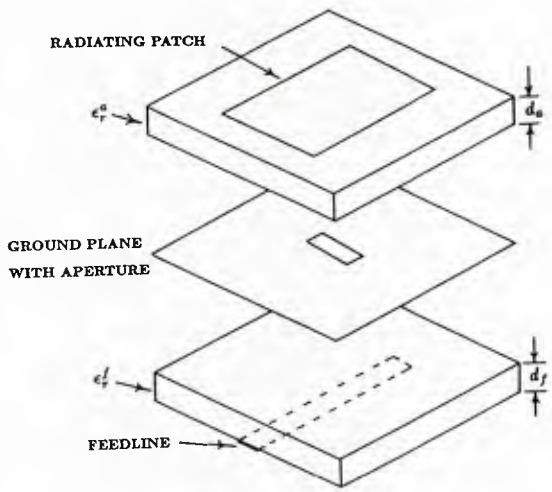

Figure 17. Microstrip radiator electromagnetically coupled to microstrip feed network in two-sided configuration.

the feed side of the ground plane has been computed and measured to be at least 20 dB below the peak of the patch radiation for the antennas that have been tested. An eight-element array with patches on $0.159 - cm$ $\epsilon_r^a = 2.2$ and feedlines on $0.064 - cm$ $\epsilon_r^f = 10.2$ has performed favorably, demonstrating the feasibility of using a substrate like GaAs for the feed network and a lower permittivity substrate for the radiating elements. The use of a low-ϵ_r antenna substrate will increase the angle at which scan blindness occurs due to surface waves on the antenna substrate. However, a blindness also will occur due to surface waves on the feed substrate and methods must be found to control this phenomenon. Spurious radiation from the feed network will not degrade side lobes and polarization because it is confined below the ground plane.

A variation of the aperture-coupled patch is shown in Figure 19 [29]. This configuration permits the feed network to occupy as much space as needed in the depth dimension. This use of depth has been essential in most microwave phased arrays that have been fabricated.

3.3.4 Linearly Tapered Slot Antenna

Endfire printed antennas operating in a traveling wave mode usually operate over wider bandwidths than broadside elements that are resonant radiators. Stripline-fed endfire notches have demonstrated broadband operation [30], but stripline is not a preferred medium for integrated millimeter wave circuits. A flared slotline (Figure 20) provides an alternative with potential for wide bandwidth operation and integration with monolithic circuits [31-33]. Also the depth dimension is easily used for circuit layout. Linearly tapered slot antennas that are $5 - 10\lambda_0$ long have been used in a focal plane array for imaging at 94 GHz. The array samples the image plane more often than other elements, yielding a resolution that is within a factor of 2 of the Rayleigh limit. Similar arrays would be useful for multiple beam applications.

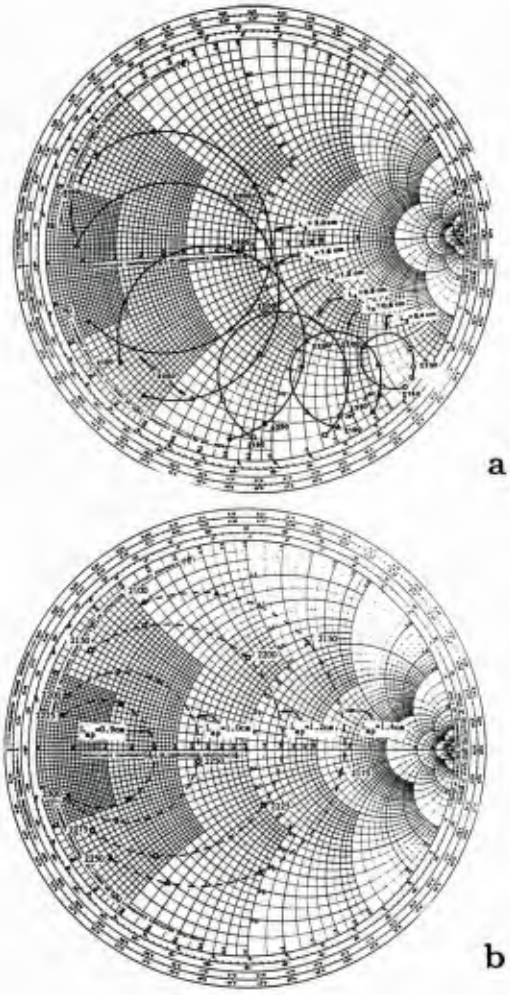

Figure 18. Impedance of aperture coupled patch for (a) various stub lengths, (b) aperture lengths. $\epsilon_r^f = \epsilon_r^b = 2.54$, $d_a = d_f = 0.16cm$, $L_ap = 1.12cm$, $W_{ap} = 0.16cm$, $L_p = 4cm$, $W_p = 3cm$.

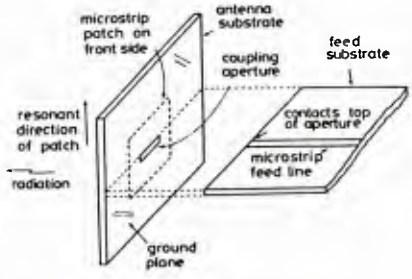

Figure 19. Aperture coupled patch with perpendicular feed network. [after 29]

One drawback of endfire elements is the difficulty of creating circular polarization or dual polarization. Dual polarization requires an eggcrate structure as in Figure 21, which would be extremely difficult to fabricate at millimeter wavelengths on GaAs substrates. A single circular polarization could be achieved by using a polarizer, but this adds loss and may limit scan range. Another possible drawback could result from surface waves on the periodic array of protruding dielectric slabs. Problems of this type have been encountered on other antennas.

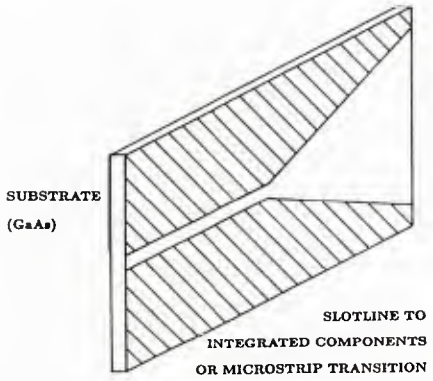

Figure 20. Linearly tapered slot on GaAs for endfire radiation.

3.4 Some Techniques for Obtaining Circular Polarization

It was noted in Section 2.1 that a rectangular microstrip antenna can be resonated in two orthogonal directions. If the antenna is square, the two resonant frequencies will be the same and a feed placed along with the nodal line of one mode (where the voltage is zero as along the centerline in Figure 5b) will couple only to the other mode. By using one feed for the horizontal mode and another for the vertical mode, two independent polarizations can be obtained. This is depicted in Figure 7. Proper combination of the two polarizations yields any desired circular or elliptical polarization. This two-feed technique can also be applied to circular disk antennas.

Because of the symmetry of the horizontal and vertical modes in the two-feed technique, the input impedances obtainable at the two feeds should be identical and circular polarization with a low axial ratio can be obtained over the entire operating band of the antenna. However, this requires the use of external circuitry (such as a 90° hybrid) to provide the equal amplitude, phase-quadrature excitations for the two feeds. Several other techniques exist for obtaining a single circular polarization over a very narrow bandwidth (typically 1/10 the bandwidth of the antenna). These techniques are generally based on feeding a patch at one point and disrupting the symmetry of the patch so that both the horizontal and vertical modes are excited and are resonant at slightly different frequencies. Then, at a frequency midway between the two resonances, one of the modes is below resonance and presents an inductive impedance while the other is above resonance and presents an equal capacitive impedance. By choosing the separation of the resonant frequencies properly, a relative phase shift of 90° between the mode currents is achieved and circular polarization can be obtained by equalizing the powers radiated by the two modes. Since the 90° phase shift results from a conjugate balancing of the resonance impedances of the patch modes, a good axial ratio is achieved only over a very narrow band of frequencies. Nevertheless, the simplicity of the single input makes this technique useful when narrow band circular polarization is required.

Several configurations for obtaining circular polarization are depicted in Figure 22. Figure 22a shows a patch antenna that is slightly longer in one direction than the other and is fed at one corner to excite both modes with equal strength [34]. A coaxial probe feed can be used also and placed anywhere along the diagonal of the patch to achieve the desired input impedance. Moving the feed to the other diagonal produces the opposite sense polarization. Another configuration that is closely related in its operation is shown in Figure 22b [35]. Slightly elliptical patches fed along a line 45° from their major axis (see Figure 22c) also produce circular polarization [36]. The configuration of Kerr [37] in Figure 22d utilizes a diagonal slot in a square metallic patch in order to couple power from the vertical mode that is excited by the feedline to the horizontal mode. A variation of the slot

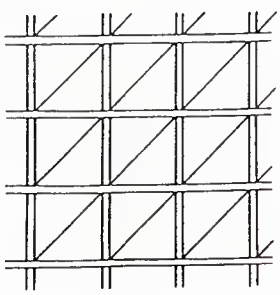

Figure 21. A configuration for obtaining dual polarization with endfire integrated antennas.

method that is actually more closely related to the techniques of Figure 22a and b is shown in Figure 22e. Still other configurations of Kerr are shown in Figures 22f and g. One feature of Kerr's slot method is that the patch can be slightly smaller than an unperturbed patch designed for the same frequency. This can be useful in array applications where a smaller element provides more space between elements. The configurations in Figure 22h-j illustrate another technique for obtaining circular polarization or for changing the resonant frequency of a microstrip antenna [13]. Small posts connect the radiating patch to the ground plane at appropriate points to load the cavity and change its resonant frequency or to couple power from one mode to an orthogonal mode. By using microwave switching diodes in conjunction with the shorting posts, a polarization diverse antenna capable pf vertical linear, right-hand circular, and left-hand circular polarization can be obtained (Figure 22j).

3.5 Some Techniques for Increasing the Operating Bandwidth

A recent study [38] has shown that the bandwidth obtainable from a microstrip antenna is approximately proportional to its volume measured in λ_0^3. This phenomenon is consistent with accepted antenna theory [39]. Therefore, the bandwidth of a simple microstrip antenna can be increased by increasing its length, width, and substrate thickness. However, the length must be approximately one-half wavelength in the dielectric substrate, so the antenna can be lengthened only if the substrate permittivity is lowered. Unfortunately, feed lines and probes radiate more on low-ϵ_r substrates, so this technique must be used with care when cross-polarization and sidelobe levels are important. Increasing the antenna's width is fairly straightforward, but higher modes of the cavity can be excited if the width is increased to one or two wavelengths. Also, elements larger than approximately $\lambda_o/2$ cannot be used in scanning arrays due to undesirable grating lobes.

Increasing substrate thickness increases the antenna's bandwidth, but leads to greater excitation of surface waves and more radiation from feed lines and probes. Nevertheless, this technique can be useful for bandwidth enhancement. This is especially true when it is combined with parasitic elements that lead to a double-tuned impedance locus, which may have twice the bandwidth of its volume-equivalent single patch. An example of this is depicted in Figure 23 [40], where a multiple-layer substrate containing a large foam-filled region to yield a low effective permittivity also contributes to the increased bandwidth. The $VSWR < 2$ bandwidth of the antenna is about 20% and circular polarization can be obtained easily by feeding the lower element with two orthogonal feeds. This kind of structure has the benefit that feed lines and probes do not radiate excessively, but the thick substrate can support undesirable surface waves.

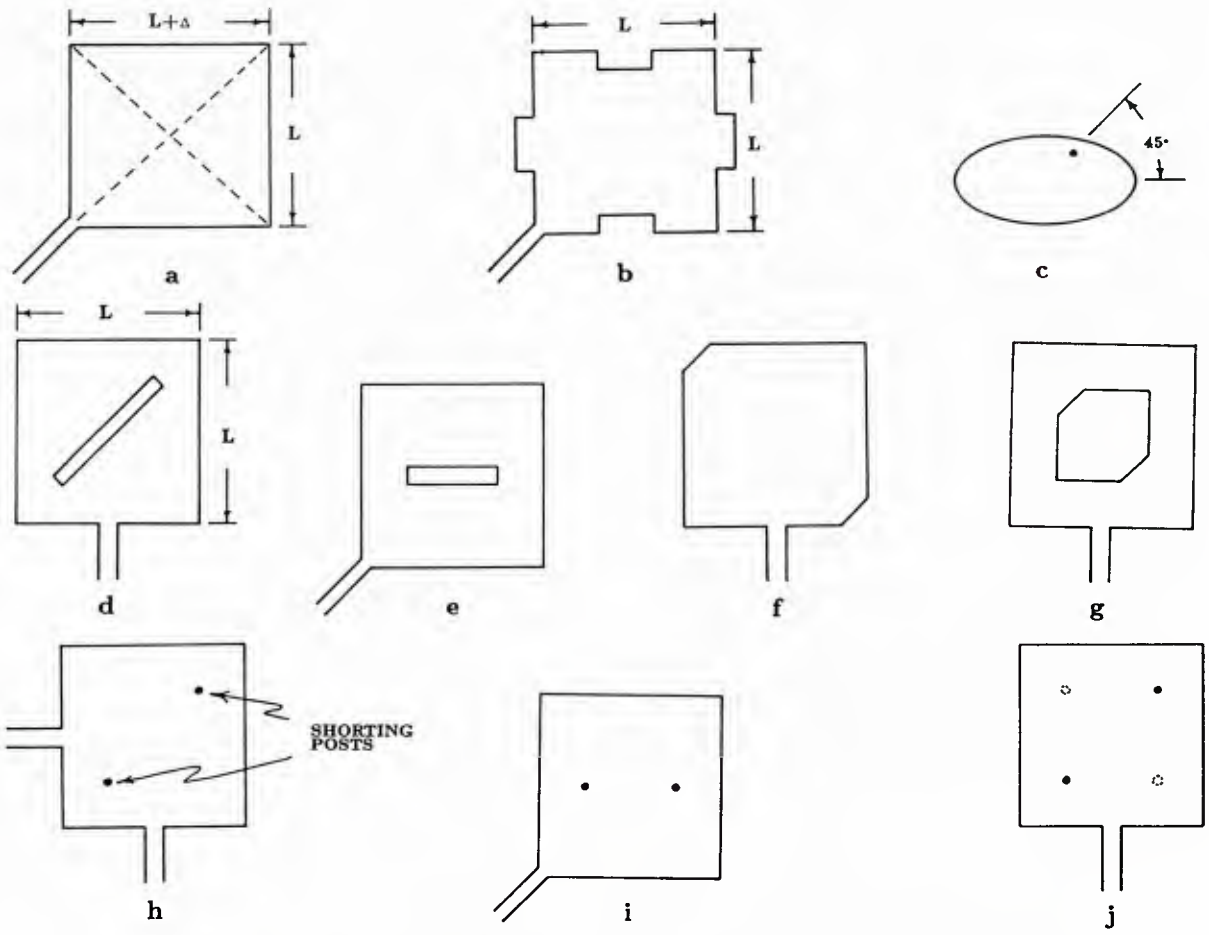

Figure 22. Antenna configurations for obtaining circular polarization with a single input port.

Other examples of bandwidth enhancement by using parasitics on the same substrate as the driven element are shown in Figure 24. Further discussion of these antennas can be found in [41-43], but they generally rely on the multiple tuning effects of coupled resonators. These effects can lead to increased bandwidth or to multiple, narrow-band operating frequencies. One of the drawbacks of these antennas is that they usually increase the dimensions of the antenna beyond $\lambda_o/2$, making them unsuitable for array applications. Also the radiation patterns may change significantly with frequency as different parasitics contribute to the radiation.

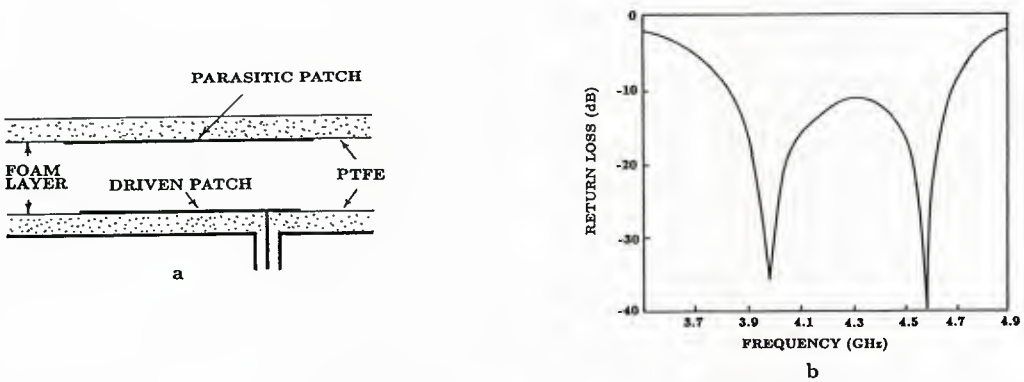

Figure 23. Electromagnetically coupled patches for enhanced bandwidth, (a) Antenna structure, (b) Return loss. [after 40]

4.0 SUMMARY

General properties of microstrip antennas have been presented with particular emphasis on characteristics that are relevant to integrated arrays for avionics. An important area of current and future research interest is computer-aided design, and some existing models that are used to analyze microstrip antennas have been described. Cavity models are numerically efficient and they lend insight into the operating characteristics of the antenna. However, the cavity model is based on assumptions that limit its accuracy and applicability. Moment method models are based on the integral equation for antenna currents and, in principal, they can yield very accurate results for complicated problems. In practice, though, computation times (which can be many minutes per data point) limit the obtainable accuracy and usefulness of results. Usable models that yield accurate estimates of input impedance for various feed types and substrates are needed.

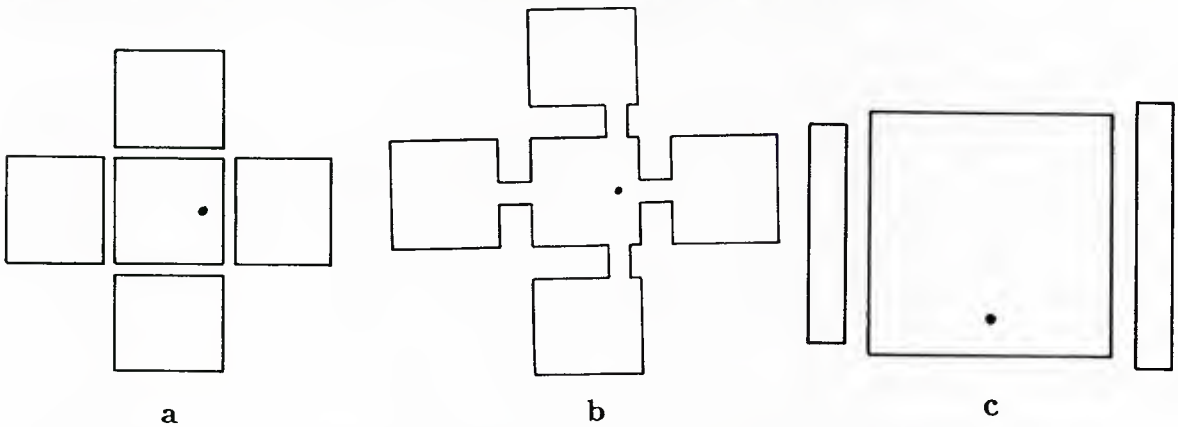

Figure 24. Some radiators with increased bandwidth obtained by using parasitic elements on the same substrate.

Methods to increase bandwidth or provide dual-frequency operation are currently being investigated, as are element and array designs for dual polarization. These investigations are motivated by system applications that require the cost reductions promised by photolithographic production of monolithic circuits and the performance achievable with waveguide or dipole elements. Conformability also may be an important consideration.

REFERENCES

1. H. D. Weinschel and K. R. Carver, "A Medium-Gain Circularly Polarized Microstrip UHF Antenna for Marine DCP Communication to the GOES Satellite System," IEEE AP-S Sym. Dig., 391-394, Amherst, MA, 1976.
2. L. R. Murphy, "SEASAT and SIR-A Microstrip Antennas," Proc. Printed Circuit Ant. Tech. Workshop, New Mexico State University, Las Cruces, 1979
3. K. D. Arkind and R. L. Powers, "Printed Circuit Antenna for Wide Bandwidth Requirements," IEEE AP-S Sym. Dig., 359-362, Los Angeles, CA, 1981.
4. Y. Yoshimura, "A Microstrip Slot Antenna," IEEE Trans. Microwave Theory Tech., Vol. MTT-20, 760-762, Nov. 1972.
5. R. J. Mailloux, "Phased Array Architecture for mm-Wave Active Arrays," Microwave Journal., Vol. 29, No. 7, 117-124, July 1986.
6. R. E. Munson, "Conformal Microstrip Antennas and Microstrip Phased Arrays," IEEE Trans. Antennas and Propagation, Vol. AP-22, 74-78, Jan. 1974.
7. I. J. Bahl and P. Bhartia, *Microstrip Antennas*, Artech House, Dedham, MA, 1980.
8. J. R. James, P. S. Hall and C. Wood, *Microstrip Antenna: Theory and Design*, Peter Peregrinus, Stevenage, UK, 1981.
9. Y. T. Lo, D. Solomon and W. F. Richards, "Theory and Experiments on Microstrip Antennas," IEEE Trans. Antennas and Propagation, Vol. AP-27, 137-145, March 1979.
10. W. F. Richards, Y. T. Lo, and D. D. Harrison, "An Improved Theory for Microstrip Antennas and Applications," IEEE Trans. Antennas and Propagation, Vol. AP-29, 38-46, Jan. 1981.
11. K. R. Carver, "Practical Analytical Techniques for the Microstrip Antenna," Proc. Printed Circuit Ant. Tech. Workshop, New Mexico State University, Las Cruces, 1979.
12. K. R. Carver and J. W. Mink, "Microstrip Antenna Technology," IEEE Trans. Ant. Propagat., Vol. AP-29, 2-24, Jan. 1981.
13. D. H. Schaubert, F. G. Farrar, A. R. Sindoris and S. T. Hayes, "Microstrip Antennas with Frequency Agility and Polarization Diversity," IEEE Trans. Ant. Propagat., Vol. AP-29, 118-123, Jan. 1981.
14. W. F. Richards and Y. T. Lo, "A Simple Theory for Reactively Loaded Microstrip Antennas," IEEE AP-S Sym. Dig., 259-262, Boston, MA, 1984.
15. W. F. Richards and S. A. Long, "An Experimental Investigation of Loaded Microstrip Antennas," IEEE AP-S Sym. Dig., 263-266, Boston, MA, 1984.
16. N. K. Uzunoglu, N. G. Alexopoulos and J. G. Fikioris, "Radiation Properties of Microstrip Dipoles," IEEE Trans. Ant. Propagat., Vol. AP-27, 853-858, Nov. 1979.
17. M. D. Deshphande and M. C. Bailey, "Input Impedance of Microstrip Antennas," IEEE Trans. Ant. Propagat., Vol. AP-30, 645-650, July 1982.
18. M. C. Bailey and M. D. Deshpande, "Integral Equation Formulation of Microstrip Antennas," IEEE Trans. Ant. Propagat., Vol. AP-30, 651-656, July 1982.
19. D. M. Pozar, "Input Impedance and Mutual Coupling of Rectangular Microstrip Antennas," IEEE Trans. Ant. Propagat., Vol. AP-30, 1191-1196, Nov. 1982.
20. J. R. Mosig and F. E. Gardiol, "General Integral Equation Formulation for Microstrip Antennas and Scatterers," IEE Proc. (London), Vol. 132, Part H, No. 7, 424-432, Dec. 1985.
21. D. M. Pozar, "Analysis of Finite Phased Arrays of Printed Dipoles," IEEE Trans. Ant. Propagat., Vol. AP-33, 1045-1053, Oct. 1985.
22. D. M. Pozar and D. H. Schaubert, "Scan Blindness in Infinite Phased Arrays of Printed Dipoles," IEEE Trans. Ant. and Propagat., Vol. AP-32, 602-610, June 1984.

23. D. M. Pozar and D. H. Schaubert, "Analysis of an Infinite Array of Rectangular Microstrip Patches with Idealized Feed Probes," IEEE Trans. Ant. Propagat., Vol. AP-32, 1101-1107, Oct. 1984.
24. D. M. Pozar and D. H. Schaubert, "Comparison of Architectures for Monolithic Phased Arrays," Microwave Journal, Vol. 29, 93-204, Mar. 1986.
25. D. M. Pozar, "Considerations for Millimeter Wave Printed Antennas," IEEE Trans. Ant. and Propagat., Vol. AP-31, 740-747, Sept. 1983.
26. H. G. Oltman and D. Z. Huebner, "Electromagnetically Coupled Microstrip Dipoles," IEEE Trans. Ant. and Propagat., Vol. AP-29, 151-157, Jan. 1981.
27. D. M. Pozar, "A Microstrip Antenna Aperture Coupled to a Microstripline," Electronics Letters, Vol. 21, 49-50, Jan. 17, 1985.
28. P. L. Sullivan and D. H. Schaubert, "Analysis of an Aperture Coupled Microstrip Antenna," IEEE Trans. Ant. and Propagat., Vol. AP-34, 977-984 Aug. 1986.
29. A. C. Buck and D. M. Pozar, "Aperture-Coupled Microstrip Antenna with Perpendicular Feed," Electronics Letters, Vol. 22, 125-126, Jan. 30, 1986.
30. L. R. Lewis, M. Fassett and J. Hunt, "A Broadband Stripline Array Element," IEEE AP-S Symp. Dig., Atlanta, GA, 335-337, June 1974.
31. P. J. Gibson, "The Vivaldi Aerial," 9th Eur. Microw. Conf., Brighton, UK, 101-105, 1979.
32. S. N. Prasad and S. Mahapatra, "A New MIC Slotline Aerial," IEEE Trans. Ant. and Propagat., Vol. AP-31, 525-527, May 1983.
33. E. L. Kollberg, J. Johansson, T. Thungren, T. L. Korziewnowski and K. S. Yngvesson, "New Results on Tapered Slot Endfire Antennas on Dielectric Substrates," 8th IEEE Intl. Conf. on Infrared and MM Waves, 1983.
34. G. G. Sanford and R. E. Munson, "Conformal VHF Antenna for the Apollo-Soyuz Test Project," IEE Int'l Conf. on Ant. for Aircraft and Spacecraft, 130-135, London, 1975.
35. L. T. Oswald and C. W. Garvin, "Microstrip Command and Telemetry Antennas," IEE Int'l Conf. on Ant. for Aircraft and Spacecraft, 217-222, London, 1975.
36. S. A. Long, L. C. Shen, D. H. Schaubert and F. G. Farrar, "An Experimental Study of the Circularly-Polarized Elliptical Printed-Circuit Antenna." IEEE Trans. Ant. Propagat., Vol. AP-29, 95-99, Jan. 1981.
37. J. L. Kerr, "Microstrip Polarization Techniques," Proc. 1978 Ant. Appl. Symp., Robert Allerton Park, Univ. of Illinois, Urbana, 1978.
38. A. Henderson, J. R. James and C. M. Hall, "Bandwidth Extension Techniques in Printed Conformal Antennas," Proc. Military Microwaves '86, 329-334, Brighton, England, 1986.
39. R. F. Harrington, *Time-Harmonic Electromagnetic Fields*, pp. 307-311, McGraw-Hill, New York, 1961.
40. C. H. Chen, A. Tulintseff and R. M. Sorbello, "Broadband Two-Layer Microstrip Antenna," IEEE AP-S Symp. Dig., 251-254, Boston, MA, 1984.
41. D. H. Schaubert and F. G. Farrar, "Some Conformal Printed Circuit Antenna Designs," Proc. Printed Circuit Ant. Tech. Workshop, New Mexico State Univ., Las Cruces, 1979.
42. G. Kumar and K. C. Gupta, "Nonradiating Edges and Four Edges Gap-Coupled Multiple Resonator Broad-Band Microstrip Antennas," IEEE Trans. Ant. Propagat., Vol. Ap-33, 173-178, Feb. 1985.
43. G. Kumar and K. C. Gupta, "Directly Coupled Multiple Resonator Wide- Band Microstrip Antennas," IEEE Trans. Ant. Propagat., Vol. AP-33, 588-593, June 1985.

SELECTIVE BIBLIOGRAPHY

This bibliography with Abstracts has been prepared to support AGARD Lecture Series No. 151 by the Scientific and Technical Information Branch of the US National Aeronautics and Space Administration, Washington, D.C., in consultation with the Lecture Series Director, Dr. Robert J. Mailloux, Rome Air Development Center, Hanscom AFB, Massachusetts.

UTTL: Satellite-borne active phased array techniques for mobile communications
AUTH: A/SHEEHAN, P. G.; B/FORREST, J. R. PAA: A/(Investors in Industry, PLC, London, England); B/(Marconi Defence Systems, Ltd., Stanmore, England)
IEE Proceedings, Part F - Communications, Radar and Signal Processing (ISSN 0143-7070), vol. 133, pt. F, no. 4, July 1986, p. 339-344. Research sponsored by the Department of Trade and Industry.
ABS: This paper investigates the design of active phased arrays for communications satellites. In particular, consideration is given to the problems occurring when active arrays are required to produce multiple beams. There is a real need to keep the complexity of the array electronics to a minimum, but this conflicts with the desire to obtain the greatest possible freedom of control of the radiation pattern produced. The paper demonstrates a method of coping with the problem. Low-gain elements are used to provide design freedom and they are grouped into subarrays to limit the complexity of the rest of the system. With appropriate configurations of subarrays, greatly improved radiation pattern characteristics can be obtained and frequency reuse between multiple beams becomes feasible. A demonstration model of 108 microstrip patches grouped into 32 subarrays, operating at 12 GHz, has been constructed and verifies that the technique is effective. 86/07/00 87A10128

UTTL: Multibeam SS-TDMA design considerations related to the Olympus specialised services payload
AUTH: A/WATT, N. PAA: A/(Marconi Space Systems, Ltd., Portsmouth, England) IEE Proceedings, Part F - Communications, Radar and Signal Processing (ISSN 0143-7070), vol. 133, pt. F, no. 4, July 1986, p. 319-325. ESA-supported research.
ABS: The paper discusses some of the particular design problems associated with a multibeam satellite-switched time-domain multiple-access (SS-TDMA) satellite payload. Contiguous beam coverage and frequency reuse between beams are shown to place some important constraints on the antenna performance. The local oscillator, switch matrix and input/output chain designs are dependent on the interbeam switching requirements. These design considerations are referenced to the Olympus Specialised Services Payload, for which a description, performance summary and link budget are presented. 86/07/00 87A10126

UTTL: A distributed array antenna system
AUTH: A/SHAW, R.; B/KOVITZ, J. PAA: B/(Lockheed Engineering and Management Services Co., Inc., Houston, TX) CORP: Lockheed Engineering and Management Services Co., Inc., Houston, Tex. IEEE Microwave Theory and Techniques Symposium, Baltimore, MD, June 2-5, 1986, Paper. 4 p.
ABS: The Space Station communication system will use microwave frequency radio links to carry digitized information from sender to receiver. The ability of the antenna system to meet stringent requirements on coverage zones, multiple users, and reliability will play an important part in the overall multiple access communication system. This paper will describe the configuration of a multibeam conformal phased array antenna and the individual microwave integrated components incoporated into this antenna system. 86/06/00 86A50286

UTTL: Aspects of lightning protection schemes for radomes
AUTH: A/BISHOP, J.; B/AKED, A.; C/POWELL, C. W.; D/RYAN, H. M. PAA: A/(Royal Aircraft Establishment, Flight Systems Dept., Farnborough, England); B/(Strathclyde, University, Glasgow, Scotland); D/(NEI Reyrolle, Ltd., Hebburn, England) IN: International Aerospace and Ground Conference on Lightning and Static Electricity, 10th, and Congres Inernational Aeronautique, 17th, Paris, France, June 10-13, 1985, Proceedings (A86-47292 23-33). Les Ulis, France, Les Editions de Physique, 1985, p. 499-507. Sponsorship: Ministry of Defence.
ABS: The feasibility of assessing aircraft radome lightning protection on the basis of lightning striking distance is demonstrated. A radome is simulated by an 8-m (in length) hemicylindrical mock radome while approaching lightning is represented by a 3-m spark; the conductors in and on the radome are earthed. A simple mathematical model describing the protection is derived and experimental results are given. It is concluded that within the bounds of unpredictability of high voltage discharges, the proposed model can explain the performance of a cylindrical case of protective conductors in terms of their pitch and distance from the internal metalwork being protected. 85/00/00 86A47338

UTTL: Corona threshold determination by three-stage physical modelling of aircraft
AUTH: A/NANEVICZ, J. E.; B/VANCE, E. F. PAA: B/(SRI International, Menlo Park, CA) IN: International Aerospace and Ground Conference on Lightning and Static Electricity, 10th, and Congres International Aeronautique, 17th, Paris, France, June 10-13, 1985, Proceedings (A86-47292 23-33). Les Ulis, France, Les Editions de Physique, 1985, p. 441-449.
ABS: Low-cost laboratory techniques for measuring the corona threshold of an aircraft protuberance are presented. A scale model of the aircraft is used together with a sample of the protuberance in question, and following one measurement on the aircraft model and two on the sample, it is possible to determine the corona threshold of the protuberance as installed on the aircraft. The present technique can aid in the exploration of alternate sites on the aircraft so as to minimize the likelihood of corona discharge. Moreover, it can suggest possible modifications to the protuberance (such as the rounding of edges) which would increase the corona threshold potential. 85/00/00 86A47333

UTTL: Survey of millimeter wave antennas
AUTH: A/SCHWERING, F. PAA: A/(U.S. Army, Communication Electronics Command, Fort Monmouth, NJ) IN: Millimeter wave technology III; Proceedings of the Meeting, Arlington, VA, April 9, 10, 1985 (A86-46659 22-33). Bellingham, WA, Society of Photo-Optical Instrumentation Engineers, 1985, p. 34-40.
ABS: A wide variety of antennas has been designed or is currently under study for the millimeter wave region. An overview over these antennas is presented. Two classes of antennas are distinguished, i.e., antennas of conventional configuration and antennas based on new design approaches. The former class consists of radiating structures, such as reflector, lens and horn antennas, whose characteristics are well established. The latter class is comprised of antennas with significant features that are peculiar to the mm-wave band and includes radiating structures such as microstrip mm-wave antennas, dielectric antennas and integrated antennas. 85/00/00 86A46664

UTTL: Arrays of microstrip spiral antennas
AUTH: A/GOSTIUKHIN, V. L.; B/GRINEVA, K. I.; C/SMIRNOV, A. B.; D/TRUSOV, V. N. Antenny (ISSN 0320-9601), no. 32, 1985, p. 94-107. In Russian.
ABS: A phased array of planar rectangular spirals with resonators is analyzed on the basis of a numerical solution of an integrodifferential equation for the magnetic current in the aperture of the spiral slot. Calculation results are presented for the amplitude and phase distributions of the field along the spiral, the input impedances, the ellipticity coefficients of the radiation field for different beam deflection angles, and radiation patterns of a single antenna in the array. Consideration is given to the mathematical modeling of a finite array of spiral antennas with allowance for the edge effects. 85/00/00 86A44731

UTTL: H-guide slot antenna shrinks sidelobes
AUTH: A/KISLIUK, M.; B/AXELROD, A. PAA: B/(Tel Aviv University, Israel) Microwaves & RF (ISSN 0745-2993), vol. 25, June 1986, p. 107, 108, 110.
ABS: For antennas with low sidelobes, a radiator is proposed that uses a slot symmetrically cut or etched in the upper plate of an H-guide (a dielectric-loaded parallel plane waveguide) that supports the dominant mode and has a zero cutoff frequency. The H-guide radiator is linearly polarized, conformal, easy to integrate, and very efficient (more than 80 percent). Its bandwidth is about 20 percent. Unlike current microstrip antennas, the H-guide slot antenna does not emit parasitic radiation from lines feeding the radiating elements. The measured radiation pattern of the H-guide antenna conforms well with the calculated pattern of a linear magnetic current for a wide frequency range (8.0 to 12.4 GHz). Means to boost efficiency and achieve better 'equal ripple' response are considered. A radiator with a guide height of 9 mm is shown to be 80 percent efficient in an 18 percent bandwidth, with 26 percent bandwidth achievable theoretically by decreasing guide height to 4.5 mm. 86/06/00 86A44302

UTTL: 'Invisible' antenna takes up less space
AUTH: A/SHELLEY, M.; B/BOND, K. PAA: B/(Cossor Electronics, Ltd., Harlow, England) Microwaves & RF (ISSN 0745-2993), vol. 25, June 1986, p. 93-95.
ABS: A compensated microstrip patch design is described that also uses grounded coplanar waveguide to permit a second, independent antenna to be mounted on any type of existing primary radar antenna aboard an aircraft without affecting its radiation. Successful integration of the IFF (identification friend or foe) antenna, which works at D-band, and the primary radar antenna is possible because of the diversity in frequency between the two antennas. Construction of a microstrip radiating element, electromagnetically invisible to the primary antenna, requires orthogonal grating elements and use of the primary antenna as the ground plane. Coplanar mounting of a stripline array

with the primary antenna reduces the manufacturing costs and increases the functional performance of the IFF antenna. 86/06/00 86A44300

UTTL: Thermal analysis technique applied to a conformal phased array antenna
AUTH: A/CAMPION, K.; B/GALLAGHER, J. J.; C/PARADIS, L. R.; D/SHUKIS, F. A. PAA: D/(Raytheon Co., Bedford, MA) (AIAA, Thermophysics Conference, 19th, Snowmass, CO, June 25-28, 1984, AIAA Paper 84-1762) Journal of Spacecraft and Rockets (ISSN 0022-4650), vol. 23, May-June 1986, p. 231-236. Research supported by the Sandia National Laboratories. Previously cited in issue 17, p. 2437, Accession no. A84-37489. 86/06/00 86A41731

UTTL: The effects of rain on a Radome's performance
AUTH: A/EFFENBERGER, J. A.; B/STRICKLAND, R. R.; C/JOY, E. B. PAA: B/(Chemical Fabrics Corp., Merrimack, NH); C/(Georgia Institute of Technology, Atlanta) Microwave Journal (ISSN 0026-2897), vol. 29, May 1986, p. 261, 262, 264 (5 ff.). 86/05/00 86A40044

UTTL: MLS - The pilot's point of view
AUTH: A/RENOUARD PAA: A/(Union de Transports Aeriens, Puteaux, France) (Seminaire sur le Systeme d'Atterrissage Hyperfrequences 'MLS' Toulouse, France, Nov. 26, 27, 1985) Navigation (Paris) (ISSN 0028-1530), vol. 34, April 1986, p. 145-166. In French.
ABS: The benefits and difficulties associated with implementing the Microwave Landing System (MLS) as standard equipment for airline passenger aircraft are considered. MLS offers an elimination of local signal distortions, three-dimensional guidance devoid of local reflectances, and usefulness even when the runway disappears beyond local terrain relief. The precision exceeds that available from current systems during categories I and II landings. Finally, calibration is easier and cheaper. The switchover to MLS from ILS is to be performed over a 12 yr period, implying that the aircraft must carry two different landing guidance systems and pilots must be qualified to operate both of them. The long period of transition would cause a higher fuel consumption rate. It is noted that current display systems do not provide the information in a clear manner, and could be improved by including the MLS in digital display CRT systems, particularly in concert with meteorological displays. Similarly, the MLS and ILS systems could be interoperative and use the same display. Tests are still needed to determine the operability of MLS during category III approaches. Finally, the various on board equipment and procedures associated with implementation of the MLS are discussed. 86/04/00 86A39557

UTTL: A technique to evaluate the accessibility of airborne receivers to interfering signals
AUTH: A/KOESTER, D. P.; B/COOK, C. E.; C/STEVENS, R. R. PAA: C/(Mitre Corp., Bedford, MA) IN: ICC '85; International Conference on Communications, Chicago, IL, June 23-26, 1985, Conference Record. Volume 2 (A86-37526 17-32). New York, Institute of Electrical and Electronics Engineers, Inc., 1985, p. 814-821.
ABS: Techniques to evaluate the accessibility of modern military airborne receivers to tactical jammers are described. Signal detection capabilities of the equipment are analyzed in relation to system performance. Problems encountered in examining adaptive antenna arrays are discussed. The procedures for calculating operability volumes are studied. The effects of radio horizon and terrain on line-of-sight communications are investigated. The contours of maximum communications range are estimated and utilized to evaluate the communications performance for a system configuration and an interference environment. 85/00/00 86A37555

UTTL: A diffraction technique for the prediction of effects of space frame radome structures on the performance of reflector antennas
AUTH: A/HOLDEN, G. J.; B/ANDERSON, A. P.; C/CHAMBERS, B. PAA: C/(Sheffield, University, England) IN: International Conference on Antennas and Propagation (ICAP 85), 4th, Coventry, England, April 16-19, 1985, Proceedings (A86-31851 14-32). London and New York, Institution of Electrical Engineers, 1985, p. 158-161.
ABS: The spectral domain plane-to-plane diffraction technique which is utilized to study the effects of radome structures on reflector antennas is described. A simulation predicting the scattered field due to a half wavelength blockage is examined. The application of the plane-to-plane technique to scattering/blockage problems is analyzed. The radiation patterns for the antenna/radome combination are evaluated. The patterns predicted by the diffraction technique and the shadow blockage technique are compared. The data reveal that the two patterns are equivalent at the boresight; however, at angles greater than or equal to 5 deg there is no correlation. 85/00/00 86A31884

UTTL: International Conference on Antennas and Propagation (ICAP 85), 4th, University of Warwick, Coventry, England, April 16-19, 1985, Proceedings Conference organized by IEE, URSI, IEEE, et al. London and New York, Institution of Electrical Engineers, 1985, 603 p. For individual items see A86-31852 to A86-31953.

ABS: The present conference considers such fields as the use of radars for atmospheric attenuation and interference studies, array antennas, slant path propagation, printed antenna designs, travelling wave antennas, millimeter and quasi-optical antennas, antenna structures, VHF antennas, millimeter-wave propagation, and measurement techniques for far field patterns, metrology, phased arrays, and dipole antennas. Also considered are topics concerning tropospheric line-of-sight effects, adaptive arrays, reflector antennas, tropospheric ducting, mobile radio systems, scattering and diffraction phenomena, prediction techniques for mobile and broadcast services, antenna feeds, HF radar propagation studies, satellite antennas, ionospheric propagation, and satellite and radio astronomy antennas. 85/00/00 86A31851

UTTL: Antennas of satellite communication earth stations

AUTH: A/POKRAS, A. M.; B/SOMOV, A. M.; C/TSURIKOV, G. G. Moscow, Izdatel'stvo Radio i Sviaz', 1985, 288 p. In Russian.

ABS: Methods of the analysis and design of axisymmetric and nonaxisymmetric antennas of satellite communication earth stations are examined. In particular, attention is given to antennas with mirror diameters of 25, 12, 7, 4, and 2.5 m operating in the ranges 4/6 or 11/14 GHz; antennas equipped with a beam mode guide are described in detail. The discussion also covers implementations of antennas of the open Cassegrain type, methods of improving the radiation patterns of antennas, antenna exciters, and the noise temperature of receiving microwave antennas. 85/00/00 86A31271

UTTL: Aperture-coupled microstrip antenna with a perpendicular feed

AUTH: A/BUCK, A. C.; B/POZAR, D. M. PAA: B/(Massachusetts, University, Amherst) Electronics Letters (ISSN 0013-5194), vol. 22, Jan. 30, 1986, p. 125, 126.

ABS: A new technique is described for feeding printed antennas. A microstrip antena on one substrate is coupled through an electrically small aperture to a microstrip feed line on a perpendicularly oriented substrate. No direct connection is made to the patch. Such a geometry allows two separate substrates to be used for the antenna and feed functions. Measurements of a prototype design are presented. 86/01/30 86A31182

UTTL: Scanning-sector expansion in double-frequency aligned waveguide phased antenna arrays

AUTH: A/PONOMAREV, L. I.; B/STEPANENKO, V. I.; C/KULKOV, M. IU. Radioelektronika (ISSN 0021-3470), vol. 29, Feb. 1986, p. 36-41. In Russian.

ABS: An analysis is made of the characteristics of double-frequency waveguide phased arrays with optimal aligned dielectric and beyond-cutoff inserts. It is shown that the scanning sector can be expanded and the gain of the array can be increased during operation in the HF subband through alignment of the radiators as well as through 'truncation' of the apertures of passive LF elements using band-stop filters. 86/02/00 86A30954

UTTL: Antenna-feed systems for space communications in the ULF-ELF bands (Review)

AUTH: A/ARKHIPOV, N. S.; B/BONDAR, L. V.; C/VITOVTSEV, A. G.; D/LOMAN, V. I. Radioelektronika (ISSN 0021-3470), vol. 29, Feb. 1986, p. 4-15. In Russian.

ABS: The published literature on microwave antenna-feed systems intended for use in satellite communication systems is reviewed. Particular attention is given to the design and operation of antenna-feed systems for stationary, transportable, airborne, and shipboard stations. 86/02/00 86A30951

UTTL: System performance in rain in a radome-enclosed environment

AUTH: A/CHANG, K.-C. PAA: A/(Electronic Space Systems Corp., Concord, MA) International Journal of Infrared and Millimeter Waves (ISSN 0195-9271), vol. 7, Feb. 1986, p. 267-289.

ABS: Computer modeling and analysis techniques have been established to evaluate performance during rain, in a radome-enclosed system. Electromagnetic transmission line theory using ray-tracing techniques is presented to compute transmission loss. Comparisons between theory and measured results are documented. Variations in water film thickness versus look angle and the resulting effect on performance are discussed. Other performance effects in rain, such as depolarization and noise temperature, are included in the analysis. The differences in performance using hydrophobic and

non-hydrophobic materials can easily be predited. Hydrophobic membrane materials are available for use with a radome, which yield excellent electromagnetic performance, even at mm wave frequencies. Recent tests are discussed which substantiate enhanced radome performance during rain. 86/02/00 86A30716

UTTL: Trends in phased array development
AUTH: A/SCHELL, A. C. PAA: A/(USAF, Rome Air Development Center, Bedford, MA) Microwave Journal (ISSN 0026-2897), vol. 29, March 1986, p. 26, 28, 30, 32.
ABS: In the past 15 years, several outstanding phased arrays have been taken into service for functions involving defense applications. It is pointed out, however, that the impact of phased array technology on radar and communications antennas has been minor in comparison to the impact of solid-state technology on the other major subsystem, the signal processor. This situation is mainly related to cost considerations, and the scale of the commercial market involved. Attention is given to details regarding the economics of phased arrays, a possible key to improved solutions to phased array construction and operation, the employment of the techniques of photolithography in the fabrication of a transversely-developed array, the need for manufacturing techniques to incorporate magnetic or electroacoustic control devices into the array, problems of heat generation, small mm-wave arrays, questions of reliability, and integrated antennas. 86/03/00 86A29776

UTTL: Technology achievements and projections for communication satellites of the future
AUTH: A/BAGWELL, J. W. PAA: A/(NASA, Lewis Research Center, Cleveland, OH) CORP: National Aeronautics and Space Administration. Lewis Research Center, Cleveland, Ohio. IN: Communication Satellite Systems Conference, 11th, San Diego, CA, March 17-10, 1986, Technical Papers (A86-29576 12-32). New York, American Institute of Aeronautics and Astronautics, 1986, p. 289-297. Previously announced in STAR as N86-17595.
ABS: Multibeam systems of the future using monolithic microwave integrated circuits to provide phase control and power gain are contrasted with discrete microwave power amplifiers from 10 to 75 W and their associated waveguide feeds, phase shifters and power splitters. Challenging new enabling technology areas include advanced electrooptical control and signal feeds. Large scale MMIC's will be used incorporating on chip control interfaces, latching, and phase and amplitude control with power levels of a few watts each. Beam forming algorithms for 80 to 90 deg wide angle scanning and precise beam forming under wide ranging environments will be required. Satellite systems using these dynamically reconfigured multibeam antenna systems will demand greater degrees of beam interconnectivity. Multiband and multiservice users will be interconnected through the same space platform. Monolithic switching arrays operating over a wide range of RF and IF frequencies are contrasted with current IF switch technology implemented discretely. Size, weight, and performance improvements by an order of magnitude are projected.
RPT#: AIAA PAPER 86-0649 86/00/00 86A29611

UTTL: The input impedance and antenna characteristics of a cavity-backed plasma covered ground plane antenna
AUTH: A/JAREM, J. M. PAA: A/(Texas, University, El Paso) IEEE Transactions on Antennas and Propagation (ISSN 0018-926X), vol. AP-34, Feb. 1986, p. 262-267. Research supported by the Sandia National Laboratories.
ABS: A description of two methods which are based on a cavity Green's function technique and a waveguide Green's technique which can be used to calculate the input impedance, electromagnetic fields, antenna probe currents, and antenna characteristics of a cavity-backed plasma covered ground plane antenna is presented. A description of the formulation of the theory behind the methods is given. Comparison of theory and experiment are made. 86/02/00 86A29046

UTTL: AN/ASC-30 upgraded SATCOM moderate gain antenna/radome subsystem
AUTH: A/JOYNER, T. E. PAA: A/(USAF, Avionics Laboratory Wright-Patterson AFB, OH) IN: NAECON 1985; Proceedings of the National Aerospace and Electronics Conference, Dayton, OH, May 20-24, 1985. Volume 2 (A86-28326 12-04). New York, Institute of Electrical and Electronics Engineers, 1985, p. 1192-1197.
ABS: An advanced EHF/SHF antenna/radome subsystem developed for the AFWAL Avionics Laboratory (WPAFB) is described. This AN/ASC-30 antenna/radome subsystem is part of a total EHF/SHF satellite communications terminal which is to be used to conduct flight-test experiments with a new DoD satellite system. The schedule called for installation on a test aircraft during the summer of 1985. The effort described is a redesigned subsystem intended to achieve frequency compatibility with the new satellite system. 85/00/00 86A28472

UTTL: Mechanical design and evaluation of a slotted CFRP waveguide antenna
AUTH: A/KNUTSSON, L.; B/BRUNZELL, S.; C/MAGNUSSON, H.
PAA: C/(Ericsson Radio Systems, AB, Moelndal, Sweden)
IN: ICCM - V; Proceedings of the Fifth International Conference on Composite Materials, San Diego, CA, July 29-August 1, 1985 (A86-27676 11-24). Warrendale, PA, Metallurgical Society, Inc., 1985, p. 475-481.
ABS: A development program for a slotted waveguide array antenna made of metallized CFRP was carried out. The main objective was to minimize the weight of the structure without degrading the electrical and mechanical performance. This paper focuses on mechanical design aspects and manufacturing methods of metallized CFRP waveguides and assembly of an antenna array. A weight saving of approximately 40 percent was accomplished by the CFRP structure compared to a corresponding aluminum structure. Electrical properties and cost were essentially equal for the two concepts. 85/00/00 86A27703

UTTL: Aircraft coupling model evaluations at SHF/EHF
AUTH: A/GENELLO, G.; B/PESTA, A. PAA: B/(USAF, Rome Air Development Center, Griffiss AFB, NY) IN: International Symposium on Electromagnetic Compatibility, Wakefield, MA, August 20-22, 1985, Record (A86-27126 11-33). New York, Institute of Electrical and Electronics Engineers, 1985, p. 72-74.
ABS: Severe overcrowding of the RF spectrum, especially at UHF, has been one primary motivator to extend military communications into the SHF and finally the EHF band. The potential interference of placing new SHF/EHF terminals on-board existing and new aircraft platforms is unknown and must be assessed. Several EMC-related computer analysis programs are available to predict the coupling between aircraft antennas. However, the models contained in these codes may not be adequate for prediction analysis at these higher frequencies. Coupling measurements have been performed on a KC-135 style aircraft and a F-16 tactical fighter to evaluate the validity of the computer models. A comparison analysis of predicted and actual coupling data is presented. 85/00/00 86A27128

UTTL: Microwave Landing System (MLS)
AUTH: A/STRONG, J. J. PAA: A/(Hazeltine Corp., Commack, NY) IN: Institute of Navigation, National Technical Meeting, San Diego, CA, January 15-17, 1985, Proceedings (A86-26426 11-04). Washington, DC, Institute of Navigation, 1985, p. 209-218.
ABS: The Microwave Landing System (MLS) which uses microwave frequencies in the 5000 MHz range and 200 operating channels to provide azimuth and elevation guidance, and continuous range information to aircraft is examined. A scanning beam concept in which the time differences between two scans of the azimuth and elevation antennas are measured to obtain angular guidance data is employed in the MLS. The azimuth, elevation and back azimuth stations, and data links of the MLS are described. The precision distance measuring equipment transponder produces range data and operates in initial and final approach modes. The implementation of the MLS worldwide for military and civilian applications, and the FAA's national implementation program for the MLS are discussed. 85/00/00 86A26444

UTTL: Antenna siting on helicopters
AUTH: A/AUDONE, B.; B/MESCHI, G. PAA: A/(Aeritalia S.p.A., Caselle Torinese, Italy); B/(Costruzioni Aeronautiche Giovannia Agusta S.p.A., Cascina Costa, Italy) Netherlands Association of Aeronautical Engineers and Technische Hogeschool te Delft, European Rotorcraft Forum, 10th, The Hague, Netherlands, Aug. 28-31, 1984, Paper. 17 p.
ABS: The antenna siting activity on helicopters is described with special attention paid to electromagnetic problems. The importance of the prediction of antenna performances at the early stage of the project is stressed pointing out the importance of computer aids. Test facilities are also described for performing antenna pattern measurements, which represent the most difficult task of the overall activity. 84/08/00 86A26133

UTTL: Processable polyimide matrix resin
AUTH: A/COBUZZI, C. A.; B/CHAUDHARI, M. A. PAA: B/(Ciba-Geigy Corp., Ardsley, NY) IN: National SAMPE Technical Conference, 17th, Kiamesha Lake, NY, October 22-24, 1985, Proceedings (A86-21701 08-23). Covina, CA, Society for the Advancement of Material and Process Engineering, 1985, p. 318-324.
ABS: This paper discusses the characteristics of CIBA-GEIGY's XU 218 polyimide, focusing on its application as a matrix resin. XU 218 is a soluble thermoplastic polyimide which has significant advantages over current polyimides. XU 218 can be used as a matrix resin for advanced composites. Due to its unique properties, prepregging and composite fabrication of XU 218 are easier than processing polyamic acid precursor-type polyimides. In addition to improved processability, XU 218 exhibits the high performance characteristics of polyimides such as good mechanical properties, high glass transition

temperature, thermal stability, and good toughness. 85/00/00 86A21728

UTTL: Comparison of calculated and measured height profiles of transverse electric VLF signals across the daytime earth-ionosphere waveguide
AUTH: A/FIELD, E. C., JR.; B/WARBER, C. R.; C/KOSSEY, P. A.; D/LEWIS, E. A.; E/HARRISON, R. P. PAA: B/(Pacific-Sierra Research Corp., Los Angeles, CA); E/(USAF, Rome Air Development Center, Bedford, MA) Radio Science (ISSN 0048-6604), vol. 21, Jan.-Feb. 1986, p. 141-149.
ABS: Airborne VLF antennas radiate energy that propagates via both transverse electric (TE) and transverse magnetic (TM) modes in the earth-ionosphere waveguide. In order to compare the structure of such signals, measurements were made using rocket probes launched from Wallops Island, Virginia. The probes measured TE and TM fields at all altitudes between the ground and the base of the ionosphere. The nearly horizontal airborne transmitting antenna radiated a TE signal that was stronger than its TM signal at altitudes above about 10 km. The signals comprised one or more well-defined TE or TM waveguide modes. Calculated height profiles agree well with the measured ones and correctly reproduce details of profile structure caused by interaction between two or more modes. 86/02/00 86A21513

UTTL: An array of possibilities for future antenna systems
AUTH: A/FORREST, J. R. PAA: A/(University College, London, England) (Journees Internationales sur les Antennes, Nice, France, Nov. 13-15, 1984) Annales des Telecommunications (ISSN 0003-4347), vol. 40, July-Aug. 1985, p. 438-444.
ABS: Possible future trends concerning antenna-system requirements in communications and radar are examined. It is argued that phased-array antennas will solve many of the existing problems. It is suggested that these arrays will contain relatively few controllable elements, and that they will be characterized by 'intelligent' signal processing based on the capabilities of multiple-beam formation and adaptive patterns. 85/08/00 86A14185

UTTL: S-Band circularly polarized microstrip phased array
AUTH: A/COOMBS, D. L. PAA: A/(Ball Aerospace, Systems Div., Boulder, CO) IN: ITC/USA/'84; Proceedings of the International Telemetering Conference, Las Vegas, NV, October 22-25, 1984 (A86-13201 03-32). Research Triangle Park, NC, Instrument Society of America, 1984, p. 643-654.
ABS: An S-Band phased array has been developed which is very efficient, has excellent scanning performance, can be steered electronically in both azimuth and elevation, and is very thin. Using microstrip elements, phase shifters and a combiner network, the following design requirements were satisfied: operation at 2.2 to 2.3 GHz, right-hand polarization with axial ratio less than 3 dB, scan volume plus or minus 60 degrees in elevation and plus or minus 10 degrees in azimuth, efficiency greater than 60 percent at midband and greater than 50 percent at the band edges, scan performance with less than 2 dB loss out of 45 degree elevation scan angles, ability to operate in ground mobile environment, and quantity production possible at reasonable cost. 84/00/00 86A13251

UTTL: ELT antenna gain distributions under simulated crash conditions
AUTH: A/ESTEP, H. PAA: A/(NASA, Goddard Space Flight Center, Greenbelt, MD) CORP: National Aeronautics and Space Administration. Goddard Space Flight Center, Greenbelt, Md. IEEE Transactions on Aerospace and Electronic Systems (ISSN 0018-9251), vol. AES-20, Nov. 1984, p. 841-843.
ABS: A study of the relative merits of ELT antenna positions, when mounted on a small aircraft, is presented. The gain distribution of the best antenna position together with the worst crash scenario is also given. 84/11/00 86A12698

UTTL: Differential mount enhances EHF antenna design
AUTH: A/CONNOLLY, A. R.; B/WILLS, J. D., JR. PAA: B/(Datron Systems, Inc., Simi Valley, CA) Defense Electronics (ISSN 0278-3479), vol. 17, Sept. 1985, p. 87, 88, 91-93.
ABS: Three competing geometries for mounting and steering the aperture were analyzed during the process of reviewing trade-offs for transportable configurations and techniques for reducing sidelobes in an optical reflecting antenna. The geometries analyzed were elevation-over azimuth, yoke, and differential. The elevation-over-azimuth arrangement is the most standard and most economical; the yoke occupies less volume than the elevation-over-azimuth; and the

differential mount is the smallest and lightest of the three and also costs less than the yoke. The performance advantages provided by the differential mount for an SHF/EHF antenna system and the design problems involved are examined. 85/09/00 85A49092

UTTL: Diagnostic measurements and analysis of wave mechanisms in radomes
AUTH: A/TRICOLES, G.; B/ROPE, E. L.; C/HAYWARD, R. A.
PAA: C/(General Dynamics Corp., Electronics Div., San Diego, CA) IN: Inverse methods in electromagnetic imaging; Proceedings of the NATO Advanced Research Workshop, Bad Windsheim, West Germany, September 18-24, 1983. Part 2 (A85-48926 24-70). Dordrecht, D. Reidel Publishing Co., 1985, p. 1223-1233.
ABS: Wavefronts in radome-bounded regions are related to boresight error; in particular, wavefront tilts are proportional to boresight error. The wavefronts and therefore boresight error depend strongly on wave polarization direction. A method for probing wavefronts was described. This diagnostic method was applied to specific, thin wall radome; it identified a wave mechanism, guided waves, which are omitted from approximate analytical methods that locally approximate curved radomes by assemblies of flat dielectric sheets. The diagnostic method has been applied to improve other radomes; it located reflecting regions. 85/00/00 85A48984

UTTL: Complex ray analysis of beam transmission through two-dimensional radomes
AUTH: A/GAO, X. J.; B/FELSEN, L. B. PAA: B/(New York, Polytechnic Institute, Farmingdale) IEEE Transactions on Antennas and Propagation (ISSN 0018-926X), vol. AP-33, Sept. 1985, p. 963-975.
ABS: Transmission through a radome is investigated using the complex ray technique. Ray tracing is performed along conventional trajectories as well as more accurate trajectories shifted laterally along the radome boundaries, and it is found from numerical comparisons that the conventional trajectories are adequate for the radome transmission problem. Wedge-tapered radomes are then considered, and the complementary roles of direct and collective treatment of internal reflections are made evident as the taper angle increases. The results establish the complex ray and collective transmission methods as an effective approach to treating radiation of large-aperture Gaussian-like fields of a dielectric radome. 85/09/00 85A48256

UTTL: Correlation of linear and nonlinear radome error induced miss distance predictions
AUTH: A/MURRAY, T. PAA: A/(Raytheon Co., Missile Systems Div., Bedford, MA) IN: 1984 American Control Conference, San Diego, CA, June 6-8, 1984, Proceedings. Volume 2 (A85-47676 23-63). New York, IEEE, 1984, p. 743-750.
ABS: A linear radome error model is defined which bridges the gap between nonlinear and linear radome error miss distance predictions. The model includes an effective slope and an effective noise variance. The effective slope and effective noise are a function of gimbal angle motion which is dependent upon guidance system disturbances such as target maneuver and range independent noise. Analytical expressions for effective slope and effective noise are derived for a sinusoidal radome error. Miss distances using the linear model correlate well with those using the sinusoidal radome. 84/00/00 85A47720

UTTL: Guidance performance analysis with in-flight radome error calibration
AUTH: A/YUEH, W. R.; B/LIN, C.-F. PAA: A/(Northrop Corp., Electronics Div., Hawthorne, CA); B/(Boeing Co., Seattle, WA) Journal of Guidance, Control, and Dynamics (ISSN 0731-5090), vol. 8, Sept.-Oct. 1985, p. 666-669.
ABS: Boresight radome errors can lead to a serious degradation of missile homing performance. For an improvement of homing performance and target intercept capability, it is therefore necessary to overcome the restrictions imposed by radome errors. The present investigation is concerned with an approach for doing this, taking into account the conduction of a guidance performance analysis with in-flight radome error calibration. Attention is given to a self-learning network scheme with an adaptive real-time estimation using a Kalman filter bank design for the switching environment in the case of high-altitude, high-speed threat. 85/10/00 85A46345

UTTL: Theoretical study of airborne electromagnetic leakage
AUTH: A/SHUBERT, K. A.; B/MEADORS, J. G.; C/BIRCHMEIER, J. R. PAA: C/(Battelle Columbus Laboratories, OH) IN: NAECON 1984; Proceedings of the National Aerospace and Electronics Conference, Dayton, OH, May 21-25, 1984. Volume 2 (A85-44976 21-01). New York, IEEE, 1984, p. 1215-1217.
ABS: A theoretical study was pursued for the characterization and control of low level EM fields associated with the transmission/reflection properties

of fine crack structures in airborne vehicles. A viable model was developed as the combination of the two EM modeling techniques. The first technique treated cracks in ground planes of finite thickness under the condition that the EM field was incident from a distance source. The second technique transformed the effects created by a distant source to effects due to a single source in the vicinity of the crack. The resulting history was implemented for specific analysis through a computer program. 84/00/00 85A45139

UTTL: Spiral antennas for ESM
AUTH: A/MORGAN, T. E. PAA: A/(Marconi Space and Defence Systems, Ltd., Stanmore, England) IEE Proceedings, Part F - Communications, Radar and Signal Processing (ISSN 0143-7070), vol. 132, pt. F, no. 4, July 1985, p. 245-251. Research supported by the Ministry of Defence (Procurement Executive).
ABS: In the absence of any published mathematical analyses of the cavity-backed spiral antennas that have become popular in Electronic Support Measures systems, the functions and operating principles of the antenna's spiral radiator, backing cavity, and balun transformer components are treated by means of elementary reasoning. As an illustration of the performance quality currently achievable with these antennas, an evaluation is conducted for the cases of a reduced size square antenna for the 0.4-4.0 GHz frequency band, a 52-mm diameter antenna covering the standard 2.0-18.0 GHz band, and an in-line, 16-mm diameter antenna and integral radome for the 18.0-40.0 GHz band, where the output is by means of a double ridge waveguide. 85/07/00 85A44947

UTTL: Tri-reflector antennas with no cross-polarized component
AUTH: A/URASAKI, S.; B/MAKINO, S.; C/KATAGI, T. PAA: C/(Mitsubishi Electric Corp., Information Systems and Electronics Development Laboratory, Kamakura, Japan) Electronics and Communications in Japan, Part 1: Communications (ISSN 8756-6621), vol. 68, Aug. 1985, p. 85-92. Translation.
ABS: Since offset antennas have good wide angle characteristics, they are used frequently for ground stations in microwave communications. However, when the frequency reuse is considered via two orthogonal polarizations, the cross-polarization components generated on the reflector surface create a problem. A method was reported in which the cross-polarization components are cancelled in the geometric optics sense in the offset Cassegrainian and Gregorian systems. In such a method, the degree of freedom in design is not large. For instance, the inclination of the axis of the conical horn used as the primary radiator is restricted. This paper studies tri-reflector antennas in which the degree of freedom is larger. The geometrical condition for eliminating the cross polarization is derived and the shape of the reflector system satisfying the condition is found. To confirm the theoretical results, an antenna has been constructed. The cross-polarization components are less than about -30 dB and hence the validity of the theory has been confirmed. 85/08/00 85A44540

UTTL: A flat antenna with an X band array
AUTH: A/MARCHAND, M. PAA: A/(LMT Radio Professionnelle, Boulogne-Billancourt, France) Revue Technique Thomson - CSF (ISSN 0035-4279), vol. 17, March 1985, p. 83-109. In French.
ABS: Design details of a flat array, high gain, low sidelobe surveillance radar antenna are described. An experimental, 512-source unit was tested at 9.6 GHz with a 1 GHz passband for rapid frequency switching. A 32 dB gain was realized with a 1 km lobe length. A 0.9 wavelength distance was established between the RF emitters and all pathways were selected by CAD studies. Printed circuits were used for the sources to reduce weight for the unit, which is a prototype of a field-erectable unit. Field test results are provided, including several performance factors which were lower than predicted. 85/03/00 85A43562

UTTL: Main stages and problems in the design of low-gain active antennas
AUTH: A/SHCHERBINA, A. A. Radiotekhnika (Kharkov) (ISSN 0485-8972), no. 69, 1984, p. 77-84. In Russian.
ABS: The paper examines the stages in the design of low-gain antenna amplifiers and antenna power amplifiers for use on flight vehicles and on the ground. An algorithm and program for the parameteric synthesis of active antennas are developed whose application significantly speeds up the production of such devices. An example of the parametric synthesis of a small antenna amplifier is given. 84/00/00 85A42106

UTTL: Giant surveillance radar squeezed into wing
AUTH: A/LERNER, E. J. Aerospace America (ISSN 0740-722X), vol. 23, July 1985, p. 29, 30, 32.
ABS: A novel airborne early warning surveillance radar has been designed for E-2 class carrier-based aircraft which uses phased array principles to blend a very

large antenna area conformally onto wing and fuselage surfaces. The antenna elements that permit this degree of conformance are end-fired devices, 'Yagis', with coupling that broadens the radiation pattern emitted by each element in the horizontal direction. The replacement of conventional radomes by such conformal systems will lead to greater aircraft loiter time through both structural weight reduction and aerodynamic efficiency improvements. 85/07/00 85A41052

UTTL: Design criterion for inclined planar radomes on radar corner reflectors used for spaceborne SAR calibration
AUTH: A/KEEN, K. M. PAA: A/(Keen Associates, Ifold, England) Electronics Letters (ISSN 0013-5194), vol. 21, June 6, 1985, p. 548-550.
ABS: Larger corner reflector ground targets currently planned for spaceborne SAR calibration will require planar A-sandwich radome covers for weather protection and mechanical stability. The radomes must be inclined with respect to reflector apertures, however, to avoid scattering cross-section uncertainties in the target beam peak direction. A criterion for inclination angle is derived here. 85/06/06 85A40144

UTTL: A circularly polarized offset reflector antenna for direct broadcasting satellites
AUTH: A/FASOLD, D.; B/LIEKE, M. PAA: B/(Messerschmitt-Boelkow-Blohm GmbH, Munich, West Germany) European Microwave Conference, 13th, Nuremberg, West Germany, Sept. 5-8, 1983, Paper. 7 p.
ABS: The design objectives and electrical performance data of a circularly polarized offset reflector antenna for the illumination of the FRG are presented. The requirements are based on the WARC regulations settled for direct broadcasting satellites. The antenna consists of an offset paraboloid reflector with an elliptical corrugated feedhorn with RF-sensor. Measured radiation pattern, gain figures and RF-sensor performance data are presented. Pattern degradations caused by reflector tilting for beam fine pointing and thermal deformations are considered.
RPT#: MBB-UR-702-84-OE 83/09/00 85A35255

UTTL: Problems of radome design for modern airborne radar. II
AUTH: A/RULF, B. PAA: A/(Radant Systems, Inc., Stow; Tufts University, Medford, MA) Microwave Journal (ISSN 0026-2897), vol. 28, May 1985, p. 265, 266, 270, 271.
ABS: Solution techniques devised for designing aircraft radomes, particularly AWACS and nose mounts, are presented. Consideration is given to the range of the angles of incidence and the ratio between polarization over the radome area. Methods are defined for selecting optimal ratios for the radome emitting/receiving segments, thus simultaneously controlling reflection and transmission effects. Nose radomes are primarily aerodynamic structures and thereby possess incidence angles of up to 80 deg. Reflected power is calculated with geometric optics. Both types of radome are constructed of carbon composite sandwich structures, which minimize reflection sufficiently to justify doubled costs. 85/05/00 85A34661

UTTL: Noise factor of active scanning antenna arrays
AUTH: A/BABENKO, A. I.; B/ZAITSEV, E. F.; C/NIKOLAEVSKII, A. L. Radiotekhnika (ISSN 0033-8486), no. 3, March 1985, p. 57-59. In Russian.
ABS: The change in the noise factor of active phased arrays during the scanning process is analyzed. Examples of this change are presented for arrays with transistor amplifiers, and it is confirmed that this change phenomenon should be taken into account in the array design. Results indicate that it is insufficient to validate the amplifiers solely on the basis of the noise factor in the nominal mode. 85/03/00 85A34172

UTTL: Dielectric dipole antennas with controlled characteristics
AUTH: A/BARZHIN, V. IA.; B/ZAIKIN, I. P.; C/OLEINIKOV, S. IU. Radiotekhnika (Kharkov) (ISSN 0485-8972), no. 71, 1984, p. 100-104. In Russian.
ABS: Numerical and experimental results are presented on the use of high-permittivity polarized piezoceramic casings to control the characteristics of dipole antennas. The effect of the casing on the amplitude and polarization patterns of the antenna is investigated. The wide applicability of piezoceramic materials in antenna technology is noted, with particular attention given to the construction of radomes that are capable of withstanding high temperatures without a significant deterioration in the strength and radio characteristics. 84/00/00 85A34167

UTTL: Shaped reflector beam waveguide and high gain antenna systems

AUTH: A/GALINDO-ISRAEL, V.; B/MITTRA, R. PAA: A/(California Institute of Technology, Jet Propulsion Laboratory, Pasadena, CA); B/(Illinois, University, Urbana, IL) CORP: Jet Propulsion Lab., California Inst. of Tech., Pasadena.; Illinois Univ., Urbana. IN: Globecom '83 - Global Telecommunications Conference, San Diego, CA, November 28-December 1, 1983, Conference Record. Volume 3 (A85-28226 11-32). New York, Institute of Electrical and Electronics Engineers, Inc., 1983, p. 1655-1659.

ABS: In this paper the problem of synthesizing dual reflector antennas for both amplitude and phase control of the final aperture distribution is discussed. An approximate procedure for the offset synthesis problem is presented and applications of the procedure to the shaping of beam waveguides and reflectors for high-gain antenna systems are illustrated. 83/00/00 85A28270

UTTL: System considerations related to active antennas

AUTH: A/FOLDES, P. PAA: A/(Foldes, Inc., Wayne, PA) IN: Globecom '83 - Global Telecommunications Conference, San Diego, CA, November 28-December 1, 1983, Conference Record. Volume 3 (A85-28226 11-32). New York, Institute of Electrical and Electronics Engineers, Inc., 1983, p. 1650-1654. Research sponsored by the International Telecommunications Satellite Organization.

ABS: The use of active satellite antennas for high volume communication in the rest of this century is surveyed, focusing on channel capacities between 50 kch and 500 kch. The subsystems constituting the payloads of future communications satellites are discussed, including their optimization and configuration, and their parameters. Alternative access and alternative modulation techniques are summarized, and microwave optics considerations are addressed. Power amplifiers for active antennas are discussed along with power-related issues. Characteristics of active antennas for C and K(u) band, far and near-field optics, FM and QPSK modulations are shown, as are the volume-weight characteristics of the CONVTOR active array integrated element feeds ad overall antenna system. 83/00/00 85A28269

UTTL: Phased arrays for communications satellites

AUTH: A/SCHULTZ, J. PAA: A/(Grumman Aerospace Corp., Bethpage, NY) IN: Globecom '83 - Global Telecommunications Conference, San Diego, CA, November 28-December 1, 1983, Conference Record. Volume 3 (A85-28226 11-32). New York, Institute of Electrical and Electronics Engineers, Inc., 1983, p. 1640-1644.

ABS: This paper describes a design approach for frequency-reuse communications satellites that use multibeam array antennas. The multibeam antenna is able to cover all or part of the earth's surface with contiguous independent circularly polarized beam spots, with overlap to minimize loss of gain between spots. The transmitting and receiving antennas are active space-fed planar arrays which use wide bandwidth elements and real time delay lines for beam formulation. The array is not phase scanned; it is a fixed, space-fed, active constrained lens. The term 'active' means that RF power amplifiers are distributed in the main aperture of the transmitting antenna, and RF pre-amplifiers are distributed in the main aperture of the receiving antenna. Multiple circularly polarized beams are produced by multiple independent antenna feeds. Good polarization isolation and low sidelobes allow a high degree of frequency reuse. 83/00/00 85A28268

UTTL: Phase III GPS integration options for aircraft platforms

AUTH: A/WIEDERHOLT, L. F.; B/KLEIN, D. PAA: B/(Intermetrics, Inc., Cambridge, MA) Navigation (ISSN 0028-1522), vol. 31, Summer 1984, p. 129-151.

ABS: The GPS User Equipment is being designed for use on various platform types (aircraft, surface ships, submarines, land vehicles and manpack) with the integrated components of the user equipment (UE) being developed as separate modules. GPS UE can be integrated on board a platform to varying levels. The system enhancements available to the individual platform are dependent on the complement of GPS UE selected and the degree to which it is being integrated onto the platform. This paper describes the GPS UE capability options available to aircraft platforms. The capability options are described as generic options (i.e., not specific to any aircraft). For each option, three topics are addressed: the benefits, possible equipment configuration and implementation issues. These topics are addressed independent of particular aircraft. 84/00/00 85A25196

UTTL: Microstrip brings radar to hostile environments
AUTH: A/COLBY, G. V.; B/BRYANOS, J. C. PAA: B/(Avco Corp., Avco Systems Div., Wilmington, MA) Microwaves & RF (ISSN 0745-2993), vol. 24, Feb. 1985, p. 96-99, 113.
ABS: Design techniques have been developed to provide conformal microstrip radar antennas for a variety of missions at acceptable costs. A current-carrying conductor is imprinted on one side of a substrate, on the other side of which is a ground plane. The thinness of the antenna permits its conformal mounting and concommitant high g and mechanical stress resistance. The antenna area is determined by the frequency and bandwidth requirements, e.g., the larger the antenna the lower the frequency. Antennas 0.020 in. thick can be built into the outside of a munitions nose cone. The antennas comprise either grid or patch configurations, with higher radiation density being available from the former, which can be arranged in linear or area arrays. A theoretical model of device performance is defined and compared with experimental results on the effects of substrate thickness, loop size, the number of loops and radiator line widths. 85/02/00 85A25155

UTTL: Seeing double improves indoor range
AUTH: A/VOKURKA, V. J. PAA: A/(Eindhoven, Technische Hogeschool, Eindhoven, Netherlands) Microwaves & RF (ISSN 0745-2993), vol. 24, Feb. 1985, p. 71-73, 75, 76, 94. Research supported by the Netherlands Technology Foundation.
ABS: The efficiency of indoor compact antenna test ranges (CATR) is aided by employing cylindrical reflectors arranged according to geometrical optics principles. Using dual reflectors opens the test window to 100 GHz and reduces the reflector dimensions by 50 percent. Two perpendicular reflectors receive a plane wave from a spherical source and cause no more than -30 dB cross-polarization. The planar wave zone of the dual reflectors can be kept to a 1.5-5.0 m diam range for small-large antennas being tested for far-field patterns. The sizes are sufficient to cover most satellite, microwave link and radar antennas presently in use. Care is, however, necessary to avoid coupling and strong radiation effects during tests. 85/02/00 85A25151

UTTL: Problems of radome design for modern airborne radar
AUTH: A/RULF, B. PAA: A/(Radant Systems, Inc., Stow, MA) Microwave Journal (ISSN 0026-2897), vol. 28, Jan. 1985, p. 145-148, 152, 153.
ABS: The operation of airborne radar involves a discrimination between targets and ground clutter. A solution of the resulting problems requires the design of antennas with special characteristics. Efforts of the antenna designer, however, will be defeated if the antenna is protected by a radome which fails to provide the same high performance as the antenna. The present investigation is concerned with problems arising in the design of high-performance radomes, taking into account two important airborne radar systems. The first example involves the E-3A (AWACS), the most modern airborne surveillance radar system now in operation. The second example is related to a typical fire-control radar in a modern tactical aircraft. 85/01/00 85A24715

UTTL: Criteria for nearly omnidirectional radiation patterns for printed antennas
AUTH: A/ALEXOPOULOS, N. G.; B/JACKSON, D. R.; C/KATEHI, P. B. PAA: B/(California, University, Los Angeles, CA); C/(Michigan, University, Ann Arbor, MI) IEEE Transactions on Antennas and Propagation (ISSN 0018-926X), vol. AP-33, Feb. 1985, p. 195-205. Research supported by the Northrop Corp.
ABS: Radiation from printed antennas is investigated with emphasis placed on producing E-bar and H-bar-plane radiation patterns that are as nearly omnidirectinal as possible. This is achieved using criteria which are derived for a nonzero radiation field extending down to the layer surface (radiation into the horizon). It is determined that this phenomenon arises when a surface wave pole coincides with a branch point in the complex plane. A simple ray optics interpretation is given for the phenomenon, and graphs are presented to easily enable design of printed antenna geometry to achieve nearly omnidirectional E-bar or H-bar-plane patterns. 85/02/00 85A24660

UTTL: Compact antenna range
AUTH: A/VOKURKA, V. J. PAA: A/(Eindhoven, Technische Hogeschool, Eindhoven, Netherlands) IN: Satellite communication antenna technology (A85-23651 09-17). Amsterdam, North-Holland, 1983, p. 583-611.
ABS: The applications of compact antenna range systems for indoor measurements under far-field conditions are discussed. Compact range systems are used to collimate the radiation from a point or a line source by means

of a lens or parabolic reflector. Some technical consideration of compact range design are discussed, including: optimal stray radiation levels; shapes and dimensions of the plane wave zone, reflector surface accuracy; and operational frequency range. A photograph is provided which shows a compact range system with two crossed-parabolic cylindrical reflectors during indoor tests of a contoured beam antenna for satellite applications. 83/00/00 85A23662

UTTL: The role of antennas in advanced communication systems

AUTH: A/REUDINK, D. O. PAA: A/(Bell Radio Research Laboratory, Holmdel, NJ) IN: Satellite communication antenna technology (A85-23651 09-17). Amsterdam, North-Holland, 1983, p. 487-534.

ABS: A historical sketch of satellite research in 1950 and 1960s is presented with special emphasis given to the problem of antenna design in active satellite systems. Some of the fundamental limitations of the performance of satellite communications antennas at frequencies greater than 10 GHz are identified, including rain and ice attenuation in the lower atmosphere, depolarization, and crosstalk at low elevation angles. Some antenna designs which maximize effective isotropic radiated power and reduce atmospheric limitations are described, including spot beam antennas, scanning beam TDMA configurations, and phased array antennas. Antenna designs for limited scanning, and multireflector arrays are also discussed. 83/00/00 85A23659

UTTL: Phased arrays for satellites and the TDRSS antennas

AUTH: A/IMBRIALE, W. A. PAA: A/(California Institute of Technology, Jet Propulsion Laboratory, Pasadena, CA) CORP: Jet Propulsion Lab., California Inst. of Tech., Pasadena. IN: Satellite communication antenna technology (A85-23651 09-17). Amsterdam, North-Holland, 1983, p. 431-486.

ABS: The design and performance of satellite phased-array systems are examined by considering several specific antennas built for spacecraft use. Particular consideration is given to: (1) the JARED (Jammer Reduction Antenna System) antenna, and adaptive phased array which can be used to null jammer signals while providing coverage to specific user areas; (2) the algorithm used in the JARED antenna; and (3) a technique that can be used to detect and locate jammers. The antennas used by the Tracking and Data Relay Satellite System (TDRSS) are then described. A significant aspect of the TDRSS is the multiple access antenna which is a 30-element phased array, providing a single steered beam on transmit and the ability to receive data from 20 simultaneous users. Also included on the TDRSS is a mesh deployable reflector and a C-band and K-band communications system. 83/00/00 85A23658

UTTL: Satellite communication antenna technology

AUTH: A/MITTRA, R.; B/IMBRIALE, W. A.; C/MAANDERS, E. J. PAA: A/(Illinois, University, Urbana, IL); B/(California Institute of Technology, Jet Propulsion Laboratory, Pasadena, CA); C/(Eindhoven, Technische Hogeschool, Eindhoven, Netherlands) CORP: Illinois Univ., Urbana.; Jet Propulsion Lab., California Inst. of Tech., Pasadena.; Technische Hogeschool, Eindhoven (Netherlands). Amsterdam, North-Holland, 1983, 667 p. For individual items see A85-23652 to A85-23663.

ABS: A general overview of current technology in the field of communication satellite antennas is presented. Among the topics discussed are: the design of multiple beam systems; frequency reuse; and polarization control of antenna measurements. Consideration is also given to: contour beam synthesis; dual shaped reflector synthesis; beam shaping; and offset reflector design. The applications of the above technologies to present and future generations of communications satellites is considered, with emphasis given to such systems as: the Intelsats; the Defense Satellite Communications System, (DSCS-III); Satellite Business System (SBS), and Comstar. 83/00/00 85A23651

UTTL: Compact gain measurements on reflector antennas

AUTH: A/HOQUE, M.; B/SMITH, M. S.; C/DAVIES, D. E. N. PAA: A/(Bangladesh University of Engineering and Technology, Dacca, Bangladesh); C/(University College, London, England) IEE Proceedings, Part H - Microwaves, Optics and Antennas (ISSN 0143-7097), vol. 131, pt. H, no. 6, Dec. 1984, p. 371-378.

ABS: The paper describes an extremely compact method of making gain measurements on parabolic reflector antennas. The concept involves making return-loss measurements on the antenna when it is located in front of a plane reflecting screen mounted parallel to the antenna aperture. This compact configuration is convenient for laboratory measurements or factory testing and has been used on reflectors of up to 12 ft (3.66 m) in diameter (in the latter case, employing a water bath to represent the plane flat reflecting surface). The return-loss measurements provide information on the various loss mechanisms which

degrade the normal operation of an antenna, and the paper provides a detailed experimental and theoretical study of such losses and their relation to the measurement system. The results show an accuracy of the order of 0.1 dB for gain measurement, aided by the fact that the system corresponds to a 2-way (transmit-and-receive) measurement on the antenna. The paper discusses various ways of using the measurement for comparative and absolute determination of antenna gain. 84/12/00 85A20166

UTTL: An experimental aeronautical satellite data link
AUTH: A/ANDERSON, S. PAA: A/(Mitre Corp., McLean, VA)
IN: Digital Avionics Systems Conference, 6th, Baltimore, MD, December 3-6, 1984, Proceedings (A85-17801 06-01). New York, American Institute of Aeronautics and Astronautics, 1984, p. 454-461.
ABS: The current status of a project to design, develop, and demonstrate an experimental aeronautical satellite data link system to provide data communication capability between the ground and aircraft flying in oceanic airspace is reported. The approach used in developing the system is described, and technical details are presented to support specific design decisions. The link beween the aircraft and satellite is at L-band (1.5/1.6 GHz), and the links between satellite and earth stations are at C-band (4/6 GHz). The system concept avoids the high cost of launching, operating, and maintaining dedicated satellites through sharing of existing commercially available satellite links (e.g., INMARSAT) with other mobile users (e.g., maritime).
RPT#: AIAA PAPER 84-2691 84/00/00 85A17869

UTTL: An analysis of the pattern of longitudinal slot antenna on the metal cylinder covered with a high collision plasma layer
AUTH: A/DONG, N.; B/XIA, S. Chinese Society of Astronautics, Journal, July 1984, p. 76-84. In Chinese, with abstract in English.
ABS: In this paper, the pattern of a longitudinal slot antenna on a metal cylinder covered with a loss plasma layer (high collision layer) is discussed. Based on Maxwell's equation, the cylindrical coordinate systems solution of the radiation field is derived, and the use of the bound value of a metal cylinder is considered. Some of the numerical results obtained in this paper approximated the experimental results. 84/07/00 85A17173

UTTL: Elliptical offset Gregorian antenna for a transportable earth station
AUTH: A/HENDERSON, R. I. PAA: A/(General Electric Co., PLC, Marconi Research Centre, Chelmsford, Essex, England) GEC Journal of Research (ISSN 0264-9187), vol. 2, no. 3, 1984, p. 186-197. Research sponsored by GEC-McMichael, Ltd.
ABS: New sidelobe regulations are being introduced for earth station antennas to allow closer satellite spacing. Conventional axisymmetric antennas can meet the lower sidelobe levels only with difficulty, and offset reflector systems are therefore receiving increasing attention. This paper describes an offset Gregorian antenna for transportable applications in the 11/14 GHz bands, designed to take advantage of an elliptical radiating aperture to reduce sidelobes preferentially in the plane of the geostationary orbit. A sophisticated profile optimization method is described which maximizes gain while keeping all sidelobes below a specified envelope. 84/00/00 85A16854

UTTL: Antenna engineering handbook /2nd edition/
AUTH: A/JOHNSON, R. C.; B/JASIK, H. PAA: A/(Geogia Institute of Technology, Atlanta, GA); B/(Eaton Corp., AIL Div., Deer Park, NY) New York, McGraw-Hill Book Company, 1984, 1356 p. No individual items are abstracted in this volume.
ABS: Essential principles, methods, and data for solving a wide range of problems in antenna design and application are presented. The basic concepts and fundamentals of antennas are reviewed, followed by a discussion of arrays of discrete elements. Then all primary types of antennas currently in use are considered, providing concise descriptions of operating principles, design methods, and performance data. Small antennas, microstrip antennas, frequency-scan antennas, conformal and low-profile arrays, adaptive antennas, and phased arrays are covered. The major applications of antennas and the design methods peculiar to those applications are discussed in detail. The employment of antennas to meet the requirements of today's complex electronic systems is emphasized, including earth station antennas, satellite antennas, seeker antennas, microwave-relay antennas, tracking antennas, radiometer antennas, and ECM and ESM antennas. Finally, significant topics related to antenna engineering, such as transmission lines and waveguides, radomes, microwave propagation, and impedance matching and broadbanding, are addressed. 84/00/00 85A16081

UTTL: The main characteristics of a synthetic-aperture radar in the case of arbitrary motion of the flight vehicle

AUTH: A/ITSKHOKI, IA. S.; B/SAZONOV, N. A.; C/TOLSTOV, E. F. Radiotekhnika i Elektronika (ISSN 0033-8494), vol. 29, Nov. 1984, p. 2164-2172. In Russian.

ABS: The effect of phase fluctuations on the azimuth resolution and accuracy of a synthetic-aperture radar is evaluated for rectilinear flight and the sidelooking regime. Arbitrary flight trajectories and observation angle are assumed, and the evaluation is carried out according to the modulus of the output-signal function. 84/11/00 85A15687

UTTL: The radiation from rectangular microstrip antennas mounted on two-dimensional objects

AUTH: A/JAKOBSEN, K. R. PAA: A/(Norges Tekniske Hogskole, Trondheim, Norway) IEEE Transactions on Antennas and Propagation (ISSN 0018-926X), vol. AP-32, Nov. 1984, p. 1255-1259.

ABS: The radiation patterns for a quadratic microstrip antenna mounted on two-dimensional objects, the circular cylinder and the strip, have been calculated using both the transmission-line model and the resonator model. Analytical expressions for the far field are presented, and calculations are compared with measurements. All measurements clearly indicate that the resonator model is better than the transmission-line model in radiation pattern calculations outside the principal planes of the antenna. 84/11/00 85A14572

UTTL: Advanced 30/20 GHz multiple beam antenna for future communications satellites

AUTH: A/CHEN, C. C.; B/MINNIN, W. A. PAA: B/(TRW, Inc., Space Communications Div., Redondo Beach, CA) CORP: TRW, Inc., Redondo Beach, Calif. IN: EASCON '83; Proceedings of the Sixteenth Annual Electronics and Aerospace Conference and Exposition, Washington, DC, September 19-21, 1983 (A85-14426 04-32). New York, Institute of Electrical and Electronics Engineers, 1983, p. 95-102.

ABS: The technologies which will be implemented in advanced satellite communications systems being studied by NASA and the intended coverage scenarios are described. The systems will function at 30/20 GHz with 2.5 GHz bandwidth for the uplink and downlink. Subfrequencies will have 500 MHz bandwidth and operations will include TDMA modes. Sample scan patterns are presented for the centerminous U.S. The signals will be broadcast from a multibeam offset Cassegrain reflector antenna to obtain a low sidelobe, wide angle scan. Three contiguous low sidelobe beams will be generated with a diplex feed cluster and a 19 element scanning beam-forming network. The same technology will be used to double the capacity of current 14/12 GHz satellites. 83/00/00 85A14436

UTTL: Device for the real-time recording of the spatial structure of the electromagnetic fields of antennas in the near zone

AUTH: A/DUDKIN, V. P.; B/OBTEMPERANSKII, IU. S.; C/PETROV, IU. N.; D/CHAIKOVSKII, V. E. Radiotekhnika i Elektronika (ISSN 0033-8494), vol. 29, Sept. 1984, p. 1806-1809. In Russian.

ABS: A CRT scanner device for the real-time recording of antenna near fields in the millimeter-wave range is described. The device operates on the principle of the passive probing of the electromagnetic field; the probe in the form of a local region of elevated conductivity is produced by an electron beam in a semiconductor layer of the plane-stratified structure of the scanner screen. The device makes possible the real-time recording of the amplitude and amplitude-phase structure of microwave fields in the form of one- and two-dimensional distributions observed on the CRT screen. A scanner with the following characteristics has been constructed: An analysis aperture with a diameter of 100 mm, a complete-frame analysis time of 0.1 s, a resolution of not worse than 2 lines/mm, and a sensitivity of 10 to the -7th W/sq cm. 84/09/00 85A10442

UTTL: Antenna radar cross section

AUTH: A/YAW, D. F. PAA: A/(Westinghouse Defense and Electronics Center, Baltimore, MD) Microwave Journal (ISSN 0026-2897), vol. 27, Sept. 1984, p. 197.

ABS: The factors that have to be considered when determining the radar cross section (RCS) of an antenna are examined. In particular, consideration is given to the backscatter response, radiation mode response, and the structural mode response of antennas. Also, the monostatic grating lobe RCS response of phased arrays is examined. Expressions are presented for estimating the radiation mode RCS and the RCS grating lobe response angles. 84/09/00 85A10018

UTTL: Broadband phased-arrays antennas
AUTH: A/MANSKY, L. PAA: A/(Sedco Systems, Inc., Melville, NY) Microwave Journal (ISSN 0026-2897), vol. 27, Sept. 1984, p. 159, 160, 162 (6 ff.).
ABS: The actual jamming-to-signal ratio achieved in an electronic countermeasures (ECM) system depends on the effective radiated power (ERP) directed toward the radar by the ECM system. The required ERP may be obtained in a phase-steered array using a variety of transmit-subsystem hardware configurations. Here, tradeoff criteria to aid in the selection of an optimal architecture are discussed. Such selection is based on minimizing the array size, backscattering cross selection, and overall system complexity. Functional elements of typical phased arrays and their principal components are descried. 84/09/00 85A10016

UTTL: Simultaneous multibeam sounding of wind and turbulence
AUTH: A/BRUN, E.; B/CROCHET, M.; C/ECKLUND, W. L. PAA: C/(National Oceanic and Atmospheric Administration, Boulder, Colo.) CORP: Toulon Univ. (France).
ABS: Most clear air radars use an antenna with either a few fixed beam positions or one that can be steered to a number of beam positions, one position at a time. For spatial studies of parameters that can change rapidly these conventional radar may be severely limited. The problem is that the fixed beam radars do not cover enough positions and the steerable radars may not be able to cover the entire field of interest in a short enough time period. Preliminary results are presented from a brief experiment that suggests a way to overcome some of these space-time problems in clear air radar research. A typical clear air radar antenna located in France was modified in a simple way to produce a number of beam simultaneouly. The radar, the modifications and the resulting beam patterns are described. Spectra is then shown obtained with the multibeam array and some results are presented on the spatial variations of reflectivity. Both the positive and negative aspects of using a multibeam antenna array for clear air radar studies are summarized. 86/06/00 87N10506

UTTL: Spacecraft multibeam antenna system for 30/20 GHz
AUTH: A/ROBERTS, T. E.; B/SCOTT, W. F. CORP: Ford Aerospace and Communications Corp., Palo Alto, Calif. CSS: (Western Development Labs. Div.)
ABS: The major technical tasks that led to the definitions of operational and demonstration multiple beam antenna (MBA) flight systems and a proof of concept model (POC) are described. Features of the POC Model and its measured performance are presented in detail. Similar MBA's are proposed for transmitting and receiving with the POC Model representing the 20 GHz transmitting antenna. This POC MBA is a dual shaped-surface reflector system utilizing a movable free array to simulate complete CONUS coverage. The beam forming network utilizes ferrite components for switching from one beam to another. Measured results for components, subsystems and the complete MBA confirm the feasibility of the approach and also show excellent correlation with calculated values.
RPT#: NASA-CR-174654 NASA4-1-5-Z-F NAS 1.26:174654 WDL-TR-10138 84/01/10 86N31760

UTTL: ACTS Experiments Program
AUTH: A/SCHERTLER, R. J. CORP: National Aeronautics and Space Administration. Lewis Research Center, Cleveland, Ohio. Proposed for presentation at Globecom '86, Houston, Tex., 1-4 Dec. 1986; sponsored by the Institute of Electrical and Electronics Engineers
ABS: An overview of the ACTS Experiments Program is presented. ACTS is being developed and will flight test the advanced technologies associated with: a Ka-band multibeam antenna, onboard signal processing and switching as well as laser communications. A nominal 3 yr experiments program is planned. Through the experiments program, the capabilities of the ACTS system will be made available to U.S. industry, university and government experimenters to test, prove the feasibility and evaluate the key ACTS system technologies. Communication modes of operation using the baseband processor and microwave switch matrix are presented, along with the antenna coverage pattern. Potential experiment categories are also presented and briefly discussed. An overall schedule of activities associated with the experiments program is outlined. Results of the ACTS Experiments Program will provide information vital to successful industry implementation of ACTS technology in a future operational system.
RPT#: NASA-TM-88820 E-3182 NAS 1.15:88820 86/00/00 86N31625

UTTL: Determination of antennae patterns and radar reflection characteristics of aircraft
AUTH: A/BOTHE, H.; B/MACDONALD, D.; C/POOL, A. CORP: Advisory Group for Aerospace Research and Development, Neuilly-Sur-Seine (France).
ABS: The different types of aircraft antennas, their

radiation characteristics and their preferred siting on the airframe are described. Emphasis is placed on the various methods for determining aircraft antenna radiation patterns (ARP) and advantages, disadvantages and limitations of each method are indicated. Mathematical modelling, model measurements and in-flight measurements in conjunction with the applied flight test techniques are included. Examples of practical results are given. Methods of determining aircraft radar characteristics are also described, indicating advantages, disadvantages and limitations of each method. Relevant fundamentals of radar theory are included only as necessary to appreciation of the real meaning of radar cross section (RCS) and angular glint. The measuring methods included are dynamic full-scale, static full-scale, sub-scale optical, ultrasonic and radio modelling. References are made to RCS measuring facilities in the USA and Europe and the UK Radio Modelling Facility is used extensively to exemplify the sub scale technique.

RPT#: AGARD-AG-300-VOL-4 ISBN92-835-1530-7 86/05/00 86N30931

UTTL: Monopole element at the center of a circular groundplane of arbitrary radius. Volume 1: Theory and results

AUTH: A/WEINER, M. M.; B/CRUZE, S. P.; C/LI, C. C.; D/WILSON, W. J. CORP: Mitre Corp., Bedford, Mass.

ABS: The Air Force SINCGARS VHF-FM radio is a frequency-hopping anti-jam device utilizing electrically short antenna to minimize aerodynamic drag on airborne platforms. The development of optimally efficient, electronically tuneable antennas for this radio is of interest. Although the antenna groundplane is platform-dependent, it is usually small compared to an rf wavelength. A circular groundplane provides a standardized geometry with which to model and evaluate candidate antennas. Accordingly, a VHF antenna range with an 8 ft. diameter circular groundplane has been constructed to evaluate candidate antennas. The electrical properties of a monopole element at the center of a circular groundplane of finite radius are of interest to this program for (1) qualifying the antenna range; (2) establishing antenna standards with which to measure test antennas; and (3) modeling candidate antennas. A survey of the literature revealed that although this antenna has the simplest geometry of any monopole antenna, its properties are neither well understood nor standardized, particularly for groundplane radii which are small or comparable to a wavelength. This paper attempts to address this deficiency.

RPT#: AD-A166991 MTR-9622-VOL-1 86/03/00 86N30908

UTTL: Near-field testing of the 30 GHz TRW proof-of-concept multibeam antenna

AUTH: A/KUNATH, R. R., JR.; B/ZAKRAJSEK, R. J. CORP: National Aeronautics and Space Administration. Lewis Research Center, Cleveland, Ohio. Proposed for presentation at the Antenna Measurements Techniques Association 8th Annual Meeting and Symposium, Ottawa, Ontario, 23-25 Sep. 1986; sponsored by the National Research Council of Canada and the AMTA

ABS: Near-field testing was conducted on the 30 GHz TRW proof-of-concept (POC) Multibeam Antenna (MBA). The TRW POC MBA is a dual offset Cassegrain reflector system using a 2.7 m main reflector. This configuration was selected to assess the ability to create both multiple fixed and scanned spot beams. The POC configuration investigated frequency reuse via spatial separation of beams, polarization selectivity and time division multiple access scanning at 30 GHz. Measurements of directivity, sidelobe level, and pattern were made at NASA Lewis Research Center's Near-Field Antenna Test Facility. Presented in this paper are complete results of these measurements. Included is a detailed discussion of all testing procedures and parameters. Results of additional testing used to evaluate diffraction effects of the subreflector and distortions of the main reflector are also presented.

RPT#: NASA-TM-87357 E-3115 NAS 1.15:87357 86/00/00 86N27578

UTTL: Multibeam lens antennas

AUTH: A/CLAPP, R. E. CORP: Department of the Air Force, Washington, D.C.

ABS: Multibeam lens antennas are often circular, and utilize propagation in disk-shaped parallel-surface regions. There is phase correction through terms in theta squared, where theta is the angle of an aperture point measured from the boresight direction. In the new designs herein, the lens comprises two portions, each being two closely spaced plates with a dielectric medium between them. One portion is formed as a surface of revolution(cyclindrical or conical) with two circular ends, one end being an aperture with element feedpoints coupled to array elements. The other portion is a cap joined to the other end of the first portion. The cap may be a disk or a segment of a sphere. The dimensions and indices of refraction are selected to provide focus points for feed ports, with each focus being for a specific beam direction. The parameters may be selected so that the focus points are within the cap, at the periphery of the cap, or at the aperture.

RPT#: AD-D012108 US-PATENT-4,558,324

US-PATENT-APPL-SN-511591 US-PATENT-CLASS-343-754
85/12/10 86N25677

UTTL: DSCS network performance software support. Revision
AUTH: A/TREES, S. V.; B/HUGHES, D.; C/HUFFMAN, S.; D/MAPLES, B.; E/SHATTUCK, J. CORP: M/A-COM Linkabit, Inc., Vienna, Va.
ABS: The purpose of this task was to evaluate the utilization of the DSCS Operational Control System (DOCS) and to provide version release test support for the DSCS Network Planning Software (DNPS). This report also examines the development of multiple beam antenna (MBA) algorithms to calculate beam weights that provide minimum mean square error (MSE) performance between desired and actual gain contour patterns.
RPT#: AD-A163530 FR-170 86/01/07 86N25163

UTTL: VHF-FM communications antennas for project SINCGARS (UH-1 tail whip and cabin roof bent whip evaluation)
AUTH: A/CARALYUS, J.; B/MILLER, J.; C/GRATACOS, C.; D/CANSLER, F. CORP: Army Aviation Systems Command, St. Louis, Mo.
ABS: The American Electronics Laboratory (AEL), Allaire, NJ, was tasked by the U.S. Army Avionics Research and Development Laboratory (SAVAA-M), Fort Monmouth, NJ, to develop replacement breadband matching modules for the CU-942B and the FM 10-30-1 antenna to satisfy specified requirements for Project SINCGARS. AEL was further tasked to test various candidate antennas provided by commercial vendors that are mechanically interchangeable with the CU-942B and the FM 10-30-1. After completion of the AEL development/test program, AVRADA tasked an independent, non-based Government antenna test facility to conduct prescribed antenna verification tests in accordance with an agreed upon test plan. This technical report describes communications antenna systems provided by Dayton-Granger, Inc (DGI), American Electronics Lab (AEL), and Avionics Antenna Systems (AVANT). The test measurements were conducted at the Naval Air Development Center, Antenna Test Facility located in Warminster, PA. The information in this report provides, in part, the technical data for the protection data package of adequate VHF-FM Communications antennas for the UH-1 helicopter when used with the new SINCGARS Radio.
RPT#: AD-A163561 USAAVSCOM-TR-85-E-3 85/12/00 86N24883

UTTL: Study of the use of lightweight shipborne terminals for maritime satellite telecommunications
AUTH: A/HAGENAUER, J.; B/HAERTER, M.; C/OETTL, H.; D/SALZER, D.; E/SCHWEIKERT, R.; F/BOMMAS, G.; G/FRITSCH, B.; H/KLAGES, W.; I/KLIMMEK, N.; J/LAUB, W. PAA: A/(DFVLR, Oberpfaffenhofen, West Germany); B/(DFVLR, Oberpfaffenhofen, West Germany); C/(DFVLR, Oberpfaffenhofen, West Germany); D/(DFVLR, Oberpfaffenhofen, West Germany); E/(DFVLR, Oberpfaffenhofen, West Germany) CORP: Dornier-Werke G.m.b.H., Friedrichshafen (West Germany).
ABS: Smaller and less expensive satellite terminals are studied in order to cover a larger fraction of the world's commercial and yachting fleets. The problem of increased multipath propagation effects is analyzed together with system alternatives to reduce its incidence. The alternatives include antenna types, transmission power, bit rates, modulation schemes and forward correcting codes. Four light weight terminal types are described. Two operate with broad pencil beams and the others with hemispheric antennas. Multipath losses of one of the models are compensated by forward error correcting coding. Final selection requires experimental verification.
RPT#: ESA-CR(P)-2115 82/09/00 86N19341

UTTL: Technology achievements and projections for communication satellites of the future
AUTH: A/BAGWELL, J. W. CORP: National Aeronautics and Space Administration. Lewis Research Center, Cleveland, Ohio. Proposed for presentation at the 11th Communications Satellite Systems Conference, San Diego, Calif., 16-20 Mar. 1986; sponsored by AIAA
ABS: Multibeam systems of the future using monolithic microwave integrated circuits to provide phase control and power gain are contrasted with discrete microwave power amplifiers from 10 to 75 W and their associated waveguide feeds, phase shifters and power splitters. Challenging new enabling technology areas include advanced electrooptical control and signal feeds. Large scale MMIC's will be used incorporating on chip control interfaces, latching, and phase and amplitude control with power levels of a few watts each. Beam forming algorithms for 80 to 90 deg. wide angle scanning and precise beam forming under wide ranging environments will be required. Satelllite systems using these dynamically reconfigured multibeam antenna systems will demand greater degrees of beam interconnectivity. Multiband and multiservice users will be interconnected through the same space platform. Monolithic switching arrays operating over a wide range of RF and IF frequencies are contrasted with current IF switch technology implemented

discretely. Size, weight, and performance improvements by an order of magnitude are projected.
RPT#: NASA-TM-87201 E-2856 NAS 1.15:87201 86/00/00 86N17595

UTTL: VHF-AM communications equipment selection and installation practices for helicopters
AUTH: A/BOLZ, E. H.; B/KING, L. D. CORP: Systems Control, Inc., West Palm Beach, Fla.
ABS: The problems helicopter operators face when using VHF communications within typical operating environments where coverage by the network of ground stations may be deficient are addressed. This is of particular interest to IFR helicopter operators. The specific reasons why communications effectiveness can be limited in mountainous or remote regions, considering typical low helicopter operating altitudes, are reviewed. Recommendations to operators for improving the airborne VHF installation, and therefore improving its coverage capabilities, are presented. Several installation-related factors are discussed. These include the characteristics of the hardware, i.e., the transceiver and the antenna, and the characteristics of the installation, including antenna installation and resulting coverage pattern, the cable run, the effects of signal availability and ways of maximizing the capture of the available signal. A set of procedures is presented which allows operators to evaluate numerically the benefit in terms of signal strength or sensitivity they may expect given that they make specific improvements to a given actual or planned installation.
RPT#: DOT/FAA/PM-85/8 AD-A163483 85/09/00 86N15518

UTTL: Quasi-optic study of dielectric radomes and lenses
AUTH: A/FELSEN, L. B. CORP: Polytechnic Inst. of New York, Farmingdale. CSS: (Microwave Research Inst.)
ABS: The results from this study confirm the utility of complex ray tracing (via ordinary complex rays, collective complex rays or hybrid forms) for Gaussian beam type fields transmitted through tapered or curved two-dimensional shell radomes. The numerical algorithm, which avoids the need for integrations over an equivalent aperture when passing from the near zone to the far zone, can be simplified substantially for a range of applications by recourse to paraxial approximations. These conclusions are expected to remain valid also for more general three-dimensional configurations. Although non-Gaussian aperture distributions are not well modeled by complex ray fields per se, recent studies indicate that general aperture fields can be expressed as discrete superpositions of Gaussian fields. This makes the results for single Gaussians reported here directly relevant for the tracking, via obstacles and interfaces, of this more general class of incident fields.
RPT#: AD-A158441 POLY-MRI-1444-85 ARO-18887.7-EL 85/08/01 86N14481

UTTL: Simulation of the enhanced traffic alert and collision avoidance system (TCAS 2)
AUTH: A/ROJAS, R. G.; B/BURNSIDE, W. D.; C/LAW, P.; D/GRANDCHAMP, B. CORP: Ohio State Univ., Columbus. CSS: (ElectroScience Lab.)
ABS: The OSU aircraft code is used to analyze and simulate the TCAS 2 circular array which is mounted on the fuselage of a Boeing 737 aircraft. It is shown that the sum and difference patterns radiated by the circular array are distorted by the various structures of the aircraft, i.e., wings, tail, etc. Furthermore, monopulse curves are calculated and plotted for several beam positions and THETA angles. As expected, the worst cases of distortion occur when the beams are pointed toward the tail of the aircraft.
RPT#: NASA-CR-176328 NAS 1.26:176328 SAR-716199-3 85/09/00 86N12216

UTTL: Theory and experiment for infinite microstrip arrays
AUTH: A/WRIGHT, S. M.; B/LO, Y. T. PAA: B/(Illinois Univ., Urbana) CORP: Saint Francis Medical Center, Peoria, Ill. CSS: (Dept. of Radiology and Medical Imaging.)
ABS: Microstrip antennas are well suited for use in large scanning arrays. To obtain greater bandwidth, it is useful to use thicker substrates, which can increase the effects of mutual coupling and lead to significant mismatch or blindness for certain scan angles. Using an infinite array formulation, the impedance of a single element in an infinite array environment was solved with the method of moments. Mutual coupling is built into the solution, and the presence of surface waves is accounted for by using the periodic Green's function for the grounded dielectric substrate. Blindness in arrays of microstrip dipoles on various substrates, both with and without radomes is demonstrated. 85/01/00 86N11406

UTTL: Considerations for millimeter wave, monolithic phased arrays
AUTH: A/SCHAUBERT, D. H.; B/POZAR, D. M.; C/YNGVESSON, K. S.; D/JACKSON, R. W. CORP: Massachusetts Univ., Amherst. CSS: (Dept. of Electrical and Computer Engineering.)
ABS: Some candidate elements for millimeter wave, monolithic phased arrays are discussed. Printed antennas on high permittivity substrates are discussed in relation to EHF array performance. Scan impedance and blindness are evaluated by analysis and experiment. Methods for interfacing active devices such as FETs with candidate array elements are discussed. 85/01/00 86N11399

UTTL: Radome analysis and design capabilities of the RF and Microwave Technology Branch
AUTH: A/OVERFELT, P. L. CORP: Naval Weapons Center, China Lake, Calif.
ABS: A description of computer codes covering boresight error prediction, flat panel reflection and transmission properties, Von Karman geometry parameters, and spherical wave propagation for radomes is presented. The theoretical basis for each code is discussed, and examples of inputs and outputs are given. Comparison of theory with experimental data shows reasonable correlation. Thus, these codes can predict many interesting and useful properties needed for adequate initial radome design without resorting to expensive and time-consuming test procedures.
RPT#: AD-A156662 AD-E900475 NWC-TP-6636 85/04/00 86N10404

UTTL: Simulation and analysis of airborne antenna radiation patterns
AUTH: A/KIM, J. J. G. CORP: Ohio State Univ., Columbus.
ABS: An accurate and efficient analytic solution for predicting high frequency radiation patterns of fuselage-mounted airborne antennas is described. This is an analytic study of airborne antenna patterns using the Uniform Geometrical Theory of Diffraction (UTD). The aircraft is modelled in its most basic form so that the solution is applicable to general-type aircraft. The fuselage is modelled as a perfectly conducting composite ellipsoid; whereas, the wings, stabilizers, nose, fuel tanks, and engines, etc., are simulated as perfectly conducting flat plates that can be attached to the fuselage and/or to each other. The composite-ellipsoid fuselage model is necessary to successfully simulate the wide variety of real world fuselage shapes. Since the antenna is mounted on the fuselage, it has a dominant effect on the resulting radiation pattern so it must be simulated accurately, especially near the antenna. Various radiation patterns are calculated for commercial, private, and military aircraft, and the space shuttle Orbiter. The application of this solution to numerous practical airborne antenna problems illustrates its versatility and design capability. In most cases, the solution accuracy is verified by the comparisons between the calculated and measured data. 84/00/00 85N31342

UTTL: Calibration methods in millimeter-wave radioastronomy
AUTH: A/ABRAHAM, Z. CORP: Instituto de Pesquisas Espaciais, Sao Jose dos Campos (Brazil). Presented at the 4th IAU Reg. Meeting, Rio de Janeiro, Nov. 1984
ABS: A calibration method for millimeter wave observations that automatically compensates the atmospheric attenuation, even in the presence of a radome, or when the mean kinetic temperature of the sky is smaller than the ambient temperature is described.
RPT#: INPE-3481-PRE/724 85/03/00 85N27778

UTTL: Development of the microwave antenna range of the national antenna test facility at Paardefontein
AUTH: A/BAKER, D. E. CORP: National Inst. for Aeronautics and Systems Technology, Pretoria (South Africa).
ABS: The development of a ground reflection test range at Paardefontein is described. In addition to presenting some aspects of the range design and the measured performance, the physical development of the site will be highlighted.
RPT#: R-NIAS-21 FF-1 83/00/00 85N25669

UTTL: Design, fabrication and testing of a multibeam forming network CORP: Ford Aerospace and Communications Corp., Palo Alto, Calif. CSS: (Western Development Lab.)
ABS: A concept for a multiple beam forming network to route signals from eight input ports to twenty-one output ports so as to form eight independent seven-element cluster radiators was designed, fabricated, and tested. The operating frequency band is 2.226 to 2.254 GHz and the maximum power to any input port is two watts. The network consists of eight seven-way power dividers connected to twenty-one seven-way power combiners. The network utilizes barline circuits between parallel ground planes for the power distribution and collection. Interconnections are made with short rigid co-axial lines built into the network. The concept, general design procedures, mechanical configuration, and electrical performance

are described. It appears that the network is quite satisfactory for demonstrating practical feasibility of the technical concept.
RPT#: NASA-CR-175695 NAS 1.26:175695 84/09/00 85N24228

UTTL: Application of pushbroom altimetry from space using large space antennas
AUTH: A/PARSONS, C. L.; B/MCGOOGAN, J. T.; C/BECK, F. B.
PAA: A/(NASA. Goddard Space Flight Center); B/(NASA. Goddard Space Flight Center) CORP: National Aeronautics and Space Administration. Langley Research Center, Hampton, Va.; National Aeronautics and Space Administration. Wallops Flight Center, Wallops Island, Va.
ABS: The capabilities of multibeam altimetry are discussed and an interferometric multibeam technique for doing precision altimetry is described. The antenna feed horn arrangement and the resulting footprint lube pattern are illustrated. Plans for a shuttle multibeam altimetry mission are also discussed. 85/04/00 85N23817

UTTL: Development concerns for satellite-based air traffic control surveillance systems
AUTH: A/MCDONALD, K. D. CORP: Federal Aviation Administration, Washington, D.C.
ABS: Preliminary results of an investigation directed toward the configuration of a practical system design which can form the baseline for assessing the applications and value of a satellite based air traffic surveillance system for future use in the National Airspace System (NAS) are described. This work initially studied the characteristics and capabilities of a satellite configuration which would operate compatibly with the signal structure and avionics of the next generation air traffic control secondary surveillance radar system, the Mode S system. A compatible satellite surveillance system concept is described and an analysis is presented of the link budgets for the various transmission paths. From this, the satellite characteristics are established involving a large multiple feed L band antenna of approximately 50 meter aperture dimension. Trade offs involved in several of the alternative large aperture antennas considered are presented as well as the influence of various antenna configurations on the performance capabilities of the surveillance system. The features and limitations of the use of large aperture antenna systems for air traffic surveillance are discussed. Tentative results of this continuing effort are summarized with a brief description of follow on investigations involving other space based antenna systems concepts. 85/04/00 85N23816

UTTL: Coordinate determination errors in measuring characteristics of radiation field of airborne antennas
AUTH: A/GAZAZYAN, E. D.; B/PANCHENKO, V. G. CORP: Joint Publications Research Service, Arlington, Va.
ABS: Expressions are derived for estimating the coordinate errors in measuring the characteristics of the radiation field of airborne antennas. Errors in six coordinates must be taken into account at any given moment: the azimuth, elevation, slant range, heading, pitch and roll of the aircraft. It is recommended that straight-line flights be employed. Maneuvers should be used only in extreme cases, such as for measurements in the upper hemisphere. Conditions are specified under which it is possible to measure the characteristics of airborne antennas not equipped with maneuvering sensors, recording means or telemetry. 85/01/23 85N22919

UTTL: A generalized solution to a class of printed circuit antennas
AUTH: A/KATEHI-TSEREGOUNIS, P. B. CORP: California Univ., Los Angeles.
ABS: The theory and design of antennas excited by a microstrip transmission line or by a gap generator are examined. The antennas and the strip transmission line may be embedded inside or printed on the substrate. A theortical approach is implemented which accounts accurately for the physical effects involved including surface waves. The Green's function was obtained by synthesizing the fields of Hertzian dipoles which are oriented in arbitrary directions and which are printed on or embedded in the substrate. The method of solution is based on solving the Pocklington integral equation by employing the method of moments with proper choice of expansion and testing functions. The excitation mechanism is taken into account effectively by considering it as part of the antenna. The current distribution is obtained both on the transmission line and the printed antennas by matrix inversion. The method accounts for conductor thickness and for arbitrary substrate parameters. As an example, printed strip dipoles excited by a transmission line embedded in the substrate or by a voltage gap generator are considered. 84/00/00 85N22882

UTTL: Gain enhancement methods for printed circuit antennas
AUTH: A/JACKSON, D. R.; B/ALEXOPOULOS, N. G. CORP: California Univ., Los Angeles. CSS: (Lab. for Integrated Electromagnetics.)
ABS: Resonance conditions for a substrate-superstrate printed antennas geometry which allow for large antenna gain are presented. Asymptotic formulas for gain, beamwidth and bandwidth are presented and the bandwidth limitation of the method is discussed. The method is extended to produce narrow patterns about the horizon, and directive patterns at two different angles.
RPT#: AD-A150090 UCLA-ENG-84-39 UCLA-15 ARO-19778.15-EL 84/11/28 85N21517

UTTL: A radome for air traffic control SSR radar systems CORP: Electronic Space Systems Corp., Concord, Mass.
ABS: A new generation of monopulse and discrete interrogation systems has evolved for air traffic control applications that presents significant challenges to total system design and performance. Reliable operation of the antenna system is essential in today's ever increasing air traffic congestion. An important component of the total system is a radome to protect the antenna from the environment and to enable consistent, reliable electromagnetic performance. The various types of radomes that have been employed over the years to protect antennas are discussed and evaluated relative to the air traffic control radar application. The sandwich radome is selected as the best option and a detailed design analysis is presented which considers the vital characteristics of transmissivity, boresight error, and sidelobe perturbations.
RPT#: AD-P004373 84/00/00 85N21467

UTTL: Image lobe analysis for large radomes
AUTH: A/PUPKO, B.; B/GORDON, D.; C/STAROBINETS, S. CORP: Israel Aircraft Industries Ltd., Lod.
ABS: Image lobe intensities resulting from radomes enclosing large antennas (D greater than or equal to 15 lambda) were evaluated using ray tracing and aperture integration of the reflected field. It is shown, that random phase approximation can be used when the greatest radius of curvature is less than D to the 2nd power/8 lambda.
RPT#: AD-P004359 84/00/00 85N21453

UTTL: Dual band radome wall design
AUTH: A/CROWE, B. J. CORP: Flight Systems, Inc., Newport Beach, Calif.
ABS: Radomes for currently-deployed air launched tactical missiles are typically designed to operate at a single frequency or narrow range of frequencies, and occasionally over a wider band of contiguous frequencies spanning an octave or slightly more. Requirements to operate against an extended threat suite, and/or to negate probable countermeasures tactics, indicate a need for future systems to encompass a multi-mode capability. Such systems will combine operations in two or more discrete segments of the electromagnetic spectrum in an integrated seeker unit. Possible mechanizations include combinations of RF/IR, IR/UV, passive RF/active RF, and microwave/millimeter wave bands. Multimode systems such as these will naturally require a matching capability from the radome. Computer analysis can permit the identification of promising wall configurations, exhibiting desirable electrical properties in physically realizable thickness combinations. This paper describes two dual-band walls designed in this manner.
RPT#: AD-P004357 84/00/00 85N21451

UTTL: Near-field effects on radome boresight errors
AUTH: A/HUDDLESTON, G. K. CORP: Georgia Inst. of Tech., Atlanta. CSS: (School of Electrical Engineering.)
ABS: A computer-aided simulation of a boresight error measurement procedure and facility was carried out to quantify the effects of separation distance and wave reflections from anechoic chamber boundaries on radome-induced boresight errors using two BSE algorithms. The 3-D radome analysis program described earlier was modified to include near-field and reflection effects.
RPT#: AD-P004356 84/00/00 85N21450

UTTL: A subaperture approach to the calculation of flashlobes introduced by airborne radomes
AUTH: A/HIZAL, A.; B/LYON, R. W.; C/CUTHBERTSON, A. CORP: Middle East Technical Univ., Ankara (Turkey).
ABS: In airborne radomes a considerable effort has been devoted to the calculation of boresight errors but little attention has been given to the computation of flashlobes. These are caused by reflections from the radome wall and generally appear at angles well away from the boresight of the enclosed antenna. In certain circumstances they can seriously compromise the sidelobe suppression of the overall system. This paper describes an efficient method for flashlobe prediction

which gives more detailed information and can be used in an optimization of radome shape and wall build. The technique is based on the subaperture method which has already been successfully used to predict other bulk radome effects.
RPT#: AD-P004355 84/00/00 85N21449

UTTL: Generalized radome BSE (radome boresight error) characterization using superposition techniques
AUTH: A/PLIMPTON, G.; B/CERULLO, M. CORP: Raytheon Co., Bedford, Mass. CSS: (Missile Systems Div.)
ABS: Measurement of radome boresight error response to both polarization and gimbal angle variations can result in excessively long measurement times if a large number of incident polarizations are to be tested. Instead, by measuring the antenna radome system response to two orthogonal polarizations, and by using electro-magnetic superposition, it is possible to completely characterize the antenna/radome BSE response as a function of any arbitrary incident polarization. This paper will focus on the details of implementing the generalized radome BSE characterization in the Bedford Automated Test Facility and will compare measured and superpositioned data.
RPT#: AD-P004354 84/00/00 85N21448

UTTL: Comparison of spherical wave ray tracing and exact boundary value solutions for spherical radomes
AUTH: A/BLOOM, D. A.; B/OVERFELT, P. L.; C/WHITE, D. J. CORP: Naval Weapons Center, China Lake, Calif.
ABS: Much radome analysis is based on plane wave ray tracing techniques which combine conceptual simplicity with reasonable accuracy. As increasing demands on the performance of airborne antennas necessitate more accurate methods of analysis for the enclosing radome, an exact idea of the limits of applicability of the ray-optical approximation becomes more critical. In an effort to contribute to this subject, we have taken a single layer spherical radome excited by a dipole source oriented parallel to the z-axis and computed its transmitted electric and magnetic fields using a spherical wave ray tracing technique and also by solving the electromagnetic boundary value problem exactly. The exact solution is used as a standard against which the ray tracing approximation can be compared. In this paper, we compare the field patterns of the two solutions by varying the dipole offset distance, the observation point position, wall thickness, dielectric constant, wavelength, and curvature. Parameter values and the compared field patterns are examined in terms of the theory, and conclusions are drawn as to which parameters affect agreement most strongly.
RPT#: AD-P004353 84/00/00 85N21447

UTTL: A computer analysis of the RF performance of a ground-mounted, air-supported radome
AUTH: A/PUNNETT, M. B.; B/JOY, E. B. CORP: Georgia Inst. of Tech., Atlanta. CSS: (School of Electrical Engineering.)
ABS: Several reports and actual operating experience have highlighted the degradation of RF Performance which can occur when SSR or IFF antenna are mounted above primary search antenna within metal space frame or dielectric space frame radomes. These effects are usually attributed to both the high incidence angles and sensitivity of the low gain antennae to sidelobe changes due to scattered energy. Although it has been widely accepted that thin membrane radomes would provide superior performance for this application, there has been little supporting documentation. A plane-wave-spectrum (PWS) computer-based radome analysis was conducted to assess the performance of a specific air-supported radome for the SSR application. In conducting the analysis a mathematical model of a modern SSR antenna was combined with a model of an existing Birdair radome design.
RPT#: AD-P004352 84/00/00 85N21446

UTTL: Electromagnetic analysis of radomes by the moment method
AUTH: A/TRICOLES, G.; B/ROPE, E. L.; C/HAYWARD, R. A. CORP: General Dynamics Corp., San Diego, Calif. CSS: (Electronics Div.)
ABS: The electromagnetic performance of radomes is usually analyzed approximately by ray tracing, surface integration, or angular spectra. A significant approximation is that the radome is locally flat, and transmittance at a point is described by a set of flat sheets of infinite extent. This approximation is significant in the analysis of wave polarization dependence of boresight error, especially near the shadow of a tip where the surface normal direction varies rapidly because of circumferential curvature. This paper describes calculations for hollow wedges; these are based on a theory of J. H. Richmond for hollow cylinders of arbitrary shape. The paper also gives a new theory for hollow cones and circular rings, and it compares computed and measured phase and intensity values for a cone and a ring.
RPT#: AD-P004351 84/00/00 85N21445

UTTL: Proceedings of the Symposium on Electromagnetic Windows (17th) held at Georgia Inst. of Technology, Engineering Experiment Station, Atlanta, Georgia on 25-27 July 1984. Part 2
AUTH: A/BASSETT, H. L. CORP: Georgia Inst. of Tech., Atlanta. CSS: (Engineering Experiment Station.)
ANN: The Seventeenth Electromagnetic Window Symposium marks 29 years of regularly scheduled symposia on electromagnetic windows. The first seven symposia were held at Ohio State University. The Georgia Institute of Technology has hosted the symposium biennially since 1966, with the U.S. Air Force cohosting the symposia of 1966, 1968, and 1972. For individual titles see N85-21445 through N85-21469.
RPT#: AD-A149125 ARO-21807.1-MS-CF-PT-2 84/00/00 85N21444

UTTL: The susceptibility of aeronautical navigational aids to interference from adjacent-band broadcast transmissions
AUTH: A/MILLARD, G. H. CORP: British Broadcasting Corp., Kingswood (England). CSS: (Engineering Div.)
ABS: Measurements to determine the susceptibility of some airborne navigation receivers to interference from VHF/FM sound transmissions are described. The measurements were designed to investigate both the response to interference radiated in-band and to intermodulation in the receivers.
RPT#: BBC-RD-1984/12 84/11/00 85N18234

UTTL: Millimeter wave antenna technology
AUTH: A/DYBDAL, R. B. CORP: Aerospace Corp., El Segundo, Calif. CSS: (Electronics Research Lab.)
ABS: Millimeter wave antenna technology has had a long history of development, and as millimeter wave systems evolve through planning to implementation, a significant amount of additional development work will be required. Millimeter wave antennas play a key role in the rationale for millimeter system designs because high spatial resolution can be achieved with modest physical dimensions. Reflector, lens, array, and horn technologies are surveyed. Multiple beam designs and adaptive processing antennas are described because these technologies afford high leverage opportunities to enhance electronic survivability and to extend communication capabilities. Ancillary components, such as radomes, are a necessary part of practical antenna designs and are discussed in some detail.
RPT#: AD-A148694 TR-0084(4925-06)-1 SD-TR-84-52 84/09/30 85N17291

UTTL: Dual mode radio frequency-infrared frequency system
AUTH: A/BRUMBAUGH, C. T.; B/PITTENGER, R. L.; C/KLEES, R. M. CORP: Department of the Air Force, Washington, D.C.
ABS: A combined RF/IR system in which a common surface is used for the dual modes of radiating and absorbing RF energy and of reflecting and focusing IR energy is discussed. The common surface is structured, configured, and used as the slotted array antenna for the RF energy and as the primary mirror of a Cassegrain optical subsystem for the IR energy.
RPT#: AD-D011402 US-PATENT-4,477,814 US-PATENT-APPL-SN-404096 US-PATENT-CLASS-343-725 84/10/16 85N16850

UTTL: Tactical HF communication for military helicopters using the NVIS mode
AUTH: A/PUCCETTI, G.; B/COMO, P. L. CORP: Elmer, Rome (Italy).
ABS: The use of loop antennas for tactical HF communications on board of military helicopters was investigated. The helo platform is considered for land or maritime scenarios. The experiments on the SH-3D helicopter compared the loop antennas and existing wire antennas. Groundwave radiated field at different azimuth angles were measured for the two antenna types, particularly at the lower end of the frequency range where the difference in the antenna geometry is more significant. A consistent better performance of the loop over the wire, typically a 16 dB to 8 dB improvement is indicated. Skywave propagation tests at different distances and altitude of the helicopter were conducted. It is found that the performance of the loop antenna is superior to the wire. It is concluded that the loop antenna is an ideal radiator for use onboard aircraft and helicopters because of its dimensions, increased efficiency, and radiation characteristics. 84/08/00 85N16807

UTTL: Tolerance synthesis of multilayer radome walls
AUTH: A/LERMAN, L. B.; B/SKURSKIY, P. P.; C/SHUMILO, T. V. CORP: Joint Publications Research Service, Arlington, Va.
ABS: The design of plane multilayer radome walls for a receiver of electromagnetic waves within a given wavelength range lambda and a given incidence sector theta is considered from the standpoint of unitary construction and quantity production. Because analytical methods of tolerancing are not practical for multi-layer structures, a method of tolerance synthesis is proposed which uses the transmission

coefficient for radio waves as the critical performance parameter. The method is applied to an N-layer wall and a linearly polarized wave of length incident at angle theta. The characteristic impedance matrix for such a wall with lossy layers is defined. 84/12/17 85N16041

UTTL: Power transfer from natural emitters to collection apertures at microwave wavelengths
AUTH: A/STACEY, J. M. CORP: Jet Propulsion Lab., California Inst. of Tech., Pasadena.
ABS: The power transfer criteria necessary and sufficient to produce a detection of the emitting object by the collecting aperture and its receiver are shown. Range equations show the transfer of microwave energy from a passive, diffuse, emitting object that is located on a planetary surface, to a collecting aperture that is carried on an aerial platform or spacecraft. The mathematical relationships show in closed form the expressions for signal to noise ratio as a function of certain key parameters. The practical case of an emitting object on the Earth and a collecting aperture in orbit is presented.
RPT#: NASA-CR-174275 JPL-PUBL-84-48 NAS 1.26:174275 84/12/01 85N15989

UTTL: A low-sidelobe space feed lens
AUTH: A/MCGRATH, D. T. CORP: Rome Air Development Center, Griffiss AFB, N.Y. CSS: (Antennas and RF Components Branch.)
ABS: A parallel-plate waveguide microwave lens, constructed as part of the concept development of completely overlapped subarray antennas, was modified and tested. The lens function is comparable to that of a Rotman lens with 16 inputs (bma ports) and 60 outputs (antenna ports). However, the input face is linear with uniformly spaced monopole elements, and the output face is circular, with monopole elements spaced uniformly in angle. Using a four-way power divider at the center four inputs and the outputs connected to a line-source array, low sidelobe patterns were measured over a 22 percent bandwidth. Over the same 8.0 to 10.0 GHz band, total power loss in the lens was between 0.3 and 1.3 dB including mismatch, spillover and reflection losses.
RPT#: AD-A147883 RADC-TR-84-116 84/05/00 85N15972

UTTL: Hardwire missile receiver coupler
AUTH: A/MILLIGAN, T. A. CORP: Department of the Air Force, Washington, D.C.
ABS: A hardware missile receiver coupled line apparatus is inserted between the antenna output port and the receiver input in a missile communication link to allow signals to be coupled directly into the missile receiver before the missile launch. At launch, the cable to the side of the missile is pulled from the side of the missile. After the cable is pulled, the open circuited cable between the side of the missile and the coupling network does not degrade the signal transmission from the antenna to the receiver.
RPT#: AD-D011350 US-PATENT-4,465,985 US-PATENT-APPL-SN-353983 US-PATENT-CLASS-333-116 84/08/14 85N15936

UTTL: Microstrip antenna for multichannel radiometer
AUTH: A/KNYAZEV, S. T.; B/NEFEDOV, Y. I.; C/PANCHENKO, B. A. CORP: Joint Publications Research Service, Arlington, Va.
ABS: A microstrip designed for installation aboard agricultural aircraft as part of a radiometric moisture meter operating in the 2, 18 and 30 bands is described, which provides minimum losses and has no horizontal side lobes. The basic parameters of the experimental array patterns at the center and boundary frequencies of the working bands are given. The use of microstrip radiators makes it possible to implement a moisture meter antenna system with superior operating and electrodynamic characteristics. 84/09/25 85N15056

UTTL: Measurements of polarization characteristics of radiation field of on-board aircraft antennas
AUTH: A/GAZAZYAN, E. D.; B/PANCHENKO, V. G. CORP: Joint Publications Research Service, Arlington, Va.
ABS: A method for measuring the polarization characteristics of onboard antennas is analyzed in which an aircraft following an assigned trajectory is tracked from the ground and its angle of evolution with respect to the center of mass and the signal parameters at the output of the master antenna on the ground are measured. It is determined that rectilinear horizontal trajectories with no pitch or roll of the vehicle should be used. The requirements for the pitch and roll transducers must be made stiffer when selecting angle of measurement means; methods based on measuring amplitude ratios should be used when selecting a method for measuring the polarization characteristics of onboard antennas with arbitrary polarization. 84/10/15 85N12230

UTTL: Airworthiness and Flight Characteristics (A and FC) test of the EH - 1X/EH - 1H helicopter configurations

AUTH: A/DOWNS, G. T.; B/ADKINS, J. M.; C/NAGATA, J. I.; D/KIMBERLY, J. L.; E/LINEHAN, J. L. CORP: Army Aviation Engineering Flight Activity, Edwards AFB, Calif.

ABS: Level flight performance tests were conducted on five EH-1X/EH-1H helicopter configurations to determine the change in drag characteristics with the addition of external mission equipment to the standard UH-1H helicopter configuration. Comparison of data from a baseline test configuration with previously published UH-1H and YUH-1H data indicated approximately 8.0 increase in equivalent flat plate area which was attributed to the external mission antennas, low reflective infrared/optical paint, and heat suppression kit with vertical exhaust ejector. Installation of the M-130 chaff/flare dispensers resulted in a further increase in equivalent flat plate area of 5.0 sq ft. Replacing the vertical exhaust ejector with the hot metal plus plume infrared suppressor, including the ALQ-144 countermeasures jammer resulted in a reduction in equivalent flat plate area of 1.5 sq ft. Installation of the direction finding antennas resulted in no measurable increase in drag. Addition of all external mission equipment and the hot metal plus plume exhaust resulted in a total increased equivalent flat plate area of approximately 11.5 sq ft. from the standard UH-1H helicopter.

RPT#: AD-A144881 84/01/00 85N10039

AGARD Lecture Series No.151
Advisory Group for Aerospace Research and Development, NATO
MICROWAVE ANTENNAS FOR AVIONICS
Published April 1987
166 pages

Even though considerable advances have been made in digital technology and signal processing, antennas continue to play a key role and their performance is often a dominating factor in defining the overall effectiveness of a system. New system requirements, and the need to provide electronic scanning capabilities have presented major challenges to the technology that require substantial improvements over what is currently available.

Over the last decade there have been notable advances in

P.T.O

AGARD-LS-151

Microwave antennas
Avionics
Radomes
Design
Improvement

AGARD Lecture Series No.151
Advisory Group for Aerospace Research and Development, NATO
MICROWAVE ANTENNAS FOR AVIONICS
Published April 1987
166 pages

Even though considerable advances have been made in digital technology and signal processing, antennas continue to play a key role and their performance is often a dominating factor in defining the overall effectiveness of a system. New system requirements, and the need to provide electronic scanning capabilities have presented major challenges to the technology that require substantial improvements over what is currently available.

Over the last decade there have been notable advances in

P.T.O

AGARD-LS-151

Microwave antennas
Avionics
Radomes
Design
Improvement

AGARD Lecture Series No.151
Advisory Group for Aerospace Research and Development, NATO
MICROWAVE ANTENNAS FOR AVIONICS
Published April 1987
166 pages

Even though considerable advances have been made in digital technology and signal processing, antennas continue to play a key role and their performance is often a dominating factor in defining the overall effectiveness of a system. New system requirements, and the need to provide electronic scanning capabilities have presented major challenges to the technology that require substantial improvements over what is currently available.

Over the last decade there have been notable advances in

P.T.O

AGARD-LS-151

Microwave antennas
Avionics
Radomes
Design
Improvement

antenna and radome design, particularly in sidelobe reduction, electronic scanning, conformal arrays, printed circuit arrays, adaptive control and millimetre wave antennas. This Lectures Series will address many of these issues in a two-day programme of lectures by noted workers in the various fields of antenna technology. Future trends and new directions for technological innovation will be subjects for round table discussions.

This Lecture Series, sponsored by the Avionics Panel of AGARD, has been implemented by the Consultant and Exchange Programme of AGARD.

The material in this publication was assembled to support a Lecture Series under the sponsorship of the Avionics Panel and the Consultant and Exchange Programme of AGARD presented on 7—8 May 1987 in Rome, Italy, 11—12 May 1987 in Guenzburg, Germany and 14—15 May 1987 in Ankara, Turkey.

ISBN 92-835-1547-1

antenna and radome design, particularly in sidelobe reduction, electronic scanning, conformal arrays, printed circuit arrays, adaptive control and millimetre wave antennas. This Lectures Series will address many of these issues in a two-day programme of lectures by noted workers in the various fields of antenna technology. Future trends and new directions for technological innovation will be subjects for round table discussions.

This Lecture Series, sponsored by the Avionics Panel of AGARD, has been implemented by the Consultant and Exchange Programme of AGARD.

The material in this publication was assembled to support a Lecture Series under the sponsorship of the Avionics Panel and the Consultant and Exchange Programme of AGARD presented on 7—8 May 1987 in Rome, Italy, 11—12 May 1987 in Guenzburg, Germany and 14—15 May 1987 in Ankara, Turkey.

ISBN 92-835-1547-1

antenna and radome design, particularly in sidelobe reduction, electronic scanning, conformal arrays, printed circuit arrays, adaptive control and millimetre wave antennas. This Lectures Series will address many of these issues in a two-day programme of lectures by noted workers in the various fields of antenna technology. Future trends and new directions for technological innovation will be subjects for round table discussions.

This Lecture Series, sponsored by the Avionics Panel of AGARD, has been implemented by the Consultant and Exchange Programme of AGARD.

The material in this publication was assembled to support a Lecture Series under the sponsorship of the Avionics Panel and the Consultant and Exchange Programme of AGARD presented on 7—8 May 1987 in Rome, Italy, 11—12 May 1987 in Guenzburg, Germany and 14—15 May 1987 in Ankara, Turkey.

ISBN 92-835-1547-1

antenna and radome design, particularly in sidelobe reduction, electronic scanning, conformal arrays, printed circuit arrays, adaptive control and millimetre wave antennas. This Lectures Series will address many of these issues in a two-day programme of lectures by noted workers in the various fields of antenna technology. Future trends and new directions for technological innovation will be subjects for round table discussions.

This Lecture Series, sponsored by the Avionics Panel of AGARD, has been implemented by the Consultant and Exchange Programme of AGARD.

The material in this publication was assembled to support a Lecture Series under the sponsorship of the Avionics Panel and the Consultant and Exchange Programme of AGARD presented on 7—8 May 1987 in Rome, Italy, 11—12 May 1987 in Guenzburg, Germany and 14—15 May 1987 in Ankara, Turkey.

ISBN 92-835-1547-1

AGARD

NATO OTAN

7 rue Ancelle · 92200 NEUILLY-SUR-SEINE

FRANCE

Telephone (1)47.38.57.00 · Telex 610 176

DISTRIBUTION OF UNCLASSIFIED AGARD PUBLICATIONS

AGARD does NOT hold stocks of AGARD publications at the above address for general distribution. Initial distribution of AGARD publications is made to AGARD Member Nations through the following National Distribution Centres.Further copies are sometimes available from these Centres, but if not may be purchased in Microfiche or Photocopy form from the Purchase Agencies listed below.

NATIONAL DISTRIBUTION CENTRES

BELGIUM
Coordonnateur AGARD — VSL
Etat-Major de la Force Aérienne
Quartier Reine Elisabeth
Rue d'Evere, 1140 Bruxelles

CANADA
Defence Scientific Information Services
Dept of National Defence
Ottawa, Ontario K1A 0K2

DENMARK
Danish Defence Research Board
Ved Idraetsparken 4
2100 Copenhagen Ø

FRANCE
O.N.E.R.A. (Direction)
29 Avenue de la Division Leclerc
92320 Châtillon

GERMANY
Fachinformationszentrum Energie,
Physik, Mathematik GmbH
Kernforschungszentrum
D-7514 Eggenstein-Leopoldshafen

GREECE
Hellenic Air Force General Staff
Research and Development Directorate
Holargos, Athens

ICELAND
Director of Aviation
c/o Flugrad
Reyjavik

ITALY
Aeronautica Militare
Ufficio del Delegato Nazionale all'AGARD
3 Piazzale Adenauer
00144 Roma/EUR

LUXEMBOURG
See Belgium

NETHERLANDS
Netherlands Delegation to AGARD
National Aerospace Laboratory, NLR
P.O. Box 126
2600 AC Delft

NORWAY
Norwegian Defence Research Establishment
Attn: Biblioteket
P.O. Box 25
N-2007 Kjeller

PORTUGAL
Portuguese National Coordinator to AGARD
Gabinete de Estudos e Programas
CLAFA
Base de Alfragide
Alfragide
2700 Amadora

TURKEY
Millî Savunma Başkanlığı (MSB)
ARGE Daire Başkanlığı (ARGE)
Ankara

UNITED KINGDOM
Defence Research Information Centre
Kentigern House
65 Brown Street
Glasgow G2 8EX

UNITED STATES
National Aeronautics and Space Administration (NASA)
Langley Research Center
M/S 180
Hampton, Virginia 23665

THE UNITED STATES NATIONAL DISTRIBUTION CENTRE (NASA) DOES NOT HOLD STOCKS OF AGARD PUBLICATIONS, AND APPLICATIONS FOR COPIES SHOULD BE MADE DIRECT TO THE NATIONAL TECHNICAL INFORMATION SERVICE (NTIS) AT THE ADDRESS BELOW.

PURCHASE AGENCIES

National Technical
Information Service (NTIS)
5285 Port Royal Road
Springfield
Virginia 22161, USA

ESA/Information Retrieval Service
European Space Agency
10, rue Mario Nikis
75015 Paris, France

The British Library
Document Supply Division
Boston Spa, Wetherby
West Yorkshire LS23 7BQ
England

Requests for microfiche or photocopies of AGARD documents should include the AGARD serial number, title, author or editor, and publication date. Requests to NTIS should include the NASA accession report number. Full bibliographical references and abstracts of AGARD publications are given in the following journals:

Scientific and Technical Aerospace Reports (STAR)
published by NASA Scientific and Technical
Information Branch
NASA Headquarters (NIT-40)
Washington D.C. 20546, USA

Government Reports Announcements (GRA)
published by the National Technical
Information Services, Springfield
Virginia 22161, USA

Printed by Specialised Printing Services Limited
40 Chigwell Lane, Loughton, Essex IG10 3TZ

ISBN 92-835-1547-1